DOCTORAL THESIS

BAX and BAK - the deadly rings

A comprehensive study of the mitochondrial apoptotic pore *in situ* with super-resolution microscopy

Dissertation

for the award of the degree

"Doctor rerum naturalium"

of the Georg-August-Universität Göttingen

within the doctoral program

"Molecular Medicine"

of the Georg-August University School of Science (GAUSS)

submitted by

Sarah Vanessa Schweighofer

Göttingen, December 2022

Members of the Thesis Committee:

Prof. Dr. Stefan Jakobs (1st Referee)
Research Group High Resolution of the Cell, Clinic of Neurology
University Medical Center Göttingen and
Research Group Mitochondrial Structure and Dynamics
Max Planck Institute for Multidisciplinary Sciences, Göttingen

Prof. Dr. Tiago Outeiro (2nd Referee)
Experimental Neurodegeneration
University Medical Center Göttingen

Dr. Ricarda Richter-Dennerlein
Department of Cellular Biochemistry
University Medical Center Göttingen

Further members of the Examination Board:

Prof. Dr. Blanche Schwappach-Pignataro
Dean of the Medical Faculty
University Clinics Hamburg-Eppendorf

Dr. Sonja Lorenz
Research Group Ubiquitin Signaling Specificity
Max Planck Institute for Multidisciplinary Sciences, Göttingen

Dr. Peter Lenart
Live-cell Imaging Facility
Max Planck Institute for Multidisciplinary Sciences, Göttingen

Date of the oral examination: 3rd of February 2023

"The path doesn’t necessarily have to be straight,
but don’t limit yourself to what you know.
Go out and try new things."

Sunita Williams, NASA astronaut
who held records for most spacewalks by a woman

Acknowledgments

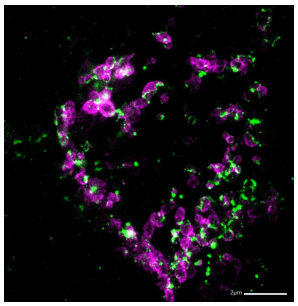

I want to thank all the amazing people who made this work possible. First and foremost Prof. Dr. Stefan Jakobs, my supervisor and Prof. Dr. Stefan Hell, our department head, who both provided me with the unique opportunity of performing my thesis work here in Göttingen at the Max Planck Institute for Multidisciplinary Sciences.

I would like to thank the members of my thesis advisory commitee, with some fluctuation over the years: Prof. Dr. Tiago Outeiro, Dr. Ricarda Richter-Dennerlein, Prof. Dr. Blanche Schwappach and Prof. Dr. Michael Meinecke, who believed in me, gave valuable advice and encouraged me when needed. Furthermore, I would like to thank the further members of my examination board, Dr. Peter Lenart and Dr. Sonja Lorenz.

Next, I want to thank all the members of the Jakobs group and the departement of NanoBiophotonics, past and present, from the bottom of my heart. There were and are so many great people who made me get up every morning and look forward to another day, not only full of exciting science, but also filled with fun, laughter and intense conversations with my wonderful colleagues.

First, I want to thank Daniel Jans, who took on the task of being my one-on-one mentor and Till Stephan, who both corrected my thesis meticulously and gave invaluable tips; Christian Brüser, Nickels Jensen and Isabell Jansen who taught me so much. Peter Ilgen, who is an essential part of the team without whom everything would break down, told me most things I know about graphic design. I also want to acknowledge our technical staff, first and foremost, Anne Folmeg, and also Sylvia Löbermann, Rita Schmitz-Salue, Tanja Koenen, Ellen Rothermel and Nicole Molitor without whose help this work would have been impossible. Cornelia Heistermann and Simone Brauer for their amazing job to keep our offices and lab spaces in perfectly clean conditions and thereby contributing enormously to the success of our work.

Very importantly, I want to thank Jan-Keller Findeisen who is such a great programmer, mentor and human being and has taught me most of the things I know about coding. The whole data science part of the thesis exists essentially thanks to you Jan, and I am eternally grateful for that! I also want to thank Mark Bates for going on a single-molecule microscopy adventure with me. I want to thank Dorian Leger and Antonio Politi from the live cell imaging facility, who were incredibly helpful in setting up the automated imaging pipeline on their STEDycon as well as Peter Lenart and Jasmin Jakobi who were always there for help in the facility. Grazvydas Lukinavicius and Ruta Gerasimaite let me use their wonderful instrumentation providing invaluable help using it.

Most importantly, I want to thank my dear "starken Männer", Daniel Stumpf and Axel Rösch - where would I be without you? I also dearly remember the unforgettable happy moments Axel and me shared with our former office colleague Florian Habenstein. Furthermore, I specifically want to thank Nickels Jensen for being such a great lab daddy and holding everything together and eating Snickers with me.

Last but not least, I want to thank my family and friends for supporting me in every aspect of life. As a biologist, I admire the miracles of nature and especially as a microscopist, I want to shed light on these mysteries. I am eternally grateful for being lucky enough to have the opportunity to wonder about such things...

Abstract

Apoptosis, the most common form of cell death in the human body, is essential for numerous physiological processes. The intrinsic apoptosis pathway can be triggered by a wide variety of stimuli and leads to the insertion of BAX and BAK, the effector proteins of the intrinsic apoptosis pathway, into the mitochondrial outer membrane (MOM). The insertion of BAX and BAK opens a pore in the MOM, which releases proteins from the mitochondrial inter-membrane space into the cytosol, thereby activating the caspase cascade, resulting in the ultimate demise of the cell.

Although the two pore-forming effector proteins, BAX and BAK, have been extensively investigated by *in vitro* studies, it is still unclear how the two proteins are arranged in the apoptotic pore in the MOM *in situ*. Using diffraction-limited microscopy, numerous studies have revealed the general sub-cellular localization of BAX and BAK, but the resolution of conventional light microscopes is insufficient to analyze the nanoscale distribution of BAX and BAK.

Therefore, in this work I employed super-resolution microscopy on apoptotic cells in order to investigate the fine structure of the apoptotic BAX-BAK pore *in situ* with sub-diffractional resolution. My results demonstrate that, when overexpressed and imaged by live-cell STED microscopy, BAX and BAK induce apoptosis, but differ in nanoscale dynamics and ultra-structures. However, the overexpression of the pore-forming proteins proved disadvantageous for the study of the apoptotic pore, because the overabundance of BAX or BAK disturbs the fragile equilibrium of pro- and anti-apoptotic proteins, leading to rapid, unphysiological cell death.

To circumvent the drawbacks of overexpression, I established a dual-color antibody staining of endogenous BAX and BAK in fixed cells suitable for STED microscopy. The super-resolved images demonstrate that BAX and BAK at endogenous expression levels formed mosaic rings together that are lining the apoptotic pore. Quantitative analysis revealed that these differently sized rings contained variable relative amounts of BAX and BAK, which tended to homogenize with the growth of the rings. Furthermore, the rings were not continuously and regularly outlined by proteins, but instead large clusters and voids were irregularly interspersed. Within this irregular arrangement along the ring outline, the two proteins had a tendency to follow similar distribution patterns rather than forming mutually exclusive assemblies. Although in wild type cells most rings were composed of both proteins, knockout cell lines of BAX or BAK demonstrated that, if one of the partners was absent, the remaining protein was able to form pores independently, corroborating the partial functional redundancy of the two proteins.

Next to immortal cell lines, I furthermore detected BAX-BAK rings in primary human cells, which suggests that the formation of complex BAX/BAK assemblies, especially mosaic rings, is a physiological and essential step during apoptosis.

Altogether, my results display BAX and BAK in apoptotic cells *in situ* and the data strongly support a toroidal pore model, where BAX and BAK proteins cover the pore rim together in an unordered fashion.

Contents

List of Figures

List of Tables

List of Abbreviations

ActD	Actinomycin D
BCL-2	B-cell lymphoma 2
BAK	BCL-2 homologous antagonist killer
BAX	BCL-2 associated X protein
BG	benzylguanine
CA	chloralkene
DKO	double-KO
FA	formaldehyde
FACS	fluorescence activated cell sorting
HDFAs	human dermal fibroblasts from adult tissue
IF	immunofluorescence
IMS	inter-membrane space
KO	knockout
MIM	mitochondrial inner membrane
MOM	mitochondrial outer membrane
MOMP	mitochondrial outer membrane permeabilization
NGS	Next Generation Sequencing
PCC	Pearson correlation coefficient
Q-VD-OPh	Quinolyl-valyl-O-methylaspartyl-[2,6-difluorophenoxy]-methylketone
SiR	silicone rhodamine
SMLM	single molecule localization microscopy
STED	Stimulated Emission Depletion
WB	Western blot

1 Introduction

1.1 Cell Death

"To be, or not to be, that is the question!" [1].
Just like human beings, all cells within an organism eventually have to die. In the human body, every second approximately one million cells die [2]. Cell death is of vital importance to every organism, because it is essential for development, efficient homeostasis and adaptation to a changing environment. Dying cells during normal embryonic development have already been discovered in 1842 in the development of a toad species [3]. However, only in 1951, a publication clearly stated that cell death is a normal part of life [4]. Today, we know of countless different pathways that lead to cell death. As many of these pathways are not yet fully defined, are overlapping by morphological features or signals activated or were previously incorrectly classified, the Nomenclature Committee on Cell Death (NCCD) was created in 2005 [5]. The nomenclature unifies criteria for the definition of cell death characteristics and morphology and is since continuously updated as new research emerges [6].

A severe cellular perturbance of physical (e.g., high pressures, temperatures, or osmotic forces), chemical (e.g., extreme pH variations), or mechanical (e.g., shear forces) nature, which leads to the instantaneous and catastrophic demise of the cell, is called accidental cell death (ACD) [6].

The vast majority of cells, however, undergo regulated cell death (RCD). No external triggers are needed for the cell to undergo RCD during development or physiological tissue turnover, as the pathways are intrinsically programmed and therefore referred to as programmed cell death (PCD). For the discovery of PCD, *Sydney Brenner, H. Robert Horvitz and John E. Sulston* were awarded the Nobel Prize in Physiology or Medicine in 2002 [7, 8, 9].

Next to development and tissue turnover, a cell also must die, if it cannot cope with different intra- or extracellular stresses. The death of the stressed cell thereby prevents the endangerment of the whole organism. This is referred to as stress-driven RCD [6] (Figure 1).
RCD is essential for the physiological fuctions of an organism and therefore needs to be tightly controlled: On the one hand, if it fails to execute when needed, the consequences can be catastrophic, manifesting as autoimmunity, cancer [10, 11] and other diseases. On the other hand, if cell death occurs by mistake, this can lead to detrimental effects, such as stroke, (neuro-)degeneration, heart attack, and other conditions [12, 13, 14, 15, 16, 2].

A plethora of (programmed and stress-driven) RCD pathways have been discovered such as necroptosis, ferroptosis, pyroptosis etc. (Figure 2). All of these pathways

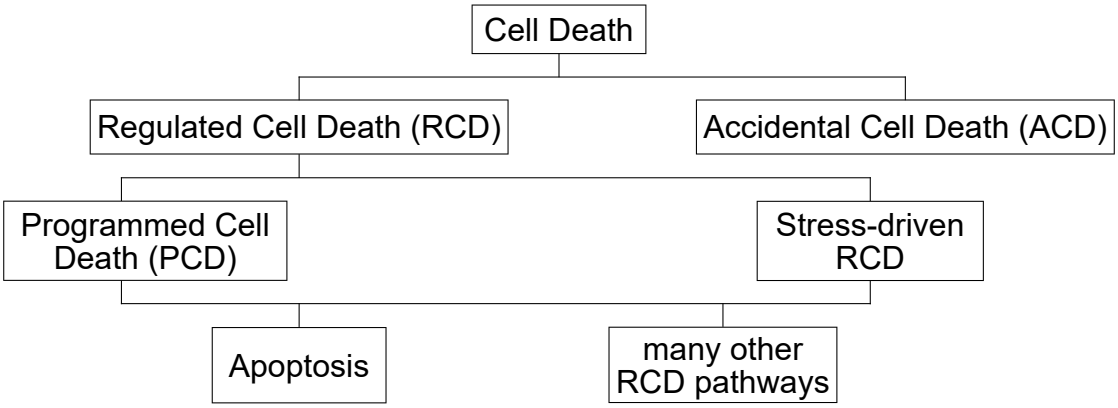

Figure 1: Categorizing cell death. Accidental cell death (ACD) happens instantaneously. However, most cells undergo regulated cell death (RCD). RCD can be distinguished into two categories: First, programmed cell death (PCD), which happens during development and physiological tissue turnover without the need for external triggers. And second, stress-driven RCD, which is triggered by perturbations of the intra- or extracellular environment. A specific cell death pathway which can be triggered during PCD or stress-driven RCD is apoptosis. There are many more RCD pathways, which contribute to PCD and/or can be elicited as stress-driven RCD (see Figure 2).

share the common feature that they rely on dedicated molecular machineries leading the cell into defined pathways of dying. The most well-known and most studied RCD pathway is apoptosis, the discovery of which began in 1972 and research on apoptosis has since grown exponentially [17].

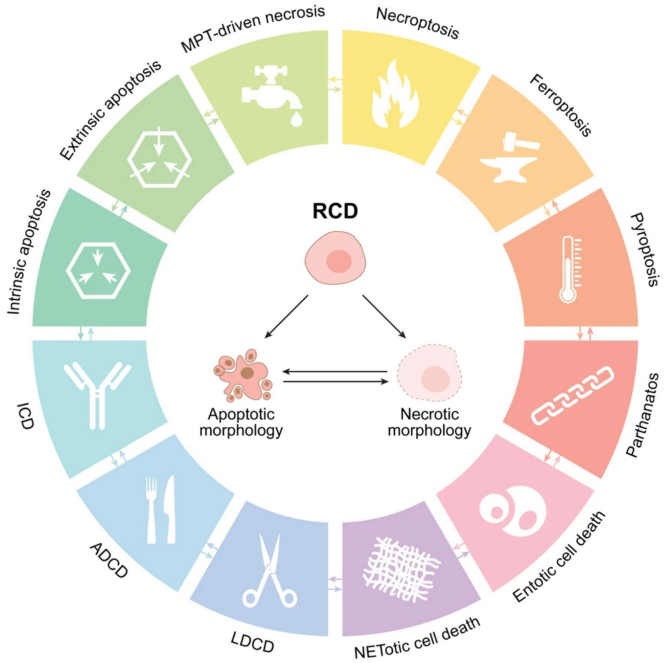

Figure 2: Regulated Cell Death (RCD) pathways. Cells which are destined to die can activate one of these many signalling pathways ultimately leading to their death. *ADCD:* autophagy-dependent cell death, *ICD:* immunogenic cell death, *LDCD:* lysosome-dependent cell death, *MPT:* mitochondrial permeability transition. (*Reproduced from* [6].)

1.1.1 Apoptosis

Apoptosis is the most common form of cell death in the human body [2]. The word apoptosis translates from ancient greek to "falling off". This was defined by *J. Kerr* in 1972 [18] because cells, which die by apoptosis, do so in an apparently random but intrinsically organized manner, just like leaves falling off a tree.

The PCD during development or tissue homeostasis relies mainly on apoptosis, which is why those two terms are often used synonymously. An example for the need of developmental apoptosis is the removal of the webbing between digits [19] (Figure 3). An example for programmed apoptosis during tissue homeostasis is the mammalian menstrual cycle [20]. However, apoptosis is not only programmed, but also occurs as stress-driven RCD, for example in cells that die after excessive UV irradiation (e.g. sunburn) [21].

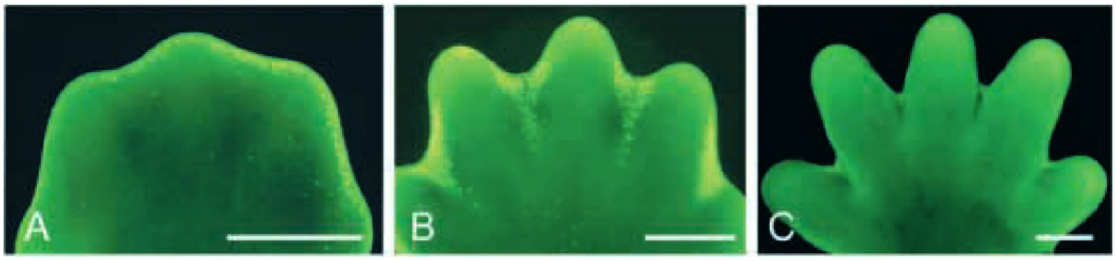

Figure 3: Removal of inter-digit webbing during embryonic development through apoptosis. Cells which are destined to die between the toes of a mouse paw become apoptotic and get phagocytosed by macrophages. Scale bars = 250 μm. (*Adapted from* [19].)

Apoptosis results in the activation of the caspase (cysteine-dependent aspartate-specific protease) cascade [22]. Caspases are proteases that cleave their substrates C-terminally of an aspartate residue, as their name suggests. Once the initiator caspases are activated, they in turn activate the effector caspases and these exert their protease activity to rapidly cleave target proteins in the cell [23], which leads to a series of events [24]: nuclear fragmentation and DNA degradation [25] occurs by endogenous endonuclease activation [26]; the Phosphatidyl-Serine (PS) flippase gets cleaved and thereby inactivated [27], which leads to PS accumulation at the outer leaflet of the plasma membrane [28, 29] to serve as degradation signal for phagocytes; all cell compartments fragment, the plasma membrane undergoes blebbing and the cell shrinks drastically. Often the cell breaks down into smaller membrane-bound fragments, the apoptotic bodies, but the contents of the dying cell remain contained within its membranes. In an organism the apoptotic cells and/or bodies are then phagocytosed and degraded by other cells like macrophages.

Independent of whether apoptosis is programmed or stress-driven, there are two different ways to trigger apoptosis which both lead to the activation of the apoptotic

caspase cascade: the extrinsic (or death receptor) pathway and the intrinsic (or mitochondrial) pathway [30] (Figure 4). The extrinsic apoptosis pathway is triggered by the binding of a ligand to a death receptor on the cell surface. This then leads to the formation of the death-inducing signaling complex (DISC) [31], which activates the caspases.

The intrinsic apoptosis pathway, in contrast, is triggered by a wide variety of stimuli, like nutrient-deprivation, DNA damage, toxins or oxidative stress [30]. Mitochondria serve as the central signaling platform in the intrinsic apoptosis pathway, by opening open a pore on the mitochondrial outer membrane (MOM), which releases proteins from the mitochondrial inter-membrane space (IMS) into the cytosol to activate caspases.

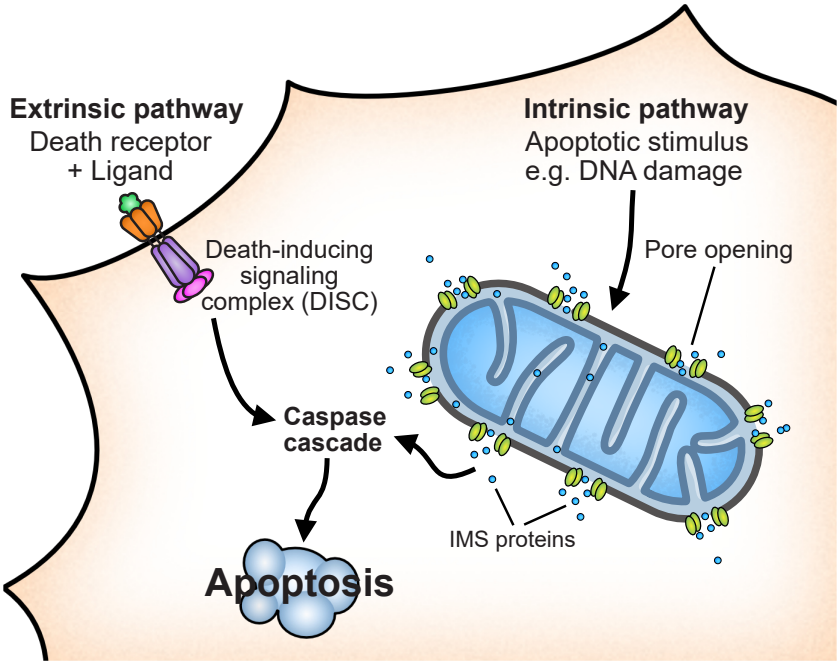

Figure 4: Apoptosis pathways. Apoptosis can be triggered extrinsically via the death-receptor pathway or intrinsically via the mitochondrial pathway. In the extrinsic (or death receptor) pathway of apoptosis, ligands bind to a death receptor on the cell surface, which leads to the formation of the death-inducing signaling complex (DISC) and consequently to the activation of the caspase cascade. The intrinsic (or mitochondrial) pathway of apoptosis is triggered by a wide variety of stimuli, which cause the opening of a pore on the MOM and therby release of IMS proteins. These proteins activate the caspase cascade, which leads to downstream events in apoptosis and the ultimate demise of the cell.

1.1.2 Mitochondria in health and disease

Mitochondria play an essential role in apoptosis. These intricate organelles are highly compartmentalized and are enveloped by two membranes [32, 33]: the mitochondrial outer membrane (MOM) and the mitochondrial inner membrane (MIM) (Fig-

ure 5A). Between the two membranes there is the inter-membrane space (IMS) and inside of the MIM the mitochondrial matrix is situated. The MIM is substantially larger than the MOM and must therefore be highly folded, which leads to the formation of invaginations of the MIM into the matrix space, the so called cristae [34, 35]. The matrix contains the mitochondrial DNA (mtDNA) [36, 37, 38], which, in humans, harbors 13 genes that encode for proteins of the electron transport chain [39]. The rest of the proteins for the electron transport chain are encoded by nuclear DNA [40, 41]. mtDNA is compacted with certain proteins into nucleoids, which appear as distinct punctae in the mitochondria [42]. In a physiological state, mitochondria are highly dynamic organelles and contrary to the classical textbook image, these organelles with a typical diameter of a couple hundred nanometers (nm) in diameter [34, 35] form a reticular network in most cell types (Figure 5B). The mitochondrial tubules undergo constant fission and fusion guided by the fusion proteins Mitofusin 1 and 2 [43, 44] as well as by the fission protein Drp1 (dynamin-related-protein1) [45, 46]. The function of the fission and fusion of mitochondria is to keep up a healthy network and rapidly adjust to local demands of the cellular environment. When parts of mitochondria are damaged, they get removed by fission and are then degraded [47].

Next to playing a crucial role in apoptosis, mitochondria have a plethora of functions in the cell (Figure 5A). They serve as hub for a multitude of signaling pathways in the cell as they have contact sites to virtually all other organelles [49]. They also supply the cell with precursors for important building blocks like amino acids, lipids and nucleotides. These precursors are derived from the tricarboxylic acid (TCA) cylce [48], a metabolic pathway, which takes place in the mitochondrial matrix.

Most importantly, mitochondria provide the cell with energy by producing ATP in a process called oxidative phosphorylation (OXPHOS). The proteins which are responsible for producing the energy are arranged in the respiratory chain or electron transport chain, which is comprised of 5 large complexes (I-V) embedded into the cristae membrane. The OXPHOS system transfers electrons from one complex to the next, thereby generating a proton (H+) gradient over the MIM. Also here, the TCA cycle provides donor molecules. Cytochrome *c* serves as mobile carrier that shuttles electrons from complex III to IV. The H^+ accumulate in the IMS and this proton gradient gets used by complex V, the ATP-Synthase, which is a powerful protein motor. When the ATP-Synthase uses H^+ to drive its rotating force, it phosphorylates an ADP molecule to produce an ATP molecule [50]. Accordingly, tissue with a high energy demand (e.g. muscles) have numerous mitochondria and can even increase the biogenesis of mitochondria upon higher demand [51].

Once a mitochondrion is functionally impaired or has expired, it is rapidly re-

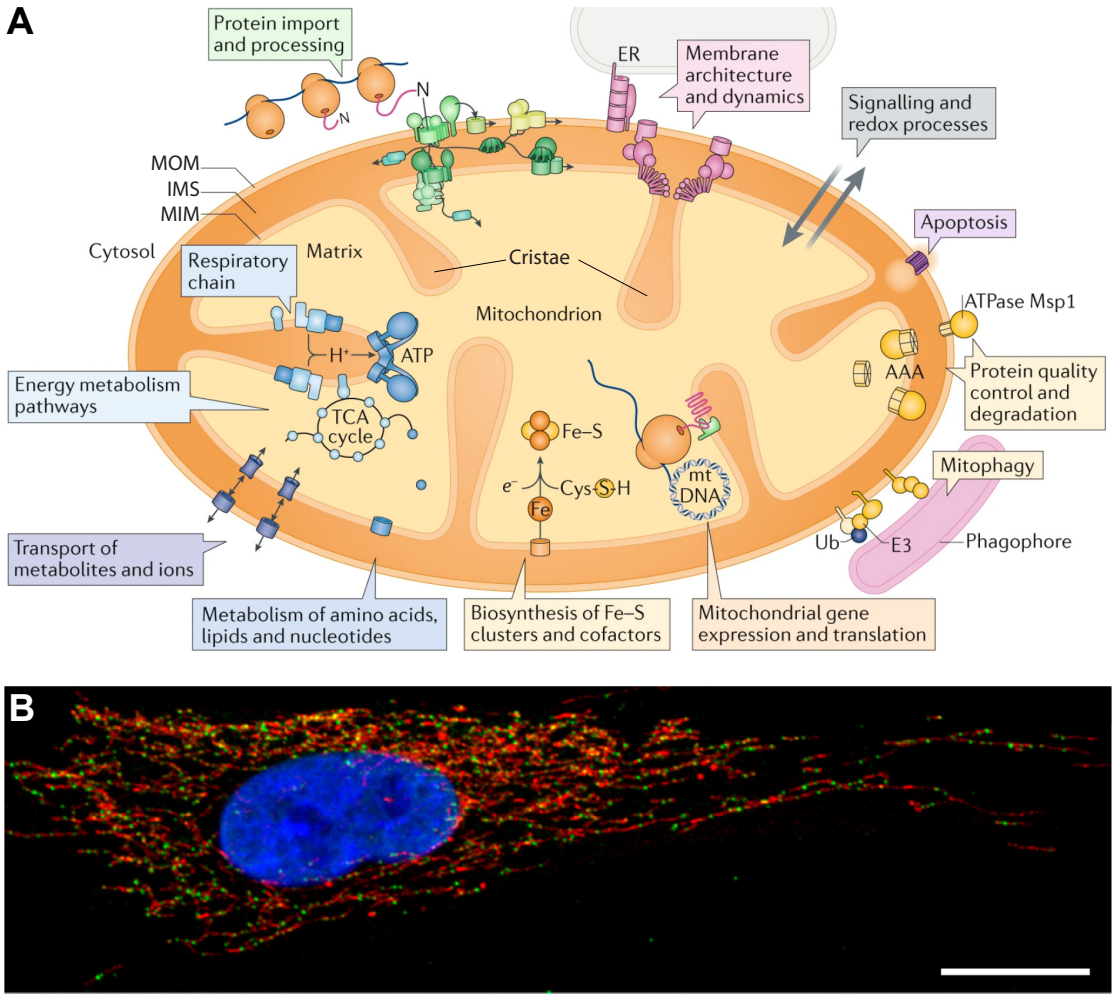

Figure 5: Mitochondrial architechture and functions. **(A)** Mitochondria consist of two membranes: the mitochondrial outer membrane (MOM) and the mitochondrial inner membrane (MIM). The space between the two membranes is called the inter-membrane space (IMS). The highly invaginated MIM forms cristae and surrounds the matrix, which contains the mitochondrial DNA (mtDNA). Mitochondria have a plethora of different functions in a cell. The tricarboxylic acid (TCA) cycle provides donor molecules for the electron transport chain. The electron transport chain or respiratory chain, which is embedded into the cristae membrane, creates energy for the organism by producing ATP via oxidative phosphorylation (OXPHOS). The TCA cycle furthermore produces precursors for the metabolism of amino acids, lipids and nucleotides. Among multiple other functions, mitochondria are in close contact with all other organelles and thereby serve as signaling hubs in the cell. (*Adapted from* [48].) **(B)** Mitochondria form a reticular network in cells. The mitochondria (red) in a human dermal fibroblast surround the nucleus (DAPI, blue) and extend over the whole cell, harboring mtDNA as nucleoids (green). Scale bar = 20 µm. (*Adapted from* [42].)

cycled by a process called mitophagy [52]. If more than single mitochondria or the whole cell has been damaged, the mitochondria fragment, release their contents and the intrinsic pathway of apoptosis is triggered [30]. In addition to activating the immunologically silent process of apoptosis, mitochondria were recently demonstrated to be multi-faceted regulators of cell death. The release of mitochondrial DNA and

RNA from the matrix has been shown to be involved in engaging inflammatory responses [30, 53], for example via the activation of the cGAS/Sting pathway [54, 55].

1.1.3 The intrinsic apoptosis pathway

When a cell fails to overcome stresses like nutrient-deprivation, DNA damage, toxins or oxidative stress, it undergoes suicide by triggering the intrinsic apoptosis pathway [30] (Figure 6). As a consequence, the balance of the pro- and anti-apoptotic players in the family of B-cell lymphoma 2 (BCL-2) proteins is shifted towards cell death and the pro-apoptotic proteins BCL-2 associated X protein (BAX) and BCL-2 homologous antagonist killer (BAK) become activated and insert into the MOM. The mitochondria round up and fragment, which leads to a collapse of the mitochondrial network. The insertion and oligomerization of BAX/BAK enables the formation of MOM pores which lead to mitochondrial outer membrane permeabilization (MOMP) [56]. Although MOMP leads to cell death in most cases and was seen as the point of no return in intrinsic apoptosis until very recently, it has now been shown that under certain circumstances cells can also survive MOMP, which results in genomic instabilty and predisposition to tumorigenesis [57, 58].

Once MOMP occurs, soluble proteins of the mitochondrial IMS are released into the cytosol. When cytochrome *c*, which is usually a part of the electron transport chain on the mitochondrial inner membrane [59, 60, 61], reaches the cytosol, it binds to Apoptotic Protease-activating Factor 1 (APAF-1) [62]. APAF-1 thereby becomes activated and binds caspase-9 [63], which is the initiator caspase of the intrinsic apoptosis pathway [64, 65]. As long as there are no apoptotic signals, caspases are inhibited in the cytosol by the inhibitor-of-apoptosis (IAP) family of proteins [66, 67]. Caspase-9 is specifically inhibited by XIAP (X-linked IAP), which prevents homo-oligomerization by keeping the caspase sequestered as a monomer and thereby preventing caspase-9 activation [68]. Smac/DIABLO (second mitochondrial activator of caspases/direct IAP binding protein with low pI) [69, 70], which is also released from the IMS during MOMP, competes with caspase-9 for binding to XIAP and thereby frees the caspase from its inhibitor [71].

The resulting complex of cytochrome *c*, APAF-1 and caspase-9 is called the apoptosome [72, 73]. Caspase-9 becomes activated by binding to Apaf-1 in the apoptosome [74], and in turn activates the executioner caspases (caspase-3 and caspase-7), which triggers the caspase cascade [75]. The executioner caspases then cleave their downstream protein targets and lead to the typical apoptotic phenotype, i. e. nuclear condensation and DNA fragmentation, PS flipping, apoptotic body formation, phagocytosis. As there are no phagocytes to clear the dead cells in a cell culture setting, the rounded-up dead cells simply detach from the substrate and float away.

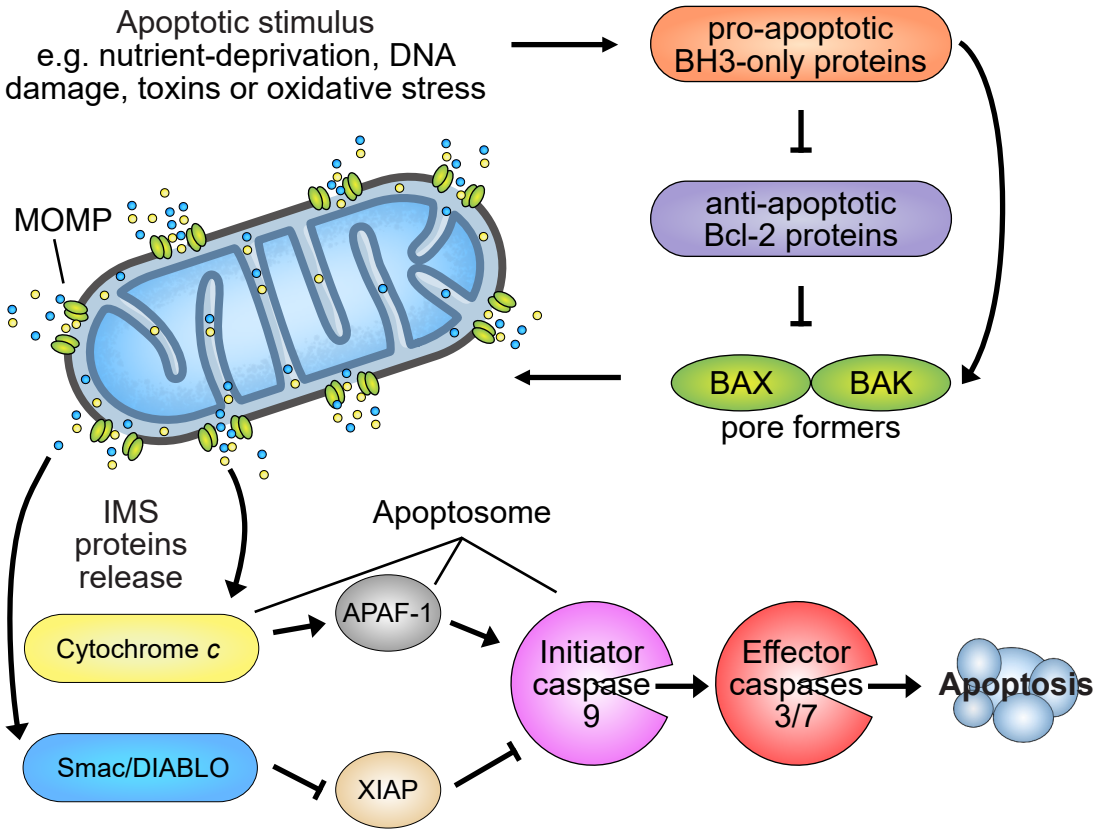

Figure 6: The intrinisic (mitochondrial) apoptosis pathway. Upon an apoptotic stimulus, a sequence of events is triggered which leads to the pore forming proteins BAX and BAK to become active and open a pore in the MOM in a process called mitochondrial outer membrane permeabilization (MOMP). Two proteins are released from the IMS into the cytosol through the newly formed apoptotic pore: cytochrome *c* and Smac/DIABLO. Cytochrome *c* activates APAF-1 and Smac/DIABLO releases Caspase-9 from its inhibitor XIAP. Cytochrome *c*, APAF-1 and caspase-9 then form a complex called the apoptosome. Caspase-9, which is the initiator caspase of the intrinsic apoptosis pathway gets activated in the apoptosome and in turn activated caspases-3 and 7, which execute downstream apoptosis.

To trigger the intrinsic apoptosis pathway, I treated the cells with Actinomycin D (ActD), a drug which binds to DNA and inhibits the synthesis of RNA [76]. In some cases, I added the BH3-mimetic ABT-737, which lead to a more uniform induction of apoptosis over the whole cell population.

Interestingly, even without caspases, cells die after MOMP. This so called caspase-independent cell death (CICD) [77] occurs when caspases are blocked by non-toxic, broad-spectrum caspase inhibitors (eg. Q-VD-OPh (Quinolyl-valyl-O-methylaspartyl-[2,6-difluorophenoxy]-methylketone) [78] or Z-VAD-FMK (N-Benzyloxycarbonyl-Val-Ala-Asp(O-Me)fluoromethylketone) [79, 80]). How exactly the cell dies during CICD is not fully understood but the most probable explanation is that the ATP production, lipid biogenesis, and other important functions of mitochondria can no longer occur efficiently after MOMP, which leads to the demise of the cell [81]. Because upstream apoptosis events like BAX and BAK activation as well as MOMP are thus decoupled

from downstream processes like caspase activation, I made use of CICD in my cell culture model by adding the caspase inhibitor Q-VD-OPh to the cells, which is a common practice when studying apoptotic cells with microscopy, as it prevents the cells from detaching from their substrate.

1.1.4 The BCL-2 protein family

The B-cell lymphoma 2 (BCL-2) proteins are the key players that initiate, regulate and execute the intrinsic apoptosis pathway upstream of mitochondrial outer membrane permeabilization (MOMP). The BCL-2 family of proteins is named after the first family member B-cell lymphoma 2 (BCL-2), which was discovered in 1984 [82]. BCL-2 was over-expressed in B-cells from a patient with acute lymphoblastic leukemia and it was later discovered that it acts as inhibitor of apoptosis [83]. Many more members of the BCL-2 family were since found [84] and are still being discovered [85]. The BCL-2 proteins interact and regulate each other tightly by binding to one another, which either leads to inhibition or activation.

All members of the of BCL-2 protein family share a common feature: they contain one or more of the four BH (BCL-2-homology) domains. The BH domains have conserved structural and functional analogies across the members of the BCL-2 family in mammals as well as other model organisms [86, 87, 88]. The BH3 domain is the main interaction surface between the proteins. The BH domains sometimes share little amino acid sequence similarity and it is therefore debated whether they should actually be called domains, or rather sequence motifs [89, 90].

To date, there are three different sub-families of BCL-2 proteins (Figure 7): the anti-apoptotic BCL-2 proteins, which have all 4 BH domains and prevent apoptosis (BCL-2, BCL-XL, BCL-W, MCL-1, A1); the pro-apoptotic BH3-only proteins, which only contain the BH3 domain and are direct and indirect activators of apoptosis (BID, BIM, PUMA, BIK, BMF, HRK, NOXA, BAD, etc.); and the pro-apoptotic effector proteins, which contain the BH1, BH2 and BH3 domains and facilitate apoptosis by causing MOMP (BAX, BAK and BOK).

In a healthy cell, the BCL-2 family members interact in a tightly controlled balance [92, 93]: the anti-apoptotic BCL-2 family members bind to the pro-apoptotic, pore-forming effector proteins, thereby preventing their activation (Figure 8). The first of these heterodimerization interactions was found between BCL-2 and BAX [94]. All anti-apoptotic proteins can inhibit all pro-apoptic effector proteins, but BCL-2 has the highest affinity for BAX, while MCL-1 preferably inhibits BAK and BCL-XL inhibits both BAX and BAK [95, 96].

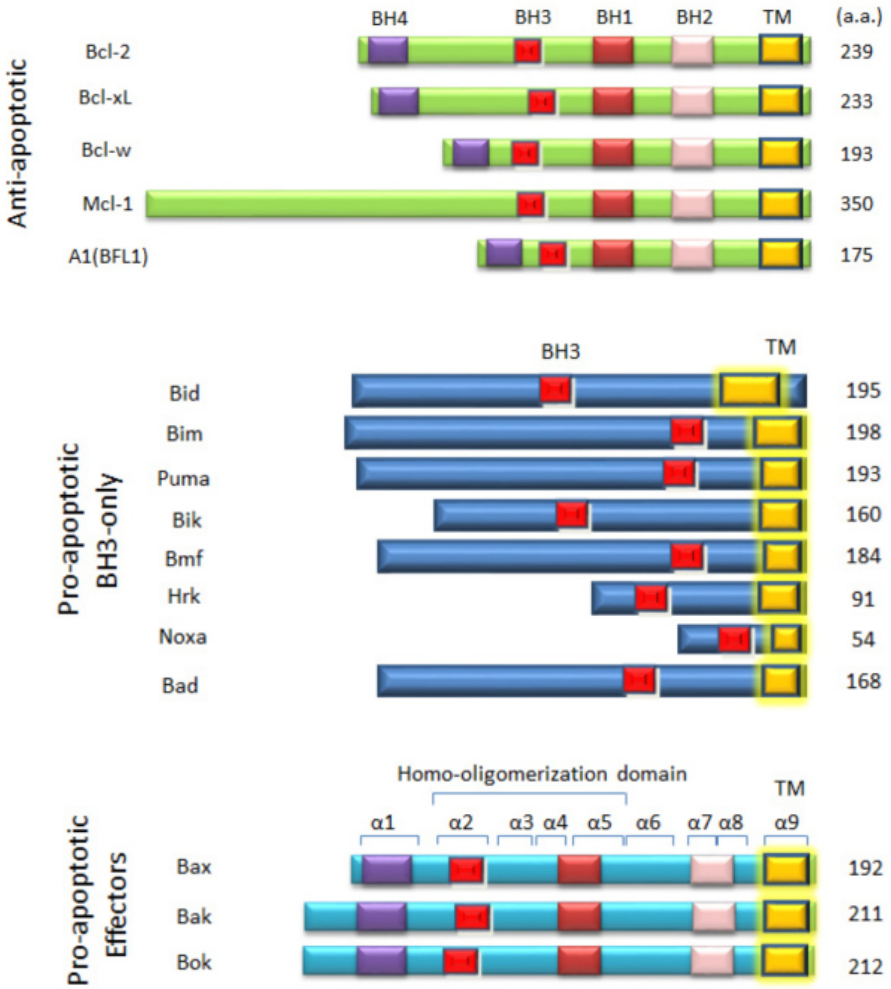

Figure 7: BCL-2 family of proteins. The BCL-2 family of proteins consists of three subfamilies: the anti-apoptotic BCL-2 proteins, which have all 4 BH domains and prevent apoptosis; the pro-apoptotic BH3-only proteins, which only contain the BH3 domain and are direct and indirect activators of apoptosis; the pro-apoptotic effector proteins, which contain the BH1, BH2 and BH3 domains and facilitate apoptosis by causing MOMP. (*Adapted from* [91].)

Once an apoptotic stimulus occurs, transcription and activation of the pro-apoptotic BH3-only proteins shifts the delicate balance of the BCL-2 proteins towards apoptosis. Some BH3-only proteins act as sensitizers by inhibiting anti-apoptotic proteins and thereby releasing the effectors from the sequestration. Other BH3-only proteins function as activators by directly activating the effector proteins [97]. Accordingly, the over-expression of anti-apoptotic BCL-2 proteins can prevent apoptosis [98], like in the cancer patient, where BCL-2 was first discovered [82]. Similarly, the over-expression of pro-apoptotic BH3-only proteins leads to the induction of apoptosis [99, 100]. Likewise, the treatment with BH3-mimetics, which mimic pro-apoptotic BH3-only proteins, leads to apoptosis. A prominent example for a BH3-mimetic is ABT-737, which disrupts the binding of the pro-apoptotic BCL-2 effector proteins to their anti-apoptotic BCL-2 inhibitors [101, 102, 103]. Thereby the sequestration of

the effectors BAX or BAK is neutralized and they are released to execute their effector function of forming the apoptotic pore. When all pro- and anti-apoptotic BCL-2 proteins are knocked out, the re-expression of BAX or BAK alone is sufficient for the cells to undergo apoptosis [104].

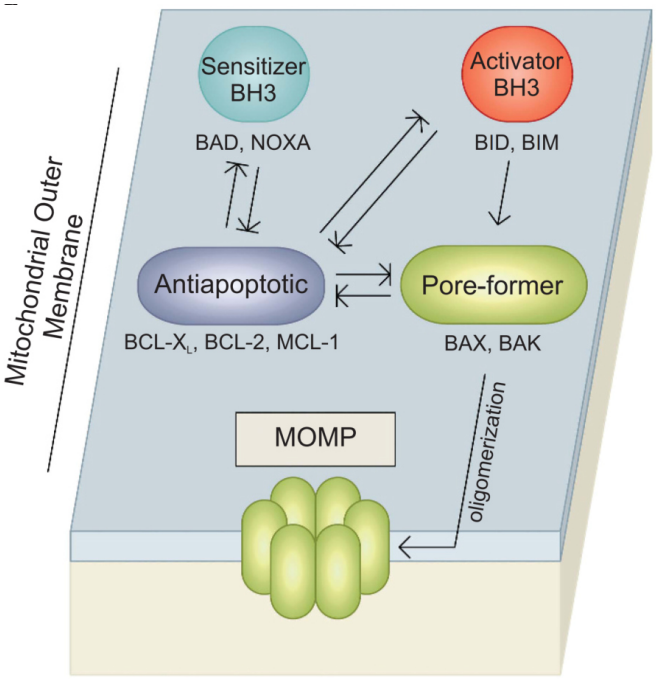

Figure 8: BCL-2 family interactions. The anti-apoptotic proteins (dark blue) inhibit both the BH3-only proteins (cyan and orange) and the pore-forming effector proteins (green). Upon an apoptotic stimulus the BH3-only proteins inhibit the anti-apoptotic proteins and activate the pore-forming effector proteins to induce apoptosis via MOMP (*Adapted from* [92].)

1.1.5 BAX and BAK

BAX and BAK are the pro-apoptotic effector proteins of the BCL-2 family, which induce MOMP when the intrinsic (mitochondrial) pathway of apoptosis has been activated. Both proteins have been discovered almost 30 years ago [94, 105, 106, 107] and are widely expressed in tissues [108, 109, 110, 111]. They were shown to be the synergistic effectors of apotosis by studies in knockout (KO) animals [112]. Only when BAX and BAK are knocked out together, developmental apoptosis is impaired. The double-KO (DKO) animals show severe defects in many organs due to failed apoptosis (e.g. vaginal openings not developed). The cells from DKO animals do not undergo MOMP or engage the mitochondrial pathway of apoptosis. Even more evidence for BAX and BAK being the pro-apoptotic effectors of apoptosis comes from cell culture studies where only BAX-BAK DKO cells resisted apoptotic stimuli. In contrast, BAX or BAK single-KO cells mostly underwent apoptosis normally [113, 114, 115, 116]. Accordingly, many cancers have lost or acquired a loss-of-function muta-

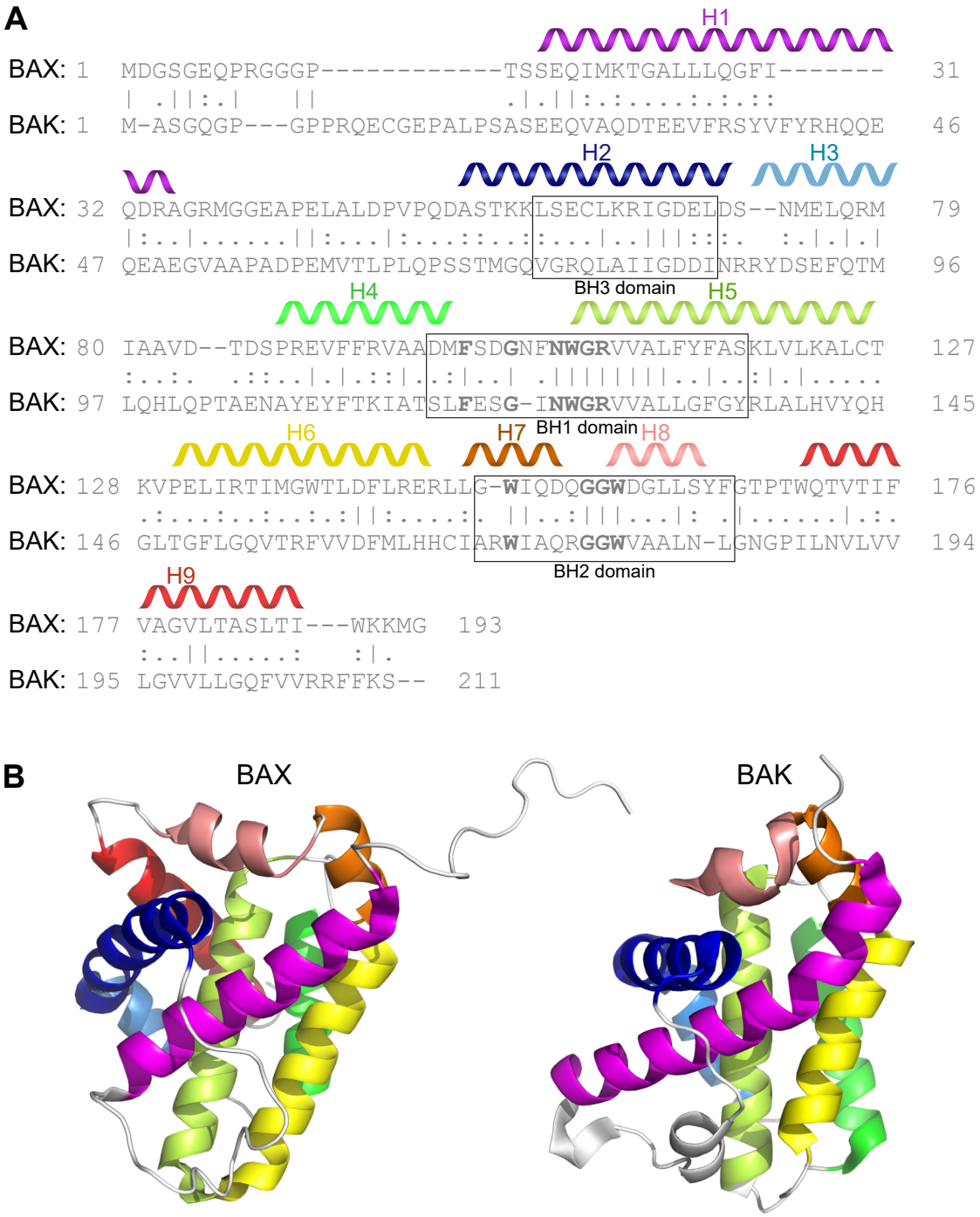

Figure 9: BAX vs BAK protein sequence and structure. **(A)** Sequence alignment of BAX and BAK. BH domains are highlighted in square boxes and helices by a helix symbol spanning the according amino acids on top (H1-H9). "|" denotes sequence identity; ":" denotes conservative substitution; "." denotes semi-conservative substitution. (Sequence alignment was generated with the EMBOSS pairwise sequence alignment tool from EMBL-EBI [123, 124]). **(B)** BAX vs. BAK protein structure. Left: BAX PDB 1F16 [121], right BAK PDB 2IMS [122]. The BAK structure does not contain the C-terminal H9 which harbors the TM domain, because it is constantly inserted in the MOM. (*Image courtesy of Daniel Stumpf.*)

tion in BAX [117] or BAK [118] or produce alternative splicing variants [119].

Although the pro-apoptotic effector proteins BAX and BAK share little sequence similarity [120] (Figure 9A), they are structurally almost identical [121, 122] (Figure 9B). They are both small proteins with 21 kDa for BAX and and 25 kDa for BAK. Both proteins contain nine alpha helices (H1-H9) of which the C-terminal H9 is the hydrophilic transmembrane (TM) domain, which is used for insertion into the MOM. BAX and BAK are continuously shuttling back and forth from the MOM to the cytosol in a process called retrotranslocation [125]. Because of their differential retrotranslocation [126] rate, BAX is predominantly localized in the cytosol with its TM domain buried inside the globular fold, whereas BAK is constitutively localized on the MOM (Figure 10, upper panel). Therefore, BAK has its TM domain constantly exposed even in a non-active state, whereas the TM domain of BAX only gets exposed when activated.

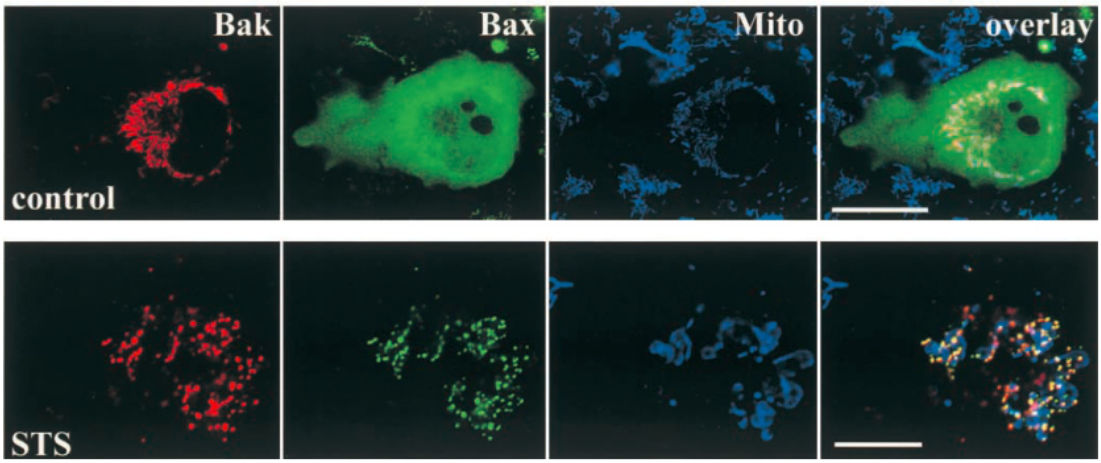

Figure 10: BAX vs. BAK localization in the cell. Under physiological conditions (control), BAX resides predominantly in the cytosol, whereas BAK is constitutively located at the mitochondria. Under apoptotic conditions (staurosporin - STS), BAX translocates to the mitochondria and both BAX and BAK coalesce into clusters at the MOM. Scale bar = 25 μm. (*Adapted from* [127].)

When a cell is in its healthy, non-apoptotic state, BAX and BAK are sequestered by anti-apoptotic BCL-2 proteins. These proteins bind the BH3 domain of BAX or BAK within their BH groove comprised of BH1, BH2 and BH3 domains. Once an apoptotic stimulus arrives, BH3-only proteins bind anti-apoptotic BCL-2 proteins and therbey release sequestered BAX or BAK. BH3-only proteins also directly activate BAX or BAK by binding to their BH groove. Upon activation, BAX and BAK undergo dramatic conformational rearrangements (Figure 11). BAX translocates to the MOM and inserts its TM domain (Figure 10, lower panel). Both BAX and BAK then expose their N-terminus (H1), which makes the "latch" region of the protein (H6 – H8) dissociate from the "core" region (H2 – H5). The conformational rearrangement exposes

the BH3 domain (in H2) of BAX and BAK. The exposed BH3 domains of the effectors can then be inserted into another BAX or BAK protein's groove. This way, the proteins form predominantly homo-dimers [128, 129, 130, 131, 132, 133] although it was suggested that they are also able to hetero-dimerize into BAX-BAK-dimers [134, 135]. The need for dimerization is further supported by an inhibitory peptide of BAK, which prevents dimerization and thereby BAK-dependent cytochrome *c* release [136]. Subsequently, more BAX and BAK molecules become activated, which leads to the oligomerization into larger order complexes on the MOM [93]. The binding interface between two dimer units is thus far elusive and it was postulated that the lipids of the MOM themselves might play a role in oligomerizing the dimers [137].

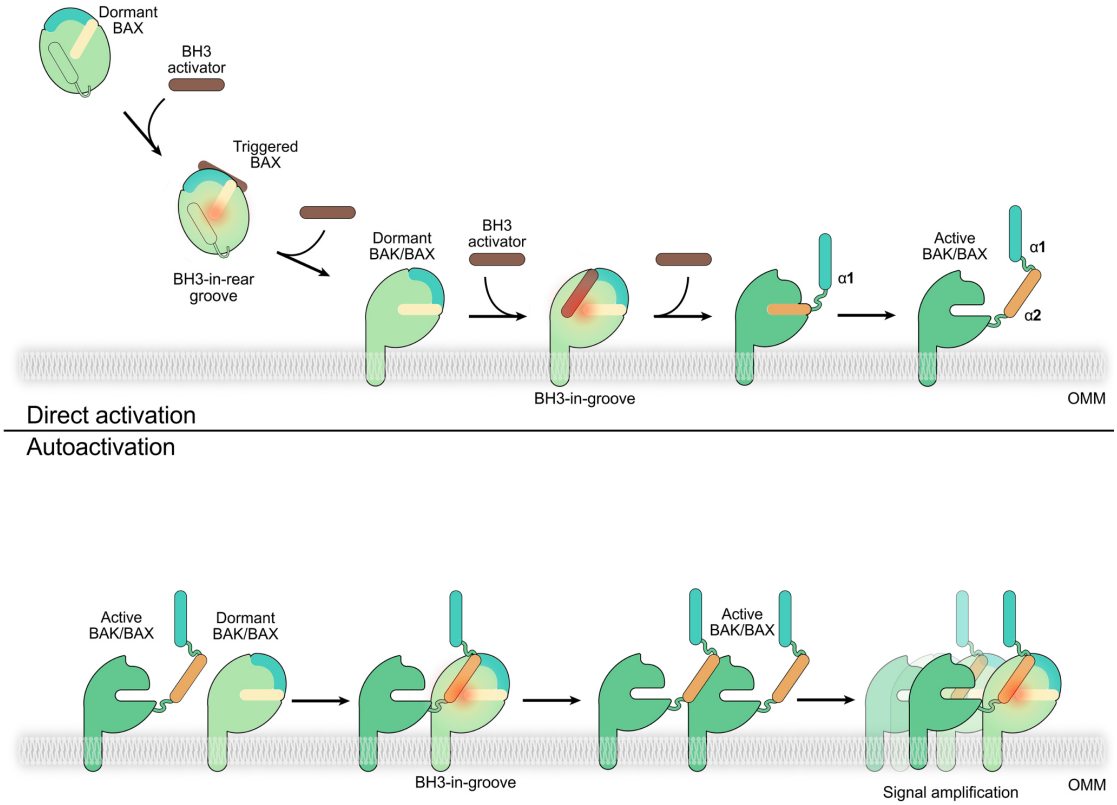

Figure 11: BAX and BAK direct and auto-activation. BH3-only proteins activate BAX and it inserts its TM domain into the MOM. BAK already resides on the MOM (here: OMM), but becomes activated by BH3-only proteins (*direct activation*). Both activated BAX and BAK then expose their N-terminus (H1, cyan) and dissociate the "latch" region of the protein (H6 – H8) from the "core" region (H2 – H5) to expose their own BH3 domain (in H2, orange). BAX and BAK then form predominantly homo-dimers and the exposed BH3 domain can subsequently activate further BAX and BAK molecules (*auto-activation*), which aggregate into higher-order oligomers at the MOM. (*Adapted from* [93].)

Note that BOK (BCL-2 related ovarian killer) has high structural similarities with BAX and BAK and is recognized as the third pore-former among the effector BCL-2 proteins [138, 139]. However, it is regulated by proteasomal degradation and not directly

involved in the canonical mitochondrial pathway of apoptosis [140]. BOK-KO mice show minimally aberrant phenotypes and are fertile [141]. Only in BAX-BAK-BOK triple-KO mice, the effect of BAX-BAK-DKO was slightly aggravated by the additional KO of BOK [142]. Because of these fundamental differences to BAX and BAK, BOK will not be a focus in this study.

1.1.6 The apoptotic pore

The formation of the apoptotic pore can be recorded using light microscopy, for example, by visualizing the release of IMS proteins [143, 144]. Furthermore activated BAX and BAK can be visualized, which reveal that they are coalescing into distinct clusters of various sizes on the MOM [127, 145, 146] (Figure 10, lower panel). However, the resolution of conventional light microscopy can only resolve clusters of BAX or BAK, which were estimated to contain hundreds [146] to thousands [127] of molecules per cluster. The underlying structural arrangement of the individual molecules in the apoptotic pore during MOMP is highly debated.

In general, proteins can form openings in membranes either by inserting into the membrane and entirely covering the lipid tails, which is called a proteinaceous pore (Figure 12A, left). Or they can from a toroidal pore, in which the lipids are bent around the pore edge so that the lipid head groups of both leaflets connect and form a barrier to prevent the lipid tails from being exposed to the aqueous environment [147] (Figure 12A, right).

BAX and BAK have been shown to homo-dimerize upon activation before they furher oligomerize [128, 121, 148, 131, 149, 133]. How the pore formation then actually happens and how the molecules arrange in the pore exactly is still not clear. Currently, there are three models of how the apoptotic pore could structurally look like: the hairpin model [150], the in-plane model [151] and the clamp model [130] (Figure 12B). The hairpin model proposes an exclusively proteinaceous pore, while the latter two models assume toroidal pores.

Although more and more evidence points towards a toroidal pore [152] (Figure 13A), a recent study using only the core alpha helices 2-5 of BAX found an conformation where the protein dimers insert into the membrane similar to the clamp model but cover the lipid tails, which supports the model of a proteinaceous pore [153] (compare Figure 12). Six of these core dimer units are needed in order to form a pore large enough to release one molecule of cytochrome *c* (Figure 13B). Many other structural studies of BAX as well as of BAK have been published, but none has defined the pore conclusively [129, 154, 155, 156, 157, 158, 159].

However, all studies investigating the apoptotic pore on a molecular level led to valuable insight into the understanding of the structural composition of the pore and

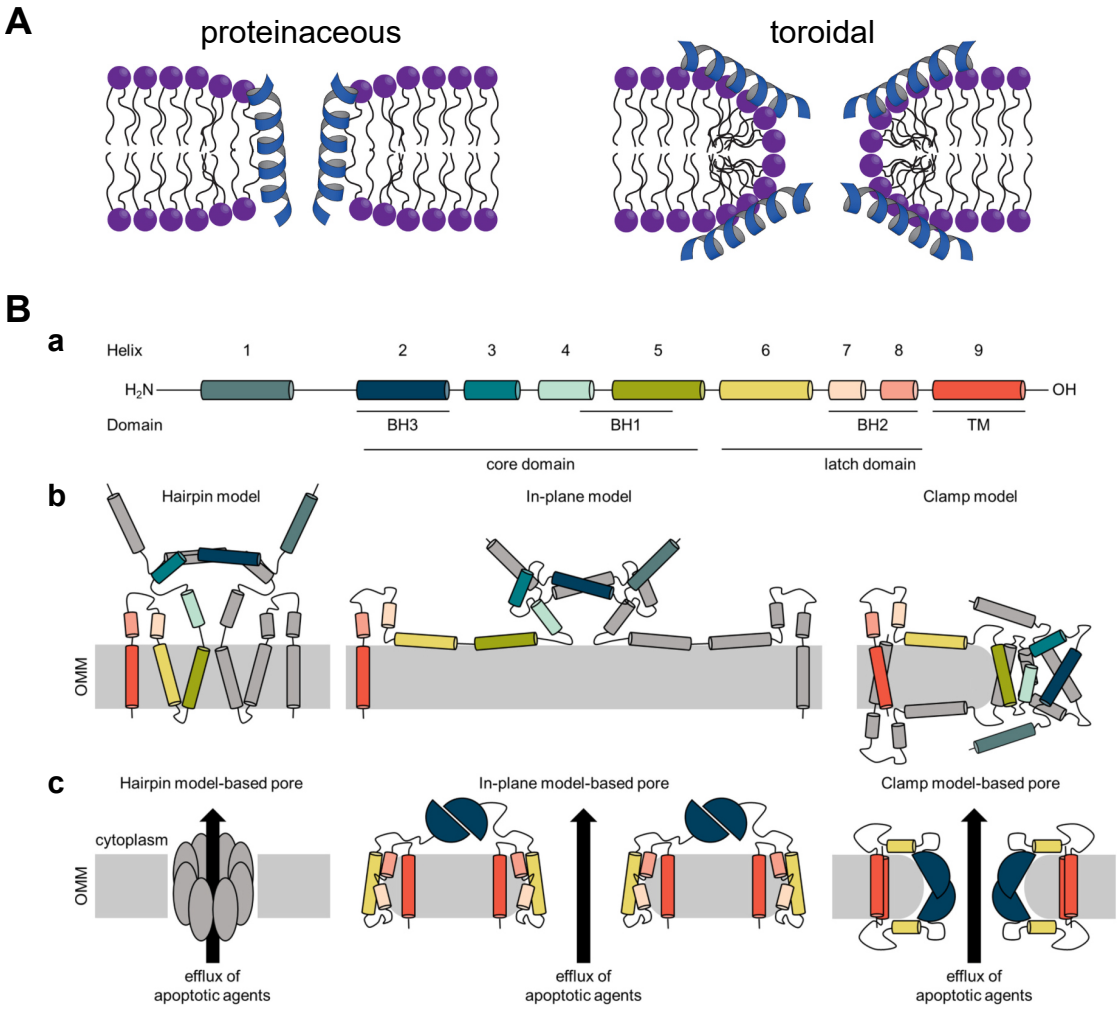

Figure 12: Apoptotic pore models of BAX and BAK. (A) *Left*: A proteinaceous pore, where the proteins cover the lipid tails and thereby prevent them from contact with the aqueous environment. *Right*: A toroidal pore, where the lipids are bent and the lipid heads cover the pore edge, which thereby prevent the lipid tails from coming into contact with the aqueous environment. (*Adapted from* [147].) **(B)** Graphical representations of the different pore-formation models of BAX and BAK. **(a)** BAX and BAK primary structure with the nine alpha helices highlighted as colored barrels. **(b)** Dimer formation in the different models. *Left*: Hairpin model, *middle*: In-plane model, *right*: clamp model. **(c)** Pore formation in the different models. *Left*: Hairpin model forming a proteinaceous pore, *middle*: In-plane model and *right*: clamp model, both forming a toroidal pore. (*Reproduced from* [160].)

the exact configuration of the individual proteins. This is especially important for designing better drugs to interfere with apoptosis [161], as deregulated apoptosis plays a major role in many diseases from cancer to neurodegeneration [161]. Structural studies have generally been performed *in vitro* with reconstituted proteins and in synthetic membranes and are thus limited to either BAX or BAK and not a combination of both. The cellular environment is highly complex and many proteins (on the MOM or in the cytosol) as well as lipids might be involved in the formation and regulation of the apoptotic pore. The lack of one of the two key proteins, an unphys-

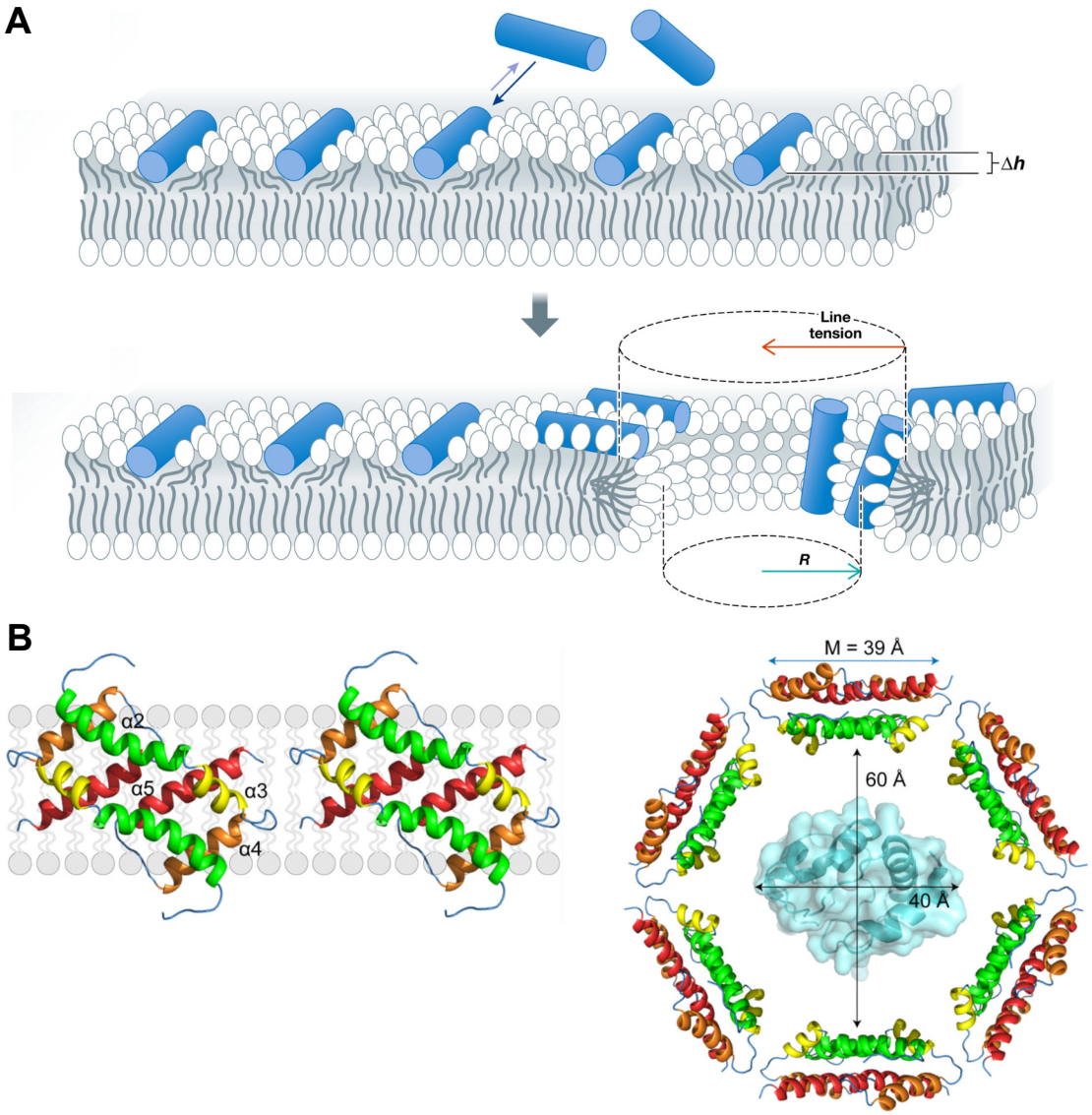

Figure 13: Models of the apoptotic BAX pore. **(A)** Model of a toroidal pore, where protein units insert into the membrane until enough tension is built so that the MOM ruptures and a pore opens up.(*Adapted from* [152].) **(B)** One model of the minimal apoptotic BAX pore. *Left*: Two core dimers of BAX comprising only H2-H5 are shown lining the wall of the apoptotic pore. In this model, they form a proteinaceous pore, shielding the lipids from the aqueous environment. *Right*: Six dimers are needed to form a pore, the size of which allows for cytochrome *c* molecule to be released. (*Adapted from* [153]).

iological lipid composition of the membrane or the absence of the cellular protein folding and degradation machinery might have significant influence on if and how the pore forms. Furthermore, the BCL-2 protein family exists in a delicate balance, which cannot be accounted for in *in vitro* studies. Therefore, it is crucial to study the apoptotic pore in the cellular context.

1.1.7 Super-resolution microscopy of the apoptotic pore

Only large clusters can be discerned, when investigating BAX or BAK in apoptotic cells with conventional microscopy [127, 146] (Figure 10). However, the invention of super-resolution microscopy allowed to image beyond the diffraction limit and revealed that many of the BAX clusters actually are ring-like structures on mitochondria [162, 163, 164] (Figure 14). BAX pores were already discovered with EM in *in vitro* systems of vesicles with mitochondria-like properties [165] as well as in cells, where BAX clusters located in vicinity to ruptures of the MOM [166]. The images of BAX rings, arcs and lines suggests a model for the pore, where the protein does not need to cover the whole pore edge in order for the cavity to form, which would support the toroidal pore even more [163, 164].

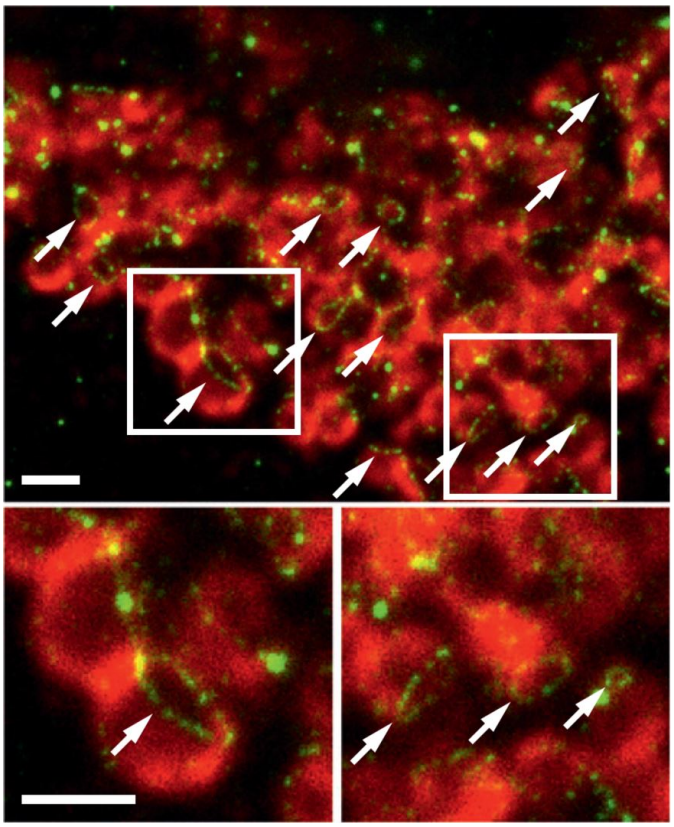

Figure 14: BAX rings in apoptotic cells in STED imaging modality. Images U-2 OS WT cells treated with of ActD. The cells were labeled with anti-BAX antibody (green) and anti-TOM20 antibody (red). BAX rings (arrows) form a pore in the MOM, visible by the absence of TOM staining within the ring. Scale bars: 1 µm. (*Adapted from* [162].)

Similarly, BAK was shown to form rings and arcs as well [167]. When simultaneously over-expressing BAX and BAK and imaging them with live cell STED microscopy, they were shown to localize in the rings together [167] (Figure 15). Furthermore, BAX and BAK were shown to influence each other regarding pore size and pore growth kinetics. Still, it remains elusive, exactly how the two players interact in the apoptotic pore

and whether they are completely functionally redundant [168, 169, 170]. Because of the small size of the apoptotic pore, the visualization requires super-resolution microscopy in order to achieve a better understanding of BAX and BAK *in situ*.

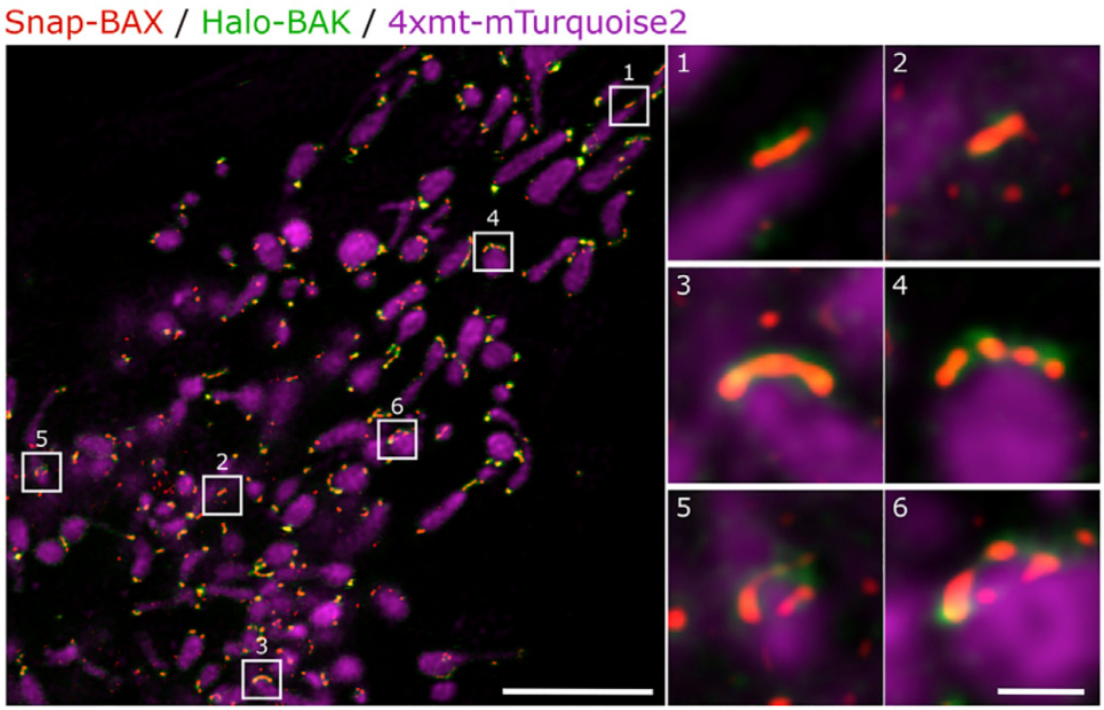

Figure 15: BAX and BAK rings (and other structures) in apoptotic cells in STED imaging modality. *Left:* Image of live U-2 OS cells over-expressing SNAP-BAX (red) and Halo-BAK (green) as well as a mitochondrial marker (magenta). The cells were labeled with SNAP-Cell SiR Janelia Fluor-549 HaloTag Ligand. Right: Enlarged regions with BAX and BAK features of interest. Rings can be discerned in boxed regions 5 and 6. Scale bars: 5 µm and 500 nm. (*Adapted from* [167].)

1.2 Light microscopy in cell biology

1.2.1 History of microscopy and the diffraction limit

In the 17th century, long before the age of super-resolution microscopy, the investigation of our surroundings by magnification through lenses was pioneered and has since been tremendously important for biological investigations. *Robert Hooke* used the simplest form of a light microscope to describe objects, plants and insects. He eventually originated the term "cell" in his famous publication "Micrographia" in 1665 [171] (Figure 16). *Van Leeuwenhoek* refined the carving of lenses significantly and could improve the magnification to up to 200 times. He discovered living bacteria and many other things which are considered the basics of biology today [172]. Light microscopes have since been refined and are essential tools for biology up to date.

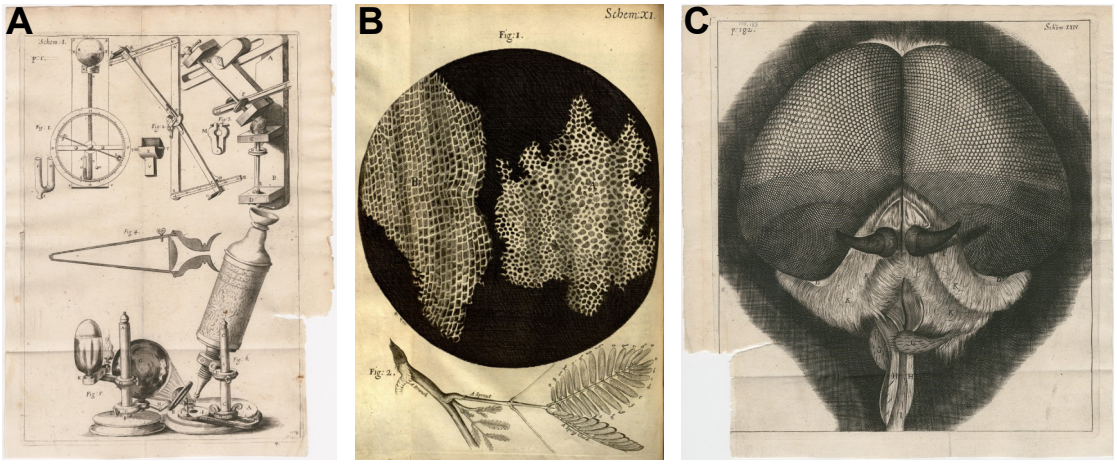

Figure 16: Robert Hooke's "micrographia" from 1665. **(A)** Hooke's instruments. The microscope is at the bottom. **(B)** The structure of cork, which lead to the term "cell". **(C)** The compound eye of a grey drone fly. (*Adapted from* [171].)

To obtain resolutions in the nanometer range, the electron microscope (EM) was invented in 1932 [173] and was immediately employed for investigations on biological specimen. In the 1950s, *George Pallade* was one of the pioneers to describe organelles within cells with EM, including mitochondria [34]. EM is still heavily used in biological research today, but despite the superior resolution of this method, there are two significant drawbacks: it is difficult and laborious to label specific proteins of interest and the sample must be fixed before imaging, preventing the observation of live cell dynamics.

Both of these problems were circumvented by the use of fluorescent proteins, the use of which started with the discovery of the green-fluorescent protein (GFP) isolated from *Aequorea victoria* in 1962 [174]. Ever since this finding, more fluorescent proteins were identified and developed. For example, mEGFP (monomeric enhanced

GFP) was derived from the original GFP, which has better photo-properties and is strictly monomeric. This led fluorescence microscopy to being one of the most important tools for cell biology today. Fluorescently labeled structures can be excited with light of one specific wavelength (excitation light) and emit light of a different wavelength (emission light). Combined with spectral filters and different excitation wavelengths, this enables multi-color imaging and the tagging of specific proteins in the cell with fluorescent proteins to investigate their sub-cellular location and live dynamics. Furthermore, antibodies can be coupled to fluorescent molecules allowing immunofluorescence (IF) staining to specifically label endogenous proteins.

Until the invention of the confocal microscope in 1955 [175], out-of-focus light was a major drawback of fluorescent microscopes, as it caused blurred images, especially in thicker specimens. To block this out-of-focus light and thereby increase the signal-to-noise ratio, a plate with a small hole (the pinhole) is installed into the beam path. The area of interest in the sample is not imaged as one frame by a camera, as is the case in widefield microscopy, but the image is assembled by scanning the area of interest and recording the signal position after position (pixel-by-pixel) by sensitive photo-detectors. Due to the barrier introduced by the pinhole, only the emission light from the focal plane is allowed to reach the detector at every recorded pixel. The focal plane in the sample is where the excitation light is focused by the objective lense. Thus, by using a pinhole and blocking the out-of-focus light, an optical sectioning effect is achieved (Figure 17A and B), which leads to crisper, less blurred images (Figure 17C).
Even with the best confocal light microscope however, there is still a resolution limit. This resolution barrier, which is a consequence of the wave-like nature of light, is called the diffraction limit. *Ernst Abbe* already postulated the diffraction limit for optical instruments in 1873 [178]:

$$d = \frac{\lambda}{2\mathrm{NA}} = \frac{\lambda}{2n * sin\alpha}$$

This equation states that in order to be resolved, the distance (d) between two objects must be equal to (or greater than) the wavelength of the used light (λ) divided by two times the numerical aperture (NA) of the objective lens. The NA, an inherent characteristic of any optical system (lens), is defined by the refractive index (n) of the immersion medium and the sine of the half angle of the cone of light that can enter or exit the lens ($sin\alpha$).

This means that, in theory, even if blue light (400 nm) and a very high NA of 1.4 was used, a resolution of no smaller than 150 nm could be achieved, implicating that the objects need to be at least 150 nm apart in order to be resolved and not to ap-

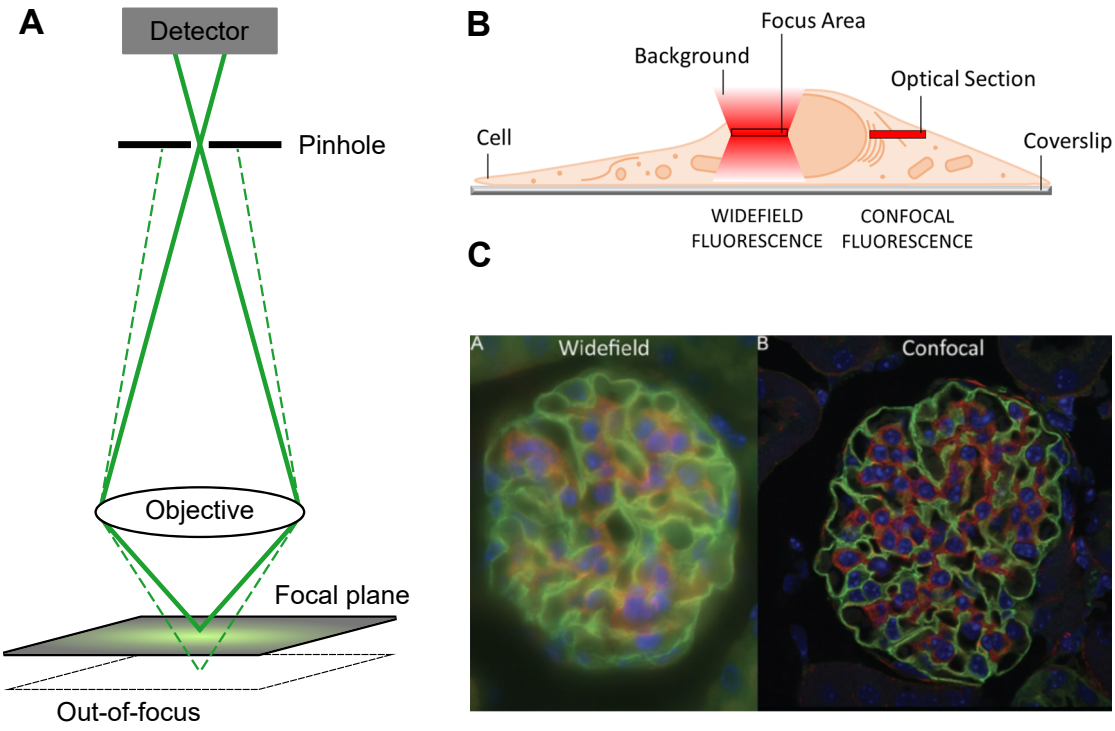

Figure 17: Confocal microscopy. **(A)** Emission beam path of a confocal microscope. After excitation (not shown), fluorescence is emitted from the focal plane in the sample as well as from regions that are out of focus. Only the light emitted from the focal plane can reach the detector (continuous green lines), while the out-of-focus-light is rejected by the pinhole (dashed green lines). **(B)** Visualization of the whole recorded signal in widefield (left) and the optical sectioning effect in confocal (right) microscopy. (*Adapted from* [176]). **(C)** Images of mouse kidney imaged with widefield (left) and confocal (right) microscopy. There is a significant reduction of out-of-focus light, identifiable by the removal of the blurred signal. (*Adapted from* [177].)

pear blurred together. Due to imperfections in lenses, this theoretical limit is hard to reach. Therefore, and because in practice usually light of 488 nm or above is used, a resolution of about half the wavelength, which is 200-300 nm can be achieved.

Due to this diffraction limit, a point source (e.g. a single fluorescent molecule) that is recorded with an optical system, appears as a blurry spot of 200-300 nm size. The blurry spot is called a point spread function (PSF). In other words, the PSF is the diffraction limited image of a point source. As this diffraction limit is based on fundamental physical laws, it cannot be broken by designing better objective lenses, which is why fluorescence microscopy was limited to structures above 200-300 nm in size for decades.

1.2.2 Super-resolution microscopy

To overcome the diffraction limit and image in the nanometer range, different super-resolution microscopy techniques were developed. All super-resolution light-micros-

copy techniques that fundamentally overcome the diffraction barrier are based on the principle of switching a fluorophore between two discernible states, usually a fluorescent (”on”) and a non-fluorescent (“off”) state. In Stimulated Emission Depletion (STED) microscopy, this happens in a spatially targeted manner, as the space from which fluorescence can be emitted is confined. In single molecule localization microscopy (SMLM) the molecules are all pushed to a dark-state and then stochastically only few of the molecules/fluorophores are excited. By this their original position can be retrieved and an image reconstructed from many frames. In MINFLUX microscopy, both of these approaches are combined to achieve unprecedented resolutions in the single-digit nanometer range.

1.2.2.1 Stimulated Emission Depletion (STED) microscopy

The principle of Stimulated Emission Depletion (STED) microscopy was proposed in 1994 by *Stefan Hell* [179]. The first functional STED setup was built in 2000 [180] and he was awarded with the Nobel Prize in Chemistry in 2014 "for the development of super-resolved fluorescence microscopy" together with *Eric Betzig* and *William E. Moerner*.

The key idea behind STED microscopy is to confine the spot in the sample, from which the molecules of interest emit fluorescence, to a space which is smaller than the diffraction limit. Even though the detection of the spot is subject to diffraction, the location in the sample from which the fluorescence was emitted, is known and thereby, the resolution barrier is overcome.

In a conventional confocal microscope, a multitude of fluorescent proteins or dye molecules (fluorophores) is excited at each pixel and the fluorescence emission is recorded. The fluorophores are excited with light of a certain wavelength (= high energy photons) and thereby transferred from the ground state to an excited electronic state (Figure 18A). Within picoseconds the fluorophores undergo vibrational relaxation to a lower vibrational energy level but still remain in the excited electronic state. From there they relax back to the ground state emitting light of a longer wavelength (= lower energy photons). This is called spontaneous emission and occurs on the order of nanoseconds. The emitted photons have a stochastic wavelength distribution according to the emission spectrum of the respective fluorophore (Figure 19).

In STED, which is a confocal microscopy technique, many fluorophores are excited at the same time at each pixel. However, in order to achieve the space confinement and thereby the super-resolution, molecules that reside outside of the very center of the excitation beam are switched off immediately after they were excited. The molecules are "switched off" by suppressing the emission of fluorescence by applying the concept of stimulated emission (Figure 18B). Stimulated emission is achieved

by introducing photons with a longer wavelength (= lower energy photons) close to the red-shifted end of the emission spectrum of the fluorophore (Figure 19). These red-shifted STED photons interact with the fluorophore while it still resides in the excited state. The lower energy of the STED photons fit the energy gap between the excited and ground state of the fluorophore and force it to the ground state. The interaction needs to occur during the nanosecond window, when the fluorophore resides in the excited state. While the fluorophore is returning to the ground state, it emits a second photon of the exact same wavelength as the STED photon that stimulated that emission. Both of these photons with longer wavelength are not visible for the photon detectors used in the microscope and the fluorophores therefore appear "depleted".

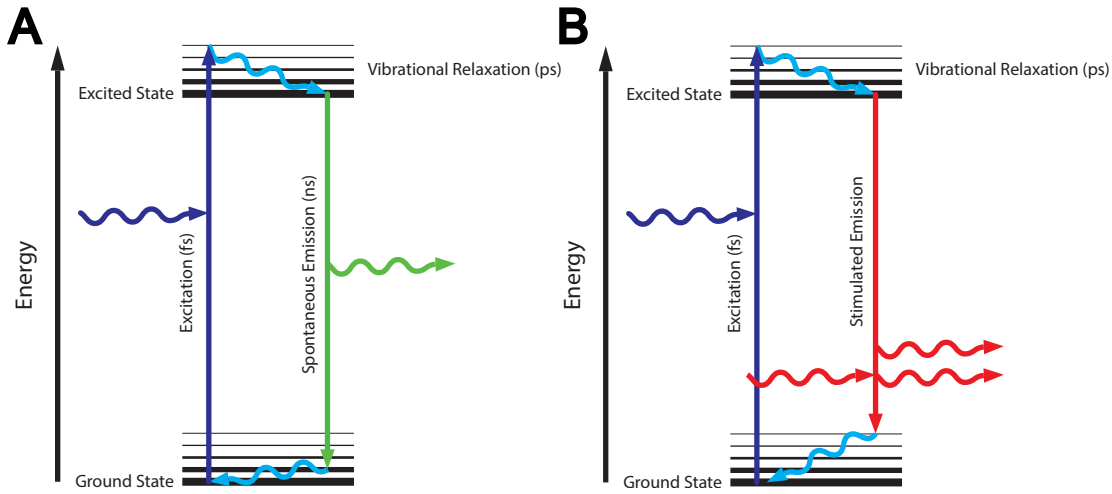

Figure 18: Energy diagram of spontaneous and stimulated emission. **(A)** A fluorophore gets excited by a photon of a certain wavelength and relaxes back to the ground state whereby it emits a photon of a higher wavelength. **(B)** A fluorophore gets excited by a photon of a certain wavelength and before it relaxes back down to the ground state a second photon of much higher wavelength is introduced. This forces the fluorophore back to the ground state whereby it emits two photons of the same wavelength as the one that was introduced. (*Image courtesy of Edward Allgeyer.*)

To practically implement STED, an additional laser is used, which emits the STED photons with a wavelength that corresponds to the red end of the emission spectrum of the fluorophore used (Figure 19). The light of this depletion (STED) laser gets modulated to have the shape of a donut and is centered exactly on the light of the excitation laser. In the middle of the donut, the intensity of the STED beam is very small (ideally zero) and therefore the molecules at this location stay in the excited state and are allowed to emit fluorescence, while molecules in the periphery of the donut get depleted (Figure 20).

To ensure that most of the fluorophores outside of the center of the donut are depleted, a large number of STED photons is required. This is controlled by the inten-

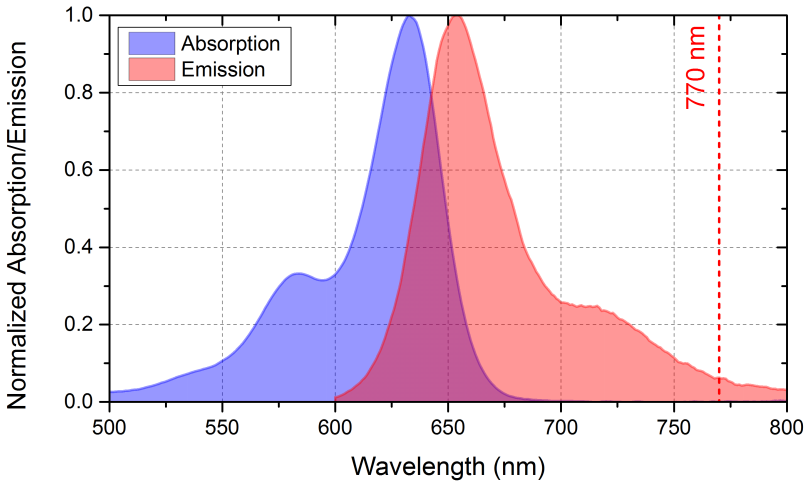

Figure 19: Excitation (absorption) and emission spectrum of a fluorophore. A fluorophore has its excitation (absorption) peak at around 630 nm and its emission peak at around 660 nm. The STED laser (dashed line) is introduced with a wavelength of 770 nm, which is at the far-red shifted end of the emission spectrum of the fluorophore. (*Image courtesy of Edward Allgeyer*).

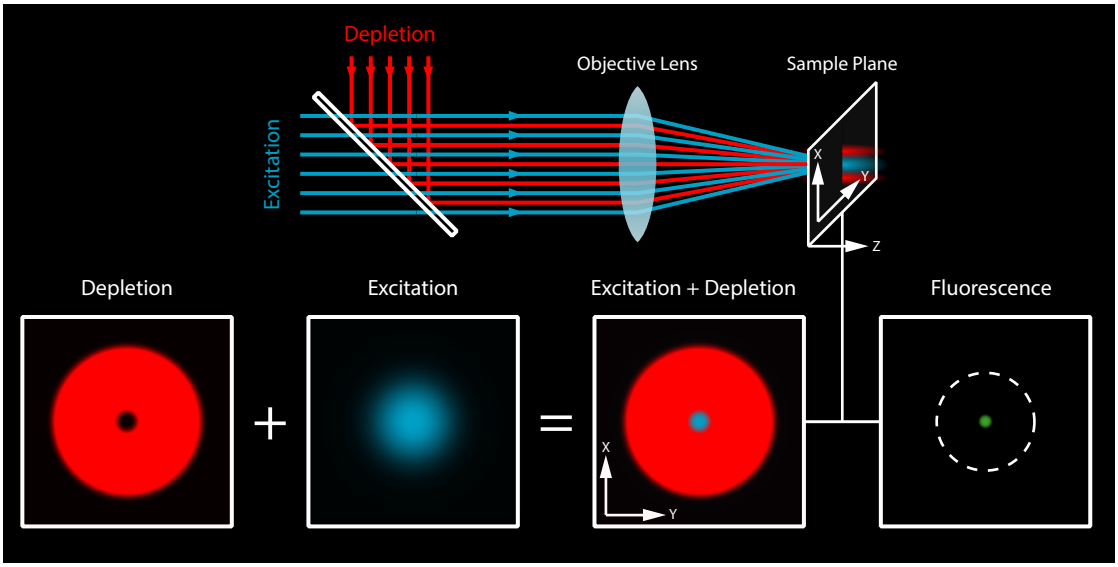

Figure 20: STED microscope setup. An excitation laser (blue) excites the fluorophores in the sample. The fluorophores would then usually relax back to the ground state by emitting light of a longer wavelength (green), a process called fluorescence. In a STED microscope, however, an additional laser with a wavelength at the red end of the emission spectrum is introduced. This depletion laser (red) gets modulated to have the shape of a donut with a zero at the center and is aligned with the excitation laser. Thereby the area which can emit fluorescence is limited to a very small fraction of the initial excitation area and resolution is therefore greatly enhanced. The image is scanned in a raster format pixel by pixel. So for every position that is scanned the collected photons are attributed to the position where they came from. (*Image courtesy of Edward Allgeyer.*)

sity of the STED laser, which influences the achievable resolution and Abbe's equa-

tion has to be modified accordingly ([179]):

$$d = \frac{\lambda}{2n * sin\alpha * \sqrt{1 + I/I_s}}$$

The more the STED laser intensity (I, on the order of MW/cm^2) exceeds the characteristic saturation intensity (I_s) of the imaged fluorophore, the smaller the resulting effective PSF and the better the resolution (therefore the distance (d) between two objects that can be resolved). In other words the resolution is inversely proportional to the STED laser intensity and the more STED power is applied, the higher the resolution will be.

The STED effect is impressively demonstrated revealing the actual size of 100 nm beads (Figure 21A vs. B). Since its invention, STED microscopy has been further developed and employed on innumerable biological questions, ranging from imaging the nuclear pores to the entry of viruses into cells. When used, for example, to investigate live mitochondria, the intricate cristae structure of the MIM is revealed by STED microscopy [35] (Figure 21C).

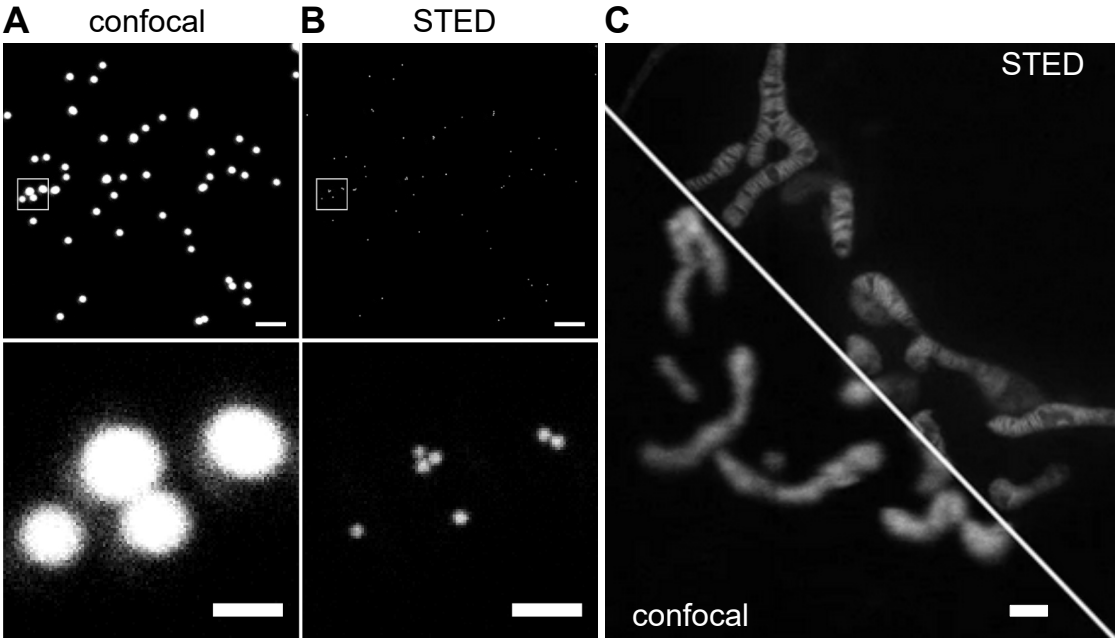

Figure 21: Visualization of resolution enhancement of STED over confocal microscopy. Beads with a size of 100 nm were recorded in **(A)** confocal and **(B)** STED mode. Lower panels show enlargement of the boxes in upper panels. Some of the diffraction limited spots in the confocal mode reveal two or more beads in STED mode. Scale bars: 2 and 0.5 µm. **(C)** STED recording of a living HeLa cell revealing the cristae structure within mitochondria in STED mode (right). Scale bar: 1 µm. (*Adapted from* [35].)

As with all microscopy tools, the number of different labels that can be used is limited and two STED channels and one or two confocal channels are common in most STED setups. The choice of structures to image is therefore a crucial one. By em-

ploying more photostable, cell-permeable dyes, the application of dual-color live cell imaging was achieved [181] and with the continuous development of dyes and applications, the possibilities are growing. In conclusion, although diffraction itself cannot be eliminated, the physical barrier that was set by diffraction has been overcome by STED microscopy with the use of two different states of fluorescent molecules.

1.2.2.2 Single molecule localization microscopy (SMLM)

In single molecule localization microscopy (SMLM), comprising photo-activated localization microscopy (PALM) [182, 183] and stochastic optical reconstruction microscopy (STORM) [184], the "on"-switching happens in a spatially stochastic manner, where only very few of the molecules are in the "on" state simultaneously. As long as one point source emits light (in this case a fluorophore) that is not overlapping with another point source (another fluorophore) and the characteristics of the optical system are known, the center of the point source (actual position of the fluorophore) can be calculated, thereby retrieving its original position. SMLM makes use of this principle by only activating single fluorophores at a time. The whole area of interest is recorded with a camera repeatedly over thousands of frames. In each frame different fluorophores emit fluorescence and by including the information from all frames, the super-resolved image can be reconstructed (Figure 22).

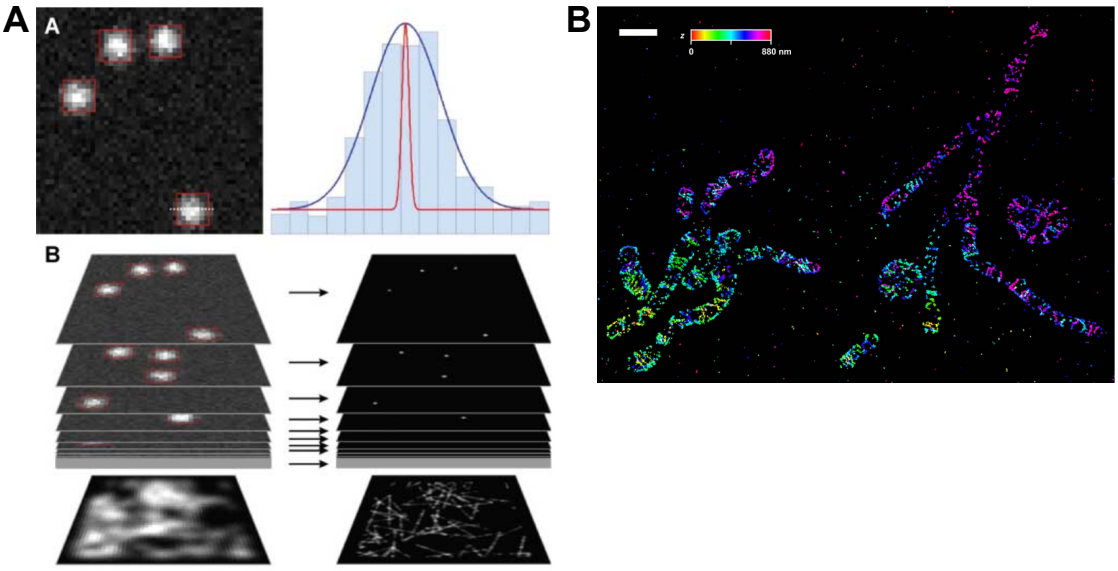

Figure 22: Single-molecule localization microscopy (SMLM) microscopy. **(A)** For PALM or STORM, a series of widefield images of a sample are acquired. The fluorophores are switching on and off in a stochastic manner over time. As only single, isolated fluorophores are recorded, their original position can be calculated. This is done for every fluorophore in every image and in the end, one super-resolved image can be reconstructed from the whole dataset (*Adapted from* [185]). **(B)** A mitochondrial protein is imaged with (4Pi-)STORM microscopy providing unprecedented localization precision and showing the characteristic cristae pattern of the MIM. Scale bar: 1 µm. (*Adapted from* [186].)

1.2.2.3 MINFLUX (MINimal photon FLUXes) microscopy

MINFLUX microscopy combines the spatially stochastic on and off switching and the spatially targeted read-out modalities to achieve resolutions in the single digit nanometer range [187, 188]. This new technique enables molecular resolution with comparatively few photons and is therefore not dependent on bright and photostable dyes. Most molecules get sent into a long-lived dark state before the MINFLUX imaging start. Some molecules are in an activated, but non-fluorescent state in a stochastic manner. An excitation laser then scans over the sample and as soon as one of the active fluorophore gets excited, the laser stays at the position of the fluorophore. The excitation laser is donut-shaped (like the depletion laser in STED microscopy). By positioning the donut-shaped excitation laser at 3 to 6 positions around the assumed first guess of the position of the fluorophore, the exact position of the fluorophore can be retrieved via the different fluorescence intensities at each of the 6 positions. Once the fluorophore has been located, the excitation laser starts scanning again for the next active fluorophore to be excited. The iterative probing process again leads to the retrieval of the exact position and is repeated for many molecules in the area of interest, thereby reconstructing the image. Even better labeling is achieved by using DNA-PAINT probes (DNA points accumulation for imaging in nanoscale topography) [189].

1.3 Aim of the thesis

Aapoptosis, the most common form of cell death, needs to be tightly controlled, because its deregulation leads to disastrous consequences for the organism. During the intrinsic apoptosis pathway, the key effector proteins BAX and BAK are responsible for permeabilizing the MOM, which leads to the release of proteins from the IMS. The IMS proteins in the cytosol activate the caspase cascade which leads to the ultimate demise of the cell.
Although the two pore-forming effector proteins, BAX and BAK, have been extensively investigated by *in vitro* studies, it is still unclear how the two proteins are arranged in the apoptotic pore on the MOM *in situ*. Using diffraction-limited microscopy, numerous studies have revealed the general sub-cellular localization of BAX and BAK, but the resolution of conventional light microscopes is insufficient to analyze the nanoscale distribution of BAX and BAK.

Therefore, the aim of this thesis was to investigate BAX and BAK in the apoptotic pore *in situ*. I asked whether the two proteins exhibited different dynamics and ultrastructures. Furthermore, I investigated the exact arrangement of BAX and BAK in the pore in apoptotic but otherwise unmanipulated cells. Finally, I enquired whether BAX and BAK were able to form apoptotic pores independently of each other.

To this end, first, an assay to perform live cell STED microscopy of BAX or BAK together with a MOM marker had to be established for the recording of temporal dynamics at sub-diffractional resolution. Then, the physiological relevance of the overexpression of the pore forming proteins needed to be tested. To incorporate temporal information while investigating proteins at endogenous expression levels in apoptotic but otherwise undisturbed cells while, a correlative live and fixed cell imaging workflow had to be developed. Furthermore, an approach needed to be set up to perform multi-color STED microscopy on the apoptotic pore of fixed cells in order to investigate super-resolved BAX and BAK simultaneously. The resulting images needed to be analyzed, which made it necessary to program a pipeline to process the imaging data. Finally, to determine whether BAX or BAK were able to form apoptotic pores independently, BAX and BAK KO cell lines had to be engineered with the CRISPR/Cas9 approach.

2 Results

In this work, I employed super resolution microscopy to study the apoptotic pore lined by the two proteins BAX (BCL-2 associated X protein) and BAK (BCL-2 homologous antagonist killer).

First, I studied the temporal dynamics of over-expressed BAX and BAK with live cell Stimulated Emission Depletion (STED) microscopy and discovered that BAX exclusively forms one ring per mitochondrion, while BAK forms smaller rings but can produce more than one ring on a mitochondrion (section 2.1).

As I discovered that the overexpression of pro-apoptotic BCL-2 proteins proved disadvantageous for physiological apoptosis induction (section 2.2), I established an immunofluorescence (IF) staining of BAX in apoptotic cells and employed it to investigate the apoptotic pore on an endogenous protein expression level with different imaging modalities. By using a 3D microscopy approach, I confirmed that most rings are revealed in two-dimensional images and therefore decided to proceed with 2D STED microscopy (section 2.3).

Then, I set up an assay to integrate temporal information into the imaging workflow by correlating live widefield recordings of cytochrome *c* release with fixed cell STED imaging of the endogenous apoptotic pore (section 2.4).

To collect super-resolved information about endogenous BAX and BAK together, I established a BAX-BAK dual-color antibody staining allowing the investigation of the apoptotic pore on physiological protein levels by fixed cell STED microscopy. With this approach, I discovered that endogenous BAX and BAK are present together in the rings, which line the apoptotic pore (section 2.5).

With a custom-written semi-automated image analysis pipeline, I analyzed the BAX-BAK rings for various properties, like size and spatial correlation of the two proteins, which unraveled novel insights regarding the composition of the apoptotic pore. BAX and BAK are positively correlated in the rings, which means that they are co-localizing and the bigger the rings, the more equal the amounts of BAX and BAK become (section 2.6). Finally, I engineered CRISPR/Cas9 knockout (KO) cells and discovered that BAX and BAK were able to form pores independently of each other (section 2.7).

2.1 Live-cell STED imaging of BAX and BAK in apoptosis reveals temporal and spatial dynamics

Apoptosis has been widely studied in a variety of assays over whole cell populations. However, apoptosis is a dynamic process with a heterogeneous onset. The cells' susceptibility to an apoptotic stimulus differs greatly and accordingly, the onset of

apoptosis varies in cultured cells on the order of hours [190]. To fully understand the timeline and individual steps of the process, apoptosis should thus be studied on a single-cell level. This approach is taken in microscopy assays, where individual cells are analyzed [146]. However, the size of the apoptotic pore is lower than the resolution limit of conventional microscopy. Therefore, in order to be able to resolve this structure, super resolution microscopy needs to be employed. So far, only slightly enhanced resolution has been applied in live cells [54] to study the dynamics of the pore. Super-resolution microscopy has also been used in live cells, but little dynamics have been previously shown [167]. For the most part, super-resolution microscopy was employed in fixed cells to study BAX and BAK rings [162, 163, 167]. Unfortunately, when fixing cells, it is impossible to know at which step in the apoptotic pathway a cell resided at the timepoint of fixation. In order to overcome these limitations and to allow for recording and analyzing the dynamics of the apoptotic pore with super-resolution microscopy in single cells, I established the visualization of BAX and BAK in live cells at sub-diffractional resolution with STED microscopy, which I will describe in the next sections.

2.1.1 Choice of cell line

For most of my experiments, I used the osteosarcoma cell line U-2 OS. Although U-2 OS cells are cancer cells, they express the tumor suppressor p53 at physiological expression levels [191, 192], which is necessary for a normal progression of the intrinsic apoptosis pathway. U-2 OS cells are very flat and have a widespread mitochondrial network, which is advantageous for super-resolution microscopy (Figure 23). Importantly, the findings from human cell lines have a higher relevance than studies from different organisms, as they can be more easily translated to human physiology and disease.

2.1.2 Generation of cell lines with suitable mitochondrial outer membrane marker

In order to monitor the intrinsic apoptosis pathway, it was crucial to find a suitable marker for mitochondria. A set of small molecule dyes called Mitotrackers (Invitrogen™/ThermoFisher) are a commonly used tool to label mitochondria as they are easy to use and cover a broad spectral range. However, during apoptosis they either get lost together with the membrane potential or get washed out when mitochondrial outer membrane permeabilization (MOMP) occurs. They are also very prone to bleaching under STED imaging conditions. Therefore, I engineered cell lines with the tagged mitochondrial outer membrane (MOM) protein OMP25 [193]. Either GFP-OMP25 or SNAP-OMP25 [194] were succesfully integrated into the safe harbor locus AAVS1

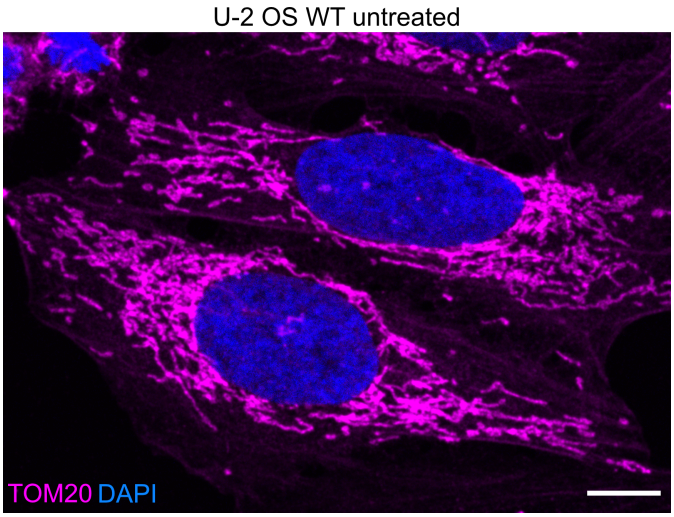

Figure 23: U-2 OS cells are flat and have a widespread reticular mitochondrial network. Confocal image of untreated U-2 OS cells, which were fixed and immunolabeled for mitochondria (anti-TOM20 (magenta)) and DNA (DAPI (blue)). Scale bar: 10 µm.

to ensure stable integration and controlled expression [195, 196]. The cells expressing SNAP-OMP25 were labeled with silicone rhodamine (SiR), a far-red STED compatible dye[197], coupled to benzylguanine (BG), which serves as the ligand for the SNAP-tag. I could observe a normal mitochondrial network in this newly created cell line. I could also visually confirm that OMP25 correctly localized to the MOM as the rim of the mitochondria was more pronounced than the central region (Figure 24) . The cells could be imaged over tens of frames under STED imaging conditions without observing significant bleaching or cellullar toxicity. Mitochondria, labeled by the tagged MOM protein, underwent normal fusion and fission events (Figure 24) and the cells were dividing at the same rate as the wild type cells in culture (doubling roughly at every 29h [198]) over many passages.

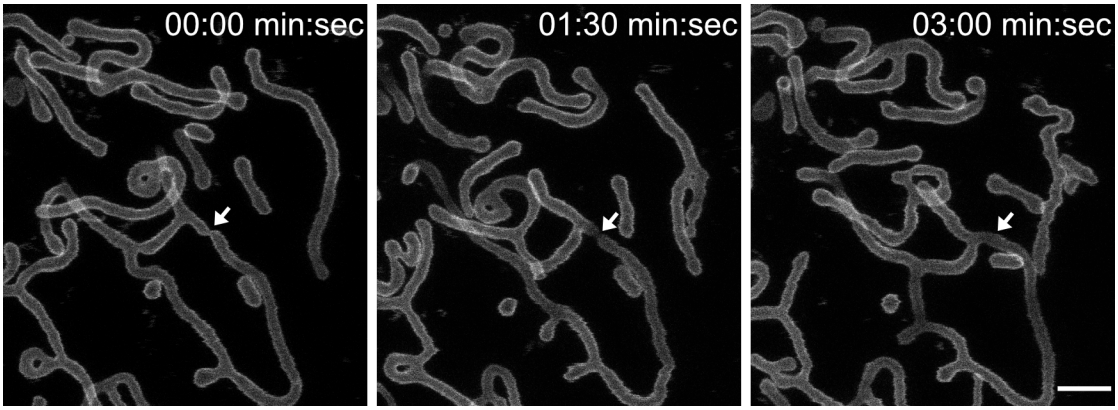

Figure 24: Cells with stably integrated MOM marker (SNAP-OMP25) are viable and photostable. Live-cell STED image sequence of U-2 OS cell line stably expressing SNAP-OMP25 in the safe harbor locus AAVS1, labeled with 500 nM SiR-BG, undergoing a fusion event (arrow). Scale bar: 2 µm.

2.1.3 Dual-color live cell STED of apoptosis

The newly generated cell line expressing a tagged MOM marker (OMP25), allowed to analyze the temporal dynamics of the apoptotic pore with super-resolution microscopy by acquiring live-cell STED videos of cells undergoing apoptosis over an extended time period. To this end, BAX or BAK with an N-terminal Halo-tag [199] were transiently expressed in the cells with stably integrated tagged OMP25. I stained the cells with SiR-BG and the photostable dye Atto590 (AttoTec™) coupled to a chloralkene (CA), which serves as ligand for the Halo-tag. This labeling strategy of combining SiR-BG and Atto590-CA shows very little background and is highly STED-compatible [181]. The labeled cells were then imaged with STED microscopy over minutes up to hours with frame times of ~ 1-3 mins, depending on the size of the field of view. The cells were imaged in the presence of 20 μM Q-VD-OPh (Quinolyl-valyl-O-methylaspartyl-[2,6-difluorophenoxy]-methylketone), a non-toxic, broad-spectrum caspase inhibitor [78], in order to prevent the detachment of the cells from the coverslips. Although it proved difficult to locate the right cells at the onset of apoptosis and determine a good tradeoff between pixel dwell time, field of view and speed, which had to be adjusted for each position individually, I succeeded in imaging the MOM together with BAX or BAK. The following two sections describe the spatial and temporal dynamics of BAX and BAK in apoptosis recorded with live cell STED microscopy.

2.1.3.1 Live cell STED imaging of BAX reveals large, dynamic rings and mitochondrial collapse

First, I investigated the spatial and temporal dynamics of BAX in apoptotic cells. I transiently transfected Halo-BAX into cells with stably expressing SNAP-OMP25 (Figure 25). The overexpression of BAX alone was sufficient to induce apoptosis, as non-transfected cells in the same dish did not undergo apoptosis (Figure 25A, upper right corner). As expected, I initially found BAX as diffuse signal in the cytosol, which shortly afterwards translocated to the mitochondria, where it formed clusters, as has been described before [127, 145, 146]. The initial small clusters were mainly located on the tips of elongated mitochondria and the mitochondria rounded up within minutes of BAX clustering (Figure 26). Some BAX clusters were also located on the side of elongated mitochondria, at sites which would subsequently constrict and undergo fission as shown by diffraction-limited imaging [200] (Figure 26, arrowheads). Unexpectedly however, some of the constrictions would also loosen again and disappear (Figure 26, arrows). Many of the small clusters on rounded up mitochondria eventually started to enlarge and some developed into rings lining a pore on the MOM (Figure 25B, arrows). The rings were visually comparable to previously published

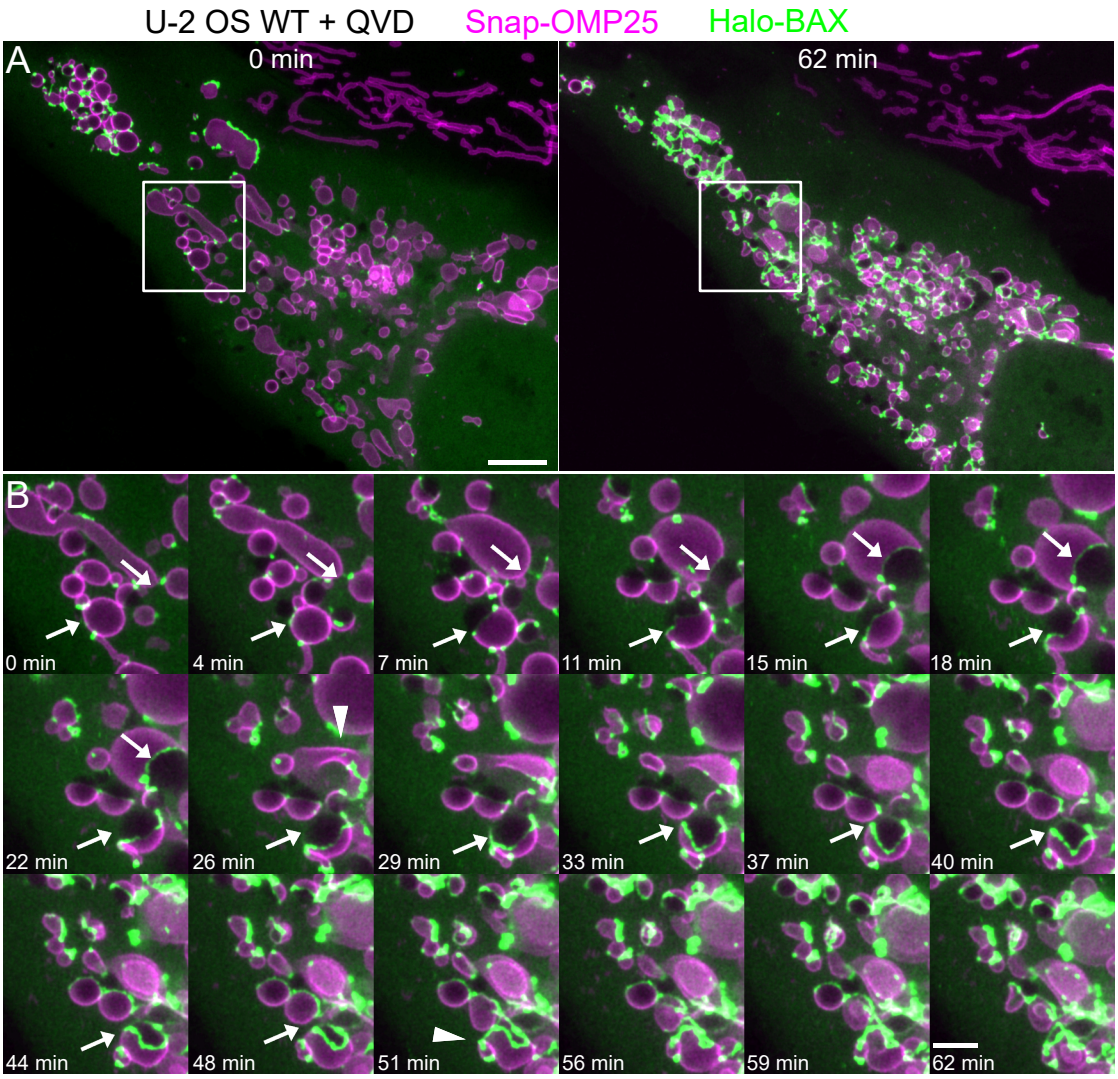

Figure 25: Live STED recording of BAX reveals large rings and mitochondrial collapse. (A) The initial (left) and final (right) frame of a live-cell STED movie of a U-2 OS WT cell undergoing apoptosis. The cells were stably overexpressing the MOM marker SNAP-OMP25 (labeled with SiR-BG, magenta) and transiently transfected with Halo-BAX (labeled with Atto590-CA, green). Movie starts slightly after apoptosis start. No apoptosis treatment was added, as the overexpression of BAX alone was sufficient to induce apoptosis. 20 µM caspase inhibitor (Q-VD-OPh) was added to prevent the detachment of the cells from the coverslips. Frame-time: 1:20 min:sec. Scale bar: 5 µm. Representative video of 16 cells from 5 replicates. **(B)** Selected frames of the enlarged inset from the movie in (A). BAX clusters develop into rings (arrows) and eventually collapse together with their respective mitochondrion (arrow heads). Scale bar: 1 µm.

rings in fixed cells [162] but the live cell STED imaging modality allowed for the first time to investigate their temporal dynamics. The time from initial cluster formation to a clearly visible ring was on the order of 5-10 minutes, however sometimes a cluster was persisting for much longer before undergoing ring formation. BAX rings generally continuously enlarged and most rings reached the maximal possible size, which was limited by the diameter of the rounded up mitochondrion they were re-

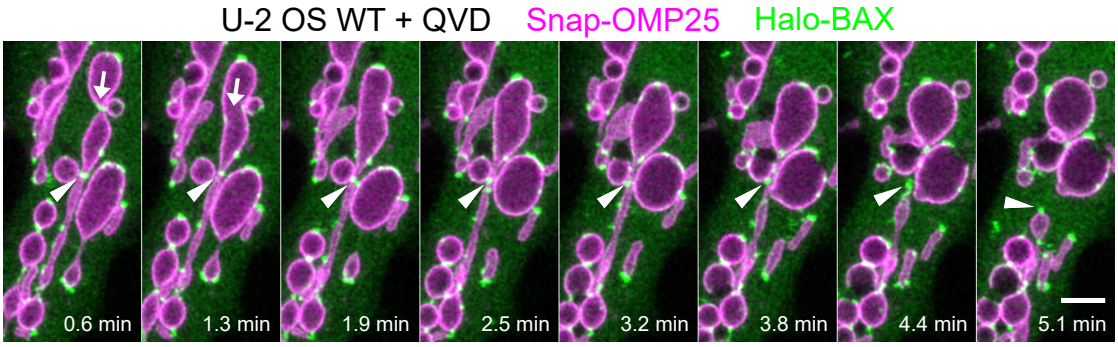

Figure 26: BAX clusters sometimes lead to mitochondrial fission. Region of interest in a live-cell STED movie of a U-2 OS WT cell undergoing apoptosis. The cells were stably overexpressing the MOM marker SNAP-OMP25 (labeled with SiR-BG, magenta) and were transiently transfected with Halo-BAX (labeled with Atto590-CA, green). No apoptosis treatment was added, as the overexpression of BAX alone was sufficient to induce apoptosis. 20 µM caspase inhibitor (Q-VD-OPh) was added to prevent the detachment of the cells from the coverslips. BAX clusters localize to mitochondrial fission (arrow head) or the constriction dissolves again and the mitochondrion rounds up (arrow). Frametime: 38 seconds. Scale bar: 2 µm.

siding on. The rings were usually enlarging for a couple of minutes and then stayed enlarged for up to tens of minutes. After their enlargement, most rings deformed and shrunk, which eventually led to the respective mitochondrion collapsing together with its BAX ring (Figure 25B, arrowheads). In all of the rings from 16 analyzed videos of 5 different experiments, there was always a maximum of only one ring per mitochondrion and the rings were found exclusively on rounded up mitochondria. During the whole apoptotic process, the initially very dynamic mitochondrial network condensed and became increasingly immotile until the whole cell finally detached from the coverslip despite the presence of Q-VD-OPh.

2.1.3.2 Live cell STED imaging of BAK reveals smaller rings and elongated linker structures

Second, I visualized the spatial and temporal dynamics of BAK in apoptotic cells. I transiently transfected Halo-BAK into cells stably expressing GFP-OMP25 (Figure 27) or SNAP-OMP25 (Figure 28). Similar to BAX overexpression, the overexpression of BAK alone was sufficient to induce apoptosis, as non-transfected cells in the same dish did not undergo apoptosis. In contrast to BAX, BAK was already localizing to the mitochondria before clustering onset, where it resides physiologically as diffuse signal [127, 146]. Similar to BAX, BAK also started forming clusters after this intial stage, and some clusters would form rings (Figure 27B, arrows). However, the BAK rings seemed in general to be smaller than their BAX counterparts and did not enlarge as much. Still, in the 13 cells from three independent experiments, about a third of the rings reached the maximal diameter of the mitochondrion they were residing on.

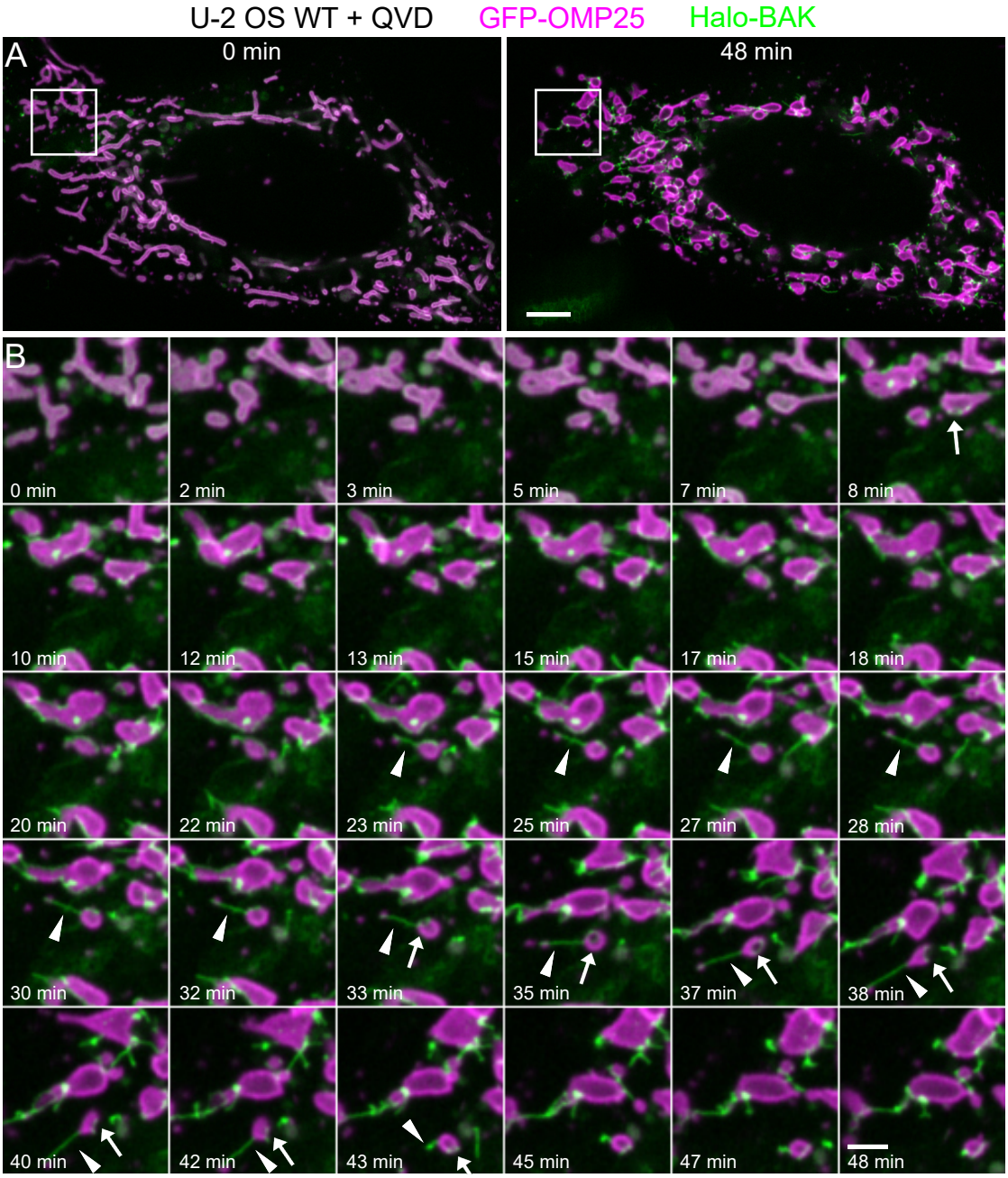

Figure 27: Live STED recording of BAK reveals smaller rings and linkers. (A) The initial (left) and final (right) frame of a live-cell STED movie of a U-2 OS WT cell undergoing apoptosis. The cells were stably overexpressing the MOM marker GFP-OMP25 (magenta) and were transiently transfected with Halo-BAK (labeled with Atto590-CA, green). Movie starts slightly before apoptosis start. No apoptosis treatment was added, as the overexpression of BAK alone was sufficient to induce apoptosis. 20 µM caspase inhibitor (Q-VD-OPh) was added to prevent the detachment of the cells from the coverslips. Frametime: 3:40 min:sec. Scale bar: 5 µm. **(B)** Selected frames of the enlarged inset from the movie in (A). BAK forms rings (arrows) and linkers (arrow heads). Scale bar: 1 µm.

Importantly, BAK rings were able to form on elongated mitochondria and I occasionally observed single mitochondria with two BAK rings (Figure 28). The time from ini-

tial cluster formation to a clearly visible ring was on the order of 5-10 minutes, however, it was sometimes difficult to distinguish individual clusters, as BAK, in contrast to BAX, was generally residing on the MOM. BAK rings were often seen to deform and reform or re-appear on a different positions on the mitochondrion, and no clear collapse of mitochondria like in the BAX overexpressing samples could be observed. Unexpectedly, I also found a high proportion of elongated, thin BAK protrusions between mitochondria, which I term "linker". The linkers were connected to the MOM at one or both ends but showed no co-localizing MOM signal on the protrusion itself (Figure 27B, arrowhead). These linkers were sometimes ejected from one mitochondrion and retracted again within one minute. Mostly however, they persisted for 20 minutes and more, while moving around before being retracted again. As with BAX overexpression, in general, the initially very dynamic mitochondrial network condensed and became increasingly immotile until the whole cell finally detached from the coverslip despite the presence of Q-VD-OPh.

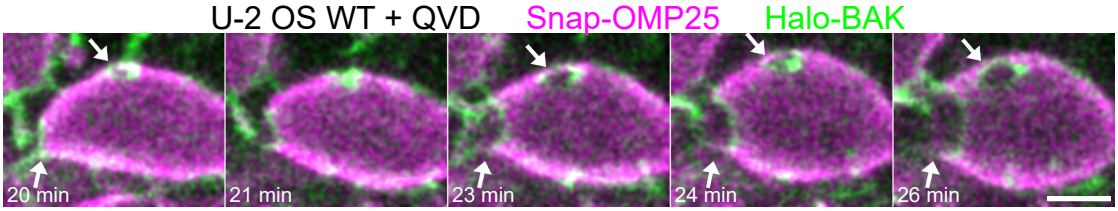

Figure 28: BAK can create two pores on one mitochondrion. Region of interest in a live-cell STED movie of a U-2 OS WT cell undergoing apoptosis. The cells were stably overexpressing the MOM marker SNAP-OMP25 (labeled with SiR-BG, magenta) and were transiently transfected with Halo-BAK (labeled with Atto590-CA, green). No apoptosis treatment was added, as the overexpression of BAK alone was sufficient to induce apoptosis. 20 µM caspase inhibitor (Q-VD-OPh) was added to prevent the detachment of the cells from the coverslips. Two BAK rings are forming and enlarging (arrows) on one mitochondrion. Frametime: 16 seconds but only some frames are shown. Scale bar: 1 µm.

In summary, I established a protocol for long-term live cell STED imaging of BAX or BAK together with the MOM in apoptotic cells at sub-diffractional resolution. A qualitative analysis of the super-resolved BAX and BAK recordings revealed insights into the dynamics of these two proteins. Both proteins are capable of forming rings within minutes after the onset of apoptosis but, I observed striking differences in the ultra-structure of the proteins and their dynamics:

1) BAX rings were only found on rounded up mitochondria and mostly grew continuously until they reached the diameter of the rounded up mitochondrion they were residing on. BAK rings also enlarged and could reach the maximal diameter, but many stayed in smaller or intermediate size stages. 2) I never found more than one BAX ring per mitochondrion. In cells with overexpressed BAK on the other hand, sometimes also two rings could be found on one mitochondrion. Additionally, the

mitochondria harboring BAK rings were sometimes still elongated. 3) BAK formed a significant proportion of elongated protrusions without MOM signal, which I termed "linkers".

Note, that I only qualitatively described the data and refrained from quantification, as the quality of most videos did not allow to extract valid and quantifiable information. In addition, most videos started or ended during the apoptotic process because it was virtually impossible to find the right cells at the right time.

Together, these findings suggest that both BAX and BAK are capable of inducing apoptosis when overexpressed. However, the differences in ring formation and size between BAX and BAK as well as differences in overall localization point to the fact that there are significant dissimilarities between the two proteins. As these experiments solely relied on the overexpression of BAX and BAK, which might interfere with the delicate balance of the B-cell lymphoma 2 (BCL-2) protein family however, I set out to investigate apoptosis induction by overexpression quantitatively in the next section.

2.2 Overexpression of BAX or BAK shifts the balance of BCL-2 proteins and induces apoptosis non-physiologically

In the previous section, I showed differences in the pore forming characteristics between BAX and BAK. The described BAX and BAK dynamics were derived from experiments in cells overexpressing the proteins. However, it is known since the end of the 20th century that BAX overexpression induces apoptosis [201, 202]. The co-incubation of MOM vesicles with active BAX alone is sufficient to produce membrane pores in these vesicles, which vary in pore diameter, frequency and kinetics depending on the GFP-BAX expression levels [165]. The capability of BAX and BAK to induce cell death without the involvement of other proteins was shown even more drastically in a cell line, where all Bcl-2 family members were knocked out, and the re-expression of BAX or BAK alone triggered apoptosis [104]. Therefore, in the following sections, I investigated the effects of overexpressing BAX in a quantitative assay with long-term live cell imaging. Furthermore, I asked, whether the tagging of BAX itself could induce apoptosis and attempted to stably integrate tagged BAX into the genome as well as tag the endogenous BAX locus.

2.2.1 Quantification of apoptosis induction by overexpressing tagged BAX

To quantify the time from BAX overexpression to apoptosis onset and the overall duration of overexpression-induced apoptosis, I transfected U-2 OS cells with GFP-BAX and monitored the GFP signal as well as cell morphology in an automated microscope for over 10 hours (Figure 29A). This assay allowed me to determine the onset and duration of apoptosis over a whole cell population in a large region of interest, in contrast to the live cell STED experiments, where I could only scrutinize a fraction of the cells in one culture dish due to technical reasons. Here, by taking a large image every 40 minutes, I discovered that the cells started expressing GFP-BAX after as little as 3-4 h after transfection. I also found that all cells, which expressed GFP-BAX, rounded up between 3-10 hours after transfection. The morphological change of the cells from flat to rounded is a clear feature of apoptosis (Figure 29B). On a cell to cell level, the onset and progression kinetics of cell death varied drastically and it was unpredictable, which cell expressed GFP-BAX and underwent morphological changes at which timepoint. These findings confirmed that the transfection of BAX resulted in fast protein overexpression and was sufficient to effectively induce apoptosis in a cell population within 10-11 h. The apoptosis onset after transfection was variable from cell to cell and different duration times of apoptosis were observed. In addition to the overall variability, the process happened generally fast. Thus, the difficulties in monitoring apoptosis by live cell STED microscopy was mainly caused by the gene-

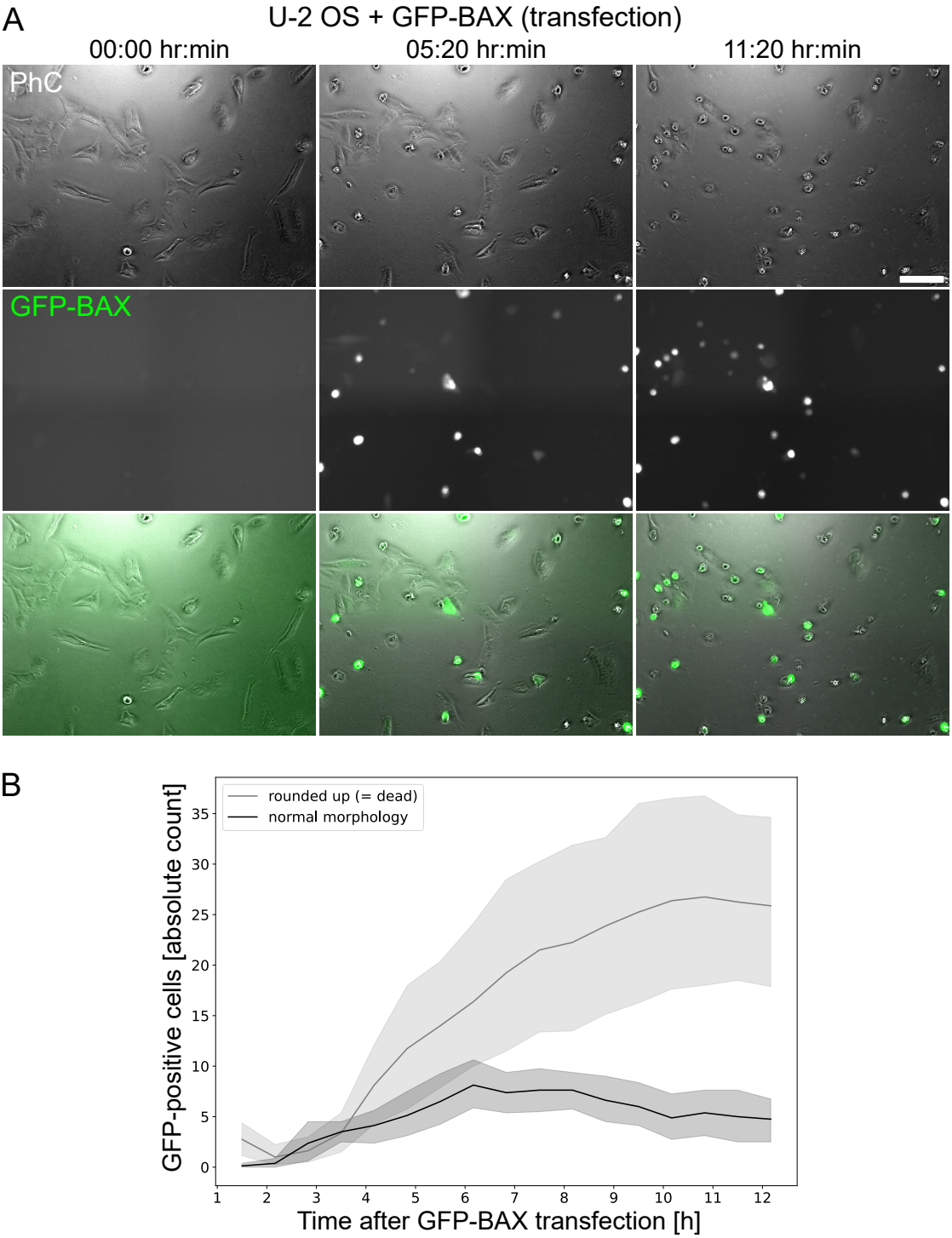

Figure 29: GFP-BAX overexpression induces apoptosis. **(A)** Three frames from a live-cell widefield movie of U-2 OS cells undergoing apoptosis after transient overexpression of GFP-BAX. The cells (Phase Contrast (PhC), grayscale) were transfected with GFP-BAX (green) directly before imaging. No additional apoptosis inducer was added. After start of expression of BAX, the rounding up and detachment from the coverslip could be observed in almost every transfected cell. Frametime: 40 minutes. Scale bar: 100 µm. **(B)** GFP-BAX positive cells with normal (black)or rounded up (gray) morphology are plotted. Solid lines are means of eight replicates with the 95 % confidence intervall shown as areas around the curve.

ral rapidity and variability in the progression of overexpression-induced apoptosis and not by the super resolution imaging procedure.

2.2.2 Transient overexpression of untagged WT and mutant BAX

In the previous experiments cells were overexpressing BAX or BAK N-terminally fused to a GFP or the Halo-tag. However, it is commonly known that tagging of proteins carries the risk of introducing an alteration into the protein conformation. BAX and BAK are globular proteins consisting of nine alpha helices that bury their N-terminus. The N-terminus gets exposed upon activation of BAX or BAK [203]. N-terminal tagging of these proteins could thus lead to constitutive activation. Therefore, in order to rule out that GFP-BAX overexpression induced apoptosis via the tag, I overexpressed untagged BAX. I included WT BAX and a mutant version of BAX, which carried a triple alanine mutation in the the BH3 domain (63-65A) [204].The BH3 domain of BAX and BAK is postulated to be involved in their oligomerization [205] and the mutant BAX thus unable to oligomerize.

I transfected the untagged BAX variants into untreated BAX-BAK-double-KO (DKO) cells (described in section 2.7), fixed them and performed an immunofluorescence (IF) staining for BAX (described in section 2.3.1). The mitochondrial morphology clearly indicated that cells, which were expressing untagged WT BAX, had become apoptotic (Figure 30A-B). Even the overexpression of the mutant version of untagged BAX 63-65A, which is supposed to be impaired in oligomerization, led to a clearly apoptotic phenotype (Figure 30C-D). This induction of apoptosis by overexpression of untagged BAX confirmed that the overexpression of BAX generally causes the induction of apoptosis, independent of N-terminal tagging. Moreover, as the cells in this assay were only imaged after fixation, the results furthermore suggest, that apoptosis induction occurs because of the overexpression independently of live-cell imaging procedures. This does not automatically rule out that tagging of BAX or BAK or imaging procedures alone might also be able to lead to apoptosis, but it shows that an over-abundance of BAX in the cell is sufficient to induce apoptosis.

In an organism, a cell usually senses an intolerable stress and induces the intrinsic apoptosis signaling pathway by activating the BH3 only proteins. These inhibit the anti-apoptotic BCL-2 proteins and liberate the physiological amount of BAX or BAK present in a cell, thereby facilitating MOMP. As the overexpression of BAX WT and even a supposed oligomerization impaired mutant version of BAX (63-65A) formed pore-like structures on the MOM and induced cell death, I concluded that the transient overexpression of BAX or BAK overcharges the system with pro-apoptotic proteins. This leads to unexpected effects on the MOM and therefore might not represent a physiological induction of the apoptosis pathway.

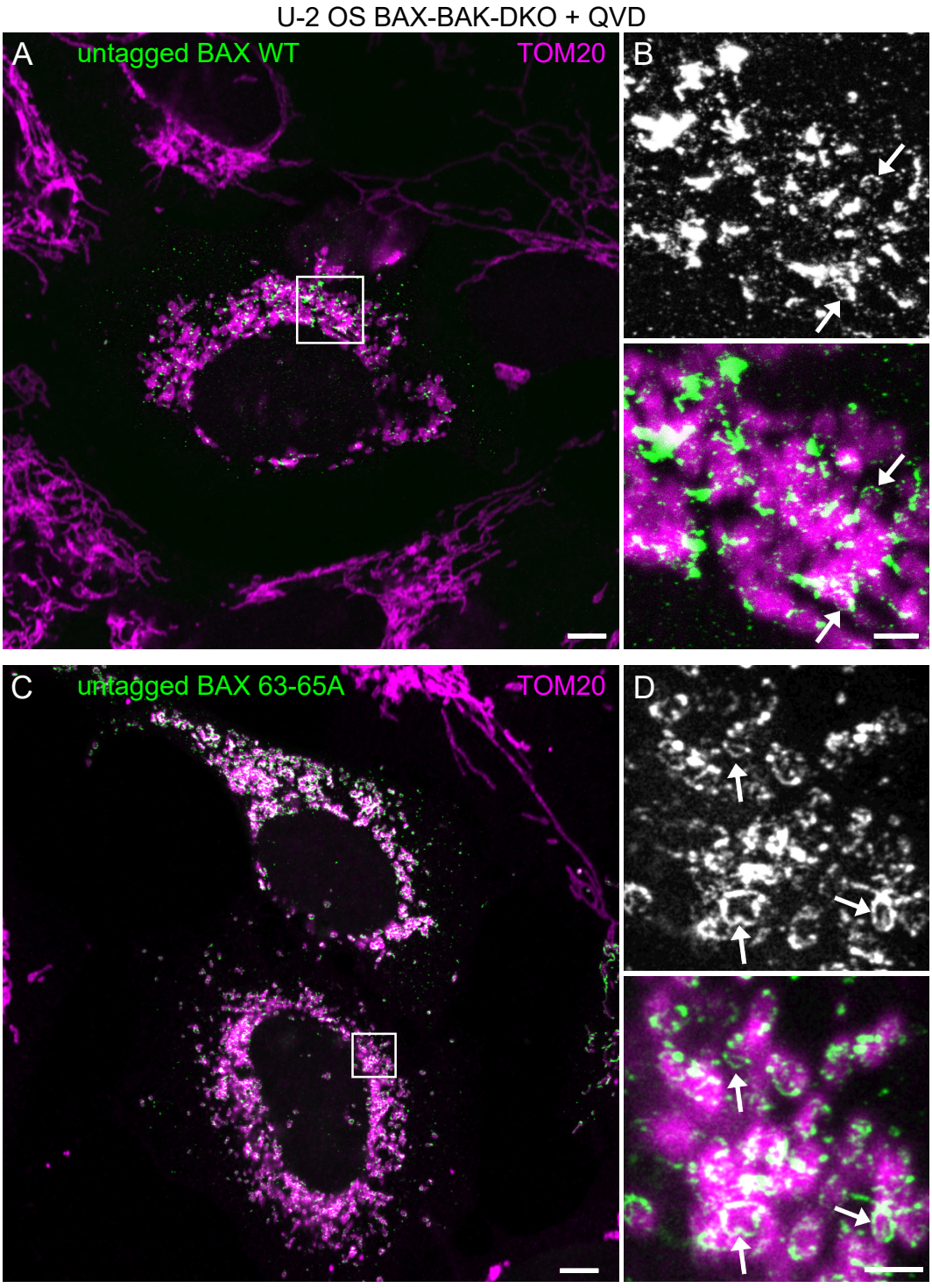

Figure 30: Over-expression of untagged BAX WT and BAX 63-65A mutant induces apoptosis. (A, C) Images of U-2 OS cells undergoing apoptosis by BAX overexpression. U-2 OS cells were transiently transfected with untagged BAX variants. After 22 h of expression, the cells were fixed and stained with anti-BAX (green) and anti-TOM20 (magenta) antibodies. Scale bars: 5 µm. **(A)** In cells overexpressing BAX WT the mitochondria round up and fragment. **(B)** Magnification of the box in (A). The overexpression of untagged WT BAX leads to BAX ring formation (arrows), but mostly BAX is present in large clusters. Scale bar: 1 µm. **(C)** In cells overexpressing BAX 63-65A the mitochondria round up and fragment as well. **(D)** Magnification of the box in (C). In cells which overexpressed the untagged 63-65A mutant, BAX predominantly formed rings (arrows) and only few large clusters. Scale bar: 1 µm.

2.2.3 Stable genomic integration of inducible Halo-BAX

The transient overexpression of tagged and untagged BAX proved to be too heterogeneous and unreliable for quantitative, physiological measurements. I therefore engineered a cell line stably expressing tagged BAX, which was expected to result in a more homogeneous apoptosis onset and longer apoptosis duration. In brief, I inserted Halo-BAX under the control of a doxycyclin-inducible promoter in the safe harbor locus AAVS1 (Adeno-associated virus integration site 1) [195] in U-2 OS cells using CRISPR/Cas9 genome editing. In order to monitor MOMP, the cell line additionally carried cytochrome *c*-mEGFP on a different allelle of the AAVS1 locus, which will be further discussed in section 2.4. I induced the expression of Halo-BAX with 1 μM of doxycyclin and added Q-VD-OPh to prevent the detachment of the cells from the coverslip. I stained the cells in imaging medium with Atto590-CA as ligand for the Halo tag. As the cells were derived from one clone, they had the same Halo-BAX expression construct inserted into their genome and I assumed that the induction of Halo-BAX expression would result in similar copy-numbers and therefore simultaneous apoptosis progression over the whole cell population. Indeed, the addition of doxycyclin lead to the release of cytochrome *c* and BAX clustering without any additional treatment (Figure 31). However, the apoptosis onset was variable from cell to cell and it was unpredictable, which cell would commence first. Additionally, the typical timeframe from normal mitochondrial morphology to cytochrome *c* release, rounding of mitochondria and BAX cluster formation was about 15 mins. The stable genomic integration of inducible BAX expression thus resulted in the same shortcomings as the transient overexpression, i.e. variable onset of apoptosis and very fast apoptosis progression. A lower concentration of doxycyclin might have slowed apoptosis progression, but would not have alleviated the problem of the cells undergoing apoptosis onset in an asynchronous manner. Therefore, this tool was equally rejected for physiological apoptosis induction.

2.2.4 Endogenous tagging of BAX impedes cellular survival

In order to circumvent the limitations of transient or inducible BAX overexpression, I attempted to tag BAX endogenously with the CRISPR/Cas9 system. In brief, I aimed for the insertion of an N-terminal Halo-tag at the endogenous BAX locus. At the same time, a GFP reporter was to be inserted into an intronic region on the inverse strand to be able to sort the cells by fluorescence activated cell sorting (FACS) for clone selection. However, although I initially detected some GFP-positive cells, no clones survived after FACS. This might indicate that cells with integration of the tag at the endogenous BAX locus did not survive the single cell sorting and clonal expansion. Due

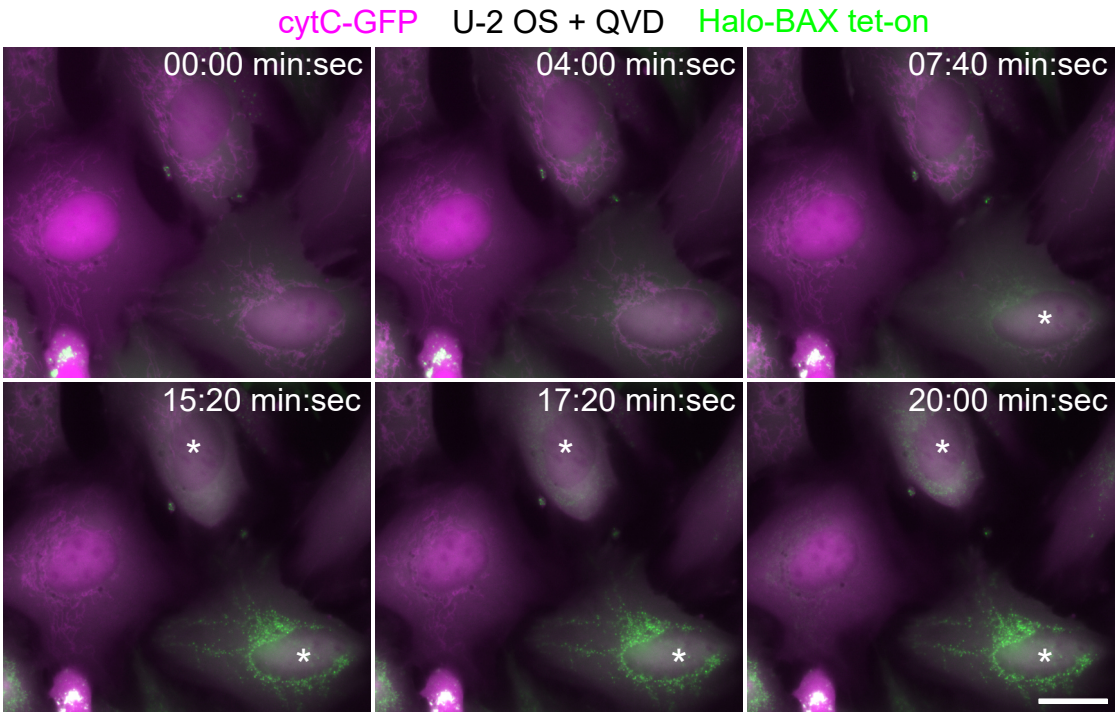

Figure 31: Doxycyclin induced BAX expression induces apoptosis. Six frames from a live-cell widefield movie of U-2 OS cells undergoing apoptosis. The cells were stably overexpressing GFP-cytochrome *c* (magenta) and doxycyclin inducible (tet-on) Halo-BAX (labeled with Atto590 dye, green). Movie starts 18h after addition of 1 µM doxycyclin. No apoptosis treatment was added. 20 µM caspase inhibitor (Q-VD-OPh) was added to prevent the detachment of the cells from the coverslips. After loss of mitochondrial cytochrome C signal, the start of BAX clustering can be observed (cells with asterisks). Frametime: 20 sec. Scale bar: 20 µm.

to the fact that a cell line with endogenously tagged BAX has not been published to my knowledge, I conclude that endogenous tagging of BAX interferes with cell physiology, which might again be due to the N-terminal tag, which renders the protein constitutively active. I therefore set out to find a way of investigating the involved pore formers in a more physiological setting.

2.3 BAX antibody staining in multiple imaging modalities

In the first part of this work, I established the use of live cell STED microscopy to record super-resolved BAX and BAK in the apoptotic pore. However, the proteins of interest in these experiments were overexpressed and I demonstrated that overexpression of pro-apoptotic Bcl-2 proteins can lead to unphysiological apoptosis induction, potentially introducing artefacts, which could lead to misinterpretations in the analysis of the apoptotic pore. Similarly, I found that endogenous N-terminal tagging hampers the clonal survival of cells. Therefore, I aimed to study the proteins in their native environment at physiological levels. To prevent the use of overexpression or tagging, I employed immunofluorescence (IF) staining of native proteins in fixed cells. In the following sections, I will present the investigation of 2D and 3D structures of endogenous BAX pores with three different imaging modalities: STED, 4Pi-STORM and MINFLUX microscopy.

2.3.1 STED microscopy of endogenous BAX

In a first step, I established 2D STED microscopy of endogenous BAX in apoptotic U-2 OS WT cells. In order to induce apoptosis , I plated the cells on coverslips and treated them between 16 and 20 h with 10 µM Actinomycin D (ActD), a drug which binds to DNA and inhibits the synthesis of RNA [76]. I also added 20 µM Q-VD-OPh, a caspase inhibitor, in order to prevent the detachment of the cells from the coverslips. After treatment and fixation, I performed an IF staining with antibodies against TOM20, cytochrome *c* and BAX. The secondary antibodies for STED microscopy were coupled to StarRed and AlexaFluore594. As established in *Große et al. 2016* [162], it is possible to label BAX with antibodies for IF staining and subsequent STED microscopy. However, because the specific antibodies of the publication were no longer available, I developed an IF staining with a mouse anti-BAX antibody (clone 2D2, Thermo #MA5-13994, hereafter called 2D2-BAX antibody, see Table 3) (Figure 32).

The apoptotic onset of individual cells is heterogeneous [190]. Typical features to discern the apoptotic cells from the non-apoptotic cells are rounded up mitochondria or cytochrome *c* loss from the inter-membrane space (IMS). These features can be observed in the recordings of cells with this IF staining (Figure 32A, top left panel and top right panel).

In healthy cells, BAX resides in the cytosol and only gets recruited to the MOM upon an apoptotic stimulus [125]. Labeling with the 2D2-BAX antibody revealed BAX clusters exclusively in the apoptotic cells (Figure 32A, top middle panel and large image), whereas it produced an almost invisible, homogeneous background staining in the cytoplasm of non-apoptotic cells (Figure 32A, top middle panel).

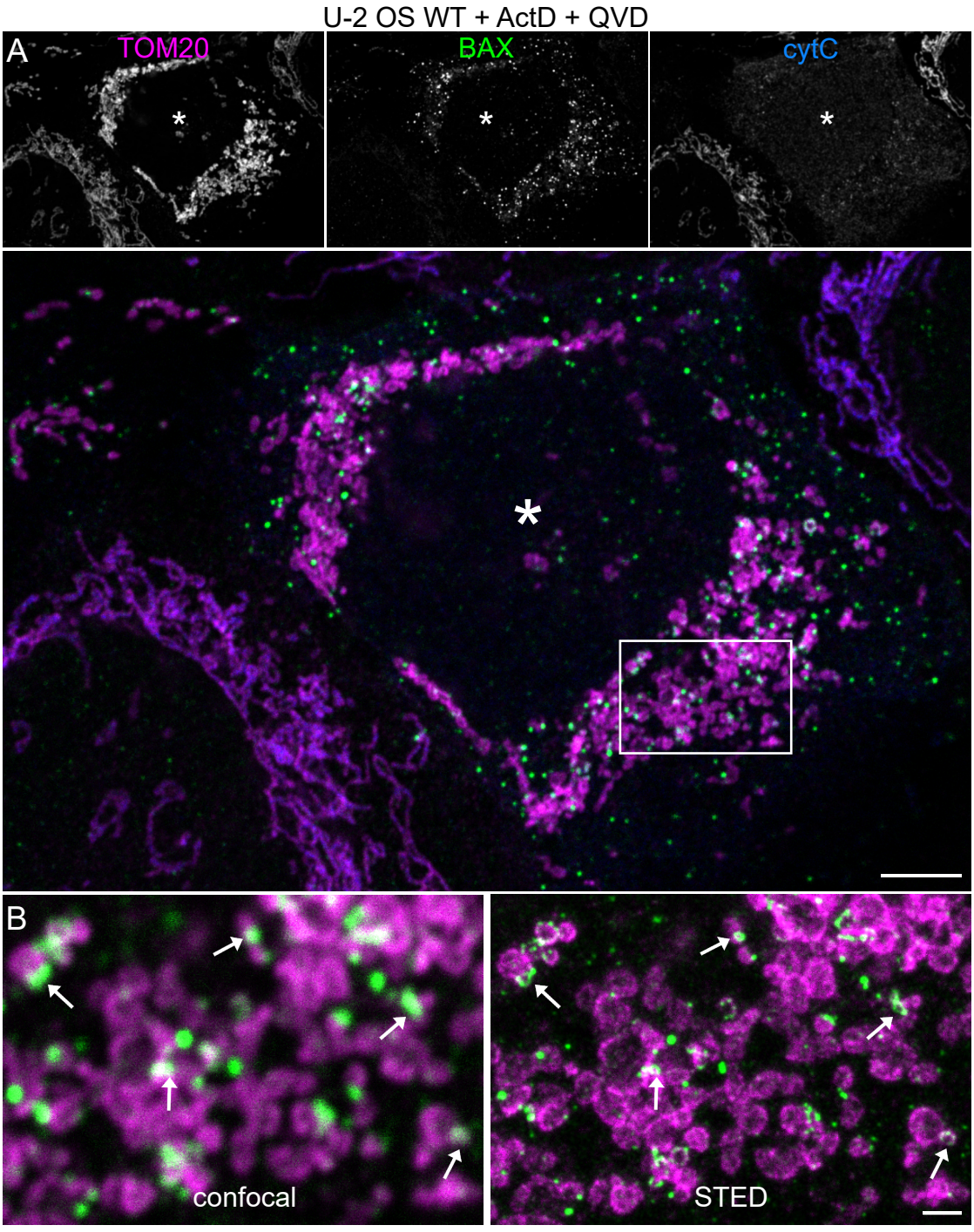

Figure 32: IF staining reveals BAX rings in STED imaging modality. **(A)** Representative image of an apoptotic U-2 OS cell (asterisk) surrounded by non-apoptotic cells. The cells were treated with 10 µM ActD. 20 µM Q-VD-OPh was added to prevent the detachment of the cells from the coverslips. The cells were fixed and labeled with the 2D2-BAX antibody (green), anti-TOM20 antibody (magenta) and anti-cytochrome C antibody (blue). Scale bar: 5 µm. **(B)** Magnification of the box in (A) containing only BAX and TOM20 channels in confocal and STED mode. BAX rings (arrows) can only be discerned in STED mode. Scale bar: 2 µm.

The 2D2-BAX antibody staining thus specifically labels apoptotic cells. When further investigating the apoptotic mitochondria harboring BAX clusters, I was able to con-

firm that, next to clusters, BAX also formed extended structures (Figure 32B). The detailed morphology of these structures, specifically rings, with sizes below the diffraction limit were only able to be resolved with STED microscopy. Therefore, the BAX (and BAK) channel will be shown in STED mode for the remainder of this thesis, unless stated otherwise.

2.3.2 MINFLUX microscopy of endogenous BAX

I successfully used the 2D2-BAX antibody staining for STED. However, this technique is still limited in resolution. In order to resolve and investigate BAX pores that are even smaller than the resolution limit of STED, I established a staining protocol for BAX in apoptotic cells for 2D MINFLUX microscopy [187] (Figure 33). U-2 OS cells

(treated with ActD and Q-VD-OPh) were fixed and immunolabeled with the 2D2-BAX antibody. In contrast to previous IF approach, the secondary antibodies were coupled to a DNA-PAINT handle [189] and labeling was performed with complementary imager strands with attached fluorophores in the imaging medium. BAX pores could be resolved with unprecedented detail below 5 nm (Figure 33B). However, the discovery of very small BAX rings proved extremely challenging, due to a number of technical limitations: MINFLUX imaging only allows for a very small field of view (typically around 3 x 3 μm). This field of view has to be chosen from a confocal overview which means that one can only guess where a small ring might be concealed behind a confocal BAX cluster. In addition, the imaging takes very long (on the order of tens of minutes) until it becomes clear whether the position was a good guess. Therefore, although I showed that BAX imaging with DNA-PAINT and 2D MINFLUX is possible, the actual application still needs some optimization. Ideally, this includes overall advancement of the technique as well as the establishment of a way to locate small BAX rings until MINFLUX can be employed for biological questions about the apoptotic pore.

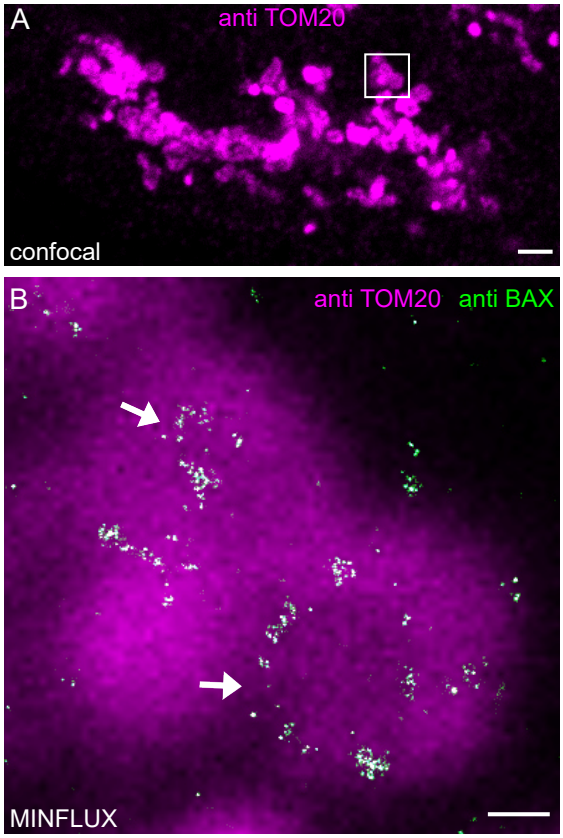

Figure 33: BAX structures resolved with MINFLUX microscopy. **(A)** Image of fragmented mitochondria labeled with anti-TOM20 antibody (magenta, confocal) in a fixed, apoptotic U-2 OS cell. Cells were treated with 10 µM ActD. 20 µM Q-VD-OPh was added to prevent the detachment of the cells from the coverslips. Scale bar: 2 µm. **(B)** MINFLUX image of BAX in apoptosis. Enlargement of the box in (A) corresponding to the actual field of view where the MINFLUX imaging was performed. Fixed cells were labeled with an anti-TOM20 antibody (magenta, confocal) and the 2D2-BAX antibody (green, MINFLUX), which was detected with a secondary antibody coupled to a DNA handle for DNA-PAINT. The sample was imaged with DNA imager strands (coupled to the fluorophore Atto655) present in the imaging medium. Scale bar: 200 nm.

2.3.3 4Pi STORM microscopy of endogenous BAX

When examining the 2D STED images of IF stainings, I discovered many more BAX structures than just rings, such as small and large clusters, and sometimes, although less frequently, lines and arcs. The protein assemblies giving rise to the structures can have any orientation in the cell and on the mitochondrion. In fact, this orientation might not be parallel to the 2D image plane, especially because apoptotic cells are rounding up substantially, and hence, rings could appear as lines or arcs in a 2D image.

To investigate the BAX assemblies in 3D and in a larger field of view than with MINFLUX microscopy, I employed 4Pi STORM microscopy on a custom-built system [186]. 4Pi-STORM microscopy provides isotropic resolution and single-digit nm lo-

calization precision while enabling a z-range of micrometers. U-2 OS cells (treated with ActD and Q-VD-OPh) were fixed, immunolabeled with the 2D2-BAX antibody, detected by a secondary Fab fragment coupled to AlexaFluor647, and imaged on the 4Pi-STORM microscope (Figure 34A). Indeed, when scrutinizing the reconstructed volume renderings, it became clear that most arc and line shaped BAX assemblies were actually rings, which only became apparent at certain angles (Figure 34B).

Although different structures, such as lines and arcs, do exist also when viewing BAX structures in 3D, they often proved to be rings, when viewed from different orientations. To get an impression of how many rings areactually concealed when looking only at 2D datasets, I quantified the 4Pi-STORM data. I investigated the percentage of rings detectable in the xy-plane compared to the total number of rings, which could be detected when examining the image volume from all angles. I found that almost 75 % of the rings can be detected in the xy-orientation (Figure 34C). Therefore, I concluded that 2D super-resolution microscopy is sufficient to detect the majority of rings.

In summary, I showed that the apoptotic pore can be studied by labeling it with the 2D2-BAX antibody and recording in different imaging modalities. The use of fast and reliable 2D STED microscopy is sufficient to resolve 75 % of the apoptotic pores as confirmed by 3D 4Pi-STORM microscopy. Therefore, the rest of the experiments in this work will be performed using 2D STED microscopy.

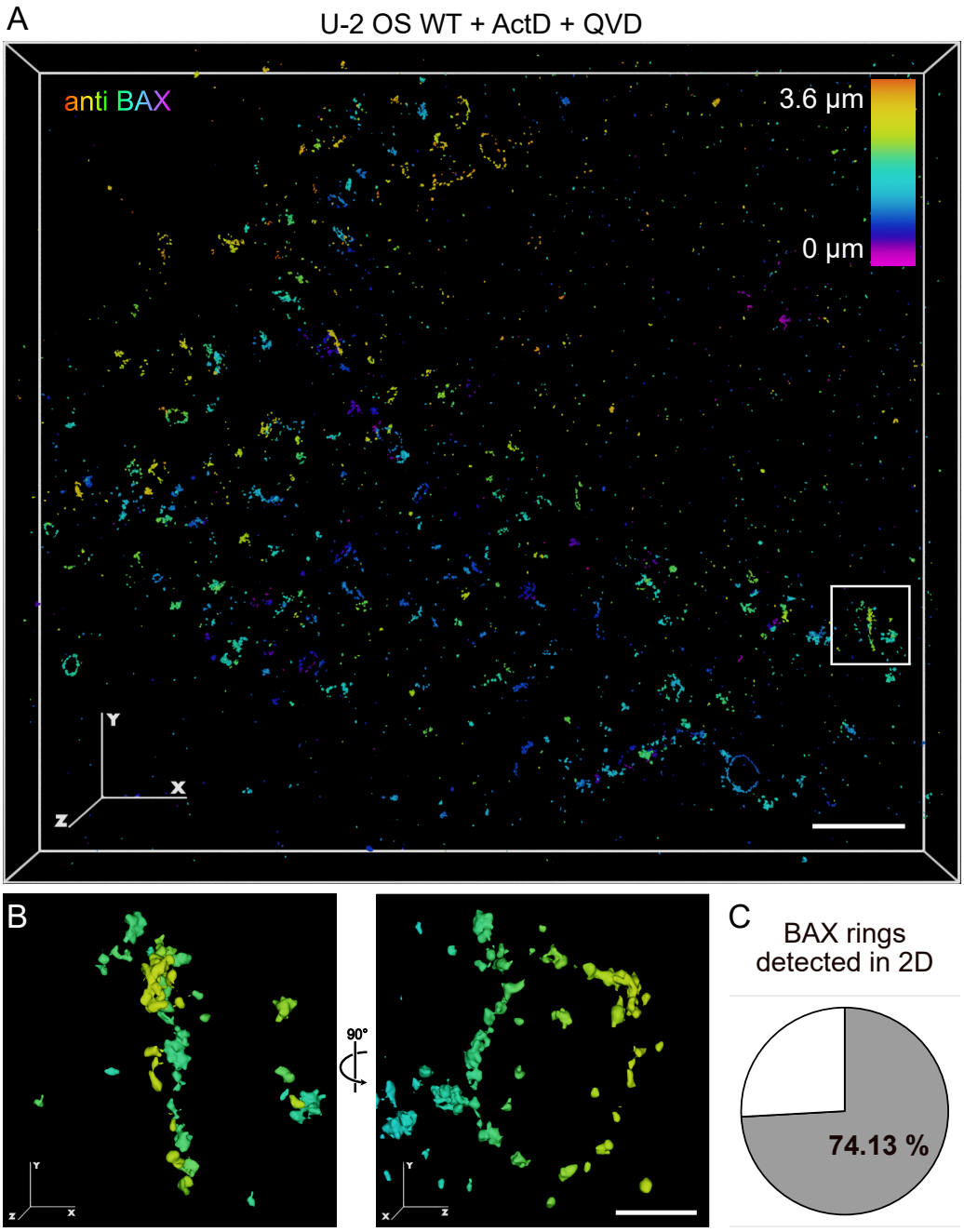

Figure 34: BAX rings are located in the cell in all spatial orientations. **(A)** 4Pi STORM image reconstruction of BAX in apoptosis. Data is displayed as perspective view along the z-axis with depth-color-coding. U-2 OS cells were treated with 10 µM ActD. 20 µM Q-VD-OPh was added to prevent the detachment of the cells from the coverslips. The apoptotic cells were fixed and labeled with the 2D2-BAX antibody, detected by a secondary Fab fragment coupled to AlexaFluor647, and prepared for 4Pi STORM imaging. The image is a representative example of three replicates. Scale bar: 2 µm. **(B)** Enlargement of the box in (A), as viewed from two angles turned by 90°, the first one showing only a line of BAX which actually is a BAX ring when viewed from the side. Scale bar: 250 nm. **(C)** Quantification of rings detected in 2D (gray area) vs 3D (full circle). Rings were counted in n = 5 images.

2.4 Establishment of a MOMP marker for the temporal resolution of apoptosis

In the previous section, I established the robust detection of endogenous BAX in apoptotic pores via IF staining and super-resolution microscopy. This allowed for the analysis of BAX pores after fixation at arbitrary timepoints during apoptosis. However, apoptosis is a very dynamic process with a heterogeneous onset [190]. Unfortunately, in IF it is impossible to know at which timepoint in the apoptotic pathway a cell resided at the time of fixation. To overcome this limitation, it is essential to include temporal information.

One way to achieve temporal resolution is live cell analysis of the proteins of interest. But because the endogenous tagging of BAX proved difficult and in order to avoid the overexpression of BAX or BAK with all the discussed drawbacks (i.e. unphysiological apoptosis induction and fast progression), I chose to establish a more physiological approach. In this section, I explain how I developed an assay, which provides a molecular ruler for apoptosis by recording a key event in live cells. After live cell imaging, the cells are fixed, immuno-labeled and imaged with STED microscopy. The occurence of the key event is then used to assign a timepoint to the STED images (Figure 35).

The key event in apoptosis, the so-called point of no return, is the permeabilization of the MOM (MOMP) [206]. During MOMP, which is an early event in the apoptotic process, the contents of the IMS get released into the cytosol. Among the released contents are many proteins, one of which is cytochrome *c*. The release of cytochrome *c* from the IMS to the cytosol occurs in a two-step process involving the remodeling of the cristae structure of the mitochondria [207, 208]. Thereby, the cytochrome *c*, which is usually bound in the electron transport chain, gets solublilized. Once cytochrome *c* is solubilized in the IMS, the release into the cytosol is rapid, complete and has successfully been used as indicator of MOMP [144].

To monitor the change in localization of cytochrome *c*, I created a cell line with stably integrated cytochrome *c*-mEGFP in the safe harbor locus AAVS1 via CRISPR/-Cas9 gene editing. The cytochrome *c*-mEGFP expressing cells were placed in imaging medium with 10 µM ABT-737, a BH3-mimetic commonly used to induce apoptosis [101]. I also added 20 µM Q-VD-OPh to prevent the detachment of the cells from the coverslips. The cells were recorded live by widefield imaging over many hours until and beyond MOMP. Indeed, the cells released cytochrome *c* at different timepoints during the recording (Figure 36A). Unexpectedly, cytochrome *c* was also found in the nucleus in this cell line. The translocation of cytochrome *c* to the nucleus has been observed in cells undergoing apoptosis [209]. Alternatively, it could also be an effect

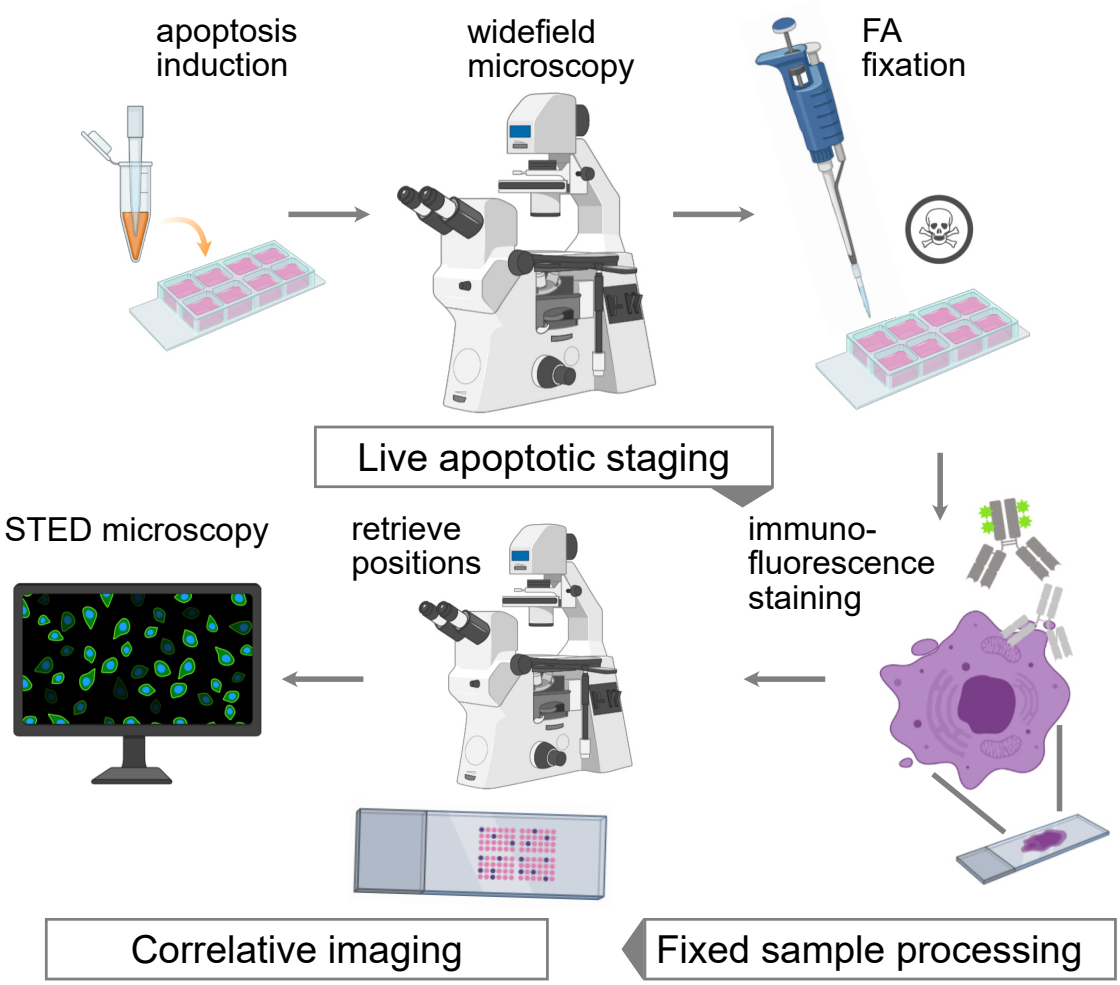

Figure 35: MOMP marker assay schematic. *Live apoptotic staging:* The cytochrome *c*-mEGFP expressing cells were treated with 10 µM ABT-737 and the positions were monitored by a widefield microscope with an automated stage. 20 µM caspase inhibitor (Q-VD-OPh) was added to prevent the detachment of the cells from the coverslips. The cells were imaged every 20 mins until MOMP (= cytochrome *c* release) and beyond. *Fixed sample processing:* The cells were then fixed with formaldehyde and IF was performed. *Correlative imaging:* The fixed and stained sample was then placed back on the microscope and with the help of a reference point on the coverslip, all positions were retrieved. The retrieved positions were then recorded with automated STED microscopy.

of the tagging, because a cytochrome *c* mutant has been shown to constitutively localize in the nucleus [210]. Though, as the cells divided normally in culture and released cytochrome *c* as expected, the nuclear localization was negligible.

After a certain amount of hours of live cell imaging, I fixed the cells and then labeled them with antibodies against TOM20 and BAX. After the IF staining was performed, I retrieved all the positions that were monitored during live-cell imaging with the help of a reference point on the coverslip. The cells at these positions were then imaged with automated STED microscopy (Figure 36B). This allowed me to record endogenous BAX rings and other structures, which I was able to link to defined time-

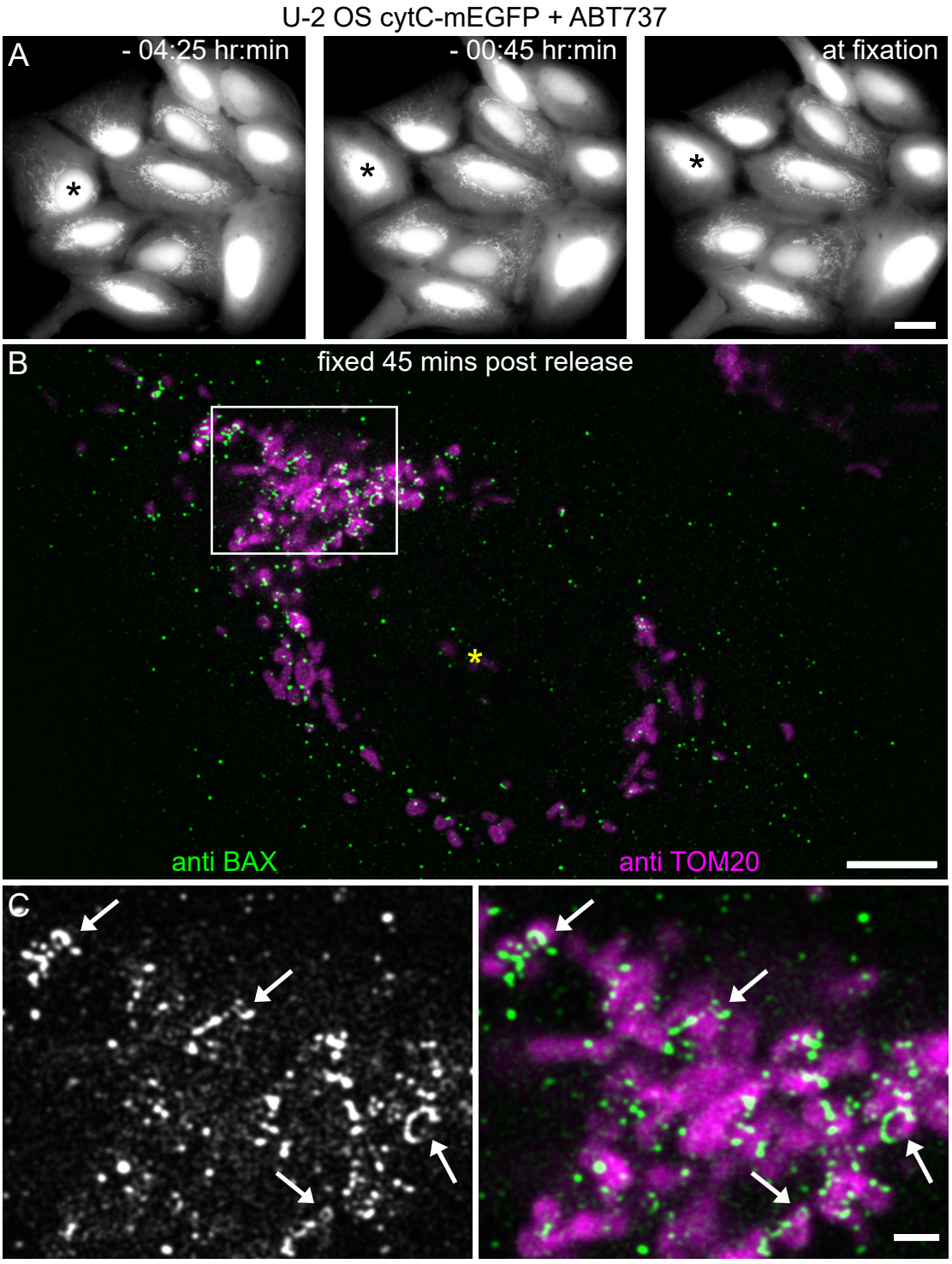

Figure 36: Cells with BAX rings post MOMP. (A) Three frames from a live cell widefield movie of U-2 OS cells undergoing apoptosis. The cells were stably overexpressing GFP-cytochrome C (gray). Movie starts 16h after addition of 10 µM ABT-737. 20 µM Q-VD-OPh was added to prevent the detachment of the cells from the coverslips. In this field of view one cell released cytochrome *c* during the imaging period (asterisk). Scale bar: 20 µm. **(B)** STED image of the same cell as the one with asterisk in (A), which was fixed 45 mins after cytochrome *c* release and then immunolabeled with the 2D2-BAX antibody (green) and an anti-TOM20 antibody (magenta). Scale bar: 5 µm. **(C)** Enlarged inset from (B) with BAX channel only (left) and a merge of TOM20 and BAX (right); arrows point at BAX rings. Scale bar: 1 µm.

points post-MOMP owing to the live cell recordings (Figure 36B-C).

Using this approach, I correlated MOMP (visualized by cytochrome *c* release) with the appearance of BAX rings, thereby adding temporal information to the super-resolved BAX images. I found that BAX rings appeared as early as 9 mins after MOMP but were also very long-lived. I still detected BAX rings in cells which had been fixed 9 hours after the release of cytochrome *c* (Figure 37). Again, these findings demonstrate the heterogeneity of apoptosis in onset and duration. The fact that BAX rings are still detectable up to 9 hours post MOMP is not in accordance with the live cell STED recordings in the first sections, where most of the mitochondria with rings collapsed after a couple of minutes and the whole cell usually detached from the coverslip after minutes to few hours. Also the live cell quantification showed that BAX overexpression eradicated a whole cell population after 10 hour. Therefore, these results substantiate that BAX overexpression intensifies apoptosis drastically and underscores the importance of investigating endogenous protein levels. In order to use this assay to also analyze BAK structures and especially the differences in time of appearance between BAX and BAK structures, a STED-compatible BAX-BAK labeling strategy needed to be established. Therefore, I developed and validated a dual-color antibody staining for BAX and BAK suitable for STED microscopy, which will be discussed in the next section.

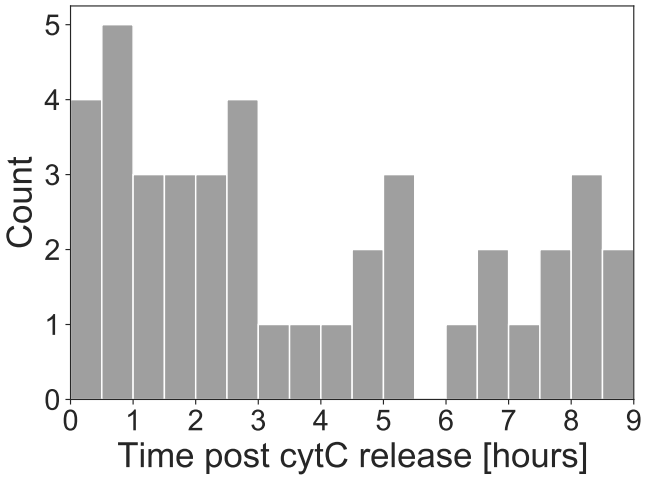

Figure 37: BAX rings are present in cells at various time points after cytochrome *c* release. Some cells already have BAX rings 10 mins after MOMP, others still have BAX rings 9 hours after MOMP, which was indicated by cytochrome *c* release. n=40 cells from one replicate. Bin width = 30 mins.

2.5 Endogenous BAX and BAK are both residing in apoptotic rings

In the previous section, I described the establishment of an assay to include temporal information in STED images of BAX in apoptosis, which revealed that BAX rings can be very long-lived and illustrated that it is crucial to investigate BCL-2 proteins at endogenous expression protein. In addition to BAX, BAK, the second effector protein of the BCL-2 family is thought to play a crucial role in forming the apoptotic pore. BAX and BAK are known to be the key players involved in MOMP and their co-localization has been shown previously [127, 146, 151, 167].

Therefore, to allow the investigation of the sub-diffractional localization of endogenous BAX and BAK simultaneously in the apoptotic pore, in the following sections, I established a dual-color antibody staining for STED microscopy of BAX and BAK in fixed cells uncovering apoptotic rings composed of both proteins. I validated the super-resolved structures with a different combination of antibodies. In addition to employing this labeling strategy in cultured cancer cell lines I was also able to reveal BAX-BAK rings in a non-cancerous cell line with this staining, which provides evidence that BAX-BAK-rings are physiologically relevant and a common phenomenon in apoptosis.

2.5.1 Dual-color antibody labeling approach imaged with STED microscopy reveals apoptotic rings comprised of BAX and BAK

In other studies, BAX or BAK rings have been investigated by re-expressing the proteins in KO cell lines [54, 167]. At endogenous protein levels, only BAX has been shown to form apoptotic rings by IF staining and STED microscopy [162]. In order to investigate both BAX and BAK together at endogenous levels, I established a dual-color antibody labeling approach of both proteins suitable for STED microscopy.

To this end, I treated U-2 OS cells with ActD and ABT-737, as well as Q-VD-OPh. The combination of ActD with the BH3-mimetic ABT-737 lead to a more uniform apoptosis induction over the whole cell population, so that most cells were apoptotic after 16-20 h of treatment, which allowed for the recording of a significant amount of images. After fixation, I labeled the endogenous proteins with BAX and BAK antibodies and detected them with secondary antibodies coupled to the STED-compatible dyes StarRed or AlexaFluor594.

In this work, I had already established the labeling of BAX with the 2D2-BAX antibody in a previous section. After testing multiple different BAK antibodies, I found a rabbit anti-BAK antibody (clone SU32-07, hereafter called SU32-BAK antibody, see Table 3) to perform well in combination with the 2D2-BAX antibody. With this BAX-BAK antibody combination I performed dual color STED microscopy of both markers

in U-2 OS cells with an additional marker in the confocal channel to label mitochondria (TOM20) (Figure 38). Like before, untreated cells showed a negligible, smooth cytosolic background staining in the BAX channel. As BAK resides canonically on the mitochondria, the labeling with the SU32-BAK antibody showed a general mitochondrial background stain. This signal was dim in comparison to the signal in apoptotic cells, so that it was easily distinguishable from the apoptotic BAK structures.

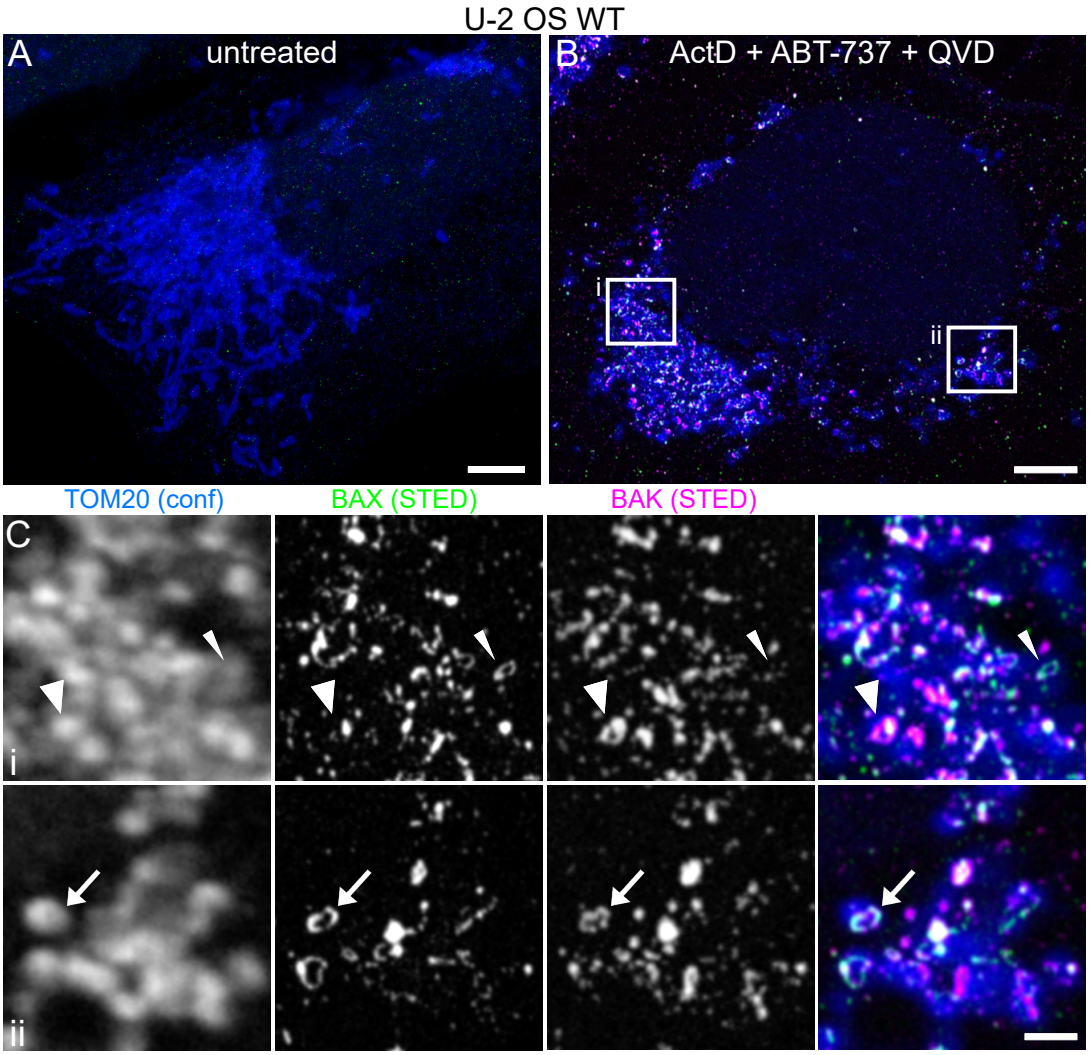

Figure 38: BAX and BAK are both residing in apoptotic rings. STED images of **(A)** untreated or **(B)** treated U-2 OS cells. The cells were treated with 10 µM ActD and 10 µM ABT-737 for 18h. 20 µM Q-VD-OPh was added to prevent the detachment of the cells from the coverslips. The cells were then fixed and immunolabeled with the 2D2-BAX antibody (STED, green), the SU32-BAK antibody (STED, magenta) and an anti-TOM20 antibody (confocal, blue). STED channels were background-subtracted and smoothed for illustration purposes. Scale bars: 5 µm. **(C)** Enlarged insets from (B). (i) Some rings consist mainly of BAK (large arrowhead) or BAX (narrow arrowhead). (ii) The by far most abundant form of rings contains both BAX and BAK (arrow). Scale bar: 1 µm.

In the resulting dual-color STED images of endogenous BAX and BAK in apoptotic cells, I observed many different structures (Figure 38A vs B). These structures con-

sisted mainly of clusters and rings as well as less frequent lines. Most of the structures and specifically the rings contained both BAX and BAK, and very few rings contained only one (or almost exclusively one) of the two proteins (Figure 38C, arrows and arrowheads). Before quantitatively analyzing and interpreting the imaging data, I first set out to corroborate the finding that most of the rings are composed of BAX and BAK.

2.5.2 Validation of BAX-BAK staining with different antibodies

In order to validate the structures observed with the BAX-BAK double antibody staining, I set out to find a different combination of antibodies with the inverse host species. After testing multiple different antibodies, I found a rabbit anti-BAX antibody which detects specific structures in apoptotic cells and produces a bright signal (clone 1C7, hereafter called 1C7-BAX antibody). I also found a mouse anti-BAK antibody, which labels the target, but has a higher background and lower signal intensity. In the end, it proved functional for the purpose, though (Bak AB-1, hereafter called AB1-BAK antibody, see Table 3). With this new BAX-BAK antibody combination, I was equally able to label apoptotic structures consisting of BAX and BAK (Figure 39). Similar to the inverse labeling strategy I had developed earlier, I found rings, lines and clusters. Indeed, almost all of the structures were made up of both BAX and BAK also in this staining. This second antibody combination thus confirmed the existence of apoptotic BAX-BAK-structures, especially rings, in an endogenous setting independently of the used antibodies. These findings suggest that although both proteins can induce apoptosis independently upon overexpression, under physiological conditions BAX and BAK cooperate to form apoptotic pores. To substantiate the physiological relevance of the discovered structures, I chose to employ the staining on a non-cancerous cell line in the next section.

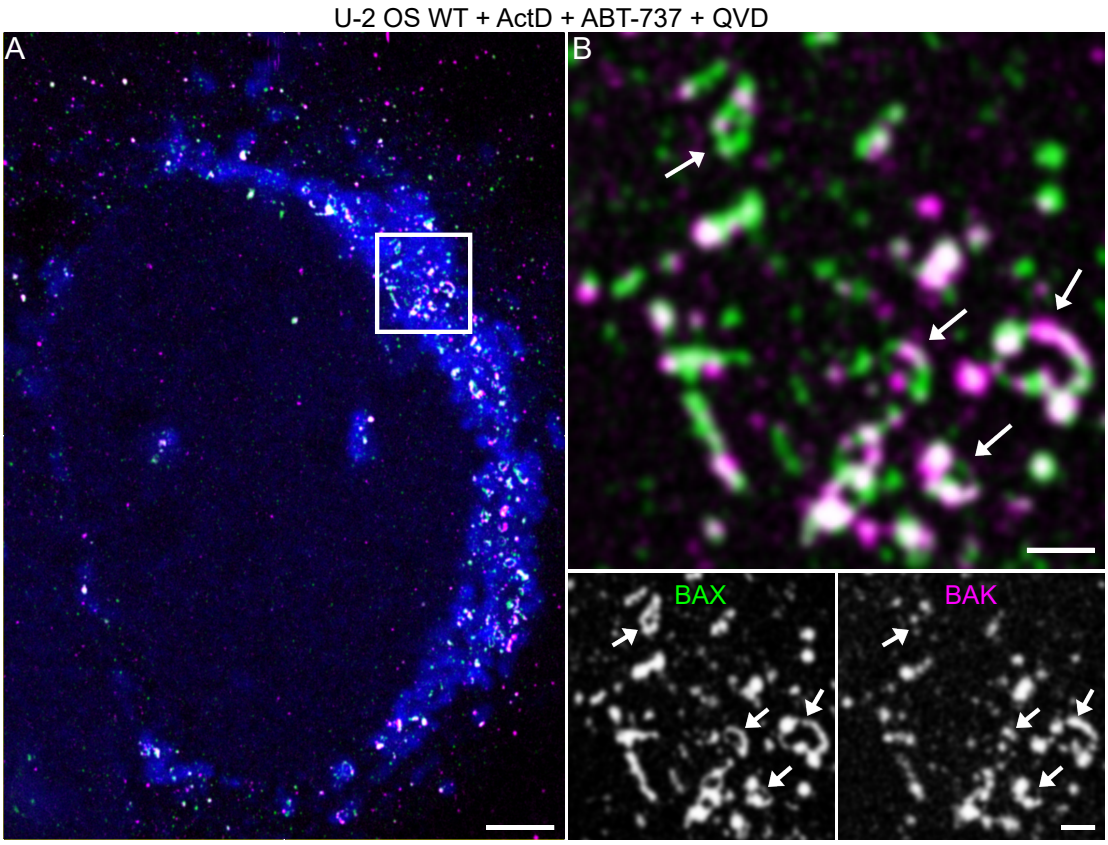

Figure 39: BAX-BAK rings can also be detected with a different antibody combination. **(A)** STED image of U-2 OS cell treated with 10 µM ActD and 10 µM ABT-737 for 20 h. 20 µM Q-VD-OPh was added to prevent the detachment of the cells from the coverslips. The cells were immunolabeled with the 1C7-BAX antibody (STED, green), the AB1-BAK antibody (STED, magenta) and an anti-TOM20 antibody (confocal, blue). Scale bar: 3 µm. **(B)** Enlarged inset from (A) showing rings (arrows). Scale bar: 1 µm.

2.5.3 BAX-BAK rings also appear during apoptosis in primary cells

So far, I had performed all experiments in the osteosarcoma cell line U-2 OS. To investigate, whether endogenous BAX-BAK rings are also a common phenomenon of apoptosis in non-cancerous cells, I used human dermal fibroblasts from adult tissue (HDFAs). I treated and immunolabeled the HDFAs with ActD and ABT-737, as well as Q-VD-OPh, and performed STED microscopy. Although HDFAs shrink substantially when they become apoptotic, which makes it difficult to locate them, I was able to identify apoptotic HDFAs (Figure 40A). The cells displayed apoptotic structures and especially rings consisting of BAX and BAK (Figure 40B). This confirms that apoptotic rings comprised of endogenous BAX and BAK indeed occur in non-cancerous cell types. The finding of BAX-BAK rings in non-cancerous cells is valuable for the basic understanding of apoptosis because cancer cell lines are often heavily mutated and do not reflect the physiological situation in the human body. Therefore, the apoptotic rings comprised of BAX and BAK in primary cells confirm that coop-

erative ring formation is a physiological phenomenon, which occurs commonly in human cells.

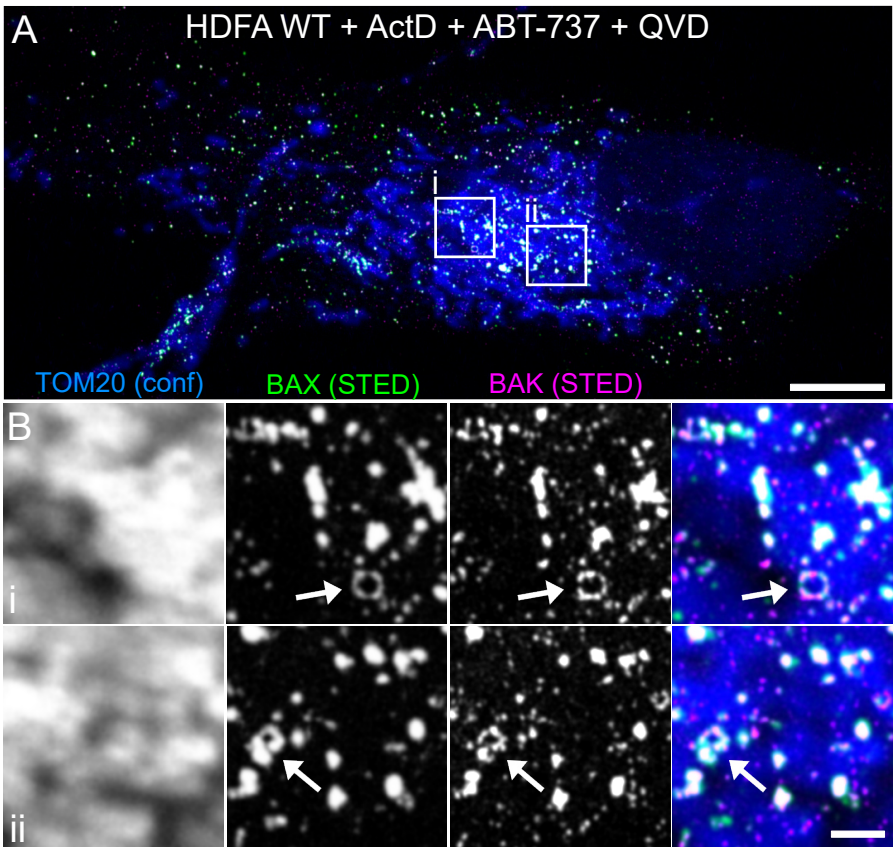

Figure 40: Rings composed of BAX and BAK are common in non-cancerous apoptotic cells. **(A)** STED image of human dermal fibroblasts from adult tissue (HDFAs) treated with 10 µM ActD and 10 µM ABT-737 for 20 h. 20 µM Q-VD-OPh was added to prevent the detachment of the cells from the coverslips. The cells were immunolabeled with the 2D2-BAX antibody (STED, green), the SU32-BAK antibody (STED, magenta) and an anti-TOM20 antibody (confocal, blue). STED channels were background-subtracted and smoothed for illustration purposes. Scale bar: 5 µm. **(B)** Enlarged insets from (A) showing BAX-BAK rings (arrows). Scale bar: 1 µm.

2.6 Semi-automated image analysis reveals heterogeneity of BAX-BAK rings

By investigating endogenous BAX and BAK with immunofluorescence (IF) stainings and dual-color STED microscopy, I showed in the previous section that both pore-forming BCL-2 proteins mostly compose the apoptotic rings together and only rarely form rings or other structures without their partner. In the following sections, I will quantify the properties of the apoptotic rings, by analyzing their size, the relative amount of BAX and BAK as well as their spatial correlation in the rings. To this end, I created a semi-automated image analysis pipeline including manual annotation of the rings, an automated FIJI [211] script to extract the information from the annotated images as well as different Python scripts to calculate and visualize the data. The analysis revealed that most rings vary in size from 0.5 to 2.5 μm with some reaching circumferences of almost 4 μm. I also found that almost exclusively all rings are composed of both BAX and BAK but that in general, rings tend to contain more BAK than BAX. However, the distribution varied drastically from ring to ring and larger rings tended to have more equal amounts of BAX and BAK. Furthermore, most rings had positively correlated BAX and BAK, meaning that BAX and BAK clusters tend to occur together at the same positions along the ring outline. Some rings also showed an anti-correlated pattern of BAX and BAK, which means that they are regularly or irregularly alternating along the ring circumference. These results are presented in detail in the next sections.

2.6.1 Line profiles of BAX and BAK along the ring

Already when attentively scrutinizing the STED images of BAX and BAK staining by eye, it became apparent that the apoptotic rings had different sizes and that the two apoptotic pore-forming members of the BCL-2 protein family covered varying amounts of the ring outline. Furthermore, they showed a variety of distribution patterns along the rings (Figure 41). Some rings were very small, others were large enough to be detected by confocal microscopy. Although some rings consisted largely of only BAX or BAK, most of them contained both proteins. Interestingly, some rings had strongly overlapping BAX and BAK signal (Figure 41, panel 1), whereas others showed a more heterogeneous distribution (Figure 41, panels 2-4).

In order to quantify all of these ring properties, I annotated the outline of 530 rings from three independent experiments manually in FIJI (Figure 42A). To ensure equal resolution for both markers, in three independent experiments, I had placed either the BAX or BAK antibody on the STED channel with the better resolution (StarRed) for 50 % of the cases. The fluorescence intensity values along the line profile of both

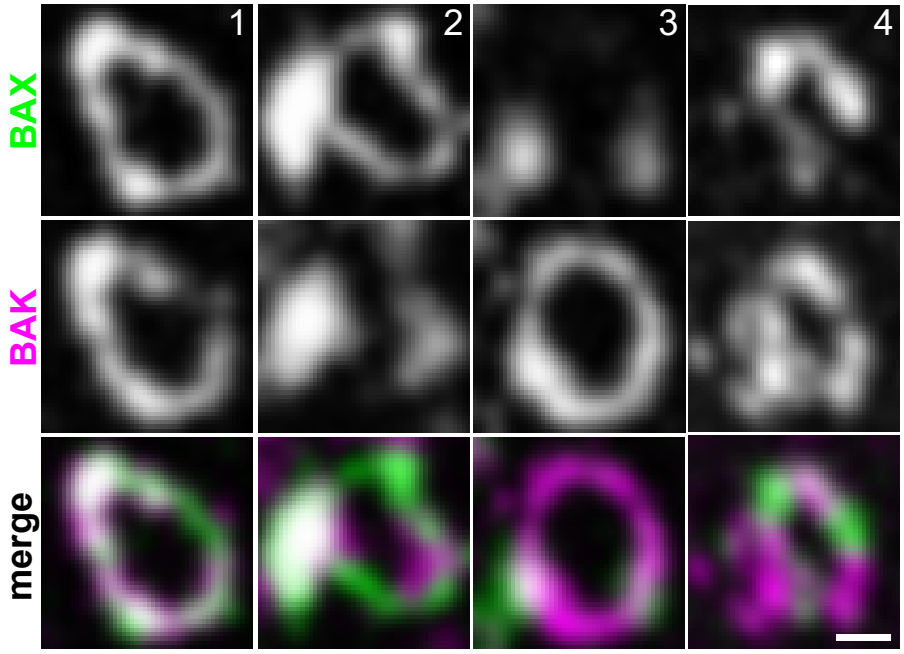

Figure 41: BAX and BAK show a heterogeneous distribution in the rings. Examples of apoptotic rings from different cells that contain different distributions of BAX and BAK. Treatment, labeling and image processing for representation as in Figure 38. Scale bar: 200 nm.

the BAX and BAK channel were measured with an automated FIJI script and saved as tables which could be visualized in the form of line plots along the ring circumference (Figure 42B, see methods section 4.10.2 and FIJI code in appendix A.1). Note, that it was crucial to label both BAX and BAK in order to visualize full rings. Still, there were numerous rings with smaller or larger segments along their outline, which displayed very little signal or were completely devoid of either BAX or BAK or both. These dimmer signals and voids, which are reflected by valleys in the line profile plots, could result from an insufficient antibody labeling, or because another protein occupies these spaces, or because the pore rim is indeed not fully covered by proteins. Many of the ring outlines also contained one or more large BAX and/or BAK cluster.

2.6.2 Ring size and BAX/BAK content varies greatly

To measure the size of the rings, I calculated the length of the line profile which is equal to the ring circumference. The rings' circumferences ranged from 0.43 to 3.81 µm with a median of 1.21 µm (Figure 43A).
Assuming that the rings were perfect circles, this would correspond to diameters of 140 to 1210 nm with a median of 380 nm. Note however, that the rings were recorded in 2D and were therefore skewed depending on their position relative to the image plane. Furthermore, unlike nuclear pores for example, only very few of the rings actually are perfect rings. To assess the circularity of the rings, I used the measure for

roundness, which is defined as:

$$Roundness = \frac{4 * Area}{\pi * MajorAxis^2}$$

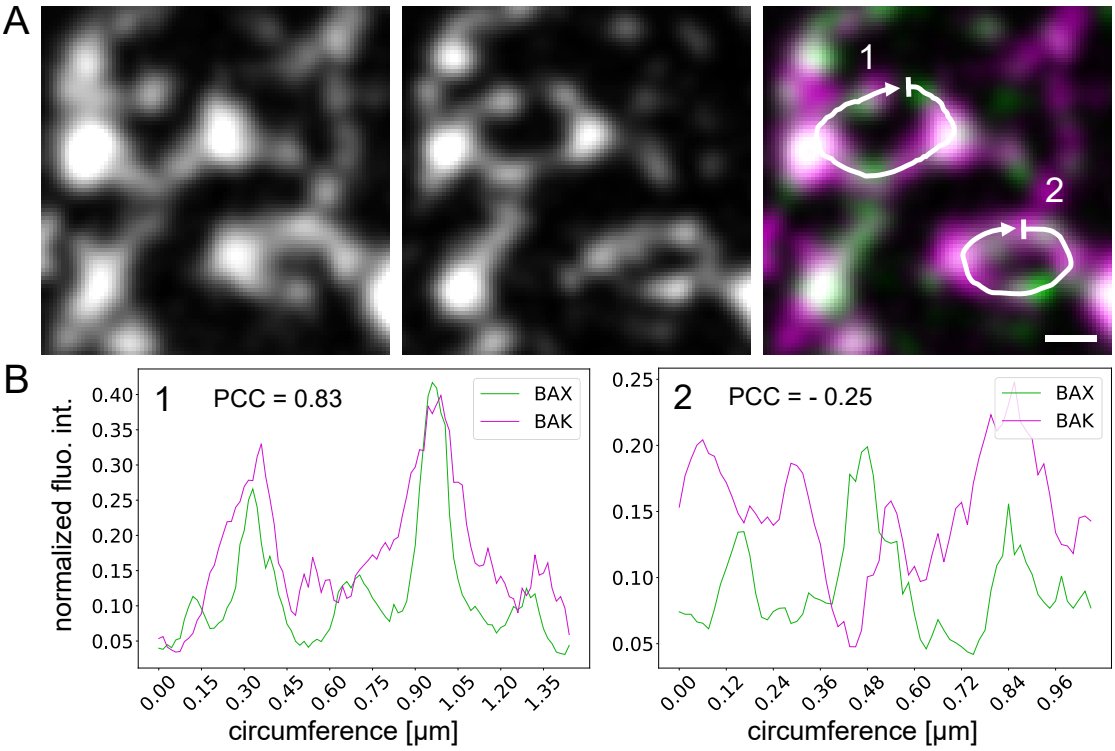

Figure 42: Representative line profiles along BAX-BAK rings. **(A)** Two adjacent rings in apoptotic U-2 OS cells with line profiles drawn along the direction of the arrows. Scale bar = 200 nm. **(B)** The line profiles were enlarged to a 5 pixel wide line. The fluorescence intensity raw data were normalized to the fluorescence intensity (fluo. int.) of all rings in the same sample. PCC = Pearson Correlation Coefficient.

For each ring, it gives a value between 1 (perfect circle) and 0 (line). For example, an ellipse with a major axis of twice the size of the minor axis would have a roundness of 0.5. The roundness of 530 rings ranged from 0.35 to 0.99 with a median of 0.77 (Figure 43B).

Overall, the obtained diameters are in good accordance with previously published values of endogenous BAX rings [162] but they are slightly larger than previously measured diameters of overexpressed BAX or BAK rings [163, 167].

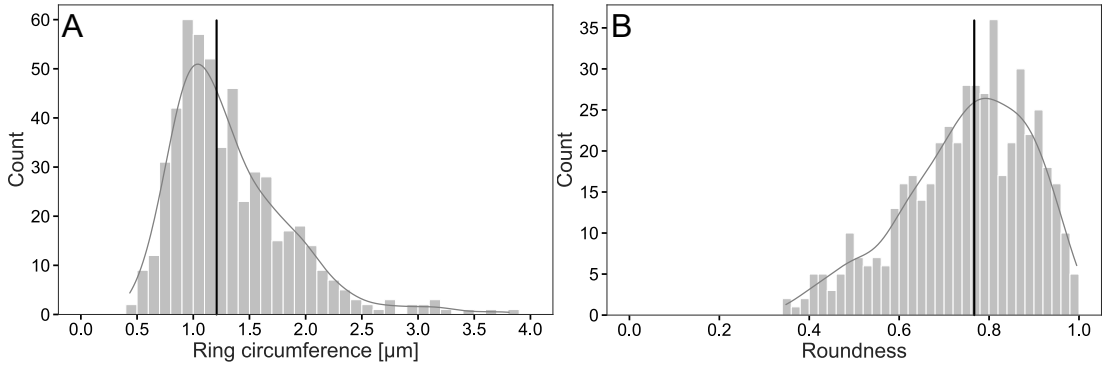

Figure 43: Circumference and roundness of BAX-BAK rings. (A) The circumference of BAX-BAK rings ranges from 0.43 to 3.81 µm. Vertical black line shows median of 1.21 µm. Bin width = 100 nm. **(B)** The roundness of BAX-BAK rings ranges from 0.35 to 0.99. Vertical black line shows median of 0.77. Bin width = 0.02. **(A and B)** Lines representing continuous data was obtained via a kernel density estimation with a Gaussian kernel. n = 530 rings from three independent experiments.

To get a better understanding of the molecular composition of the rings, I investigated their relative BAX and BAK content. For this, I measured the minimal and maximal fluorescence intensity values of BAX and BAK in all annotated ring line profiles. I normalized the individual fluorescence intensity values to the minimal and maximal values of the corresponding sample. I then determined the prevalent protein in the ring by summing up the normalized fluorescence intensity values of BAX or BAK along the ring (Python code in Appendix B.1). In 530 rings, BAK was on average more prevalent in the rings than BAX, occupying between 20 and 100 % of the ring outline with a median of 64 %. BAX was accordingly occupying between 0 and 80% of the ring outline with a median of 36 % (Figure 44).
I next analyzed whether the relative amounts of BAX and BAK would change with regards to the ring length. I calculated a rolling mean over the data (Python code in appendix B.2) and found that with increasing ring size, the mean of the relative amounts of BAX and BAK in the ring approached 50 % (Figure 45). This suggests that BAX and BAK are needed to be present in an equal ratio in order to form large rings.

2.6.3 BAX and BAK are spatially correlated in the rings

In the previous section, I showed that BAX and BAK appear together in apoptotic rings. Each of the two proteins covered varying amounts of the ring outline and BAK was generally more prominent in the rings. However, the previous analysis did not consider their spatial distribution along the rings. Therefore, I set out to investigate the positioning of BAX and BAK along the ring outline with regards to each other.

A core BAX (or BAK) dimer in the apoptotic pore has a size of around 4 nm [153]. With unlimited resolution in all three dimensions, it would be possible to resolve in-

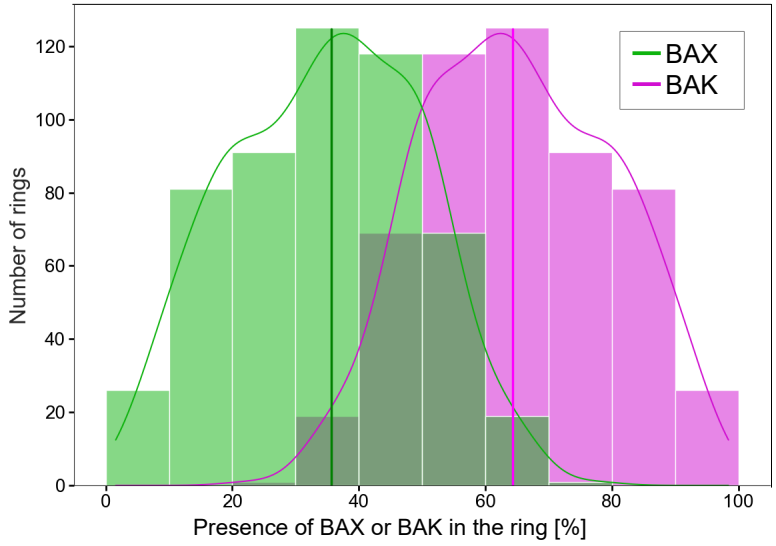

Figure 44: BAK is more prevalent in the rings. Relative amounts of ring outline occupied by BAX (green) and BAK (magenta) in the ring are plotted. Vertical lines show medians of 36 % for BAX and 64 % for BAK. Bin width = 10 %. Lines representing continuous data are obtained via a kernel density estimation with a Gaussian kernel. n = 530 rings in three independent experiments.

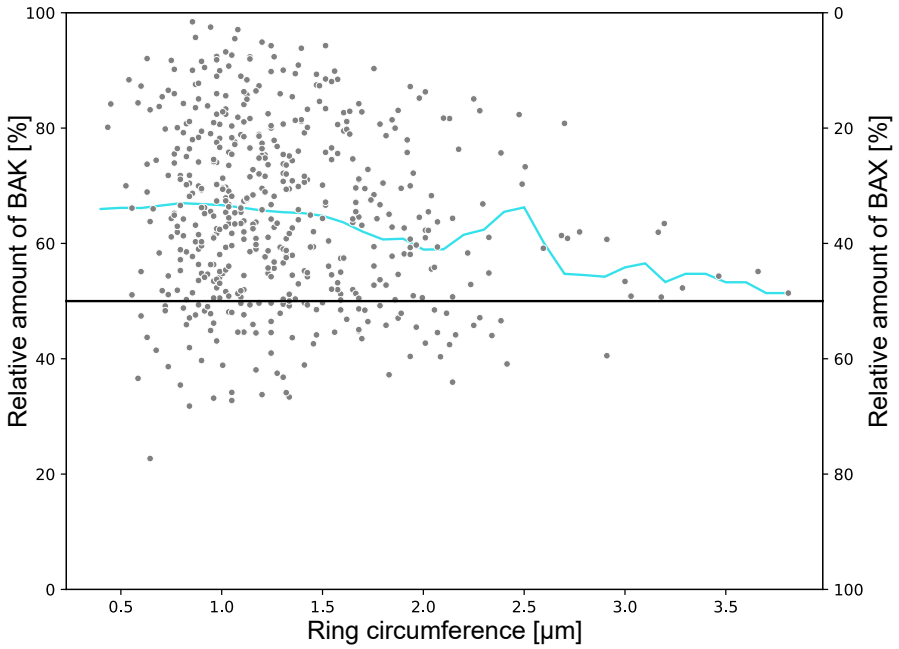

Figure 45: Relative amounts of ring outline occupied by BAX and BAK approach 50 % in larger rings. Relative amounts of BAK (left y-axis) and BAX (right y-axis) are plotted against the ring length (circumference). Black horizontal line at 50% shows equal distribution of BAX and BAK along the ring. Turquoise line shows rolling mean of BAX/BAK content over windows of 400 nm length with a stepsize of 100 nm. n = 530 rings of three independent experiments.

dividual BAX and BAK molecules. In this case, the images of rings would be expected to show mutually exclusive BAX and BAK signals, because one molecule cannot occupy the same space as another molecule. For biological applications, though, the

resolution in STED microscopy is in practice limited to around 50 nm. Thus, in a STED image, every 4 nm BAX or BAK dimer appears as a blurred 50 nm spot. This limitation makes it impossible to resolve how many BAX and/or BAK molecules are present within an area of 50 nm, or how they are distributed with regards to each other in this area. Therefore, only spots of 50 nm in size and above can be considered.

In practice, the line profiles of BAX and BAK along the ring are continuous intensity value distributions. Individual clusters of BAX or BAK can not be determined as there are no defined borders in between the intensity peaks and valleys of the BAX or BAK line profiles (see line profiles in Figure 42B). To circumvent this issue, I asked whether BAX and BAK follow the same overall distribution pattern along the ring outline. This analysis determined whether they tended to appear together on a larger scale or whether they followed an independent or alternating distribution pattern.

To determine the degree of correlation of the BAX and BAK distribution patterns along the ring outline, I calculated the Pearson correlation coefficient (PCC) of the normalized fluorescence intensities along the line profiles for each ring (Python code in Appendix B.3). BAX and BAK intensity values are represented by x and y in the following formula for the PCC [212, 213, 214]:

$$PCC = \frac{\sum_{i=1}^{n}(x_i - \bar{x})(y_i - \bar{y})}{\sqrt{\sum_{i=1}^{n}(x_i - \bar{x})^2}\sqrt{\sum_{i=1}^{n}(y_i - \bar{y})^2}}$$

This analysis of the spatial correlation between the BAX and BAK line profiles allowed to investigate whether the molecules co-localized along the ring. A PCC of 1 reflects perfect correlation, i.e. co-localization. The BAX and BAK molecules in this case would always appear together. A PCC of -1 reflects perfect anti-correlation, i.e. a (regularly or irregularly) alternating pattern of BAX and BAK on the large scale (Figure 46A). A PCC of 0 would reflect a random distribution, where the two molecules are distributed in an independent manner from each other.

When calculating the PCCs of 530 ring line profiles, I found a distribution from -0.74 to 0.98 with a median of 0.47 (Figure 46B). The dataset thus represents a population of rings with most PCCs in the positive range. The positive correlation indicates that in most rings BAX and BAK clusters overlap to some extent at the same positions along the rings. The overlap occurs more than would be expected by chance in a random distribution. In the rings with negative PCCs, many or most BAX and BAK clusters are arranged in an alternating, mutually exclusive distribution, which I had also observed before (e. g. ring examples in Figure 41, panel 4). In summary, the wide distribution of the PCCs of BAX and BAK with a positive median corroborates the visual impressions from the STED data: 1) that a vast variety of rings with differ-

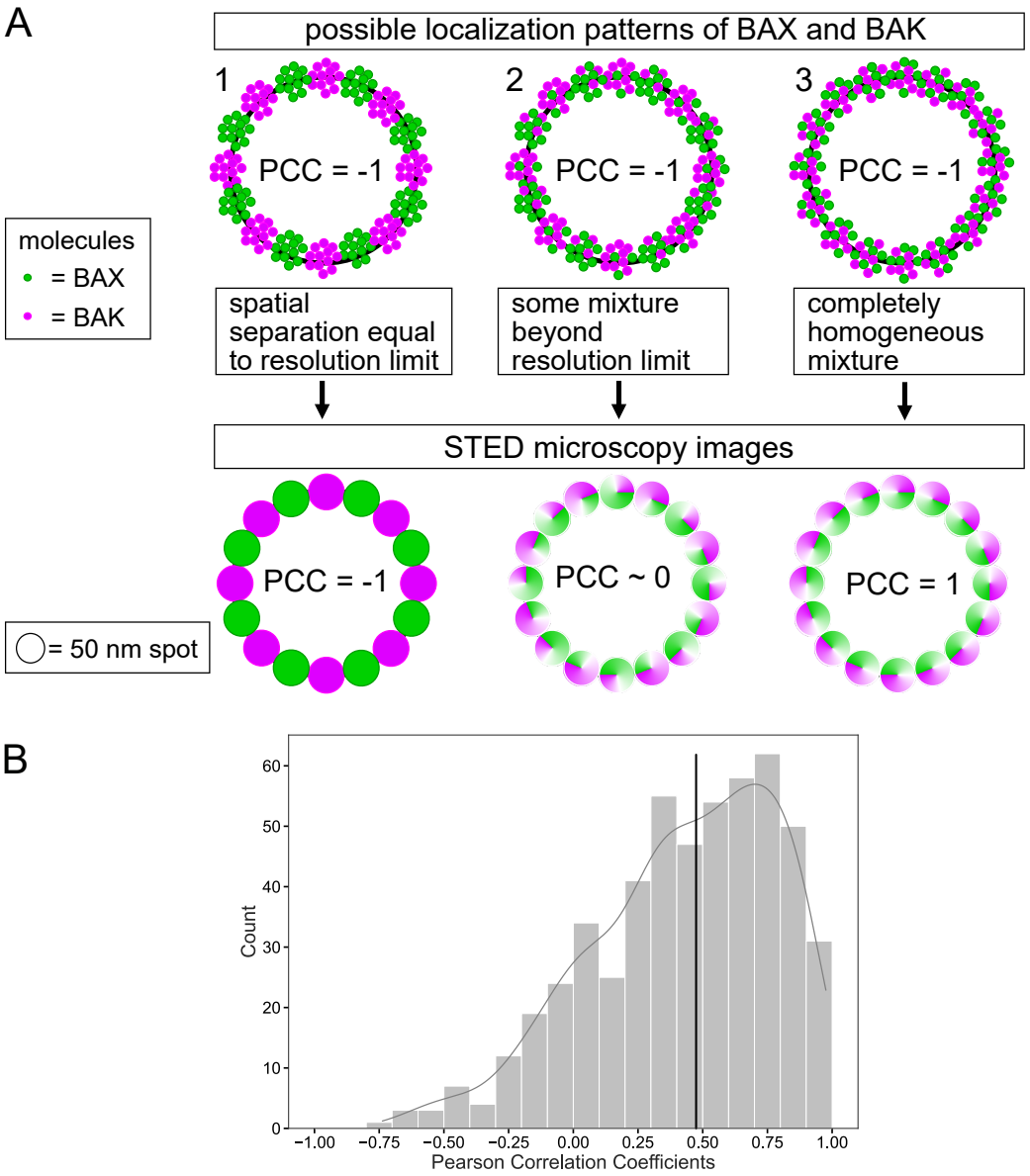

Figure 46: In most rings BAX and BAK are positively correlated to various extents. (A) Schematic of BAX (green) and BAK (magenta) molecules (not drawn to scale) in apoptotic rings. In the actual sample (top row), BAX and BAK molecules never occupy the same space and therefore always have a Pearson correlation coefficient (PCC) of -1, which reflects perfect anti-correlation. When the rings are imaged with STED microscopy (bottom row), the smallest possible resolution is 50 nm. If BAX and BAK were (regularly or irregularly) alternating on this scale (scenario 1), they would result in a PCC of -1 even with STED microscopy. If they were arranged in a rather random or mixed distribution, meaning that sometimes there are some BAX molecules intermixed in a group of BAK molecules and vice versa (scenario 2), this would result in some of the 50 nm spots to appear more green and others more magenta leading to a PCC between -1 and 1. If the BAX and BAK molecules were appearing in the same spots to the same extent together along the ring outline (scenario 3), in a STED image, every 50 nm spot would harbor the same amount of green and magenta, which would result in a PCC of 1, which reflects perfect correlation, i.e. co-localization. Note, that these schematics are oversimplified perfect world examples and do not reflect the heterogeneity of the rings, which is better represented by the actual PCCs: **(B)** The PCC of BAX and BAK ranged from - 0.74 to 0.98 with a median at 0.47 (vertical black line). Bin width = 0.1. Line representing continuous data was obtained via a kernel density estimation with a Gaussian kernel. n = 530 rings of three independent experiments.

ent distribution patterns of BAX and BAK exists and 2) that in most rings BAX and BAK clusters tend to overlap along the outline of the ring rather than exclude each other or localize in an independent, random manner.

2.6.4 Pearson correlation coefficient is dependent on amount of BAX vs BAK and ring size

In the previous section, I found various degrees of positive correlation between BAX and BAK, which suggests that they have a tendency to cluster together in a non-random manner along the outline of the apoptotic pore instead of alternating along the ring outline. However, the PCC does not include the abundance of BAX and BAX, because it only analyzes whether the data follow the same overall trajectory.

Therefore, I next investigated whether there was a link between the spatial correlation of BAX and BAK (i.e. PCC) and their relative abundance in the ring. I discovered a slight trend that rings with a higher relative BAK content had a lower mean PCC of BAX and BAK. This suggests that only if there is sufficient amount of BAX present in the ring, it will cluster together with BAK. Otherwise, in rings with more BAK content the small number of corresponding BAX clusters is slightly less likely to follow the same pattern as the BAK signal. Instead it is more likely to be randomly distributed together with or even interspersed into the BAK clusters.

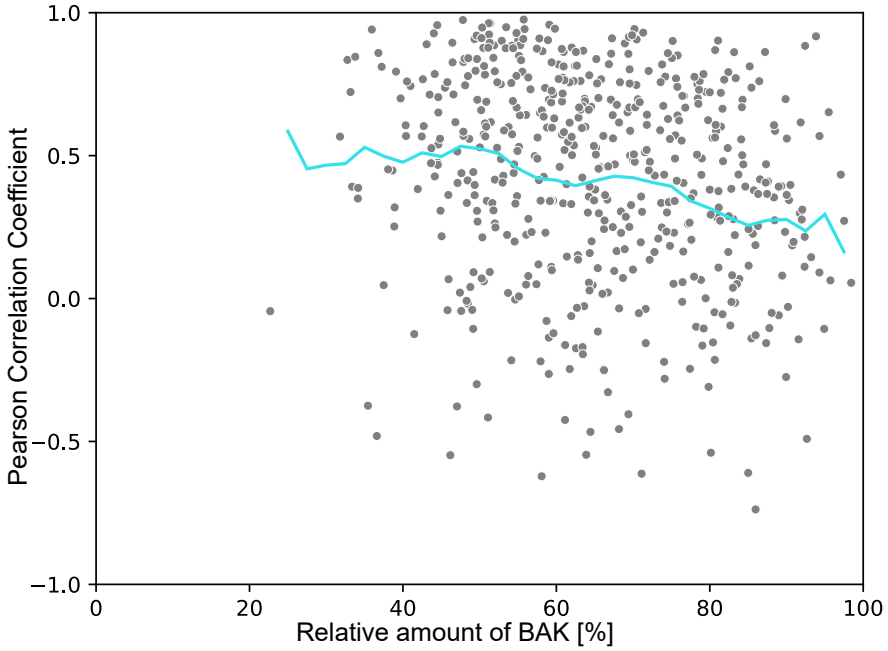

Figure 47: Rings with a higher amount of BAK have a lower PCC. PCCs of BAX and BAK in the rings were plotted with regard to the amount of BAK in the ring. Turquoise line shows rolling mean of PCC over windows of 10 % BAK content with a stepsize of 2.5 %. n = 530 rings of three independent experiments.

The calculations so far did not take the ring size into account. Therefore, I asked whether the PCC of BAX and BAK changed with different ring sizes. I observed that larger rings had more positively correlated BAX and BAK (Figure 48). This result suggests that larger rings contain more positions along their outline where BAX and BAK occur together. This could simply be due to the fact, that larger rings contain a larger outline, where overlap could happen by chance. On the other hand, I have shown in previous sections that larger rings have more similar amounts of BAX and BAK (Figure 45). And more equal amounts of BAX and BAK result in a higher PCC (Figure 47). Which property is causative of which can not be determined without further experiments.

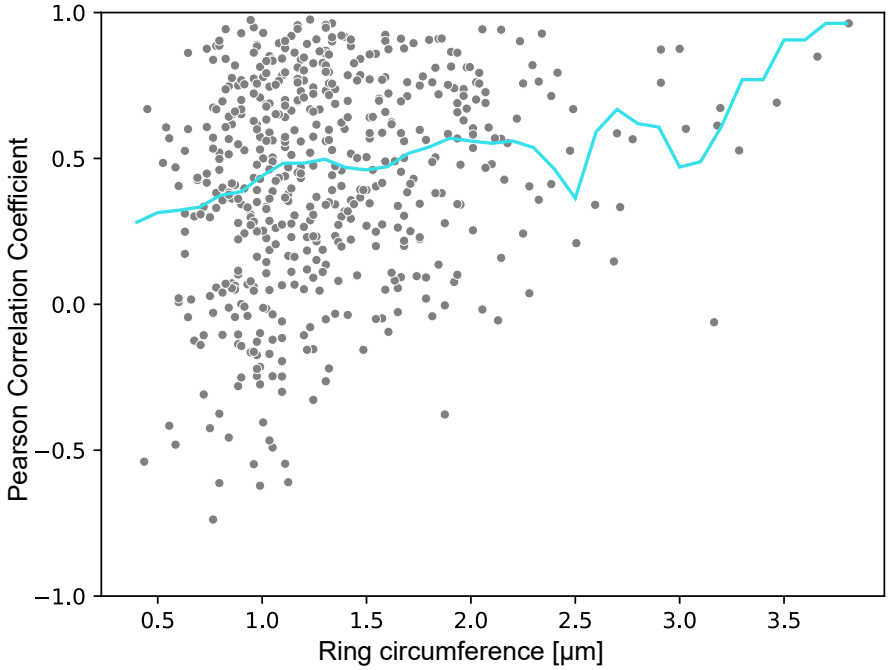

Figure 48: Pearson correlation coefficient (PCC) shows a positive trend towards larger rings. Smaller rings have all variations of correlation of BAX and BAK. Larger rings tend to cluster on the positive PCC end of the spectrum. Turquoise line shows rolling mean of PCC content over windows of 400 nm ring circumference with a stepsize of 100 nm. n = 530 rings of three independent experiments.

In conclusion, rings came in a variety of sizes, BAX-BAK amounts and PCC. The ring circumference ranged from 0.43 to 3.81 µm. The PCC varied from negative to positive with a positive median at 0.47. Generally, larger rings tended to have more equal amounts of BAX and BAK and a higher PCC. Together, these analyses revealed that together with a growing ring, an assimilation arises between the BAX and BAK localization patterns. This similar pattern is not prevailing initially, as smaller rings generally contained more BAK and had a lower PCC. These results will contribute to further elucidate the properties of the apoptotic pore in a cellular context and provide directions for future research in targeting the apoptotic pore with specific drugs.

2.7 BAX and BAK are able to form apoptotic rings independently

In previous sections in this work, I demonstrated that BAX and BAK are residing together in apoptotic rings of varying sizes. I furthermore showed that they have a tendency to cluster together at positions along the ring outlines, although the relative abundance of BAX and BAK in the rings can differ drastically. Furthermore, I showed in the first section of my work that BAX and BAK overexpression alone triggered apoptosis and when imaged with super-resolution STED microscopy, the proteins were found to form, among other structures, rings on the mitochondria. The fact that BAX and BAK are capable of forming rings independently that line the apoptotic pore was corroborated by studies, in which the two proteins were overexpressed in cells on a DKO background and also formed rings [163, 167]. In line with this, it has been described in literature that BAX and BAK have redundant functions in apoptosis, dependent on cell type and which agents were used to induce apoptosis [116]. Both proteins have to be knocked out for impaired developmental apoptosis in mice [112]. However, it is unknown whether the endogenous proteins are also capable of forming rings without their partner. Therefore, I will show in the following sections, how I generated BAX and BAK single KO cell lines in U-2 OS via CRISPR/Cas9 as well as a BAX-BAK-DKO control cell line and investigated whether BAX or BAK alone at endogenous expression levels were still able to form rings during apoptosis.

2.7.1 Generation of U-2 OS BAX and BAK single and double-KO cell lines

In order to generate BAX or BAK single knockout (KO) cell lines, I transfected U-2 OS WT cells with Cas9 plasmids containing gRNAs targeting Exon 1 of BAX or BAK. For the double-KO (DKO) cell line both plasmids were transfected simultaneously. After confirmation of protein depletion by Western blot (WB) (Figure 49A) with the E63-BAX and polyclonal anti-BAK antibodies (see Table 2), individual cell clones were investigated by IF staining with the 2D2-BAX antibody and the SU32-BAK antibody (see Table 3) and subsequent microscopy recordings. Indeed, the IF staining confirmed the absence of the proteins in the respective KO clones (Figure 49B).
To confirm the KO on a genomic level, I amplified the region around the cut site of Cas9 in Exon 1 by PCR from genomic DNA, the individual alleles were separated by TOPO cloning and sent for subsequent Sanger sequencing. No WT alleles were found in these sequences, indicating a homozygous disruption of the BAX and BAK gene, respectively.

2.7.1.1 Importance of antibody recognition site for KO confirmation

The genomic locus of BAX in U-2 OS has three alleles [215, 216]. After a DNA dou-

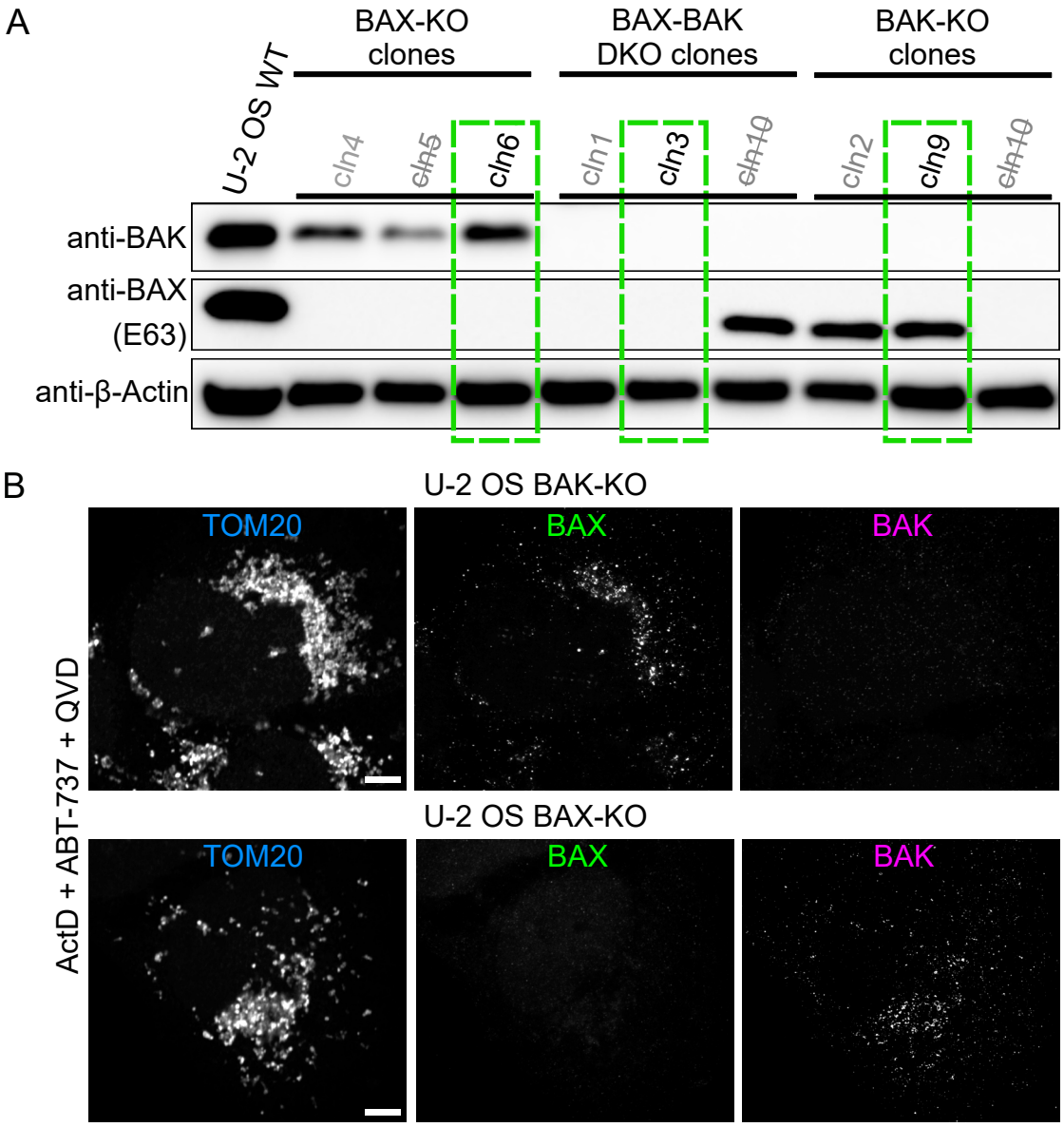

Figure 49: BAX and BAK KO clone validation by WB and IF. (A) WB analysis of potential KO clones. E63-BAX and polyclonal anti-BAK antibodies were used. The selected final clones are highlighted by green dashed line. β-Actin was used as loading control. **(B)** Confocal images of IF staining of U-2 OS KO cells treated with 10 µM ActD and 10 µM ABT-737 for 20 h. 20 µM Q-VD-OPh was added to prevent the detachment of the cells from the coverslips. The cells were immunolabeled with 2D2-BAX antibody (STED, green), SU32-BAK antibody (STED, magenta) and anti-TOM20 (confocal, blue). Scale bar: 5 µm.

ble strand break obtained by CRISPR/Cas9, the genomic locus is usually repaired by non-homologous end-joining (NHEJ). NHEJ restores each allele separately in a random manner [217]. Frequently, this repair mechanism leads to a frame-shift, a large deletion or insertion and the gene becomes defective and therefore knocked-out.

To obtain detailed information about the genomic rearrangements introduced by NHEJ after CRISPR/Cas9 in the selected clones, I performed Next Generation Sequencing (NGS). NGS yields a deeper sequence coverage than Sanger sequencing

(hundreds to thousands of reads for a PCR fragment versus one read per every colony picked in the TOPO cloning + Sanger sequencing method).

The NGS result of the alleged BAX KO (clone 6) confirmed the genomic rearrangements observed in Sanger sequencing. However, surprisingly, one allele, which was not found previously, showed a triple T insertion right after the cut site of Cas9. This triplet insertion led to a conversion of Glycine 10 to Valine and Cysteine. One of three BAX alleles was thus still translated without a frame shift, but with an in-frame insertion of one amino acid (Figure 50).

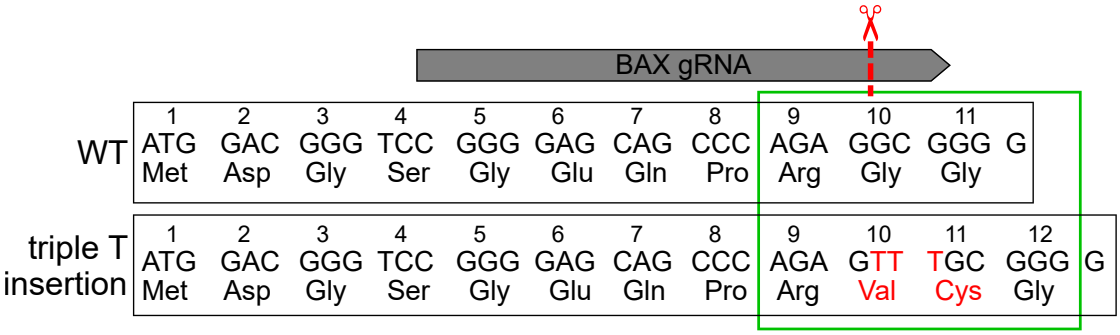

Figure 50: CRISPR/Cas9 modifications in BAX locus led to epitope mutation by triple T insertion. Genomic region of BAX surrounding the cut site of Cas9 (red dashed line), which is determined by the gRNA (gray, on top). Top sequence = WT, bottom sequence = Triple T insertion via NHEJ, converting Glycine 10 into Valine and Cystein (red letters). Part of the epitope recognition site of the E63-BAX antibody used for Western blotting (amino acids in green box) is destroyed by the mutation.

If an antibody is commercially available, the peptide sequence of the immunogen used to produce the antibody is generally proprietary. This was also the case for the E63-anti-BAX antibody, which I had previously used for Western blotting. The supplier homepage stated about the immunogen (July 2022): "Synthetic peptide within Human Bax aa 1-100 (N terminal). The exact sequence is proprietary." After obtaining information that the antibody binds exactly around amino acid 10, which is targeted by the CRISPR/Cas9 approach (Figure 50), I used a different antibody, anti-BAX-EPR18284, which binds further C-terminal in the protein. Indeed, this new antibody could detect BAX protein in the assumed BAX KO (clone 6), which falsified the previously confirmed results and proved that clone 6 is not a KO after all, which was thus discarded (Figure 51).

These results showed the importance of identifying the exact biding site of the detection antibody in the protein of interest and deep sequencing with NGS. An absent band in the Western blot did not proof a knock-out.

The 2D2-BAX antibody, which I had used for IF staining (Figure 49), surprisingly neither revealed any BAX structures in the presumed BAX-KO. Whether it also binds the BAX epitope at the triple T insertion position of BAX and thereby was not able to

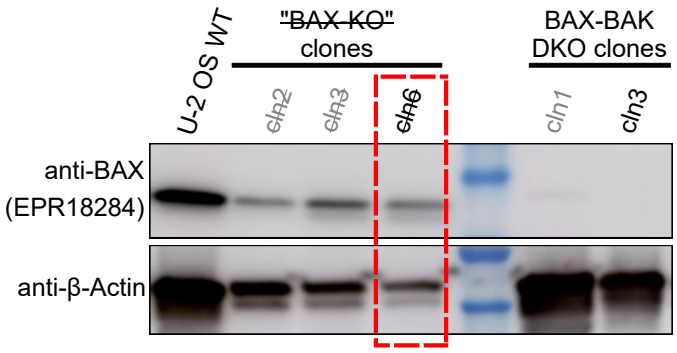

Figure 51: BAX mutated by CRISPR/Cas9 can be detected by Western blotting with a different antibody. The new WB antibody anti-BAX clone EPR18284 detected BAX in U-2 OS WT (lane 1) and in the assumed BAX-KO (lanes 2-4), but not in a BAX-BAK-DKO cell line (lanes 6-7), which proved that the antibody really detects BAX.

detect the mutated BAX in the rings needs to be tested. The precise epitope binding site was not known to the company since no epitope mapping was performed. Another possibility is that the protein derived from the triplet-inserted BAX allele is nonfunctional and therefore does not localize to the rings.

2.7.2 Cells only containing BAX die faster under treatment

In order to quantitatively assess and compare the susceptibility of cells to apoptosis treatment, I plated U-2 OS WT, BAK KO and DKO cells in 24-well plates. (I was not yet able to include an NGS-confirmed BAX KO in this analysis.) I stained the cells with 50 ng/mL Hoechst33342 and 50 nM Sytox Orange and treated them with 10 µM ActD and 10 µM ABT-737. After the addition of the treatment and staining reagents in imaging medium, I placed the cells on a Lionheart automated microscope and monitored the cells for 24 h, recording one image every hour (Figure 52A). As expected, the DKO cells did not respond to treatment. The WT cells started to die around 5 hours after treatment start, but the BAK-KO cells, which express BAX only, started to die already after 3 hours and died faster (Figure 52B). These results might indicate that BAK is needed to balance BAX in apoptosis, as is consistent with the live cell imaging data in the first section as well as previously published results, which suggest that BAX and BAK regulate each other in pore growth and apoptosis induction [167]. However, an apoptosis induction curve of confirmed BAX-KO cells, only containing BAK, first needs to be recorded and assessed in order to deduce any further conclusions from these results.

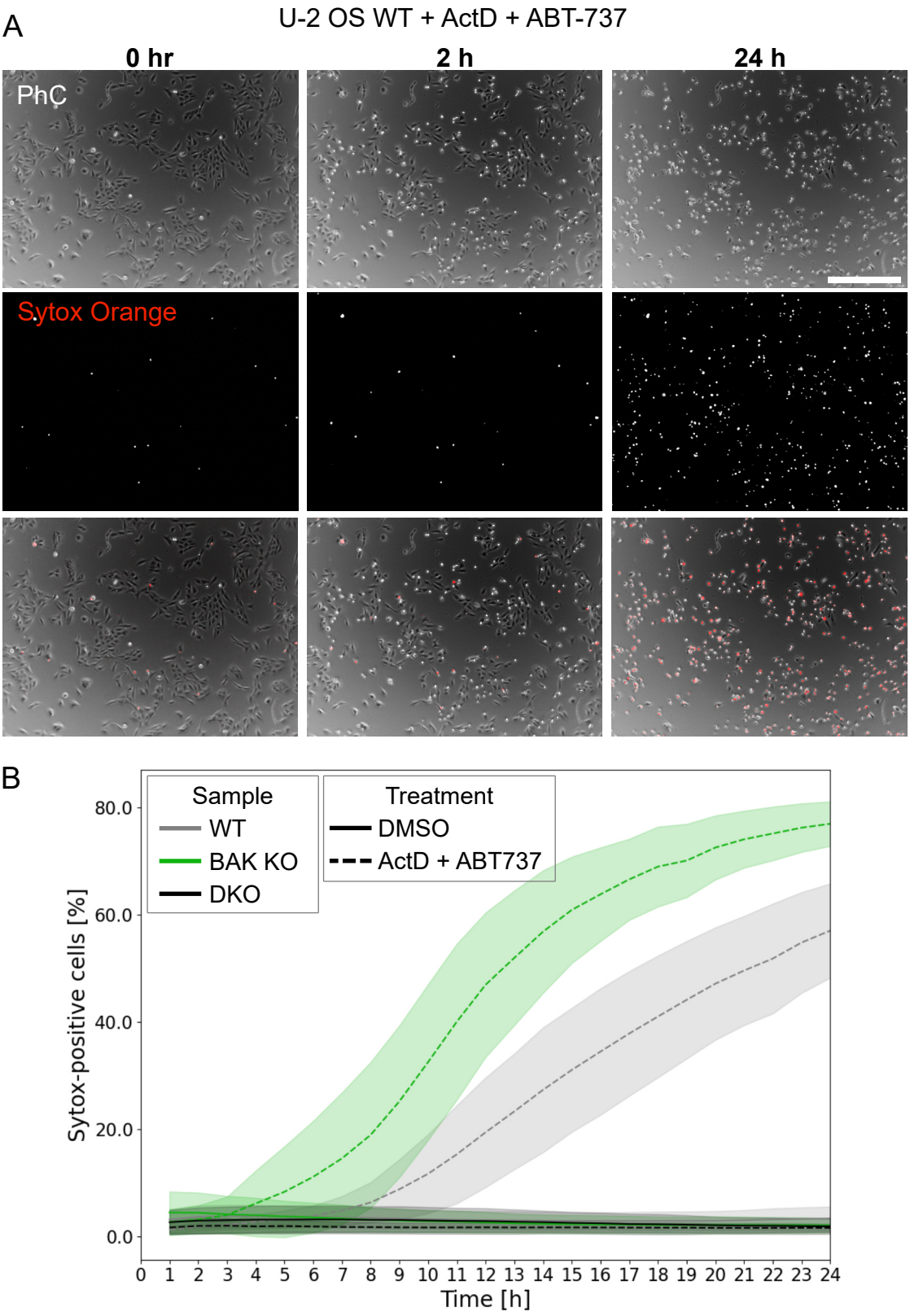

Figure 52: BAK-KO cells die faster than WT cells. **(A)** Three frames from a live-cell wide-field movie of U-2 OS cells undergoing apoptosis. The cells (Phase Contrast (PhC), grey) were treated with 10 µM ActD and 10 µM ABT-737 and monitored for Sytox-orange signal (red). Frametime: 1 hour. Scale bar: 500 µm. **(B)** The percentage of Sytox-orange positive cells versus total cells (measured by DAPI) was plotted over time.

2.7.3 BAX and BAK form apoptotic rings independently of each other

I eventually succeded to create a new BAX-KO cell line (clone 2-3) that I confirmed via WB with the new antibody (Figure 53) as well as NGS.

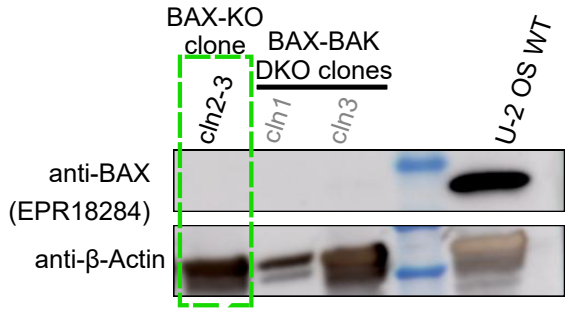

Figure 53: Final BAX-KO cell line. The final BAX-KO was confirmed by WB with the reliable detection antibody.

The BAK-KO cell line as well as the newly generated BAX-KO cell line enabled the investigation of whether the endogenously expressed proteins BAX and BAK were able to form rings independently from each other. After apoptosis treatment and IF staining, I indeed detected rings in both of the cell lines (Figure 54). As a control,

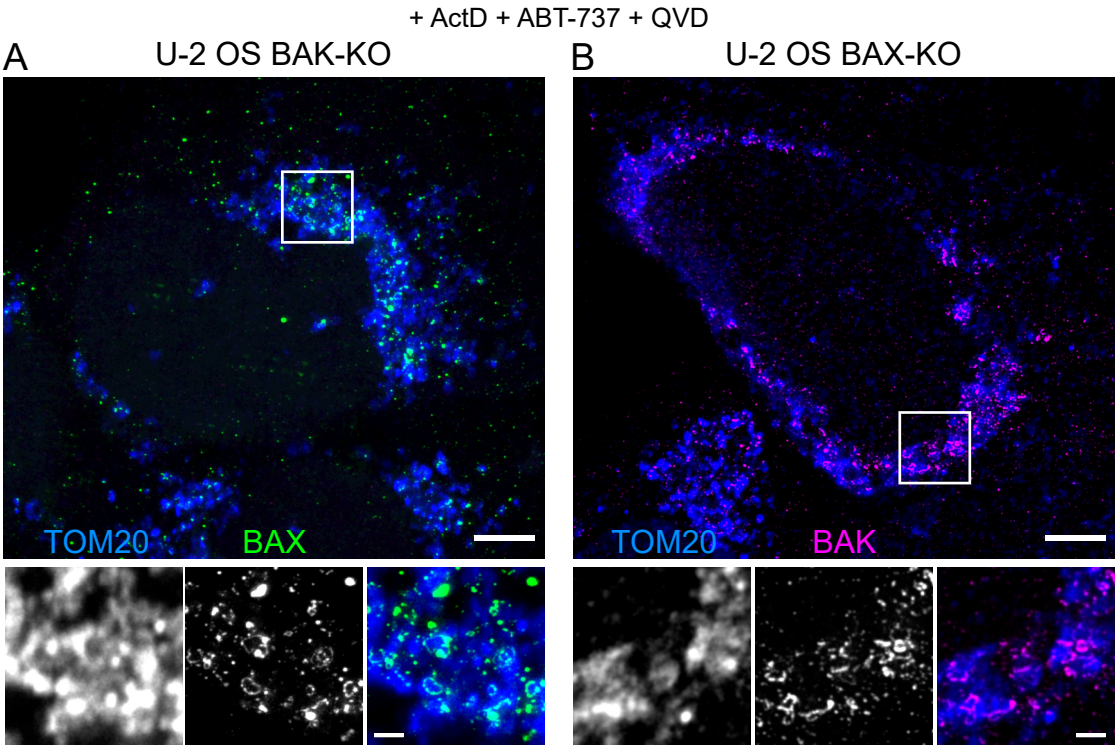

Figure 54: BAX and BAK form apoptotic rings independently of each other. U-2 OS single KO cell lines were treated with treated with 10 µM ActD and 10 µM ABT-737 for 20 h. 20 µM Q-VD-OPh was added to prevent the detachment of the cells from the coverslips. **(A)** BAK KO cells were immunolabeled with 2D2-BAX antibody (STED, green). **(B)** BAX KO cells were immunolabeled SU32-BAK antibody (STED, magenta). Both were also labeled with an anti-TOM20 antibody (confocal, blue). Scale bars: top: 5 µm, bottom: 1 µm.

when performing the same labeling in a DKO cell line, I did not detect any signal of BAX or BAK. These results demonstrate that although we find BAX and BAK primarily located together in apoptotic rings, they can equally form rings by themselves without being dependent on their partner. Notably, the IF data from this experiment correspond to the live cell STED data in terms of ring formation of both proteins. However, there was a striking difference: the fixed cell endogenous data contained essentially no linkers, neither in the BAK-KO (BAX only) nor in the BAX-KO (BAK only) cells.

In summary, I showed in this work that BAX and BAK exhibited different ultra-structures and dynamics when overexpressed and imaged with live-cell STED microscopy. However, overexpression of the pore-forming BCL-2 proteins proved disadvantageous for the study of the apoptotic pore, because the overabundance of effector proteins induces a rapid and potentially unphysiological cellular demise. Therefore, I developed a correlative imaging approach, which allows to include temporal information into the STED imaging workflow, while analyzing endogenous proteins using IF staining. In order to use the correlative assay with more than one color, I developed a dual-color antibody staining of BAX and BAK suitable for the use with STED microscopy. By employing this antibody labeling in U-2 OS as well as non-cancerous cells, I found that BAX and BAK generally reside in the apoptotic rings together. Quantitative analysis revealed that the rings contained highly variable relative amounts of BAX and BAK and that the two proteins were clustering together along the ring outline to various extents. Finally, I produced KO cell lines and showed that endogenous BAX and BAK can form rings independently from each other. The super resolved images of endogenous proteins unmasked the BAK linkers, which were detected in live cell STED imaging as potential overexpression artefacts. This knowledge contributes to a better understanding of the structural changes happening to mitochondria during apoptosis as well as to the involved pore-forming proteins, which will lead to better drug design in order to treat diseases which are caused by deregulated apoptosis.

3 Discussion

3.1 Summary of results

Permeabilization of the MOM by apoptotic pore formation and subsequent cytochrome *c* release is essential for the progression of apoptosis. However, the exact composition of the pore under physiological conditions with endogenous expression levels of the involved proteins remains elusive [169, 170].

In this work, I established live cell STED imaging of overexpressed BAX and BAK, which revealed new insights into the ultra-structural dynamics of these two key players in apoptosis. Super-resolved time-lapse recordings showed distinct oligomerization behaviors of BAX and BAK leading to the formation of different, overall highly dynamic multi-protein assemblies. However, my data also demonstrated that overexpression of BAX and BAK strongly affected the temporal progression of apoptosis. Furthermore, the apoptotic structures that appeared under overexpression conditions were clearly different from the structures present under physiological conditions with endogenous expression levels.

Therefore, in this work I investigated endogenous BAX and BAK and demonstrate that together, they form mosaic rings that are lining the apoptotic pore. STED microscopy revealed that in WT cells these rings contain both BAX and BAK in various relative amounts. If, however, one of the two proteins was absent, in KO cell lines of either BAX or BAK, the remaining protein was able to form rings independently during apoptosis, pointing to partially redundant functions of the two proteins.

In addition, the data presented in this thesis demonstrates that the mosaic BAX-BAK rings are a hallmark of apoptosis not only in human cancer cells, but also in primary human cells. This suggests that the formation of complex BAX/BAK assemblies, especially rings, is an essential step during apoptosis under physiological conditions.

3.2 Protein-overexpression vs. endogenous labeling of BAX and BAK in apoptosis

It is crucial to investigate apoptosis on a single cell level as its onset and progression kinetics are highly variable from cell to cell [190]. Therefore, fluorescence microscopy had become an essential tool for the investigation of apoptosis long before the era of super-resolution microscopy. For decades, most microscopy studies investigated the function of pro-apoptotic BCL-2 proteins such as BAX and BAK by protein overexpression [218, 127, 146, 126, 104]. These studies have revealed important insights, for example the different subcellular localization patterns of BAX and BAK as well as their co-localization into clusters on the MOM during apoptosis. Until recently,

insights into the apoptotic pore using super-resolution microscopy were also almost exclusively based on experiments, in which the involved proteins were overexpressed [163, 55, 54, 167]. However, there is rising evidence presented by this study and by the literature that the overexpression of BAX and BAK can lead to apoptosis without the need for any additional apoptosis inducer [202, 164].

3.2.1 BAX or BAK overexpression generally induces apoptosis

When quantifying apoptosis kinetics (Figure 29), I determined that the apoptosis onset induced by BAX-overexpression alone was rapid and had eradicated an entire cell population at 10 hours after transfection. The onset as well as the progression kinetics of apoptosis were asynchronous over the cell population, varying from minutes to hours from cell to cell. The different progression kinetics might be due to the fact that the cells encountered different expression levels of GFP-BAX, which might also partially explain the unsynchronized onset of apoptosis. However, apoptosis onset and progression kinetics are inherently variable because the cells reside in different states of so called apoptotic priming [219, 220]. This was corroborated by experiments in the current work studying cells with stably integrated tet-on Halo-Bax. These cells equally displayed an asynchronous apoptosis onset (Figure 31), although the clonal cell line had the same amount of Halo-BAX integrated into its genome, which was induced by the same concentrations of doxycyclin in every cell. Thus, even with the same amount of overexpressed protein present, individual cells respond differently to this stimulus, suggesting that the onset of apoptosis is controlled by a multitude of factors.

Surprisingly, even the overexpression of a BAX mutant with a disrupted BH3 domain (BAX-63-65A), which is supposed to be oligomerization impaired, induced apoptosis, indicating that the mitochondrial residence of BAX might be more important for driving apoptosis than its oligomerization [221].

In a physiological situation, the BCL-2 protein family is in a delicate balance. Usually, when a cell in an organism senses an intolerable stress, it induces the intrinsic apoptosis signaling pathway by activating the BH3 only proteins. These inhibit the anti-apoptotic BCL-2 proteins and liberate the physiological amount of BAX or BAK present in a cell, thereby facilitating MOMP.

Because the overexpression of GFP-BAX induced rapid cell death, BAX WT and even a supposed oligomerization impaired mutant version of BAX (63-65A) formed ring-like structures on the MOM and thereby also induced cell death, I concluded that the transient overexpression of BAX or BAK may cause an overload of the delicately balanced system with pro-apoptotic proteins, leading to apoptosis.

In the current study, I quantified the kinetics of apoptosis induced by overexpres-

sion of BAX. Similar rapid apoptosis progression kinetics can be expected from overexpressed BAK, as the onset of apoptosis was equally rapid in the live cell STED experiments with BAK overexpression.

Together, these results demonstrate that the overexpression of (tagged or untagged) BAX (or BAK) is sufficient to induce apoptosis. This isolated overexpression of individual players presumably disrupts the BCL-2 protein family equilibrium, which can lead to unexpected effects on the MOM and therefore might not represent a physiological induction of the intrinsic apoptosis pathway.

Overexpression experiments can thus be used to assess fundamental questions about the sub-cellular localization of certain BCL-2 proteins, their oligomerization behavior and MOMP. But especially the detailed composition of structures observed in super-resolution experiments must be interpreted with caution.

In addition to the fact that the variable apoptosis onset and progression kinetics in the overexpression model are inconvenient for live cell imaging, I also found substantial differences between the live overexpressed super-resolution images, and the fixed endogenous images, which I will discuss in the next section.

3.2.2 Live cell dynamics and BAK-overexpression artefacts

I used the effect that BAX or BAK overexpression induced apoptosis in the current work to perform live-cell STED experiments to image the spatial and temporal dynamics of the two pore-forming proteins without the addition of any drug. I only added the caspase inhibtor Q-VD-OPh, which acts downstream of MOMP, in order to prevent the detachment of the cells from the coverslip. The mere overexpression of BAX or BAK allowed to monitor temporal dynamics of the individual players during apoptosis. Both BAX and BAK were able to polymerize into extended structures, which changed their shape and orientation on the mitochondria. This indicates that apoptotic pores are flexible structures.

With the help of sub-diffraction live cell STED imaging, I also observed some interesting differences between the temporal dynamics of BAX and BAK. BAK rings generally seemed to be smaller than BAX rings and mitochondria with BAK rings were sometimes still elongated. BAX formed rings exclusively once per fragmented mitochondrion, while BAK was sometimes found to also form two rings on a single mitochondrion. Furthermore, I found BAK to form extended "linkers", which are MOM-devoid BAK protrusions extending from one mitochondrion, sometimes connecting it to another one, sometimes merely reaching into the cytosol.

Clusters and lines located on the MOM and especially the rings lining the apoptotic pore had been described before [163, 162, 167]. However, I found especially in the BAK overexpressing cells an abundance of linkers, which were not located on the

MOM and had not been described in literature. Judging from the long thin shape and the absence of MOM signal, one could speculate that these protrusions might be a subpopulation of BAK populating ER tubules. However, when comparing the live cell STED data with images of endogenously labeled BAK in the BAX-KO cells, it became apparent that the linkers were by far not as prominent in endogenous BAK structures. Another feature that was not detectable in the fixed cell STED images, was a mitochondrion with two BAK rings. This discrepancy might have different underlying causes. One of them could simply be that the linkers or double-rings might be an artefact of overexpression, as it has been demonstrated with other proteins [222].

Alternatively, it could also be a stage-specific phenomenon: Apoptosis runs through a number of stages from initial BAX/BAK cluster formation via small and large rings, all the way to mitochondrial collapse. The linkers and double-rings might only appear in a special stage, which was not captured in the fixed cell STED images.

Further scrutinizing the images of endogenous BAK in the BAX-KO cell line will elucidate whether these novel structures are overexpression artefacts or rare events. In the course of this work, I also established an assay (Figure 35), which adds temporal information to the fixed cell STED images and thus could provide time-resolved images post-MOMP to reveal whether at any point in time the linkers or double-rings also appear in endogenous BAK structures.

3.2.3 Differences in overexpressed vs. endogenous ring size

When comparing the data of rings in fixed cells from this work as well as earlier work from others [162] with previously published data of rings from live cell overexpression experiments [163, 167], I found a discrepancy in ring size. The endogenous BAX + BAK rings were by a factor of 5-10 larger than the overexpressed ones. Many potential reasons could explain these differences. It might once again simply be an overexpression artefact, although it seems less likely that a higher abundance of pore formers via overexpression would lead to smaller pores, but rather the opposite would seem plausible. Alternatively, the different imaging modalities and their respective resolution might play a role. The data for analysis in this work had been recorded on a STED microscope with resolution limits above 50 nm, whereas the ring images from other overexpression experiments were performed with SMLM [163, 167], which has much better resolution, down to a couple of nm.

A very likely reason for the ring size differences could also be the different apoptosis induction methods. The cells in the current study were treated with ActD and ABT-737 for 18 h, whereas the cells in previous studies overexpressed BAX or BAK and additionally were treated with the commonly used apoptosis inducer staurosporin (STS). STS is thought to act much faster than ActD as it inhibtis most kinases in the

cell [223] and already after a couple of minutes the cells start to die [167]. Therefore the two treatment regimes are hard to compare and the resulting differences in the advancement of the individual cells in the apoptotic stages might differ greatly. Furthermore, the combination of overexpression and drug treatment with STS might kill the cells so fast, that they have no time to develop larger pores.

Moreover, the current work investigated both endogenous BAX and BAK together in WT cells, whereas the previous studies employing overexpression only investigated the individual proteins in a single-KO or DKO background. The isolated overexpression of only one of the two players could influence the pore growth to a certain degree. Finally, the use of different cell types and the corresponding differences in mitochondrial diameter and/or composition might have an influence on the pore size instead of being a difference between overexpression and endogenous protein levels after all (see section 3.3.1.1).

In general, research in the cell death field has no common protocol to induce apoptosis. Instead, different treatment regimes or overexpression on different KO backgrounds are used in different cell types with different treatment times, which makes it overall difficult to compare studies.

In summary, my data suggests that the overexpression of BAX or BAK- or more broadly of any player of the BCL-2 protein family - is indeed very helpful for general localization studies, and does reveal valuable insights into the dynamics of the individual players. However, the super-resolved structures, which are revealed when BCL-2 proteins are overexpressed need to be analyzed with care and best confirmed by endogenous labeling. The same is true for the absolute and even relative timeline of apoptosis as the expression levels might have a significant influence on that.

3.2.4 Possible alternative endogenous tagging attempts

The endogenous tagging of BAX and/or BAK will reconcile the two methods of live cell imaging and endogenous protein labeling. However, to my best knowledge, endogenous tagging of BAX proved impossible so far. A potential explanation for the failure to engineer a cell line with N-terminally tagged BAX could be that the N-terminal tag renders the protein constitutively active. Therefore, soon after the modifications at the BAX locus by CRISPR/Cas9 have occured, all the cells with the correct integration undergo apoptosis. The tag itself might also be interfering with the binding to other BCL-2 proteins and thus the tagged BAX is not properly inhibited but free to exert its function and kill the cells in an uncontrolled manner. One possible solution to find out whether N-terminal tagging is possible at all, will be to test whether

smaller tags, like the FLAG-tag [224] combined with tag-detecting anti- or nanobodies, might produce better results.

Furthermore, one could try to internally tag the protein in a loop structure where a tag would not alter the protein function. However, in a small globular protein like BAX or BAK, mainly composed of alpha helices, it is hard to imagine where a large tag like Halo, SNAP or even FLAG-tag, might fit into the amino acid sequence without interfering with the protein folding or function. A way to circumvent the insertion of a large tag could be to expand the gentic code and perform a site-specific exchange of single residues with amino acids, which contain side chains that can be labeled with "click-chemistry", thereby providing minimally intrusive labeling of the protein of interest [225].

3.3 Properties of the apoptotic pore composed of BAX and BAK

As discussed above, it is crucial to avoid overexpression and to endogenously label BAX and BAK, the effector proteins of the apoptotic pore. By employing IF labeling and STED microscopy together with an automated imaging and semi-automated image analysis pipeline, I was able to extract information from over 500 rings lining the apoptotic pore. I found significant variations in the analyzed ring parameters, like size, relative protein abundance and their localization relative to each other in the ring: 1) Rings have various sizes and can get very large. 2) There seems to be more BAK in the rings, especially when they are smaller, and the relative amounts of BAX vs. BAK equalize when the rings reach larger sizes. 3) BAX and BAK have a tendency to cluster together along the ring outline as was demonstrated by a median positive Pearson correlation coefficient.

3.3.1 Ring size

3.3.1.1 Large rings

One finding from the ring analysis was that BAX-BAK-rings can become surprisingly large. In this work, I measured ring circumferences ranging from 500 nm to over 3.5 μm with a median of a little more than 1 μm. This corresponds to circles with diameters of 140 nm to 1.2 μm with a median of 380 nm. As discussed above, these measurements revealed a certain difference between the sizes of endogenous BAX-BAK-rings in this work and ring diameters in previous works, where the samples had been prepared by overexpressing BAX or BAK. Nevertheless, even when considering that the overexpressed rings were found to be 5-10 times smaller, still the rings measure tens of nanometers in diameter.

This is surprising, when considering the fact that the release of a single cytochro-

me *c* molecule from the IMS was postulated to require only a minimal pore size of 6 nm in diameter, which corresponds to 6 BAX core dimers covering the rim of the apoptotic pore [153]. Another previous study also suggested that in single cells only a minimal accumulation of BAX on the MOM is needed to induce pore formation [226].

Conventional microscopy images in earlier studies already demonstrated that BAX and BAK form large clusters at the MOM during apoptosis, which were estimated to contain hundreds [146] to thousands [127] of molecules per cluster. The present work as well as previous works demonstrated that these clusters often revealed rings, when imaged with super-resolution microscopy [163, 162, 167]. (Note, that when scrutinizing the microscopy images of earlier publications, large BAX or BAK rings are sometimes observable even without super-resolution.) One study investigated artificial membrane vesicles from Xenopus egg extracts that were co-incubated with active BAX. The resulting electron micrographs showed that the mere presence of BAX at these MOM vesicles lead to the induction of growing membrane pores up to diameters of 300 nm with a mean around 100-160 nm [165]. Thus, typical rings composed of BAX and/or BAK contain at least hundreds of molecules.

The typical diameter of a healthy mitochondrion measures from a couple hundred nm up to one μm in special cases [34, 35]. Healthy mitochondria are present as a network throughout the cell and the individual mitochondrial tubules can measure many μm in length. During apoptosis, these organelles fragment and swell, until most of the mitochondria resemble spheres. If a mitochondrion with 500 nm diameter would fragment to pieces with 2 μm in length, which then rounded up to a sphere, the resulting diameter of the sphere would be roughly 1 μm. If the pore growth is not limited by the number of BAX or BAK molecules, but the maximum diameter of the sphere, the rings would continuously grow until they reach 1 μm in this example. 1 μm diameter in a sphere roughly corresponds to 3 μm in circumference, which perfectly fits the larger ring circumferences measured in the current study. It is therefore highly probable that the size of the BAX-BAK pores is solely limited by the size of the mitochondrion the pore is located on.

So why do the rings grow so large?
It was postulated that the BAX-BAK pores on the MOM do not only serve to release IMS contents but that the mitochondrial inner membrane (MIM) also emerges through the BAX/BAK pores, thereby forming so called herniations. The MIM herniations reach into the cytosol, eventually break open and release mitochondrial matrix content. Especially the release of mtDNA was found to trigger inflammatory responses, like the activation of the cGAS/STING pathway [54, 55]. In order to release something as large as an extrusion of the MIM, the MOM definitely needs to develop pores with a different size scale than would be necessary to only release small IMS proteins.

Indeed, very large MOM pores during apoptosis had already been demonstrated in earlier EM studies, which clearly showed the MIM herniations through the MOM [227, 228, 229, 230, 231]. The MOM pores in these studies were described to measure 100-250 nm in diameter, which is on the same order of magnitude as the mean diameter of 380 nm measured in the present study.

It is therefore very probable that the BAX-BAK pores in the current study also extrude MIM herniations through the MOM, but further microscopical research will be necessary to elucidate this question. How the MIM then ruptures in order to release matrix components - especially mtDNA and mtRNA - is still elusive.

3.3.1.2 Small rings

Not only large, but also smaller rings were detected in the current study. The smallest possible rings I detected in the current work were 140 nm in diameter. However, much smaller rings of sizes down to 40 nm for BAX and 30 nm for BAK have been reported [163, 167]. It might very well be that even smaller rings exist, like the postulated 6 nm pore [153], but we simply cannot resolve them.

In the current work I detected a large quantity of BAX/BAK clusters all over the cell, even in the cytosol. The clusters on the MOM might indeed be unstructured clusters, or some might be rings, which were not possible to resolve. In an attempt to find minimal BAX pores, I employed MINFLUX microscopy, which has an unprecedented resolution in the single digit nm range for biological samples. However, although I succeeded in imaging BAX pores with MINFLUX, I was unable to detect minimal pores. There were a number of limitations, of which the most restraining was the fact that it proved impossible to know which BAX "cluster" might reveal a small ring and which might actually just be an unstructured cluster, which many were. Furthermore, MINFLUX has a very limited field of view. Once it will be possible to image whole cells at an adequate speed with the superior resolution of MINFLUX microscopy, it should be easy to either confirm or rule out the existence of the minimal pore. Another way of tackling this problem could be the employment of expansion microscopy, which in its newest version would also provide some ultrastructural context [232].

It is a plausible possibility, though, that the minimal pore of only a dozen molecules might simply not exist in a cellular setting. Enough tension for the MOM to rupture might only be created when there are many BAX or BAK molecules clustered together. Furthermore, it was postulated, that the clusters of BAX and BAK in the membrane might first form lines and arcs as intermediate stages, until they become full rings [163, 167]. Thus, the rings might only exist in sizes starting at certain diameters. In the current work, I very rarely observed arcs and lines, but this could again be a phe-

nomenon of staging of apoptosis. The structures are very dynamic, as seen in the live cell STED data, and thus lines and arcs might be very short-lived intermediates compared to clusters and rings. Again the MOMP-marker assay could provide an answer to that problem.

Conclusively, rings come in a broad range of sizes, which most likely reflect their growth, which is limited by the mitochondrial diameter (of apoptotic rounded up mitochondria). The ring size distribution in this work might not have captured the small rings at the lower end of the spectrum due to the employed imaging techniques. Furthermore, it is very likely, that there is some selection bias, as all rings were annotated by hand. The same might likewise be true for all other analyzed parameters. I explored many different ways of automated ring detection: Together with a colleague, I tried to implement a hard-coded heuristic; I tested the supervised machine-learning program with graphical user interface Ilastik [233] and a custom written program for ring detection ASAP [234]; and together with physicists in my team, we even attempted ring detection by a custom machine learning pipeline. Unfortunately, none of the methods worked reliably to detect rings, which are the most difficult shapes for object detection (oral communication with image analysis experts). Thus, in summary, an automated image analysis pipeline still needs to be developed in order to remove experimenter bias.

3.3.2 Ring composition

3.3.2.1 BAX vs. BAK amounts in the rings

BAX-BAK rings are not only heterogeneous in size but also the relative amounts of BAX and BAK covering the outlines of the ring vary drastically in relation to one another. I found that almost all rings were composed of both BAX and BAK. Probably even the few rings that seemed to be composed of only one protein in the STED images, have a couple of molecules of the other protein interspersed that could not be detected. Over the whole ring population of over 500 rings, BAK generally covered more of the ring outline with 64 % compared to BAX with 36 %. When the rings grew larger, there was a more equal distribution of the two players along the ring outline. This could have various reasons: It could result from an artefact that the used BAK antibody might have a higher binding affinity for its target. To avoid introducing any bias via the STED image procedure, I distributed the secondary antibody on both STED channels equally for both proteins.

Another, more biologically relevant and plausible reason might be that BAK canonically resides on the MOM even under non-apoptotic conditions. This would allow BAK to start forming clusters and then rings, while BAX is still being recruited to

the MOM. Furthermore, it has been hypothesized that BAK monomers might have a higher affinity to themselves compared to BAX [167]. BAX, which might then get recruited to the membrane by BAK or another mechanism, catches up and the difference in amounts in larger rings is leveled out. This is consistent with previously published data of *Cosentino et al.* [167] who postulated that BAK shows faster cluster formation kinetics, but needs BAX in order to grow large pores. This is corroborated even more by the live cell STED experiments in this work, where I observed that the rings in cells overexpressing BAK remained smaller than their BAX counterparts.

The results from the ring analysis furthermore showed that if there is little BAX in the rings the chances are lower that it will follow the same distribution pattern along the rings as BAK. Likewise, smaller rings have less of a tendency to contain overlapping BAX and BAK. These two results might point to the fact that small rings and rings with little BAX are the same species of rings, which might represent an early intermediate. Only if the rings grow larger, they accumulate more BAX which is then more likely to be found in all the BAK clusters. This might be due to a simple stochastic event, because if there is much less BAX than BAK not every BAK cluster can have BAX molecules. Furthermore, the pores might initially open quite fast, which is corroborated by the live cell data of this work as well as published results [167] and further substantiated by the fact that comparatively few small rings were detected in the ring analysis. The longer the pore is open, the slower it grows, until it reaches the maximal diameter of the mitochondrion. Thus, when the ring is small, the BAX molecules might also find a "free" spot along the outline of the pore, where they can integrate, while at a later stage of pore growth, the newly recruited BAX or BAK molecules are most likely to accumulate at places, where other molecules are already present and therefore the Pearson correlation coefficient heightens with increasing ring size.

Ultimately, whether the differences in recruitment kinetics are the underlying reason for the different BAX-BAK composition of the pores requires further experiments. One solution could be the employment of the MOMP marker assay, as it will rule out whether the different recruitment kinetics are simply due to the overexpression of the proteins.

3.3.2.2 Clusters and voids along the ring outline

Interestingly, in addition to rings with a fully labeled outline, I also found numerous rings with smaller or larger segments along their outline, which displayed very little BAX and/or BAK signal or were completely devoid of either BAX or BAK or both. Other parts of the rings were occupied by very large clusters with high signal intensities. Generally the thickness and intensity of the pore outline varied drastically between these two extremes (Figure 42). This heterogeneity in coverage of the pore rim

is interesting in two ways: First, the fact that some positions along the ring seem to be devoid of BAX and BAK suggests that a pore outline does not need to be fully covered by these two proteins for a stable pore to form. This corroborates the model of a toroidal pore, where the lipids are bent around the pore edge so that the head groups shield the hydrophobic tails and the edge is only partially covered by proteins. Second, the clusters and thicker and thinner lining of the pore point to the fact that BAX and/or BAK dimers are not neatly organized in a single-layer lining the pore, but we find a rather chaotic arrangement of BAX and BAK along the ring.

The absence of signal on the pore outline could also be due to incomplete labeling by the antibody. However, the gaps in labeling were of different sizes and sometimes substantially large. Such large gaps in labeling would most likely not occur due to inefficient binding of the antibody, where a more homogeneous pattern of missing labeling would be expected. Alternatively, the BAX or BAK molecules at the unlabeled positions might have undergone a different conformational rearrangement, which prevents binding of the antibody, but also this seems unlikely, given the fact that the antibodies used for IF staining bind N-terminally in the proteins and the exposure of the N-terminus is the first step of activation of BAX or BAK.

Another possibility might be that there are other players occupying the voids left by BAX and BAK. An obvious candidate is BOK, as it is the postulated third effector protein of the BCL-2 family [138]. However, it is regulated by proteasomal degradation, not directly involved in the canonical mitochondrial pathway of apoptosis [140]. Furthermore, only a small portion of the BOK proteins even localizes to the MOM [139]. It is therefore very unlikely that BOK plays a role in the apoptotic rings of the current work.

Taken together, the voids in the ring outline are most likely not occupied by any protein and the presumably toroidal pore is stable even with an incomplete protein lining of the pore edge.

Just like the voids, large BAX-BAK-clusters were found to be a quite common phenomenon on the ring outlines. Studies have proposed that, once activated, BAX and BAK dimer units are randomly aggregating together on the MOM forming disordered clusters [135]. It could be imaginable that the initial clusters (most likely mainly comprised of BAK) might serves as "nucleation centers" which accumulate more and more BAK as well as BAX molecules until eventually the MOM ruptures. After MOMP, the clusters might continue growing at the same rate as the newly formed pore rim, because dimers might just randomly attach to other dimers and this continued aggregation might happen independently of whether the dimers attach to dimers in the

rim of a pore or to dimers in a big cluster.

In order for this continued growth of the pore rim as well as the formation of large clusters to happen, dimers must interact. However, the inter-dimer interface is highly debated and proposed to occur at different sites [134, 235, 149] or even randomly as mentioned above [135].

Alternatively, it was postulated that the lipids of the MOM can bridge two dimers with their acyl chains [137]. This could explain how the dimers are recruited to the rings lining the pores, specifically on the membrane. However, the dimers in large clusters must ultimately be detached from the membrane because if a cluster of hundreds of molecules forms in a very small area, inherently, not all molecules can be associated with the membrane. The clusters were sometimes even so large, that they were noticably elevated from the membrane in STED images. Therefore, lipids might not be the only glue between dimers. After all, it is difficult to speculate how the dimers form large clusters, which are detached from the membrane. Certainly, there must be a very efficient mechanism to link dimers, as most BAX or BAK molecules get recruited to distinct visible structures like clusters and rings within a relatively short time frame during apoptosis. This can be observed in the live cell data of the current and other works [146] as the BAX and BAK background signal from the cytosol and MOM dissapears at the same time as clusters start to form.

Taken together, it seems very likely, that the pore outline is indeed very heterogeneous, containing voids, clusters and everything in between, due to the random aggregation ability of BAX and BAK. The presence of BAK on the membrane in healthy cells might explain the predominance of BAK in smaller (=earlier) rings, while BAX might get recruited to the rings with a slight delay. Again, either endogenous tagging or the MOMP marker assay, could further corroborate that BAK clusters serve as "nucleation centers" and precede BAX recruitment to the MOM and ring formation.

3.4 If one player is missing

My results demonstrated that BAX and BAK are usually localizing together in rings lining the apoptotic pore. However, if one of the two proteins is missing, the remaining partner can form rings independently. I showed this in single-BAX- or BAK-KO cell lines, which still formed rings during apoptosis, which I detected via IF labeling of endogenous proteins in fixed cells and recorded with STED microscopy. The rings looked comparable to the WT rings and the cells showed no otherwise unexpected phenotype.

It has clearly been shown that BAX and BAK form homodimers, although there is

significant debate about how exactly they dimerize [128, 129, 130, 131, 236, 132, 133]. The fact that, in my hands, the overexpression of a supposed oligomerization impaired mutant of BAX (63-65A) was able to induce apoptosis and form apoptotic structures on the MOM resembling those of WT BAX in many regards is thus striking, but indicative of the fact that there might be more dimerization or oligomerization interfaces than previously thought. The need for BAX and BAK dimerization in apoptosis is widely accepted and is supported by an inhibitory peptide of BAK, which prevents dimerization and thereby BAK-dependent cytochrome *c* release [136]. However, little is known about the affinities between full length activated BAX and BAK molecules with themselves or their partner. The affinity of BAX was defined for a couple of different BH3 peptides [237], including the BAX BH3 peptide. Interestingly, the affinity was not high (dissociation constant (K_D) = 150 μM). These NMR experiments were performed on BAX with a truncated C-terminus. However, the presence of the C-terminal domain as well as the residue composition is essential for the subcellular localization, as was derived from mutant studies [121]. Furthermore, there is a substantial conformational rearrangement happening when BAX gets activated [121] and therefore a K_D value from natively folded BAX with only the BH3 domain of BAX might not represent the cellular reality. Still, the BAX BH3 peptide triggered significant BAX dimerization [237].

Thus, although we know little about the strength of the interaction, it became clear that the dimerization is crucial for apoptosis. In order to form the apoptotic pore, the homodimer units then further oligomerize. These steps can be fulfilled efficiently by BAX and BAK without the need for their partner. This explains why the two proteins can act completely independently from their partner and execute apoptosis on their own. This redundant killing ability was demonstrated with BAX- or BAK-single-KO animals, which were able to undergo developmental apoptosis almost normally with no or very mild phenotypes [112].

Interestingly, although BAX and BAK can act completely independently, potential hetero-dimer interactions have been shown [238, 239, 134, 135]. Other studies showed that antibody-induced as well as light-induced BAK activation could in turn activate BAX [240, 167], but it is not known whether this happens on the dimer or the monomer level. Thus, there probably are BAX-BAK interactions but these interactions are not necessary for successful apoptosis completion [112].

So, if BAX and BAK are perfectly capable of executing apoptosis by themselves and do not have to interact, then why do both exist and maybe do interact?
A simple explanation for the the molecular redundancy might be that it is a mecha-

nism of the cell to ensure efficient killing at any time. Even if one of the two players is accidentally impaired, the other on can still trigger MOMP and thereby launch the whole apoptosis machinery. Also, the players up- and downstream of BAX and BAK, like the pro-apoptotic BCL-2 proteins as well as caspases are redundant. This guarantees the prevention of aberrant cell proliferation and thus protects the organism against cancer.

Another reason why both are needed, in addition to executing apoptosis redundantly and being each others safety net, could be the regulation of the speed with which apoptosis occurs and thereby they influence the footprint a dying cell leaves behind. It has recently been shown that apoptotic cells release pro-survival factors, which protect neighboring cells against apoptosis for a couple of hours [241, 242]. This protective effect, called apoptosis induced survival (AiS), occured even in BAX-BAK-DKO cells, which means that it occurs irrespective of MOMP [241].

So, maybe the tuning of the pore growth does not only serve to adjust the speed of mtDNA release and inflammatory signal transduction, as proposed recently [167]. The speed of pore growth might also regulate the speed of apoptosis altogether, in order to allow the dying cell enough time for the release of the pro-survival factors into the surroundings. This way, by tuning the pore growth, a cell might not only regulate the level of inflammation it induces, but also, how much survival of neighboring cells it will facilitate. Therefore, the outcome of the apoptotic tuning could be very dependent on the tissue the dying cell is embedded in as well as the stress that initially induced apoptosis of this very cell.

Interestingly, this work shows that the cells which only contained BAX (BAK-KO), died faster than the WT. This suggests that BAK has some sort of slowing function on cellular apoptosis. This is hard to reconcile with the previously proposed mechanism where BAK initially oligomerizes faster, which would instead suggest that BAK-only containing cells should die faster than BAX-only containing cells [167]. Maybe, although the fast oligomerization of BAK at the start is missing, cells only containing BAX are still able to grow large pores very fast once BAX reached the membrane. Even though they initially have slower recruitment kinetics, because BAX is not in the membrane, once inserted into the MOM, BAX might even have a higher affinity to itself than BAK. This would also explain the fact that BAX is continusouly shuttled back in the cytosol, because it would be too dangerous for a cell to have BAX residing at the membrane. The BAK-KO cells then die faster than the WT, because they are not limited in pore size by BAK, but further research is needed to interpret these findings. Especially, the dying speed of the BAK-only cell line (BAX-KO) created in the current work, still needs to be determined.

Furthermore, it has been postulated that BAK rings are smaller than BAX rings

[167]. Although my live cell STED data corroborate these findings, an automated analysis of the endogenous fixed cell data of the BAK rings in the BAX-KO cells will ultimately provide clarity, whether this is an overexpression artefact or BAK rings are really smaller. The molecular interactions behind a restricted pore size of BAK needs to be investigated using other techniques.

Apoptosis was thought to be immunologically and otherwise silent for decades and the research into this area has only just begun. Along these lines, it will be interesting to elucidate, whether in a BAX or BAK single-KO, which might potentially be speeding up or slowing down apoptosis progression, AiS is reduced or enhanced.

Ultimately, a cell decides whether it is "nobler in the mind to suffer the slings and arrows of outrageous fortune", thus survive after an insult, potentially risking DNA or other damage "or to take arms against a sea of troubles, and by opposing end them?" [1], thus induce apoptosis and end its misery. In addition though, a cell might also decide about the faith of its neighboring cells, by fine tuning the speed of apoptosis and apoptotic pore growth, by which the release of inflammatory and pro-survival factors are tightly regulated.

3.5 Conclusion and Outlook

In summary, my work reveals unprecedented details of the temporal and spatial dynamics of BAX and BAK in apoptotic pores and highlights the importance of studying the apoptotic pore on an endogenous protein level with super-resolution microscopy methods. BAX and BAK together form the rings that line the apoptotic pore but if only one of the two proteins is present, it is capable of forming rings independently. It is most likely that the pore size, when both proteins are present, is solely limited by the diameter of the harboring mitochondrion. BAK-only pores are suggested to be smaller than mosaic BAX-BAK pores or BAX-only pores, but this needs to be quantitatively verified on single-KO data from the newly generated cell line.

STED, MINFLUX and 4Pi STORM super-resolution data suggest, that the apoptotic pore edge does not have to be fully delineated by BAX or BAK. Furthermore BAX and BAK do not seem to form an ordered wall of single-layered BAX or BAK dimers around the pore edge but rather a chaotic arrangement of BAX and BAK, with voids and large BAX-BAK-clusters on the ring outline. This strongly supports the model of a toroidal BAX-BAK pore, growing from small clusters (Figure 55).

The big remaining questions are: 1) Are there size differences between the single-KO rings and compared to the WT rings? 2) How do BAX and BAK interact on a molecular level? 3) Is the MIM herniating through rings delineating endogenous pores? 4) If so, how is the MIM ruptured? 5) What is the minimal size of a BAX or BAK pore? 6) Do BAX or BAK single-KO cells have a reduced or enhanced ability to induce AiS?

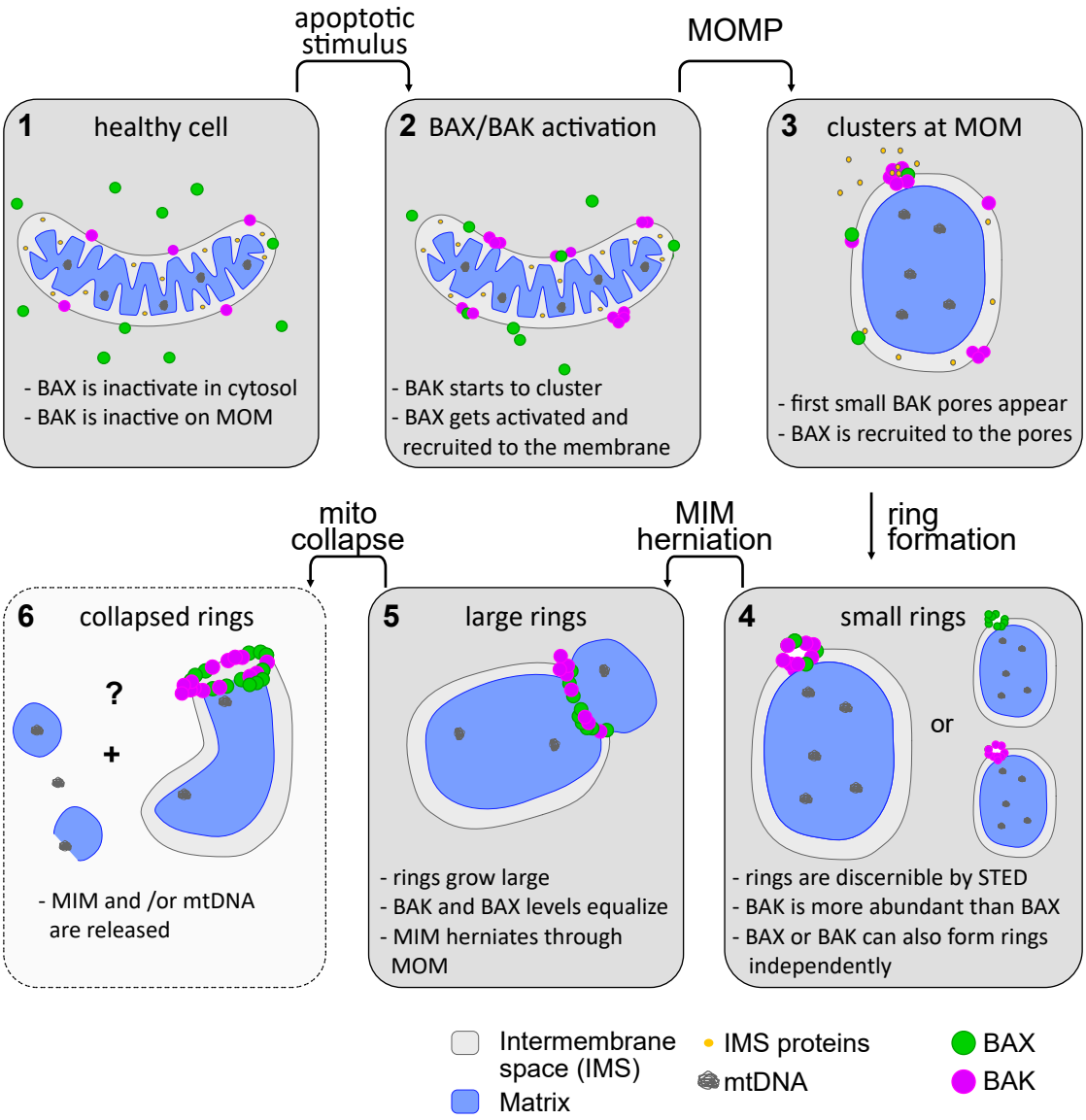

Figure 55: Model of BAX and BAK forming apoptotic rings together. **1** *Healthy cell*: BAX is actively transported back from the MOM into the cytosol, where it resides in its native globular fold. BAK is predominantly localized at the MOM with its transmembrane domain inserted into the membrane but in an inactive state. **2** *BAX/BAK activation*: An apoptotic stimulus triggers the intrinsic apoptosis pathway. BAK gets activated at the MOM, starts dimerizing and BAX gets activated and recruited to the membrane and dimerizes as well. Both undergo striking conformational rearrangements to insert into the membrane. It is unknown whether BAX/BAK heterodimers exist. **3** *Clusters at MOM*: BAK dimers randomly aggregate and thereby initiate cluster formation, BAX dimers get recruited into the clusters and the MOM gets permeabilized (MOMP) and IMS proteins released. **4** *Small rings*: The rings become large enough to be resolved by STED microscopy. At this early stage they contain more BAK than BAX. If, however, one of the two effector proteins is missing, the other one can form rings independently. **5** *Large rings*: Rings harboring big clusters as well as voids continuously enlarge by the steady recruitment of more BAX and BAK. If only BAK is present, the rings stay smaller. The MIM eventually herniates through the MOM into the cytosol. **6** *Collapsed rings*: The MIM herniations somehow release their content to trigger downstream inflammatory pathways, the mitochondrion collapses and with it the ring.

4 Materials & Methods

4.1 Molecular biology

4.1.1 PCR

By default Q5 High-Fidelity DNA Polymerase (NEB #M0491S) was used for PCR with the standard 5x Q5 reaction buffer. Also most of the time 2% DMSO was added to the reaction mixture, as most PCRs were done on genomic DNA to check for CRISPR edited loci. dNTPs were thawed on ice. Each reaction mixture was set up on ice in PCR tubes:

10 µL 5x Q5 reaction buffer
1 µL DMSO
1 µL 10 mM dNTPs
2.5 µL 10 µM forward primer
2.5 µL 10 µM reverse primer
1-10 µL DNA template
0.5 µL Q5
22.5 - 31.5 µL molecular grade water
50 µL total

Samples were put into a thermocycler at the following settings:

98 °C - 2 min (or 10 min if genomic)
30x [98 °C - 20 sec; 50 to 70 °C (annealing temperature according to primers) - 30 sec;
72 °C - 30 sec to 3 min (elongation time according to template size and manufacturer's specifications (Q5 polymerase: 2kb/min))
72 °C - 10 min;
4 °C - forever;

4.1.1.1 Frequently used primers

In Table 1, frequently used PCR primers for sequencing are listed.

#	name	sequence (5' -> 3')
7428	Bax fw	tacacaaacacaaacattcgagtcatgactg
7429	Bax rv	cttgagacactcgctcagcttcttggtggac
9553	Bak fw	ccaggaacagctaaaaaccccccaggctc
9554	Bak rv	gtagctgcggcccagaaaagtcacacagg

Table 1: Frequently used primers

4.1.2 Agarose DNA gel

6X DNA loading dye: 10 mL

6 mL TAE 10X
3 mL Glycerol
15 mg Bromphenol blue
15 mg Xylencyanol

To check DNA fragments for their presence, size and abundance, e.g. after PCR or cloning, agarose gels ranging between 0,8 up to 2 % agarose (w/v) (my Bio-Budget #10-35-1020) in 1x TAE buffer were used. The gels were cast ultra-thin in home-made chambers and run at 80 V for 30 mins covered with 1x TAE buffer. The DNA samples were mixed with 6x loading dye and loaded. As a marker usually 5 µL of GeneRuler 1 kb DNA Ladder (Thermo Scientific #SM0311) was used. After running the gels were put into an ethidium bromide bath (1 mL of EtBr (Ethidium Bromide solution 1% AppliChem #A1152.0025) in ca. 1000 mL of water) for 10 mins and then analyzed under UV light.

4.1.3 Gel purification

If two or more DNA fragments had to be separated, a gel purification was performed with the QIAquick® Gel Extraction Kit (Qiagen # 28706). The DNA fragments were excised as narrowly as possible from the gel under UV light and put into a fresh Eppendorf tube. It was weighed and per 100 mg of gel 100 µL of buffer QG were added. This was incubated at 65 °C for 3 min shaking. 1 volume of isopropanol was added. The mixture was applied to a QIAquick spin column and spun for 30 sec at full speed (repeated multiple times if volume exceeded 750 µL). The flowthrough was discarded and 750 µL of buffer PE were added, 30 sec full speed, discard flowthrough. The column was spun once more to remove residual buffer. It was then placed in a new Eppendorf tube, 30 µL of buffer EB were added to the center of the column, incubated for 1 min and spun for 1 min full speed to elute purified DNA.

4.1.4 Whole protein lysates

Lysis buffer:

50 mM Tris-HCl pH7.4
4 mM MgCl2
0,1 mM DTT
1% SDS

Mix 1000 µL of lysis buffer freshly with:

50 µL cOmplete solution (cOmplete, EDTA-free Protease inhibitor cocktail tablet, Merck # 5056489001; 25X stock solution prepared according to manufacturer's instructions)
2 µL Benzonase (Sigma/Merck # E1014)

Sample buffer: 6X

0.05 M Tris-HCl pH6.8
2 % SDS
1 % ß-Mercaptoethanol
10 % Glycerin
0.01 % Bromphenolblau

Per pellet of a confluent 6-well of U-2 OS, I used 75 µL of lysis buffer and resuspended the pellet very well. Then I added 15 µL sample buffer WITH b-ME, resuspend well again. This was incubated at 95°C for 5 mins to denature the proteins. (The prepared lysates could be stored at -80 °C. Before use they were heated at 90 °C for 5 min again.)

4.1.5 Western blot

4.1.5.1 Buffers for Western blot

PAGE running buffer 10x

For 2 L:
0,250 M Tris 60,6 g
1,925 M Glycin 288,4 g
1 % SDS 20 g
pH 8,3

Ponceau stain

0,1 % Ponceau
in 5 % Acetic Acid
fill up with water

10X TBS

For 1 L:
24 g Tris base (formula weight: 121.1 g)
88 g NaCl (formula weight: 58.4 g)
Dissolve in 900 mL distilled water
pH to 7.6 with HCl
Add distilled water to a final volume of 1 L

1X TBS-T

Prepare 1 L of 1X TBS
Add 0.1% (1 mL) of Tween (AppliChem # A4974.0500)

block buffer

1 L of 1X TBS
Add 5% dried milk powder (AppliChem # A0830.1000)

4.1.5.2 Antibodies for Western blot

In Table 2, all the antibodies used for Western Blots are listed.

4.1.5.3 Western blot protocol

Any kD gels (BioRad 4–15 % Mini-PROTEAN® TGX™ Precast Protein Gels, 15-well, 15 µL #4561086 OR BioRad Any kD™ Mini-PROTEAN® TGX™ Precast Protein Gels, 10-well, 30 µL #4569033 or any other combination of slot size and gel composition, depending on the specific proteins to be analyzed) were placed into a BioRad gel tray after removing the green seal from the bottom. Rubber lip of the tray was properly sealed by gel to ensure that no buffer was running out from the middle. Insert dummy on the other side (writing facing inside), if only one gel used. 1 L of 1X PAGE running buffer (ca. 800 mL needed for one tank), was prepared to fill the inside of the two gels and the tank. After removal of the combs, according amounts of lysates were filled intot the gel pockets. 5 µL of ladder was loaded (PageRuler™ Prestained Protein

Antibody	Supplier	Cat#	Dilution
Rabbit anti human monoclonal recombinant Anti-Bax antibody [EPR18284] (**good** for checking BAX KOs!)	abcam	# ab182734	1:1000
Rabbit anti human monoclonal recombinant Anti-Bax antibody [E63] (**bad** for checking BAX KOs!)	abcam	# ab32503	1:800
Rabbit anti human polyclonal Anti-Bak Antibody, NT (**good** for checking BAK KOs!)	Merck/ Millipore	# 06-536	1:1000
Mouse anti pigeon Purified Anti-Cytochrome C, Clone 7H8.2C12 (RUO), reactivity to human	BD Biosciences	# 556433	1:2500
Rabbit polyclonal Anti-GFP antibody	abcam	# ab6556	1:2500
Mouse anti human Monoclonal Anti-β-Actin antibody (**loading control**)	Sigma	# A5441	1:4000
Goat Anti-Rabbit Peroxidase-AffiniPure IgG (H+L), Conjugation: Horseradish Peroxidase (HRP)	Dianova	# 111-035-144	1:5000
Goat Anti-Mouse Peroxidase-AffiniPure IgG (H+L), Conjugation: Horseradish Peroxidase (HRP)	Dianova	# 115-035-062	1:5000

Table 2: Antibodies used for Western blot

Ladder, 10 to 180 kDaThermo Scientific™ # 26617), as well as empty wells filled with 2.5 µL 6X loading dye. The gels were run at 200V for 30mins. In the meantime block buffer (=milk) was always prepared freshly by adding 5 % milk to TBS.

After running, the gels were blotted onto nitrecellulose membranes (iBlot stack, invitrogen # IB23002) by using the iBlot 2 system (invitrogen #IB21001) according to the manufacturer's instructions. After this blotting step, the success of the protein transfer was briefly checked by covering the membrane with Ponceau stain and destaining with dH_2O until bands were visible. If needed, membranes could be cut with a scalpel at this point. Destaining was continued shortly and the membrane was immersed in block buffer for 1 hr at RT (or at 4 °C overnight).

The blocking solution was discarded and the primary AB diluted in block buffer was added directly. The membrane with 1° AB solution was incubated o/n at 4 °C (either sealed in small bags or in multi-position trays). The next day the antibody solutions were recovered (they could be reused for a long time) and the membrane was washed 3 x 5 min with TBS-T on RT shaking.

Then the secondary AB was added diluted in block buffer. The secondary AB cou-

pled to HRP (see Table 2) was prepared fresh every time and according to the species of the primary antibody. It was incubated at RT for 1 hr shaking and shielded from light. Then the membrane was washed 3 x 5 min with PBS-T on RT shaking again. After a brief rinse in TBS, ECL solution (Immobilon Forte Western HRP substrate, Millipore #WBLUF0100) was used to develop the membranes, which were imaged on an Amersham™ Imager 600.

4.2 Cloning

4.2.1 Gibson assembly

Next to classical restriction-ligation cloning, Gibson assembly was frequently performed to generate new plasmids. The primers were designed with the nebuilder tool [243] to have a 20 bp sequence for binding and approximately a 30 bp overhang. The vector was cut at the approximate site of insertion and the primers contained overhangs that would fit to the exact integration site. The whole Gibson assembly process was performed *in silico* with Snapgene® to make sure all sequences were correct. The reaction was performed with the Gibson Assembly® Master Mix (neb, #E2611L). Vector and DNA fragment(s) were assembled in a 1:3 molar ratio together with 1X Gibson Mastermix. Eg.: 30 fmol of a 10000 bp vector with 90 fmol of a 700 bp insert. The mixture was incubated at 5 °C for 15 min and could then be stored on ice.

4.2.2 Electroporation of bacteria

Home-made electrocompetent *E. coli* DH5α (50 µL) were thawed on ice (!). 60-260 µL of ice-cold water was added and pieptted gently up and down once or thwice to thaw the bacteria. In a cuvette, 2 µL of plasmid DNA were inserted as drop against the wall. 50 µL of the bacteria were used per electroporation reaction and pipetted onto the DNA spot in the cuvette. After gently taping the cuvette to make the mixture sit on the bottom of the cuvette without bubbles, it was inserted into the electroporator (BioRad Gene Pulser™ together with a Pulse controller, ca. 1990). The settings were as follows: 200 Ohm and 25 µFarad as well as 2.5 Volts. After successfull electroporation (time constant above 4), the bacteria were resuspended in 1 mL LB and incubated at 37 °C for 1 h shaking. The bacteria were then plated on antibiotic-containing agar plates with ColiRollers™.

4.2.3 TOPO cloning

When DNA pieces of different sequences (eg. PCR of a genomic locus after mutation by CRISPR) needed to be separated for Sanger sequencing, TOPO cloning was

performed with Zero Blunt™ TOPO™ PCR Cloning Kit (Invitrogen™ # 450245).

4 µL of the gelexed PCR (loaded all 50 µL on agarose) of genomic DNA surround -ing the wanted locus

1 µL salt solution

1 µL water

1 µL fresh pCR-Blunt II – TOPO vector

Incubate 30 mins on RT.

Diluted with 18 µL of water to 24 µL total.

2 µL of this was electroporated into electro-competent E. coli.

Plated the whole electroporation reaction on Kanamycin plates.

Sequence Ecoli overnight seq with primer M13 from seqlab

4.3 Plasmids

4.3.1 Overexpression plasmids

4.3.1.1 Halo-BAX plasmid

hBax C3-EGFP, which was a gift from Richard Youle (Addgene plasmid # 19741), was linearized by using the restriction endonucleases AgeI and SacI. The Halo tag was amplified by PCR from plasmid pENTR4-HaloTag (w876-1), which was a gift from Eric Campeau (Addgene plasmid # 29644), with the following primers:
Halo_fw_AgeI: 5'-gctaccggtcgccaccatggcagaaatcggtac-3'
Halo_rv_SacI: 5'-tgagctcgagatctgagtagccggaaatctcgagcgtcgaca-3'
The amplified Halo-tag was also cut with the restriction endonucleases AgeI and SacI and then inserted into the linearized Bax plasmid by ligation.

4.3.1.2 Halo-BAK plasmid

EGFP-Bak, which was a gift from Richard Youle (Addgene plasmid # 32564), was linearized by using the restriction endonucleases AgeI and XhoI. The Halo tag was amplified by PCR from plasmid pENTR4-HaloTag (w876-1), which was a gift from Eric Campeau (Addgene plasmid # 29644), with the following primers:
Gibson_fw_Halo-Bak_AgeI: 5'-gatccgctagcgctaccggtatggcagaaatcggtactggc-3'
Gibson_rv_Halo-Bak_XhoI: 5'-agccataagcttgagctctagatctgagtagccggaaatctcgagc-3'
The amplified Halo-tag was then inserted into the linearized Bak plasmid via Gibson assembly.

4.3.1.3 Untagged BAX WT and BAX 63-65A plasmids

The untagged BAX WT and BAX 63-65A plasmids were kind gifts of Frank Edlich, and

contained the BAX WT coding sequence, or a mutant version with amino acids 63 to 65 changed to alanines, respectively in the pcDNA vector.

4.3.2 CRISPR gRNA plasmids

4.3.2.1 BAX and BAK gRNA plasmids for gene knockout

The gRNA+Cas9 plasmids pX458-BAX or pX458-BAK to cut the the first exon of the genes was derived from pSpCas9(BB)-2A-GFP (PX458), which was a gift from Feng Zhang (Addgene plasmid # 48138). The following oligonucleotides were annealed and integrated into pX458 after linearization with the BbsI restriction endonuclease:

BAX-gRNA1-KO-px458_F: 5'-caccgCGGGGAGCAGCCCAGAGGCG-3'
BAX-gRNA1-KO-px458_R: 3'-aaacCGCCTCTGGGTGCTCCCCGc-3'
BAK-gRNA2-KO-px458_F: 5'-caccGTCTCCGCACTCCTGCCTGGG-3'
BAK-gRNA2-KO-px458_R: 5'-aaacCCCAGGCAGGAGTGCGGAGAC-3'

4.3.2.2 BAX gRNA plasmids for genomic integration of N-terminal tag

To generate pX330_BAX_gRNA1, the gRNA+Cas9 plasmid pX330-U6-Chimeric_BB-CBh-hSpCas9, which was a gift from Feng Zhang (Addgene plasmid # 42230) was linearized with the BbsI restriction endonuclease. The following oligonucleotides were annealed and integrated into pX330 after linearization:

SVSgRNA1f_Bax-gRNA1_fw: 5'-caccgTGAAGGACGCACGTTCAGCG-3'
SVSgRNA1r_Bax-gRNA1_rv: 5'-aaacCGCTGAACGTGCGTCCTTCAc-3'

4.3.2.3 gRNA plasmids for the safe harvbor locus AAVS1

The plasmid PX330-AAVS1-gRNA was generated by Till Stephan [244]. To generate PX330-AAVS1-gRNA, the gRNA+Cas9 plasmid pX330-U6-Chimeric_BB-CBh-hSpCas9, which was a gift from Feng Zhang (Addgene plasmid # 42230) was linearized with the BbsI restriction endonuclease. The following oligonucleotides were annealed and integrated into pX330 after linearization:

AAVS1-gRNA FW: 5'-CACCGTGTCCCTAGTGGCCCCACTG-3'
AAVS1-gRNA REV: 5'-AAACCAGTGGGGCCACTAGGGACAC-3'

4.3.3 CRISPR donor plasmids

4.3.3.1 HDR template for endogenous Halo-BAX

The HDR template to insert an N-terminal Halo-tag into the BAX-locus was ordered and fully synthesized as plasmid. The Halo-tag was inserted shortly before the N-terminus of BAX with a short linker. The linker "YSDLELKL" was derived from the

original plasmid hBax C3-EGFP, which was a gift from Richard Youle (Addgene plasmid # 19741). An inverse GFP reporter cassette flanked by loxP sites was inserted on the inverse strand in intron 1.

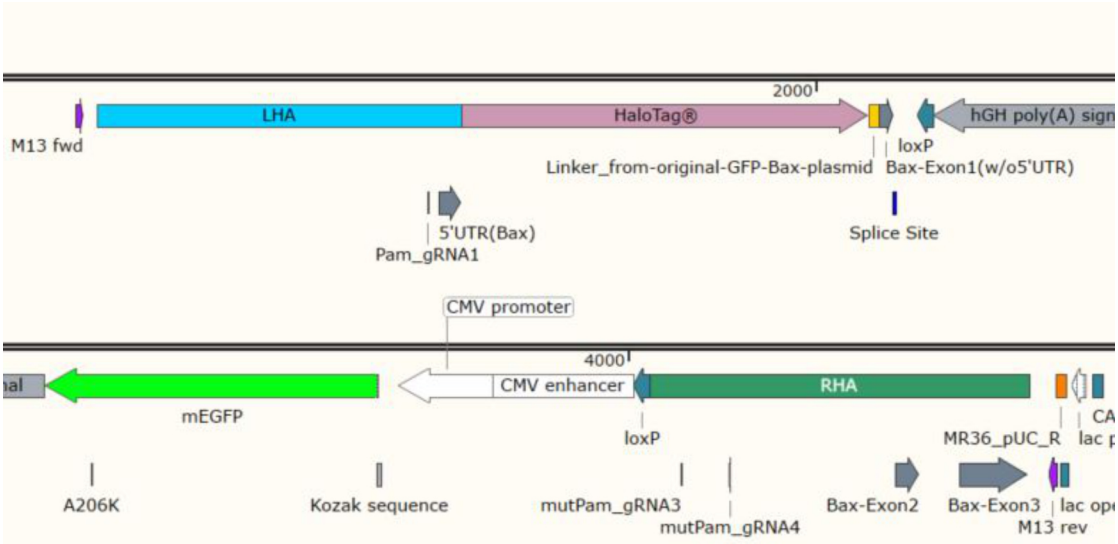

Figure 56: Donor plasmid for endogenous Halo-BAX with inverse GFP. LHA = left homoly arm, RHA = right homolgy arm.

4.3.3.2 HDR templates for safe harbor (AAVS1) integration of SNAP-OMP25 and GFP-OMP25

To generate the donor plasmid to integrate SNAP-OMP25 or GFP-OMP25 into the safe harbor locus, the plasmids AAVS1-Snap-OMP25 and AAVS1-GFP-OMP25 were created. For this, AAVS1-Basticidin-CAG-Flpe-ERT2, which was a gift from Su-Chun Zhang (Addgene plasmid #68461), was linearized by using the restriction endonucleases SalI and EcoRV. GFP-OMP25 and Snap-OMP25 were kind gifts from the Bewersdorf lab (Yale University) and are described elsewhere [181]. OMP25 with the respective tag was amplified by PCR using the primers given below and subsequently integrated into the linearized AAVS1 plasmid by Gibson assembly.

Gibson_AAVS1_Snap-OMP25_fw:
5'-tcattttggcaaagaattcgtcgacgccgccaccATGGACAAAGACTGCGAAAT-3'
Gibson _Snap-OMP25_AAVS1_rv:
5'-tgattatcgataagcttgatatcTCAAAGTTGTTGCCGGTATC-3'
Gibson_AAVS1_GFP-OMP25_fw:
5'-tcattttggcaaagaattcgtcgacGCCGCCACCATGGTGAGC-3'
Gibson_GFP-OMP25_AAVS1_rv:
5'-gttgattatcgataagcttgatatctcaaagttgttgccggtatctcatg-3'

4.3.3.3 HDR templates for safe harbor (AAVS1) integration of cytC-mEGFP

To generate cytochrome *c*-mEGFP, the cytochrome *c* coding sequence was amplified with the following primers to add BamHI and KpnI restriction sites.

SVS5_CYCS_rev_BamHI:

5'-GTGGCGACCGGTGGATCCCCctcattagtagctttttgagataagc-3'

SVS5_CYCS_fw_KpnI:

5'-CAGTCGACGGTACCatgggtgatgttgagaaaggc-3'

The PCR product as well as the vector p-mEGFP-N were digested with these two enzymes and ligated. The resulting linker was the remnant of the multiple cloning site "GDPPVAT". In order to avoid GFP expression, the ATG start codon of mEGFP was removed by mutagenesis PCR.

To generate the donor plasmid to integrate cytochrome *c*-mEGFP into the safe harbor locus, the resulting cytochrome *c*-mEGFP (without ATG) was then amplified with the following primers:

9942_SVS26_AAVS1_cytC-mEGFP_fw:

5'-tcattttggcaaagaattcgtcgacgccgccaccatgggtgatgttgagaaag-3'

9943SVS27_cytC-mEGFP_AAVS1_rv:

5'-tgattatcgataagcttgatatcctacttgtacagctcgtcca-3'

To generate the donor plasmid to integrate cytochrome *c*-mEGFP into the safe harbor locus (AAVS1), the plasmid AAVS1-Basticidin-CAG-Flpe-ERT2, which was a gift from Su-Chun Zhang (Addgene plasmid #68461), as well as the cytochrome *c*-mEGFP fragment were digested by using the restriction endonucleases SalI and EcoRV and merged by Gibson assembly.

4.3.3.4 HDR templates for safe harbor (AAVS1) integration of tet-on Halo-BAX

To generate the donor plasmid to integrate Halo-BAX under a tetracyclin (doxycyclin in my case) inducible promoter into the safe harbor locus (AAVS1), the plasmid AAVS1-TRE3G-EGFP, which was a gift from Su-Chun Zhang (Addgene plasmid # 52343), was linearized by using the restriction endonucleases SalI and MluI. Halo-BAX was amplified with the following primers:

SVS49_Gibson_fw_Halo-Bax-AAVS1-TREG-SalI:

5'-acttcctaccctcgtaaagtcgacATGGGATCCGAAATCGGTACTG-3'

SVS50_Gibson_rv_Halo-Bax-AAVS1-TREG-MluI:

5'-gcaggctagccatatgacgcgtTCAGCCCATCTTCTTCCAGATGGTGAG-3'

The PCR product was equally digested with SalI and MluI. The insert was then inserted into the vector via Gibson assembly.

4.4 Sequencing

4.4.1 Sanger sequencing

DNA was sent for over-night sequencing to Microsynth Seqlab. The purified DNA was premixed with water and primer according to the guidelines: 12 µL DNA template solution plus 3 µL 10 µM sequencing primer solution. 40-100 ng/µL plasmid DNA or 1.5 ng/µL per 100 bp of PCR product. E.coli overnight sequencing could also be ordered: a single colony was picked and put into the prefilled tubes from Microsynth. Chromatograms were visualized with SNAPGene®.

4.4.2 Next Generation Sequencing (NGS)

4.4.2.1 Sample preparation for Illumina NGS

DNA was prepared by tagmentation with the DNA Prep, (M) Tagmentation (96 Samples, IPB) kit (Illumina® # 20060059) and according to "Illumina DNA Prep Reference Guide Document # 1000000025416 v09 June 2020". In brief, the DNA was enzymatically fragmented into pieces of 350 bp, then the DNA was amplified while adding the adapters (IDT® for Illumina® DNA/RNA UD Indexes Set A, Tagmentation (96 Indexes, 96 Samples) #20027213) for cluster generation and unique index sequences were added. After cleanup, all samples were pooled, denatured and loaded onto the machine.

Detailed protocol of NGS sample prep:

0. Measure accurate DNA concentration on qbit (or equivalent instrument) according to manufacturer's instructions.
(Qubit™ 4 Fluorometer, mit WiFi; ThermoFisher #Q33238)

1. Tagment DNA
Material:
BLT [4°C]
TB1 (health hazard!) [-20°C]

Bring BLT and TB1 to room temperature.
Prepare Beads Mastermix (times your n° samples + appropriate surplus):
10 µL BLT
10 µL TB1
Vortex properly and DO NOT spin.
Put 100-500ng DNA into a PCR tube.

[If you have less, consult original Illumina protocol]
Add water to add up to 30 µL.
Add 20 µL of Beads Mastermix.
Resuspend.
Run „Tagment“ program in thermocycler:
Lid-heating
55°C 15min
Hold 10°C

2. Post tagmentation cleanup
Material:
TSB [RT]
TWB [RT]

Add 10µL TSB to the tagmentation reaction.
Run „Tagment Clean“ program in thermocycler:
Lid-heating
37°C 15min
Hold 10°C
Put tubes on magnetic stand and wait until liquid is clear.
Discard supernatant.
2x Wash:
Add 100 µL TWB very slowly to the beads and resupspend.
Put tubes on magnetic stand and wait until liquid is clear.
Discard supernatant.
Add 100 µL TWB very slowly to the beads and resupspend.

3.Amplification of tagmented DNA
Material:
EPM (health hazard!) [-20°C]
Index adapters in 96-well plate [-20°C]

Prepare ice bucket
Thaw EPM on ice, takes at least 15mins.
Thaw index adapter plate on RT.
Prepare PCR Mastermix (times your n° samples + appropriate surplus):
20 µL EPM
20 µL H2O

Vortex properly and spin.
Put sample tubes on magnetic stand and wait until liquid is clear.
Discard supernatant.
Add 40 µL PCR Mastermix very slowly to the beads and resupspend.
Spin down.
Add 10 µL of a different adapter pair of
„pre-paired i7 and i5 index adapters“ to each sample.
Resuspend properly and spin.
Run „TagmentPCR“ program in thermocycler:

Lid-heating
68°C 3min
98°C 3min
5 cycles of:
98°C for 45 seconds
62°C for 30 seconds
68°C for 2 minutes
68°C 3min
Hold 10°C

SAFE STOPPING POINT
If you are stopping, store at 2°C to 8°C for up to 3 days

4. Final cleanup
Material:

SPB [4°C]
RSB [-20°C]
EtOH abs.

Bring SPB and RSB to RT and vortex
Prepare 80 % EtOH from EtOH abs.
Put sample tubes on magnetic stand and wait until liquid is clear.
Transfer 45 µL of the supernatant into a fresh tube.
Add 40 µL H2O to the samples.
Vortex and invert SPB thouroughly.
Add 45µL SPB to the samples. Resuspend well.
[This step presumably mainly removes primers
and leaves PCR product behind in the supernatant.]
Incubate for 5 min.

Vortex and invert SPB thouroughly.
Add 15 µL of fresh SPB into new tubes
Put sample tubes on magnetic stand and wait until liquid is clear.
Transfer 125 µL supernatant from each sample into the corresponding new tube (containing 15 µL fresh SPB), resuspend properly and discard the old tube.
Incubate for 5 min.
[This step presumably mainly binds the PCR products to the beads, as the primers should be gone.]
Put sample tubes on magnetic stand and wait until liquid is clear.
Discard supernatant.
2x Wash:

> Add 200 µL fresh 80 % EtOH to the beads on the magnetic stand and DO NOT resupspend.
> Incubate for 30 sec.
> Discard supernatant.

Remove and discard residual EtOH
Air dry for 5 min.
Add 32 µL RSB to the beads and resuspend thoroughly.
Incubate for 2 min.
Put sample tubes on magnetic stand and wait until liquid is clear.
Transfer 30 µL supernatant to a new tube.

SAFE STOPPING POINT
If you are stopping, store at -25°C to -15°C for up to 30 days.

5. Pooling of libraries and loading
When all samples are ready:
Material:

> 10mM Tris pH8.5
> 200mM Tris-HCl, pH7.0
> Hyb(ridization) Buffer

Measure DNA concentration again with qbit.
Dilute all samples to 1 nM with 10mM Tris pH8.5
Pool samples to one library pool, vortex, spin.
Mix 5 µL of pooled library with 5 µL of 0.1N NaOH [this step denatures the DNA]
Vortex, spin and incubate at RT for 5min.
Add 5 µL of 200mM Tris-HCl, pH7.0
Vortex and spin

Add 985 µL of prechilled Hybridization Buffer to the tube of denatured library pool. This gives a total volume of 1 mL at 5 pM.
Dilute this to 1.2 pM (120 µL library + 380 µL Hyb buffer).
Spike in PhiX (1-30%, here eg. 30%):
150 µL denatured and diluted PhiX + 250 µL library pool.
Load sample onto cartridge: Total load volume is 500 µL.

4.4.2.2 Setting up a NGS run on the Miniseq and data analysis

Readily prepared and pooled samples were loaded onto a cartridge (cartridge needs to thaw on RT at least 2h), which contains all the necessary reagents (MiniSeq Mid Output Kit (300-cycles), Illumina® #FC-420-1004). A sequencing run should not exceed cluster density >20k clusters/cm2, otherwise data might be unreliable. Once the run was completed, data were investigated by running the "PCR amplicon" or "resequencing" modules from the local run manager. Sample names, read length (151 bp), index length (10bp) and sequencing modality (paired end) had to be selected. The analysis compiled fastq files for every samples from the raw data and then aligned it to the reference genome. The resulting .bam files and the corresponding .bai (index) files were visualized with the software Integrated Genome Viewer (IGV).

4.5 Eukaryotic cell culture

4.5.1 Routine cell culture

U2OS cells (HTB-96™) were ordered from ATCC and cultured in McCoy's 5A medium with 10% FBS and 1mM sodium pyruvate. HeLa cells (CCL-2™) and human dermal fibroblasts from adult tissue (HDFA, PCS-201-012™) were also order from ATCC and cultured in Dulbecco's Modified Eagle Medium (DMEM) with 4.5 g/L glucose, GlutaMax™, 1 mM sodium pyruvate and 10% FBS.

Bacterial contamination of all cell lines was suppressed by addition of 100 µg/ml streptomycin and 100 U/ml penicillin to the culture medium. The cells were grown in a CO2 incubator at 37 °C, 5% CO2 and 90% humidity. Before the cells reached confluency, they were split by trysinisation up to a 1:10 dilution and discarded upon reaching p20.

Cells were frozen in antibiotic-free medium supplemented with 20% FBS and 10% DMSO and placed at -80 °C in a freezing container cooling down slowly. Mycoplasma tests were performed by an external provider on the supernatants on a regular basis.

4.5.2 Transfection of eukaryotic cells

4.5.2.1 Electroporation Electroporation of eukaryotic cells was performed with the Amaxa® Cell Line Nucleofector®. The trypsinized cells were resuspended in PBS and adjusted to 1×10^6 cells/100 µL. These 100 µL were transferred to an electroporation cuvette, where 0.5-2 µg of the DNA of interest had been added. The cuvette containing this mixture was put into the electroporator and the according program was applied, eg. X-001 for U-2 OS. The electroporated cells were then resuspended in 1000 µL of fresh medium and plated in an appropriate vessel.

4.5.2.2 Lipofection 5 µL of Lipofectamine® 2000 Reagent (ThermoFisher #11668-019) was diluted in 250 µL of optiMEM (ThermoFisher #11058021). In a separate tube 2 µg of DNA were mixed with 250 µL optiMEM. These two preparations were incubated for 5 min and then combined and incubated for 15-20 min in order for the DNA-lipid complexes to form. The total of 500 µL were then added to cells in a 6-well that were ~ 75 % confluent. No media change was immediately required, but was performed the next day most of the time. If smaller vessel were to be transfected, the amount of the mixture that was applied was lowered accordingly. After 24h-48h of expression the cells were monitored. If BAX or BAK plasmids were expressed, the observation of cell death already started at 4h after transfection and cells were usually mostly dead the next day.

4.5.3 Apoptosis treatment

In order to induce apoptosis, cells were plated and let attach for at least 24 h. They were then treated for 16-20h by exchanging the medium with pre-warmed normal medium containing the required reagents. Usually cells were treated with 10 µM ActD (Merck/Calbiochem # 114666-5MG) and/or 10 µM ABT-737 (Apexbio #A8193). 20 µM Q-VD-OPh (Apexbio #A1901) was added as well in order to prevent the detachment of the cells from the coverslip. These reagents were kept frozen in small aliquots as 8-10 mM stock solutions in DMSO.

4.5.4 Harvest cell pellets

Cells from a confluent 6-well plate were harvested by trypsinisation and spinning at 300 g for 5 mins and the pellet could be stored at -80 °C. When needed, the pellet was resuspended in lysis buffer to generate whole cell protein lysates or used for the extraction of genomic DNA.

4.5.5 Eukaryotic DNA isolation

DNA was isolated of eukaryotic cells with the GenElute™ Mammalian Genomic DNA Miniprep Kit (Sigma # G1N350). A 6-well of confluent U-2 OS cells was harvested by trypsinization, spun down and the pellet thoroughly resuspended in 500 µL of the extraction solution. The kit was used according to manufacturere's instructions. The DNA could then be used right away or frozen at -20 °C.

4.5.6 Fluorescence activated cell sorting (FACS)

Cells from a T-75 were detached by trypsinisation, recovered in normal medium, spun down once and resuspended in 2 mL of PBS. Right before sorting, the cells were passed through a cell strainer with 35 µm mesh size (Falcon® 5 mL Round Bottom Polystyrene Test Tube, with Cell Strainer Snap Cap #352235). The cells were then sorted at a Sony Sorter SH800 by setting the gates according to an untransfected negative and (if possible) a positive control into 96-well plates at a concentration of 1 cell per well.

4.6 CRISPR cell line production

4.6.1 BAX and BAK KO and double KO cells

To generate cell lines with knocked out BAX or BAK or both (DKO), U-2 OS cells were (co-) transfected by electroporation with the plasmids pX458-BAX and/or pX458-BAK, which expressed a gRNA against Exon1 of the respective gene and a GFP (plasmids in section 4.3). Three days after transfection, single cells were transferred into 96-well plates via FACS for GFP. After about 3 weeks, single cell clones were expanded and checked for the absence of the protein by Western Blot. Selected clones were then analyzed by Sanger and/or Illumina sequencing of the targeted exon.

4.6.2 Endogenous tagging of BAX with Halo-tag

To generate cell lines with N-terminally tagged BAX at the endogenous locus, U-2 OS cells were co-transfected by electroporation with the plasmids pX330_BAX_gRNA1, which expressed a gRNA against Exon1 of BAX, as well as the HDR template for genomic Halo-BAX with a GFP reporter in the intronic region between Exon1 and Exon 2 of BAX (plasmids in section 4.3). Three days after transfection, single cells were transferred into 96-well plates via FACS for GFP. After about 3 weeks, single cell clones should have been expanded but none had surivived.

4.6.3 Safe harbor AAVS1 integration

To generate cell lines with a gene inserted into the safe harbor locus AAVS1 [195, 196], U-2 OS cells were co-transfected by electroporation with pX330-AAVS1-gRNA and the respective AAVS1 HDR template plasmid. Three days after transfection, 2,5 - 5 μg/mL Blasticidin (Invivogen #ant-bl-1) for the CMV promoter containing HDR templates (GFP-OMP25, SNAP-OMP25 and cytochrome *c*-mEGFP), or 0.25-1 μg/mL Puromycion (Invivogen #ant-pr-1) for the tet-on promoter containing plasmids (tet-on Halo-BAX), was added to the cells diluted in normal medium in order to select the clones with integration. The surviving clones were single cell sorted into 96-well plates via FACS.

4.7 Labeling of cells

4.7.1 Expression of tagged proteins for live cell imaging

Cells were either stably overexpressing proteins (e.g. SNAP-OMP25) or they were transiently transfected, which was routinely done vie electroporation for most plasmids. Only plasmids which contained BAX or BAK were transfected by lipofection and the cells needed to be processed within a few hours after transfection, otherwise massive cell death would prevent any further experiment.

4.7.2 Induction of expression of tet-on system

Doxycyclin (Sigma #D9891-5G - Lot #36M4008V - CAS-Number: 24390-14-5) was dissolved in sterile water at a stock concentration of 10 mg/mL. A working stock solution was prepared in PBS at 1 mg/mL. This was then diluted in normal medium containing tet-free FBS (Takara/Clontech #631106) instead of normal FBS. The concentration applied to cells was usually 1 μg/mL and expression was monitored 18 h later.

4.7.3 Live cell labeling with STED compatible dyes

Atto590-chloralkene (CA) and SiR-BG were synthesized by the Facility for Synthetic Chemistry, Max-Planck Institute for Multidisciplinary Sciences. The cells were incubated with 250 nM Atto590-chloralkene (CA) and 500 nM SiR-BG in full medium for 30 min - 1 hr, followed by a washout of 30 min - 1 hr. The cells were then rinsed once and subsequently placed in imaging medium.

4.7.4 Immunofluorescence (IF) staining

4.7.4.1 Antibodies for IF staining

In Table 3, the antibodies used for IF are listed.

Antibody	Supplier	Cat#	Dilution
Primary antibodies			
Mouse anti human BAX Monoclonal Antibody (2D2) **"2D2-BAX"**	invitrogen	# MA5-13994	1:50
Rabbit anti human BAX antibody, clone 1C7, ZooMAb® Monoclonal **"1C7-BAX"**	Merck/ Sigma-Aldrich	# ZRB 1103 -4X25U	1:100
Rabbit anti human BAK Recombinant Monoclonal Antibody (clone # SU32-07) **"SU32-BAK"**	invitrogen	# MA5-32111	1:100
Mouse anti human Anti-Bak (Ab-1) mAb (clone #TC-100) **"Ab-1-BAK"**	Merck/ Sigma-Aldrich	# AM03	1:100
Rabbit anti human monoclonal Recombinant Anti-TOMM20 antibody [EPR15581-39]	abcam	# ab186 734	1:100
Mouse anti human Purified Anti-TOM20 Clone 29/TOM20 (RUO)	BD Biosciences	# 612278	1:100
Secondary antibodies			
AffiniPure Sheep Anti-Mouse IgG (H+L), home-coupled to StarRed (Abberior #1-0101-011-3)	Jackson Immuno	# 515-005-062	1:200
AffiniPure Goat Anti-Rabbit IgG (H+L), home-coupled to StarRed (Abberior #1-0101-011-3)	Jackson Immuno	# 111-005-144	1:200
Goat anti-Mouse IgG (H+L) Highly Cross-Adsorbed Secondary Antibody, Alexa Fluor™ 594	invitrogen	# A11032	1:200
Goat anti-Rabbit IgG (H+L) Highly Cross-Adsorbed Secondary Antibody, Alexa Fluor™ 594	invitrogen	# A11037	1:200
F(ab')2-Goat anti-Rabbit IgG (H+L), Alexa Fluor™ 647 **"for 4Pi STORM"**	invitrogen	# A-21246	1:500
Tertiary antibodies			

Rabbit anti human TOMM20 antibody [EPR15581-39], coupled to Alexa Fluor® 488	abcam	# ab205 486	1:50
Mouse anti human cytochrome C clone 6H2.B4, coupled to Alexa Fluor® 488	BD	# 560263	1:50

Table 3: Antibodies used for immunofluorescence

4.7.4.2 Buffers for IF staining

fix: 8% formaldehyde (FA), which was obtained by diluting 16 % FA (Thermo Scientific™/Pierce™ #28908) with PBS
perm: 0.5 % Triton™ X-100 (Merck/Millipore #1086031000) in PBS
block: 5% BSA (Albumin (BSA) Fraction V, (pH 7.0), AppliChem # A13910500) in PBS
wash: PBS, homemade
mount: Prolong Diamond mounting media with or without DAPI (ThermoFisher # P36966 or #P36965)

4.7.4.3 IF staining protocol

Cells were seeded on 12 mm 1.5H coverslips (Marienfeld # 0117520) and let attach at least over night. After an eventual treatment, they were fixed with 8% FA for 10 mins. The coverslips were then washed 3x with PBS and permeabilized for 5 mins. After another 3x wash with PBS, the coverslips were blocked for 30 mins. The primary antibodies were diluted in block buffer and added onto the coverslips in a wet chamber for 1 h at room temperature. After 3x wash, the secondary antibodies, also diluted in block buffer, were added for 1h at room temperature. After another 3x wash, the samples were then mounted with Prolong Dimaond on glass slides (Microscopic Slides with Ground Edges Fisherbrand™ # 11562203). For stainings, which included an antibody directly coupled to a fluorophore (from here on called tertiary antibody), the samples were incubated for 1h with a blocking antibody raised in the same species as the tertiary antibody in order to block unbound epitopes of the secondary antibody. Then the sample was washed 3x and the tertiary antibody was added in block buffer for 1h at room temperature. After washing again 3x, the samples were mounted as described above.

4.8 Microscopy

4.8.1 STED imaging

4.8.1.1 Live cell STED

Live cell STED videos were acquired on a quad scanning STED microscope (Expert Line, Abberior Instruments) equipped with a UPlanSApo 100x/1,40NA oil objective (Olympus), 488, 596 and 650 nm excitation and a 3 W 775 nm depletion lasers. The detection bandwidth of the APD filters were 500-550, 580-630, 650-720 nm. The pinhole was set to 0.9 Airy units and a pixel size of 20 nm with a pixel dwell time of 5-8 µsec and three line accumulations was used. The STED power was set to 20-30 % depending on the channel, the sample brightness and overall equipment performance. Some of the shown fixed cell STED images were acquired on the same microscope with 15 nm pixel size, 10 µsec pixel dwell time, STED powers of 25-60 % and otherwise identical settings as above.

4.8.1.2 Automated fixed cell STED

Some of the shown fixed cell STED images were acquired on the same microscope as above with 15 nm pixel size, 10 µsec pixel dwell time, STED powers of 25-60 % and otherwise identical settings as above. Most of the fixed cell STED recordings, especially all of the images for the quantifications were acquired on a STEDycon (Abberior Instruments) mounted on a Nikon inverted microscope (Ti-2) with a CFI PlanApo 100x/1.45NA oil objective (Nikon). The system was equipped with 405, 488, 561, 640 nm excitation lasers and a 1.5 W 775 nm depletion laser. Detection bands of the APDs were 500-550, 580-630 and 650-700 nm. The pinhole size was set to 1.13 Airy units and a pixel size of 15 nm with a pixel dwell time of 10 µsec and three line averages was used. The STED power was set to 40-70 % depending on the channel, the sample brightness and overall equipment performance. Multi-position acquisition was enabled through the Nikon software and an automated pipeline was programmed to automatically acquire multiple STED images by sending out a TTL trigger signal to the STEDycon software at every pre-definded position (see Appendix C.1).

4.8.2 Correlative live and fixed cell imaging for temporal investigation of apoptosis

The microscope for all correlative assays was a Nikon body with a mounted STEDycon as described above in section 4.8.1.2. All correlative imaging was performed in 8-well dishes (ibidi #80807). One well of the dish was left free and a marker cross was drawn as a unique reference point on the surface of the glass on the inside of the well. The dish with the seeded cells in imaging medium was positioned on the stage, firmly

pressed into one corner of the stage holder and fixed with sticky rubber pads. The cells were recorded in any imaging mode (widefield, confocal, STED) for as long as needed (mostly overnight). The dish was then quickly taken off stage, cells fixed and labeled with IF in the wells (see IF staining protocol 4.7.4.3). After adding mounting medium and an 8mm-coverslip on top of each well, the dish was ready for correlative imaging. The marker cross as reference point on the coverslip was localized manually. All positions from the live cell imaging session including the reference point had been saved in the NIS elements acquisition software from Nikon. By updating the reference point, all other positions could be updated as well and thereby localized again with incredibly high precision and reliability. (I love the Nikon setup and software!) The same cells, which were monitored live were then ready to be recorded fixed with automated STED microscopy as in section 4.8.1.2.

4.8.3 Live cell monitoring in Lionheart automated microscope

Cells were plated in a 24-well glass bottom plate (Greiner #662892) and let attach over night. They were then treated depending on the specific experiment. Just before imaging the medium was replaced with FluoroBrite™ DMEM (Gibco #A1896701) supplemented with 10 % FCS. Depending on the assay, the imaging medium was also supplemented with 20 μM Q-VD-OPh or 10 μM ActD + 10 μM ABT-737 + 20 μM Q-VD-OPh and/or 50 ng/mL Hoechst33342 and/or 50 nM Sytox orange. The microscope was pre-heated to 37°C and 5% CO2 was supplied.

4.8.4 4Pi STORM imaging

The samples for 4 Pi STORM imaging were prepared like described in section 4.7.4.3 with slight differences (see also [186]): The cells were seeded on custom-made coverslips, which had been sputter-coated with a thin aluminum layer covering one-quarter of the glass, to create a mirror surface needed for alignment of the sample and microscope objectives. After the usual treatment, fixation and primary antibody staining, the secondary antibody was replaced by Fab fragments coupled to Alexa Fluor 647 (Thermo Fisher, A21246; dilution 1:500). Fiducial beads were added to the samples and they were mounted in imaging buffer by placing a second coverslip on top. This sandwich of coverslips (containing the cell layer with beads in between) was sealed and mounted vertically on the stage of the microscope.

4.8.5 MINFLUX imaging

The samples for MINFLUX imaging were prepared like described in section 4.7.4.3 with slight differences (also see [189]): The cells were seeded, treated, fixed and stained

as usual. The secondary antibody contained a DNA-PAINT [245] docking strand instead of a fluorophore. Fiducial gold particles (BBI solutions #SKU EM.GC150/4) were then placed on the sample and after a quick wash, the sample was mounted on microscope slides with cavities (BRAND® cavity slides #BR475535-50EA) containing imaging buffer (Massive Photonics) with 2-4 nM DNA-PAINT imager strand coupled to Atto655 corresponding to the DNA strand on the secondary antibody (Massive Photonics).

4.9 Data representation for illustrations

For image representation in figures (but never before data analysis), images were contrast enhanced, in BAX and BAK channels the background was subtracted with a rolling ball algorithm with a pixel size of 20 and most channels were filtered with a Gaussian filter with sigma of 1 or 2 in FIJI. For live cell STED videos the MOM channel was bleach corrected with the FIJI-in-built histogram-match.

4.10 Quantifications of microscopy data

4.10.1 GFP-BAX overexpression death curve analysis

Images of GFP-BAX overexpressing cells were analyzed with a custom FIJI script. They were adjusted for brightness and contrast and a Gaussian blur of sigma 5 was applied. The "Intermodes" threshold was used and of the resulting particles the ones with a circularity above 0.8 were considered "rounded up" and thus dead.

4.10.2 Ring length and Pearson correlation coefficient of BAX and BAK in the ring

Rings were quantified in a semi-automated manner. The ring circumferences were manually annotated in FIJI in images from 3 independent replicates. The line width was then adjusted to 5 pixels and the circumference length as well as fluorescence intensity profiles were plotted on unprocessed raw data with FIJI and saved as .csv files (for FIJI code see subsection A.1). The fluorescence intensities were then normalized to the fluorescence of all rings in the same sample (for Python code see subsection B.1). The Pearson correlation coefficient between the BAX and BAK intensities was calculated in a custom Python script (for Python code see subsection B.3). All other calculations were also performed with Python

Appendices

Appendix A FIJI code

A.1 Semi-automated analysis of BAX-BAK rings

```
/*prompts the user to open a directory with tiffs, where an enhanced
 * image with both Bax and Bak channels is available.
 * User choses one ring and draws a line around it
 * the script then edits the selection to a 5pixel wide line,
 * adds it to ROI manager.
 * Then opens the corresponding raw data file
 * chooses Bax and Bak channels separately
 * draws a line profile of the selected structure from
 * the ROI manager on the raw data files
 * saves the line profile as csv
 * also saves the ROI with the same name as the image file
 * Sarah Schweighofer, Mar 2022, MPINAT, Göttingen
*/


// choose source directory
filepath_obf = getDirectory("Choose Source Directory ");
//CHOOSE THE LOCATION OF THE ORIGINAL HERE!
filepath = filepath_obf + "/tifs"
 filelist = getFileList(filepath);

// choose save directory
savepath ="P:/Private/practice/quantification_of_imaging_experiments/
    manual_ring_quantification_all-rings/"

for (i = 0; i < filelist.length; i++) {
  filename = filelist[i];
  print(filename);

  //if you find your_string anywhere in the filename - user can change this to any
    string wanted
  your_string = "_merge.STED-enh99.9.tiff.jpg";
```

```
31  if (endsWith(filename, your_string)) {
32     file  = filepath  + "/"  + filename;
33     print( file );
34     open(file);
35     title  = getTitle();
36
37     //select rings
38     waitForUser("ROI", "Please select freehand tool and draw ROIs. Then add them
       to the ROI manager by pressing t. Click OK when done.");
39
40     //  open the original raw data
41     original_title  = replace(filename, your_string, ".obf");
42     original_file  = filepath_obf + original_title;
43     run("Bio-Formats Importer",
44     "open=original_file autoscale color_mode=Default open_files open_all_series
       rois_import=[ROI manager] view=Hyperstack stack_order=XYCZT");
45
46     Bax = original_title  + "  - Bax.STED";
47
48     Bak = original_title  + "  - Bak.STED";
49
50     //now I look at the ROIs on the original images
51     count = roiManager("count");
52
53     //only if  user chose at least  one ROI,
54     //I  want to execute the following code:
55     if (count > 0) {
56       for  (j  = 0;  j  < count; j++) {
57          //rename the ROIs
58          roiManager("select", j);
59          roiManager("Set Line Width", 5);
60          roiManager("Rename", title+"ROI"+j+1);
61          //i  starts  with 0 but I  want to start  counting with 1
62
63
64          //look at  the ROIs on the Bax image and plot profile and get values
65          selectImage(Bax);
66          roiManager("select", j);
```

```
67          run("Plot Profile");
68          Bax_values =
69          Plot.getValues(Bax_microns, Bax_intensities);
70
71          //same for Bak
72          selectImage(Bak);
73          roiManager("select", j);
74          run("Plot Profile");
75          Bax_values = Plot.getValues(Bak_microns, Bak_intensities);
76          //20220621: I think this is an error, I said Bax_values again although it
        should be Bak_values.
77          //On the other hand it doesn't matter, cause the variable is not used. I don't
        want to change the code now
78
79
80          // create new results table
81          Table.create("line_profiles");
82          // set length column
83          Table.setColumn("µm", Bax_microns);
84          // set Bax column
85          Table.setColumn("Bax Intensities", Bax_intensities);
86          // set Bak column
87          Table.setColumn("Bak Intensities", Bak_intensities);
88
89          saveAs("Results", savepath + "Plot_Values_" + original_title + "_ROI" + j+1 +
        ".csv");
90          selectWindow("Plot_Values_" + original_title + "_ROI" + j+1 + ".csv");
91
92          //close the table;
93          run("Close" );
94
95          //save the ROI in its boundingbox as jpg
96          selectImage(title);
97          roiManager("select", j);
98          roiManager("Set Line Width", 30);
99          run("To Bounding Box");
100         run("Duplicate...", "duplicate");
101         // save ROIs as is
```

```
102         save_title = replace(title, ". tif", "_ROI" + j+1 + ".jpg");   //i starts with 0
    but I want to start counting with 1
103         saveAs("Jpeg", savepath + save_title);
104
105         // in order to save the ROIs with their original line width I need to set it
    back
106         roiManager("select", j);
107         roiManager("Set Line Width", 5);
108       }
109
110       //now save the ROI set as zip so that it can be opened on the corresponding
    image again
111       roiManager("Save", savepath + original_title + "RoiSet.zip");
112
113       //clear the ROI manager
114       selectWindow("ROI Manager");
115       run("Close" );
116     }
117
118
119     //close all open images
120     close ("*");
121   }
122 }
```

Appendix B Python code

B.1 Normalization of BAX BAK rings

```
'''
NORMALIZATION SCRIPT 1
This program opens csv files of ring line profiles raw data in one folder.
Then reads out all Bax and Bak raw values and calculates the min and max for all the samples in the folder and saves it in a new csv.
This can then be used to ormalize values to this general MIN/MAX values – see other scripts.
User needs to just run the script, everything else is asked for.
Göttingen, August 2022, Sarah Vanessa Schweighofer, MPI–NAT
'''

import os
from tkinter import filedialog
import pandas as pd
import seaborn as sns
import matplotlib.pyplot as plt
import numpy as np



def main():
    # let the user choose the folder containing the tables
    root_path = filedialog.askdirectory() # prompts user to choose directory. From tkinter
    # prints out the number of files in the selected folder with the wanted file format and adds them to a list
    file_format = ".csv"
    filenames = [filename for filename in sorted(os.listdir(root_path)) if filename.startswith(("Plot_"))]
    print("There are {} files with this format.".format(len(filenames)))
    if not filenames: # pythonic for if a list is empty
        print("There are no files with this format.")

```

```
29  Bax_maxes = [] # empty list for all mins and maxes, all of these are gonna be
    our columns in the final csv.
30  Bak_maxes = []
31  Bax_mins = []
32  Bak_mins = []
33
34  for filename in filenames:
35      print(filename)
36      file_path = os.path.join(root_path, filename)
37      df = pd.read_csv(file_path, encoding='latin1') # latin1 encocing needed in
    order to be able to read special chars like "µ"
38      print(df)
39
40      ###### save all maximumn and minumum Bax and Bak values in one large
    csv ####################
41      Bax_max = df["Bax Intensities"].max() # in order to calculate the max of
    each colum
42      Bak_max = df["Bak Intensities"].max()
43      Bax_min = df["Bax Intensities"].min()
44      Bak_min = df["Bak Intensities"].min()
45
46      Bax_maxes.append(Bax_max)
47      Bak_maxes.append(Bak_max)
48      Bax_mins.append(Bax_min)
49      Bak_mins.append(Bak_min)
50
51  # create the min/max output table
52
53  data = {"filenames": filenames,
54          "Bax max": Bax_maxes,
55          "Bak max": Bak_maxes,
56          "Bax min": Bax_mins,
57          "Bak min": Bak_mins}
58
59  print(data)
60
61  df = pd.DataFrame(data)
62
```

```
63      result_path = os.path.join(root_path, 'results')
64      if not os.path.isdir(result_path):
65          os.makedirs(result_path)
66      savepath = os.path.join(result_path, "mins_maxes.csv")
67      df.to_csv(savepath)
68
69
70  if __name__ == '__main__':
71      main()
72
73  '''
74  NORMALIZATION SCRIPT 2
75  This program opens line plot raw csv files.
76  Then calculates the relative Bax or Bak values by using the min-max-value csv
        created with Bax-Bak-min-max_over-replicate.py.
77  Then saves a new csv of these relative values.
78  From this it then plots the line profile with matplotlib and saves it as png.
79  User needs to just run the script, everything is asked for.
80  Göttingen, August 2022, Sarah Vanessa Schweighofer, MPI-NAT
81  '''
82
83  import os
84  from tkinter import filedialog
85  import pandas as pd
86  import seaborn as sns
87  import matplotlib.pyplot as plt
88  import numpy as np
89
90
91
92  def main():
93      # let the user choose the folder containing the tables
94      root_path = filedialog.askdirectory()  # prompts user to choose directory. From
        tkinter
95
96      ###### open the csv with all the min and max values from this repliccate,
        created with "Bax-Bak-min-max_over-replicate.py"
97      result_path = os.path.join(root_path, 'results')
```

```
98      file_path = os.path.join(result_path, "mins_maxes.csv")
99      min_max = pd.read_csv(file_path, encoding='latin1')  # better already sort the
        csv manually before importing
100
101     ###### calculate min and max intensity of all the rings in this replicate
        ####################
102     Bax_min = min_max["Bax min"].min()  # in order to calculate the min of the Bax
         values
103     Bak_min = min_max["Bak min"].min()  # in order to calculate the min of the Bax
         values
104     Bax_max = min_max["Bax max"].max()
105     Bak_max = min_max["Bak max"].max()
106
107     # prints out the number of files in the selected folder with the wanted file
        format and adds them to a list
108     file_format = ".csv"
109     filenames = [filename for filename in sorted(os.listdir(root_path)) if filename.
        startswith(("Plot_"))]
110     print("There are {} files with this format.".format(len(filenames)))
111     if not filenames: # pythonic for if a list is empty
112         print("There are no files with this format.")
113     for filename in filenames:
114         print(filename)
115         file_path = os.path.join(root_path, filename)
116         df = pd.read_csv(file_path, encoding='latin1')  # latin1 encocing needed in
        order to be able to read special chars like "µ"
117         print(df)
118
119         ########## normalize the raw values to the overall brightness of this
        channel in this raplicate #######
120         Bax_norm = (df["Bax Intensities"] - Bax_min) / (Bax_max - Bax_min)
121         Bak_norm = (df["Bak Intensities"] - Bak_min) / (Bak_max - Bak_min)
122
123         ##### create a new csv with these normalized values ######
124         df2 = pd.concat([df["µm"], Bax_norm, Bak_norm], axis=1)
125         print(df2)
126
127         new_filename = filename[12:-4]
```

```
128         print(new_filename)
129         output_file = os.path.join(result_path, new_filename + "_normalized-by-
        rings-replicate.csv")
130         print(output_file)
131         df2.to_csv(output_file)
132         ####################################
133 
134         #### plot the whole story with pandas/matplotlib ######
135         my_x_ticks = df["µm"]
136         plt.figure(figsize=(11.7, 8.27))
137         plt.plot(my_x_ticks, Bax_norm, label='Bax', color='#0EB30E')
138         plt.plot(my_x_ticks, Bak_norm, label='Bak', color='#D10FD1')
139 
140         plt.xticks(my_x_ticks) #df["nm"]
141         plt.locator_params(axis='x', nbins=10)
142 
143         # TODO: set size of the tickmark labels with matplotlib
144         # plt.set_xticklabels(plot.get_xticks(), size=16)
145         #       # plot.set_yticklabels(plot.get_yticks(), size=16)
146 
147         plt.title(filename, y=0.9, fontsize=24) # y is a relative coordinate system.
        1 is at the very top, 0.9 a little below and so on
148         plt.xticks(fontsize=20)
149         plt.yticks(fontsize=20)
150         plt.xlabel('length [µm]', fontsize=24)
151         plt.ylabel('normalized fluorescence intensity [a.u.]', fontsize=24)
152         plt.legend(fontsize=16, title_fontsize=24, loc="lower right")
153 
154         new_filename = filename[12:-4]
155         output_file = os.path.join(result_path, new_filename + "line-
        plot_normalized-to-repl-rings.png")
156         plt.savefig(output_file)
157 
158         ## plt.show() #needs to come after savefig, otherwise saved plot will be
        blank...    ################################################
159 
160 if __name__ == '__main__':
161     main()
```

B.2 Rolling mean function definition

```
1  def rolling_mean(window_size, starting_value, x_series, y_series, max_x_value,
       roll_factor):
2      '''
3      :param window_size: how big is the window sliding over the dataset
4      :param starting_value: where does the sliding start
5      :param x_series: series of pandas dataframe containing the independent x
       values
6      :param y_series: series of pandas dataframe containing the dependent y values
7      :param max_x_value: where should the while loop stop, eg 100% Bax content or
       maximal ring length etc
8      :param roll_factor:in which increments should the window slide over the data
9      :return: rollmeans: the means for each slided window and rollmean_x: the
       according x values
10     '''
11     # x is the independent, y the dependent variable
12     x_slices = []
13     x_slice_indices = []
14     rollmeans = []
15     rollmean_x = []
16
17     # schleife mit stepsize
18     i = starting_value
19     while i < max_x_value: # 100 is the maximal possible amount
20         # find all the x values in a certain window of the series (= slice)
21         x_slice = x_series[(x_series >= i) & (x_series < (i + window_size))].
       sort_values() # find all the values between x and (x plus stepsize) and sort the
       list ascending
22         print(i)
23         print(x_slice)
24         x_slices.append(x_slice)
25
26         # find the index values of the x values in the slice
27         slice_index = x_slice.index
28         x_slice_indices.append(slice_index)
29         print(slice_index)
30
```

```
31          # find the according y values at the given indices
32          y_values = y_series.iloc[slice_index]
33          print(y_values)
34
35          # calculate the y mean in each y slice
36          mean = y_values.mean()
37          rollmeans.append(mean)
38
39          # create column with adequate window size
40          rollmean_x.append(i)
41
42          i += window_size / roll_factor # increase i with window size durch 2 oder 4
        etc um wirklich nen rolling zu haben!!!
43
44      print(x_slices)
45      print(x_slice_indices)
46      print(rollmeans)
47      print(len(rollmeans))
48      print(len(rollmean_x))
49
50      return rollmeans, rollmean_x
```

B.3 PCC of BAX BAK rings

```
'''
This program opens a folder with csv files.
Then calculates the Pearson correlation coefficient.
Göttingen, March 2022, Sarah Vanessa Schweighofer, MPI-NAT
'''

import os
from tkinter import filedialog
import pandas as pd
import seaborn as sns
import matplotlib.pyplot as plt



def main():
    names = [] #empty list for all filenames, both of these are gonna be our columns in the final csv.
    pearsons = [] #empty list for alle the pearson coefficients
    # let the user choose the folder containing the images to be converted
    root_path = filedialog.askdirectory() # prompts user to choose directory. From tkinter

    # prints out the number of files in the selected folder with the .tiff file format
    file_ending = "replicate.csv"
    file_list = []
    # spaziert durch alle Subdirectories und sucht sich alle Files und packt sie in ne neue Liste, die ich oben neu kreiert habe
    for root, dirs, files in os.walk(root_path):
        for name in files:
            file_list.append(os.path.join(root, name))
            print(name)
    print( file_list )
    filenames = [filename for filename in file_list if filename.endswith(file_ending)]
    print("There are {} files with this format.".format(len(filenames)))
    if not filenames: # pythonic for if a list is empty
```

```
33          print("There are no files with this format.")
34
35      for filename in filenames:
36          print(filename)
37          names.append(filename)
38          file_path = os.path.join(root_path, filename)
39          table = pd.read_csv(file_path, encoding='latin1') #latin1 encocing needed
        in order to be able to read special chars like "µ"
40          print(table)
41
42          Bax = table["Bax Intensities"]  # in order to calculate the mean of each
        colum
43          Bak = table["Bak Intensities"]
44
45          pearson = Bax.corr(Bak, method="pearson")
46          print(pearson)
47
48          pearson = pearson.iat[0, 1] #as it spits out a correlation matrix between all
        columns in a dataframe, again as datafram itself, I need to pick the value out of
        the datafram, then correlates the two columns with each other
49          print(pearson)
50
51          pearsons.append(pearson)
52
53      print(names)
54      print(pearsons)
55
56      #create the final output table
57
58      data = {"filenames": filenames,
59              "pearson coefficient": pearsons}
60
61      print(data)
62
63      df = pd.DataFrame(data)
64
65      # calculate the median
66      median = df["pearson coefficient"].median()
```

```
67
68      print(df)
69      print("The median is: {}.".format(median))
70
71      savepath = os.path.join(root_path, "Pearsons.csv")
72      df.to_csv(savepath)
73
74      # # visualize as histogram with pandas
75      # hist = df.hist(column='pearson coefficient', bins=10)
76      # plt.hist
77      # plt.show()
78
79      # visualize as histogram with seaborn
80      sns.set_style("white")
81      hist = sns.displot(x='pearson coefficient', data=data, kde=True, color="#808080
        ", binwidth=0.1, binrange=(-1, 1), height=8.27, aspect=11.7/8.27) # height=8.27,
        aspect=11.7/8.27 so stellt man die Größe beim displor ein, bei anderene gehts ü
        ber figsize; das sind die Werte für A4 in inches
82      # kde = kernel density estimation distribution aka the line over te histogram,
        length measures in inch!!
83      plt.title('Spatial Correlation of Bax and Bak in the ring', y=0.97, fontsize=24) #
        y is a relative coordinate system. 1 is at the very top, 0.9 a little below and so
         on
84      plt.xticks(fontsize=20)
85      plt.yticks(fontsize=20)
86      plt.xlabel('Pearson Correlation Coefficients', fontsize=24)
87      plt.ylabel('Count', fontsize=24)
88      plt.tight_layout() #damits keine legends abschneidet und so
89      # add the vertical line for the median
90      plt.axvline(x=median, ymax=0.95, color='black', lw=2.5) #ymax makes the line
        not go into the title, the variable median comes from above
91      plt.hist
92      plt.show()
93
94      ################################## write text file with median and
        number of analyzed rings ##########################################
95      savepath = os.path.join(root_path, "lengths.txt")
96      with open(savepath, "w") as f: # Opens file and casts as f
```

```
97          f.write("The median is " + str(median) + ". I analyzed " + str(len(df)) + "
        rings.")  # Writing
98          # File closed automatically
99
100
101 if __name__ == '__main__':
102     main()
```

Appendix C Nikon NIS-Elements code

C.1 Automated acquisition of 1 STED image per 1 widefield position

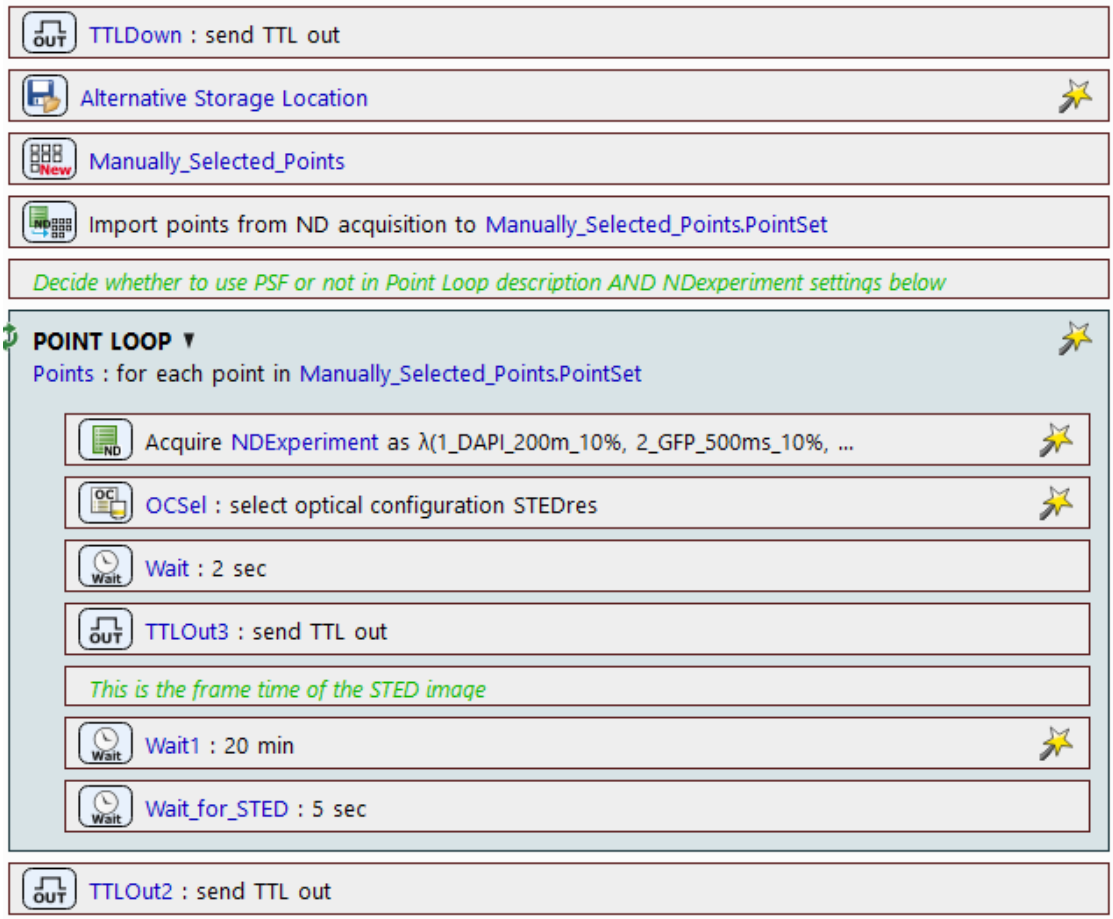

Figure 57: Code for automated acquisition of STED images. It was necessary to write custom code in the graphical programming language of the Nikon software NDAcquisition to acquire 1 STED image for every selected position via sending TTL triggers out to the STEDycon software.

References

[1] William Shakespeare. *Hamlet*. Wordsworth classics. Wordsworth Classics, Ware, 1601.

[2] Douglas R. Green. A matter of life and death. *Cold Spring Harbor perspectives in biology*, 14(1), 2022. URL: https://cshperspectives.cshlp.org/content/14/1/a041004.full, doi:10.1101/cshperspect.a041004.

[3] Carl Vogt. *Untersuchungen über die Entwicklungsgeschichte der Geburtshelferkröte (Alytes obstetricans)*. Jent & Gassmann, 1842. URL: https://books.google.de/books?id=FjtOAAAAcAAJ&printsec=frontcover&hl=de#v=onepage&q&f=false.

[4] A. Glücksmann. Cell deaths in normal vertebrate ontogeny. *Biological reviews of the Cambridge Philosophical Society*, 26(1):59–86, 1951. URL: https://onlinelibrary.wiley.com/doi/abs/10.1111/j.1469-185X.1951.tb00774.x.

[5] G. Kroemer, W. S. El-Deiry, P. Golstein, M. E. Peter, D. Vaux, P. Vandenabeele, B. Zhivotovsky, M. V. Blagosklonny, W. Malorni, R. A. Knight, M. Piacentini, S. Nagata, and G. Melino. Classification of cell death: recommendations of the nomenclature committee on cell death. *Cell Death & Differentiation*, 12 Suppl 2:1463–1467, 2005. URL: https://www.nature.com/articles/4401724, doi:10.1038/sj.cdd.4401724.

[6] Lorenzo Galluzzi, Ilio Vitale, Stuart A. Aaronson, John M. Abrams, Dieter Adam, Patrizia Agostinis, Emad S. Alnemri, Lucia Altucci, Ivano Amelio, David W. Andrews, Margherita Annicchiarico-Petruzzelli, Alexey V. Antonov, Eli Arama, Eric H. Baehrecke, Nickolai A. Barlev, Nicolas G. Bazan, Francesca Bernassola, Mathieu J. M. Bertrand, Katiuscia Bianchi, Mikhail V. Blagosklonny, Klas Blomgren, Christoph Borner, Patricia Boya, Catherine Brenner, Michelangelo Campanella, Eleonora Candi, Didac Carmona-Gutierrez, Francesco Cecconi, Francis K-M Chan, Navdeep S. Chandel, Emily H. Cheng, Jerry E. Chipuk, John A. Cidlowski, Aaron Ciechanover, Gerald M. Cohen, Marcus Conrad, Juan R. Cubillos-Ruiz, Peter E. Czabotar, Vincenzo D'Angiolella, Ted M. Dawson, Valina L. Dawson, Vincenzo de Laurenzi, Ruggero de Maria, Klaus-Michael Debatin, Ralph J. DeBerardinis, Mohanish Deshmukh, Nicola Di Daniele, Francesco Di Virgilio, Vishva M. Dixit, Scott J. Dixon, Colin S. Duckett, Brian D. Dynlacht, Wafik S. El-Deiry, John W. Elrod, Gian Maria Fimia, Simone Fulda,

Ana J. García-Sáez, Abhishek D. Garg, Carmen Garrido, Evripidis Gavathiotis, Pierre Golstein, Eyal Gottlieb, Douglas R. Green, Lloyd A. Greene, Hinrich Gronemeyer, Atan Gross, Gyorgy Hajnoczky, J. Marie Hardwick, Isaac S. Harris, Michael O. Hengartner, Claudio Hetz, Hidenori Ichijo, Marja Jäättelä, Bertrand Joseph, Philipp J. Jost, Philippe P. Juin, William J. Kaiser, Michael Karin, Thomas Kaufmann, Oliver Kepp, Adi Kimchi, Richard N. Kitsis, Daniel J. Klionsky, Richard A. Knight, Sharad Kumar, Sam W. Lee, John J. Lemasters, Beth Levine, Andreas Linkermann, Stuart A. Lipton, Richard A. Lockshin, Carlos López-Otín, Scott W. Lowe, Tom Luedde, Enrico Lugli, Marion MacFarlane, Frank Madeo, Michal Malewicz, Walter Malorni, Gwenola Manic, Jean-Christophe Marine, Seamus J. Martin, Jean-Claude Martinou, Jan Paul Medema, Patrick Mehlen, Pascal Meier, Sonia Melino, Edward A. Miao, Jeffery D. Molkentin, Ute M. Moll, Cristina Muñoz-Pinedo, Shigekazu Nagata, Gabriel Nuñez, Andrew Oberst, Moshe Oren, Michael Overholtzer, Michele Pagano, Theocharis Panaretakis, Manolis Pasparakis, Josef M. Penninger, David M. Pereira, Shazib Pervaiz, Marcus E. Peter, Mauro Piacentini, Paolo Pinton, Jochen H. M. Prehn, Hamsa Puthalakath, Gabriel A. Rabinovich, Markus Rehm, Rosario Rizzuto, Cecilia M. P. Rodrigues, David C. Rubinsztein, Thomas Rudel, Kevin M. Ryan, Emre Sayan, Luca Scorrano, Feng Shao, Yufang Shi, John Silke, Hans-Uwe Simon, Antonella Sistigu, Brent R. Stockwell, Andreas Strasser, Gyorgy Szabadkai, Stephen W. G. Tait, Daolin Tang, Nektarios Tavernarakis, Andrew Thorburn, Yoshihide Tsujimoto, Boris Turk, Tom Vanden Berghe, Peter Vandenabeele, Matthew G. Vander Heiden, Andreas Villunger, Herbert W. Virgin, Karen H. Vousden, Domagoj Vucic, Erwin F. Wagner, Henning Walczak, David Wallach, Ying Wang, James A. Wells, Will Wood, Junying Yuan, Zahra Zakeri, Boris Zhivotovsky, Laurence Zitvogel, Gerry Melino, and Guido Kroemer. Molecular mechanisms of cell death: recommendations of the nomenclature committee on cell death 2018. *Cell Death & Differentiation*, 25(3):486–541, 2018. URL: https://www.nature.com/articles/s41418-017-0012-4, doi:10.1038/s41418-017-0012-4.

[7] S. Brenner. The genetics of caenorhabditis elegans. *Genetics*, 77(1):71–94, 1974. URL: https://academic.oup.com/genetics/article/77/1/71/5991065, doi:10.1093/genetics/77.1.71.

[8] H. Ellis. Genetic control of programmed cell death in the nematode c. elegans. *Cell*, 44(6):817–829, 1986. URL: https://www.sciencedirect.com/science/article/pii/0092867486900048, doi:10.1016/0092-8674(86)90004-8.

[9] H. R. Horvitz and J. E. Sulston. Isolation and genetic characterization of cell-lineage mutants of the nematode caenorhabditis elegans. *Genetics*, 96(2):435–454, 1980. URL: https://academic.oup.com/genetics/article/96/2/435/5994280, doi:10.1093/genetics/96.2.435.

[10] D. L. Vaux, S. Cory, and J. M. Adams. Bcl-2 gene promotes haemopoietic cell survival and cooperates with c-myc to immortalize pre-b cells. *Nature*, 335(6189):440–442, 1988. URL: https://www.nature.com/articles/335440a0, doi:10.1038/335440a0.

[11] Douglas Hanahan and Robert A. Weinberg. Hallmarks of cancer: the next generation. *Cell*, 144(5):646–674, 2011. URL: https://www.cell.com/fulltext/S0092-8674(11)00127-9, doi:10.1016/j.cell.2011.02.013.

[12] J. H. Su, A. J. Anderson, B. J. Cummings, and C. W. Cotman. Immunohistochemical evidence for apoptosis in alzheimer's disease. *Neuroreport*, 5(18):2529–2533, 1994. URL: https://journals.lww.com/neuroreport/Abstract/1994/12000/Immunohistochemical_evidence_for_apoptosis_in.31.aspx, doi:10.1097/00001756-199412000-00031.

[13] G. A. MacGibbon, P. A. Lawlor, E. S. Sirimanne, M. R. Walton, B. Connor, D. Young, C. Williams, P. Gluckman, R. L. Faull, P. Hughes, and M. Dragunow. Bax expression in mammalian neurons undergoing apoptosis, and in alzheimer's disease hippocampus. *Brain Research*, 750(1-2):223–234, 1997. URL: https://www.sciencedirect.com/science/article/pii/S0006899396013510, doi:10.1016/S0006-8993(96)01351-0.

[14] S. Shimohama. Apoptosis in alzheimer's disease–an update. *Apoptosis : an international journal on programmed cell death*, 5(1):9–16, 2000. URL: https://link.springer.com/article/10.1023/A:1009625323388, doi:10.1023/A:1009625323388.

[15] Isidro Ferrer. Apoptosis: future targets for neuroprotective strategies. *Cerebrovascular diseases (Basel, Switzerland)*, 21 Suppl 2(Suppl. 2):9–20, 2006. URL: https://www.karger.com/Article/FullText/91699, doi:10.1159/000091699.

[16] Brad R. S. Broughton, David C. Reutens, and Christopher G. Sobey. Apoptotic mechanisms after cerebral ischemia. *Stroke*, 40(5):e331–9, 2009. URL: https://www.ahajournals.org/doi/10.1161/STROKEAHA.108.531632, doi:10.1161/STROKEAHA.108.531632.

[17] D. L. Vaux. Apoptosis timeline. *Cell Death & Differentiation*, 9(4):349–354, 2002. URL: https://www.nature.com/articles/4400990, doi:10.1038/sj.cdd.4400990.

[18] J. F. Kerr, A. H. Wyllie, and A. R. Currie. Apoptosis: a basic biological phenomenon with wide-ranging implications in tissue kinetics. *British Journal of Cancer*, 26(4):239–257, 1972. URL: https://www.nature.com/articles/bjc197233, doi:10.1038/bjc.1972.33.

[19] W. Wood, M. Turmaine, R. Weber, V. Camp, R. A. Maki, S. R. McKercher, and P. Martin. Mesenchymal cells engulf and clear apoptotic footplate cells in macrophageless pu.1 null mouse embryos. *Development (Cambridge, England)*, 127(24):5245–5252, 2000. URL: https://journals.biologists.com/dev/article/127/24/5245/41046/Mesenchymal-cells-engulf-and-clear-apoptotic, doi:10.1242/dev.127.24.5245.

[20] K. Kokawa, T. Shikone, and R. Nakano. Apoptosis in the human uterine endometrium during the menstrual cycle. *The Journal of Clinical Endocrinology & Metabolism*, 81(11):4144–4147, 1996. URL: https://academic.oup.com/jcem/article/81/11/4144/2649595?login=true, doi:10.1210/jcem.81.11.8923873.

[21] A. Schwarz, R. Bhardwaj, Y. Aragane, K. Mahnke, H. Riemann, D. Metze, T. A. Luger, and T. Schwarz. Ultraviolet-b-induced apoptosis of keratinocytes: evidence for partial involvement of tumor necrosis factor-alpha in the formation of sunburn cells. *The Journal of investigative dermatology*, 104(6):922–927, 1995. URL: https://www.sciencedirect.com/science/article/pii/S0022202X15421967, doi:10.1111/1523-1747.ep12606202.

[22] N. A. Thornberry and Y. Lazebnik. Caspases: enemies within. *Science (New York, N.Y.)*, 281(5381):1312–1316, 1998. URL: https://www.science.org/doi/10.1126/science.281.5381.1312, doi:10.1126/science.281.5381.1312.

[23] Markus Rehm, Heiko Dussmann, Reiner U. Janicke, Jeremy M. Tavare, Donat Kogel, and Jochen H. M. Prehn. Single-cell fluorescence resonance energy transfer analysis demonstrates that caspase activation during apoptosis is a rapid process. role of caspase-3. *The Journal of biological chemistry*, 277(27):24506–24514, 2002. URL: https://www.sciencedirect.com/science/article/pii/S0021925819666287, doi:10.1074/jbc.M110789200.

[24] Rebecca C. Taylor, Sean P. Cullen, and Seamus J. Martin. Apoptosis: controlled demolition at the cellular level. *Nature reviews. Molecular cell biology*, 9(3):231–241, 2008. URL: https://www.nature.com/articles/nrm2312, doi:10.1038/nrm2312.

[25] J. R. Williams, J. B. Little, and W. U. Shipley. Association of mammalian cell death with a specific endonucleolytic degradation of dna. *Nature*, 252(5485):754–755, 1974. URL: https://www.nature.com/articles/252754a0, doi:10.1038/252754a0.

[26] A. H. Wyllie. Glucocorticoid-induced thymocyte apoptosis is associated with endogenous endonuclease activation. *Nature*, 284(5756):555–556, 1980. URL: https://www.nature.com/articles/284555a0, doi:10.1038/284555a0.

[27] Katsumori Segawa, Sachiko Kurata, Yuichi Yanagihashi, Thijn R. Brummelkamp, Fumihiko Matsuda, and Shigekazu Nagata. Caspase-mediated cleavage of phospholipid flippase for apoptotic phosphatidylserine exposure. *Science (New York, N.Y.)*, 344(6188):1164–1168, 2014. URL: https://www.science.org/doi/10.1126/science.1252809, doi:10.1126/science.1252809.

[28] V. A. Fadok, D. R. Voelker, P. A. Campbell, J. J. Cohen, D. L. Bratton, and P. M. Henson. Exposure of phosphatidylserine on the surface of apoptotic lymphocytes triggers specific recognition and removal by macrophages. *Journal of immunology (Baltimore, Md. : 1950)*, 148(7):2207–2216, 1992. URL: https://www.jimmunol.org/content/148/7/2207.long.

[29] S. J. Martin, C. P. Reutelingsperger, A. J. McGahon, J. A. Rader, R. C. van Schie, D. M. LaFace, and D. R. Green. Early redistribution of plasma membrane phosphatidylserine is a general feature of apoptosis regardless of the initiating stimulus: inhibition by overexpression of bcl-2 and abl. *Journal of Experimental Medicine*, 182(5):1545–1556, 1995. URL: https://rupress.org/jem/article/182/5/1545/25769/Early-redistribution-of-plasma-membrane, doi:10.1084/jem.182.5.1545.

[30] Florian J. Bock and Stephen W. G. Tait. Mitochondria as multifaceted regulators of cell death. *Nature reviews. Molecular cell biology*, 21(2):85–100, 2020. URL: https://www.nature.com/articles/s41580-019-0173-8, doi:10.1038/s41580-019-0173-8.

[31] F. C. Kischkel, S. Hellbardt, I. Behrmann, M. Germer, M. Pawlita, P. H. Krammer, and M. E. Peter. Cytotoxicity-dependent apo-1 (fas/cd95)-associated proteins form a death-inducing signaling complex (disc) with the receptor. *The EMBO journal*, 14(22):5579–5588, 1995. URL: https://www.embopress.org/doi/abs/10.1002/j.1460-2075.1995.tb00245.x, doi:10.1002/j.1460-2075.1995.tb00245.x.

[32] M. Lévy, R. Toury, and J. André. Purification et caractérisation enzymatique de la membrane externe des mitochondries. *Comptes rendus hebdomadaires des seances de l'Academie des sciences. Serie D: Sciences naturelles*, 263(22):1766–1769, 1966. URL: https://www.sciencedirect.com/science/article/pii/0005273667900922.

[33] C. Schnaitman, V. G. Erwin, and J. W. Greenawalt. The submitochondrial localization of monoamine oxidase. an enzymatic marker for the outer membrane of rat liver mitochondria. *The Journal of cell biology*, 32(3):719–735, 1967. URL: https://rupress.org/jcb/article/32/3/719/16904/THE-SUBMITOCHONDRIAL-LOCALIZATION-OF-MONOAMINE, doi:10.1083/jcb.32.3.719.

[34] G. E. PALADE. The fine structure of mitochondria. *The Anatomical Record*, 114(3):427–451, 1952. URL: https://onlinelibrary.wiley.com/doi/10.1002/ar.1091140304, doi:10.1002/ar.1091140304.

[35] Till Stephan, Axel Roesch, Dietmar Riedel, and Stefan Jakobs. Live-cell sted nanoscopy of mitochondrial cristae. *Scientific Reports*, 9(1):12419, 2019. URL: https://www.nature.com/articles/s41598-019-48838-2, doi:10.1038/s41598-019-48838-2.

[36] S. NASS and M. M. NASS. Intramitochondrial fibers with dna characteristics. ii. enzymatic and other hydrolytic treatments. *The Journal of cell biology*, 19(3):613–629, 1963. URL: https://rupress.org/jcb/article/19/3/613/1267/INTRAMITOCHONDRIAL-FIBERS-WITH-DNA-CHARACTERISTICS, doi:10.1083/jcb.19.3.613.

[37] D. J. LUCK and E. REICH. Dna in mitochondria of neurospora crassa. *Proceedings of the National Academy of Sciences of the United States of America*, 52(4):931–938, 1964. URL: https://www.pnas.org/doi/10.1073/pnas.52.4.931?url_ver=Z39.88-2003&rfr_id=ori:rid:crossref.org&rfr_dat=cr_pub%20%200pubmed, doi:10.1073/pnas.52.4.931.

[38] G. Schatz, E. Haslbrunner, and H. Tuppy. Deoxyribonucleic acid associated with yeast mitochondria. *Biochemical and Biophysical Research Communications*, 15(2):127–132, 1964. URL: https://www.sciencedirect.com/science/article/pii/0006291X64903110, doi:10.1016/0006-291X(64)90311-0.

[39] S. Anderson, A. T. Bankier, B. G. Barrell, M. H. de Bruijn, A. R. Coulson, J. Drouin, I. C. Eperon, D. P. Nierlich, B. A. Roe, F. Sanger, P. H. Schreier, A. J. Smith, R. Staden, and I. G. Young. Sequence and organization of the human mitochondrial genome. *Nature*, 290(5806):457–465, 1981. URL: https://www.nature.com/articles/290457a0, doi:10.1038/290457a0.

[40] L. Bogorad. Evolution of organelles and eukaryotic genomes. *Science (New York, N.Y.)*, 188(4191):891–898, 1975. URL: https://www.science.org/doi/10.1126/science.1138359, doi:10.1126/science.1138359.

[41] Einat Hazkani-Covo, Raymond M. Zeller, and William Martin. Molecular poltergeists: mitochondrial dna copies (numts) in sequenced nuclear genomes. *PLOS Genetics*, 6(2):e1000834, 2010. URL: https://journals.plos.org/plosgenetics/article?id=10.1371/journal.pgen.1000834, doi:10.1371/journal.pgen.1000834.

[42] Christian Kukat, Christian A. Wurm, Henrik Spåhr, Maria Falkenberg, Nils-Göran Larsson, and Stefan Jakobs. Super-resolution microscopy reveals that mammalian mitochondrial nucleoids have a uniform size and frequently contain a single copy of mtdna. *Proceedings of the National Academy of Sciences of the United States of America*, 108(33):13534–13539, 2011. URL: https://www.pnas.org/doi/10.1073/pnas.1109263108?url_ver=Z39.88-2003&rfr_id=ori:rid:crossref.org&rfr_dat=cr_pub%20%200pubmed, doi:10.1073/pnas.1109263108.

[43] G. J. Hermann, J. W. Thatcher, J. P. Mills, K. G. Hales, M. T. Fuller, J. Nunnari, and J. M. Shaw. Mitochondrial fusion in yeast requires the transmembrane gtpase fzo1p. *The Journal of cell biology*, 143(2):359–373, 1998. URL: https://rupress.org/jcb/article/143/2/359/15913/Mitochondrial-Fusion-in-Yeast-Requires-the, doi:10.1083/jcb.143.2.359.

[44] A. Santel and M. T. Fuller. Control of mitochondrial morphology by a human mitofusin. *Journal of cell science*, 114(Pt 5):867–874, 2001. URL: https://journals.biologists.com/jcs/article/114/5/

867/982/Control-of-mitochondrial-morphology-by-a-human, doi:10.1242/jcs.114.5.867.

[45] E. Smirnova, D. L. Shurland, S. N. Ryazantsev, and A. M. van der Bliek. A human dynamin-related protein controls the distribution of mitochondria. *The Journal of cell biology*, 143(2):351–358, 1998. URL: https://rupress.org/jcb/article/143/2/351/15875/A-Human-Dynamin-related-Protein-Controls-the, doi:10.1083/jcb.143.2.351.

[46] Arnaud M. Labrousse, Mauro D. Zappaterra, Daniel A. Rube, and Alexander M. van der Bliek. C. elegans dynamin-related protein drp-1 controls severing of the mitochondrial outer membrane. *Molecular Cell*, 4(5):815–826, 1999. URL: https://www.sciencedirect.com/science/article/pii/S1097276500803913, doi:10.1016/S1097-2765(00)80391-3.

[47] Tatjana Kleele, Timo Rey, Julius Winter, Sofia Zaganelli, Dora Mahecic, Hélène Perreten Lambert, Francesco Paolo Ruberto, Mohamed Nemir, Timothy Wai, Thierry Pedrazzini, and Suliana Manley. Distinct fission signatures predict mitochondrial degradation or biogenesis. *Nature*, 593(7859):435–439, 2021. URL: https://www.nature.com/articles/s41586-021-03510-6, doi:10.1038/s41586-021-03510-6.

[48] Nikolaus Pfanner, Bettina Warscheid, and Nils Wiedemann. Mitochondrial proteins: from biogenesis to functional networks. *Nature reviews. Molecular cell biology*, 20(5):267–284, 2019. URL: https://www.nature.com/articles/s41580-018-0092-0, doi:10.1038/s41580-018-0092-0.

[49] Martin Picard and Orian S. Shirihai. Mitochondrial signal transduction. *Cell Metabolism*, 34(11):1620–1653, 2022. URL: https://www.sciencedirect.com/science/article/pii/S1550413122004594, doi:10.1016/j.cmet.2022.10.008.

[50] James A. Letts and Leonid A. Sazanov. Clarifying the supercomplex: the higher-order organization of the mitochondrial electron transport chain. *Nature Structural & Molecular Biology*, 24(10):800–808, 2017. URL: https://www.nature.com/articles/nsmb.3460, doi:10.1038/nsmb.3460.

[51] M. Benjamin Hock and Anastasia Kralli. Transcriptional control of mitochondrial biogenesis and function. *Annual review of physiology*, 71:177–203, 2009. URL: https://www.annualreviews.org/doi/10.1146/annurev.physiol.010908.163119, doi:10.1146/annurev.physiol.010908.163119.

[52] Mashun Onishi, Koji Yamano, Miyuki Sato, Noriyuki Matsuda, and Koji Okamoto. Molecular mechanisms and physiological functions of mitophagy. *The EMBO journal*, 40(3):e104705, 2021. URL: https://www.embopress.org/doi/full/10.15252/embj.2020104705, doi:10.15252/embj.2020104705.

[53] Saverio Marchi, Emma Guilbaud, Stephen W. G. Tait, Takahiro Yamazaki, and Lorenzo Galluzzi. Mitochondrial control of inflammation. *Nature Reviews Immunology*, pages 1–15, 2022. URL: https://www.nature.com/articles/s41577-022-00760-x, doi:10.1038/s41577-022-00760-x.

[54] Kate McArthur, Lachlan W. Whitehead, John M. Heddleston, Lucy Li, Benjamin S. Padman, Viola Oorschot, Niall D. Geoghegan, Stephane Chappaz, Sophia Davidson, Hui San Chin, Rachael M. Lane, Marija Dramicanin, Tahnee L. Saunders, Canny Sugiana, Romina Lessene, Laura D. Osellame, Teng-Leong Chew, Grant Dewson, Michael Lazarou, Georg Ramm, Guillaume Lessene, Michael T. Ryan, Kelly L. Rogers, Mark F. van Delft, and Benjamin T. Kile. Bak/bax macropores facilitate mitochondrial herniation and mtdna efflux during apoptosis. *Science (New York, N.Y.)*, 359(6378), 2018. URL: https://www.science.org/doi/10.1126/science.aao6047, doi:10.1126/science.aao6047.

[55] Joel S. Riley, Giovanni Quarato, Catherine Cloix, Jonathan Lopez, Jim O'Prey, Matthew Pearson, James Chapman, Hiromi Sesaki, Leo M. Carlin, João F. Passos, Ann P. Wheeler, Andrew Oberst, Kevin M. Ryan, and Stephen Wg Tait. Mitochondrial inner membrane permeabilisation enables mtdna release during apoptosis. *The EMBO journal*, 37(17):e99238, 2018. URL: https://www.embopress.org/doi/full/10.15252/embj.201899238, doi:10.15252/embj.201899238.

[56] Nigel J. Waterhouse, Jean-Ehrland Ricci, and Douglas R. Green. And all of a sudden it's over: mitochondrial outer-membrane permeabilization in apoptosis. *Biochimie*, 84(2-3):113–121, 2002. URL: https://www.sciencedirect.com/science/article/pii/S0300908402013792, doi:10.1016/S0300-9084(02)01379-2.

[57] Gabriel Ichim, Jonathan Lopez, Shafiq U. Ahmed, Nathiya Muthalagu, Evangelos Giampazolias, M. Eugenia Delgado, Martina Haller, Joel S. Riley, Susan M. Mason, Dimitris Athineos, Melissa J. Parsons, Bert van de Kooij, Lisa Bouchier-Hayes, Anthony J. Chalmers, Rogier W. Rooswinkel, Andrew Oberst, Karen Blyth, Markus Rehm, Daniel J. Murphy, and Stephen W. G.

Tait. Limited mitochondrial permeabilization causes dna damage and genomic instability in the absence of cell death. *Molecular Cell*, 57(5):860–872, 2015. URL: https://www.sciencedirect.com/science/article/pii/S1097276515000192, doi:10.1016/j.molcel.2015.01.018.

[58] Halime Kalkavan, Mark J. Chen, Jeremy C. Crawford, Giovanni Quarato, Patrick Fitzgerald, Stephen W. G. Tait, Colin R. Goding, and Douglas R. Green. Sublethal cytochrome c release generates drug-tolerant persister cells. *Cell*, 185(18):3356–3374.e22, 2022. URL: https://www.sciencedirect.com/science/article/pii/S0092867422009783, doi:10.1016/j.cell.2022.07.025.

[59] C. A. MacMunn. Vi. researches on myohamatin and the histohæmatins. *Philosophical Transactions of the Royal Society of London*, 177:267–298, 1886. URL: https://royalsocietypublishing.org/doi/10.1098/rstl.1886.0007, doi:10.1098/rstl.1886.0007.

[60] D. Keilin. On cytochrome, a respiratory pigment, common to animals, yeast, and higher plants. *Proceedings of the Royal Society of London. Series B, Containing Papers of a Biological Character*, 98(690):312–339, 1925. URL: https://royalsocietypublishing.org/doi/10.1098/rspb.1925.0039, doi:10.1098/rspb.1925.0039.

[61] E. F. Hartree. The discovery of cytochrome. *Biochemical Education*, 1(4):69–71, 1973. URL: https://www.sciencedirect.com/science/article/pii/0307441273900745, doi:10.1016/0307-4412(73)90074-5.

[62] Hua Zou, William J. Henzel, Xuesong Liu, Alexis Lutschg, and Xiaodong Wang. Apaf-1, a human protein homologous to c. elegans ced-4, participates in cytochrome c–dependent activation of caspase-3. *Cell*, 90(3):405–413, 1997. URL: https://www.sciencedirect.com/science/article/pii/S0092867400805012, doi:10.1016/S0092-8674(00)80501-2.

[63] Joe Rodriguez and Yuri Lazebnik. Caspase-9 and apaf-1 form an active holoenzyme. *Genes & Development*, 13(24):3179–3184, 1999. URL: http://genesdev.cshlp.org/content/13/24/3179.long.

[64] H. Duan, K. Orth, A. M. Chinnaiyan, G. G. Poirier, C. J. Froelich, W. W. He, and V. M. Dixit. Ice-lap6, a novel member of the ice/ced-3 gene family, is activated by the cytotoxic t cell protease granzyme b. *The Journal of biological chemistry*, 271(28):16720–16724, 1996. URL: https://www.sciencedirect.

com/science/article/pii/S0021925818319367, doi:10.1074/jbc.271.28.16720.

[65] Peng Li, Deepak Nijhawan, Imawati Budihardjo, Srinivasa M. Srinivasula, Manzoor Ahmad, Emad S. Alnemri, and Xiaodong Wang. Cytochrome c and datp-dependent formation of apaf-1/caspase-9 complex initiates an apoptotic protease cascade. *Cell*, 91(4):479–489, 1997. URL: https://www.sciencedirect.com/science/article/pii/S0092867400804341, doi:10.1016/S0092-8674(00)80434-1.

[66] C. S. Duckett, V. E. Nava, R. W. Gedrich, R. J. Clem, J. L. van Dongen, M. C. Gilfillan, H. Shiels, J. M. Hardwick, and C. B. Thompson. A conserved family of cellular genes related to the baculovirus iap gene and encoding apoptosis inhibitors. *The EMBO journal*, 15(11):2685–2694, 1996. URL: https://www.embopress.org/doi/abs/10.1002/j.1460-2075.1996.tb00629.x, doi:10.1002/j.1460-2075.1996.tb00629.x.

[67] Q. L. Deveraux, R. Takahashi, G. S. Salvesen, and J. C. Reed. X-linked iap is a direct inhibitor of cell-death proteases. *Nature*, 388(6639):300–304, 1997. URL: https://www.nature.com/articles/40901, doi:10.1038/40901.

[68] Eric N. Shiozaki, Jijie Chai, Daniel J. Rigotti, Stefan J. Riedl, Pingwei Li, Srinivasa M. Srinivasula, Emad S. Alnemri, Robert Fairman, and Yigong Shi. Mechanism of xiap-mediated inhibition of caspase-9. *Molecular Cell*, 11(2):519–527, 2003. URL: https://www.sciencedirect.com/science/article/pii/S1097276503000546, doi:10.1016/S1097-2765(03)00054-6.

[69] Anne M. Verhagen, Paul G. Ekert, Miha Pakusch, John Silke, Lisa M. Connolly, Gavin E. Reid, Robert L. Moritz, Richard J. Simpson, and David L. Vaux. Identification of diablo, a mammalian protein that promotes apoptosis by binding to and antagonizing iap proteins. *Cell*, 102(1):43–53, 2000. URL: https://www.sciencedirect.com/science/article/pii/S009286740000009X, doi:10.1016/S0092-8674(00)00009-X.

[70] Chunying Du, Min Fang, Yucheng Li, Lily Li, and Xiaodong Wang. Smac, a mitochondrial protein that promotes cytochrome c–dependent caspase activation by eliminating iap inhibition. *Cell*, 102(1):33–42, 2000. URL: https://www.sciencedirect.com/science/article/pii/S0092867400000088, doi:10.1016/S0092-8674(00)00008-8.

[71] S. M. Srinivasula, R. Hegde, A. Saleh, P. Datta, E. Shiozaki, J. Chai, R. A. Lee, P. D. Robbins, T. Fernandes-Alnemri, Y. Shi, and E. S. Alnemri. A conserved

xiap-interaction motif in caspase-9 and smac/diablo regulates caspase activity and apoptosis. *Nature*, 410(6824):112–116, 2001. URL: https://www.nature.com/articles/35065125, doi:10.1038/35065125.

[72] H. Zou, Y. Li, X. Liu, and X. Wang. An apaf-1.cytochrome c multimeric complex is a functional apoptosome that activates procaspase-9. *The Journal of biological chemistry*, 274(17):11549–11556, 1999. URL: https://www.sciencedirect.com/science/article/pii/S0021925819734620, doi:10.1074/jbc.274.17.11549.

[73] Loretta Dorstyn, Christopher W. Akey, and Sharad Kumar. New insights into apoptosome structure and function. *Cell Death & Differentiation*, 25(7):1194–1208, 2018. URL: https://www.nature.com/articles/s41418-017-0025-z, doi:10.1038/s41418-017-0025-z.

[74] Srinivasa M. Srinivasula, Manzoor Ahmad, Teresa Fernandes-Alnemri, and Emad S. Alnemri. Autoactivation of procaspase-9 by apaf-1-mediated oligomerization. *Molecular Cell*, 1(7):949–957, 1998. URL: https://www.sciencedirect.com/science/article/pii/S1097276500800957, doi:10.1016/S1097-2765(00)80095-7.

[75] E. A. Slee, M. T. Harte, R. M. Kluck, B. B. Wolf, C. A. Casiano, D. D. Newmeyer, H. G. Wang, J. C. Reed, D. W. Nicholson, E. S. Alnemri, D. R. Green, and S. J. Martin. Ordering the cytochrome c-initiated caspase cascade: hierarchical activation of caspases-2, -3, -6, -7, -8, and -10 in a caspase-9-dependent manner. *The Journal of cell biology*, 144(2):281–292, 1999. URL: https://rupress.org/jcb/article/144/2/281/16044/Ordering-the-Cytochrome-c-initiated-Caspase, doi:10.1083/jcb.144.2.281.

[76] H. M. Sobell. Actinomycin and dna transcription. *Proceedings of the National Academy of Sciences of the United States of America*, 82(16):5328–5331, 1985. URL: https://www.pnas.org/doi/10.1073/pnas.82.16.5328?url_ver=Z39.88-2003&rfr_id=ori:rid:crossref.org&rfr_dat=cr_pub%20%200pubmed, doi:10.1073/pnas.82.16.5328.

[77] S. W. G. Tait and D. R. Green. Caspase-independent cell death: leaving the set without the final cut. *Oncogene*, 27(50):6452–6461, 2008. URL: https://www.nature.com/articles/onc2008311, doi:10.1038/onc.2008.311.

[78] T. M. Caserta, A. N. Smith, A. D. Gultice, M. A. Reedy, and T. L. Brown. Q-vd-oph, a broad spectrum caspase inhibitor with potent antiapoptotic properties. *Apoptosis : an international journal on programmed cell death*,

8(4):345–352, 2003. URL: https://link.springer.com/article/10.1023/A:1024116916932, doi:10.1023/a:1024116916932.

[79] I. Rodriguez, K. Matsuura, C. Ody, S. Nagata, and P. Vassalli. Systemic injection of a tripeptide inhibits the intracellular activation of cpp32-like proteases in vivo and fully protects mice against fas-mediated fulminant liver destruction and death. *Journal of Experimental Medicine*, 184(5):2067–2072, 1996. URL: https://rupress.org/jem/article/184/5/2067/51122/Systemic-injection-of-a-tripeptide-inhibits-the, doi:10.1084/jem.184.5.2067.

[80] C. J. van Noorden. The history of z-vad-fmk, a tool for understanding the significance of caspase inhibition. *Acta Histochemica*, 103(3):241–251, 2001. URL: https://www.sciencedirect.com/science/article/pii/S0065128104700719, doi:10.1078/0065-1281-00601.

[81] Lydia Lartigue, Yulia Kushnareva, Youngmo Seong, Helen Lin, Benjamin Faustin, and Donald D. Newmeyer. Caspase-independent mitochondrial cell death results from loss of respiration, not cytotoxic protein release. *Molecular biology of the cell*, 20(23):4871–4884, 2009. URL: https://www.molbiolcell.org/doi/10.1091/mbc.e09-07-0649, doi:10.1091/mbc.e09-07-0649.

[82] L. Pegoraro, A. Palumbo, J. Erikson, M. Falda, B. Giovanazzo, B. S. Emanuel, G. Rovera, P. C. Nowell, and C. M. Croce. A 14;18 and an 8;14 chromosome translocation in a cell line derived from an acute b-cell leukemia. *Proceedings of the National Academy of Sciences of the United States of America*, 81(22):7166–7170, 1984. URL: https://www.pnas.org/doi/10.1073/pnas.81.22.7166, doi:10.1073/pnas.81.22.7166.

[83] D. Hockenbery, G. Nuñez, C. Milliman, R. D. Schreiber, and S. J. Korsmeyer. Bcl-2 is an inner mitochondrial membrane protein that blocks programmed cell death. *Nature*, 348(6299):334–336, 1990. URL: https://www.nature.com/articles/348334a0, doi:10.1038/348334a0.

[84] D. T. Chao and S. J. Korsmeyer. Bcl-2 family: regulators of cell death. *Annual review of immunology*, 16:395–419, 1998. URL: https://www.annualreviews.org/doi/10.1146/annurev.immunol.16.1.395, doi:10.1146/annurev.immunol.16.1.395.

[85] Sebastian Ruehl, Clifford S. Guy, Zhenrui Li, Mao Yang, Tudor Moldoveanu, and Douglas R. Green. *Anti-apoptotic BH3-only proteins inhibit Bak-*

dependent apoptosis. 2022. URL: https://www.biorxiv.org/content/10.1101/2022.07.24.499430v1, doi:10.1101/2022.07.24.499430.

[86] X. M. Yin, Z. N. Oltvai, and S. J. Korsmeyer. Bh1 and bh2 domains of bcl-2 are required for inhibition of apoptosis and heterodimerization with bax. *Nature*, 369(6478):321–323, 1994. URL: https://www.nature.com/articles/369321a0, doi:10.1038/369321a0.

[87] T. Chittenden, C. Flemington, A. B. Houghton, R. G. Ebb, G. J. Gallo, B. Elangovan, G. Chinnadurai, and R. J. Lutz. A conserved domain in bak, distinct from bh1 and bh2, mediates cell death and protein binding functions. *The EMBO journal*, 14(22):5589–5596, 1995. URL: https://www.embopress.org/doi/abs/10.1002/j.1460-2075.1995.tb00246.x, doi:10.1002/j.1460-2075.1995.tb00246.x.

[88] C. Borner, I. Martinou, C. Mattmann, M. Irmler, E. Schaerer, J. C. Martinou, and J. Tschopp. The protein bcl-2 alpha does not require membrane attachment, but two conserved domains to suppress apoptosis. *The Journal of cell biology*, 126(4):1059–1068, 1994. URL: https://rupress.org/jcb/article/126/4/1059/14972/The-protein-bcl-2-alpha-does-not-require-membrane, doi:10.1083/jcb.126.4.1059.

[89] Marc Kvansakul and Mark G. Hinds. Chapter three - the structural biology of bh3-only proteins. In Avi Ashkenazi, Junying Yuan, and James A. Wells, editors, *Methods in Enzymology : Regulated Cell Death Part A: Apoptotic Mechanisms*, volume 544, pages 49–74. Academic Press, 2014. URL: https://www.sciencedirect.com/science/article/pii/B9780124171589000030, doi:10.1016/B978-0-12-417158-9.00003-0.

[90] Abdel Aouacheria, Christophe Combet, Peter Tompa, and J. Marie Hardwick. Redefining the bh3 death domain as a 'short linear motif'. *Trends in Biochemical Sciences*, 40(12):736–748, 2015. URL: https://www.sciencedirect.com/science/article/pii/S096800041500184X, doi:10.1016/j.tibs.2015.09.007.

[91] Xu Luo, Katelyn L. O'Neill, and Kai Huang. The third model of bax/bak activation: a bcl-2 family feud finally resolved? *F1000Research*, 9:935, 2020. URL: https://f1000research.com/articles/9-935/v1, doi:10.12688/f1000research.25607.1.

[92] Justin Kale, Elizabeth J. Osterlund, and David W. Andrews. Bcl-2 family proteins: changing partners in the dance towards death. *Cell Death & Dif-*

ferentiation, 25(1):65–80, 2018. URL: https://www.nature.com/articles/cdd2017186, doi:10.1038/cdd.2017.186.

[93] Giridhar Sekar, Adedolapo Ojoawo, and Tudor Moldoveanu. Protein-protein and protein-lipid interactions of pore-forming bcl-2 family proteins in apoptosis initiation. *Biochemical Society Transactions*, 50(3):1091–1103, 2022. URL: https://portlandpress.com/biochemsoctrans/article/50/3/1091/231272/Protein-protein-and-protein-lipid-interactions-of, doi:10.1042/BST20220323.

[94] Zoltán N. Oltval, Curt L. Milliman, and Stanley J. Korsmeyer. Bcl-2 heterodimerizes in vivo with a conserved homolog, bax, that accelerates programed cell death. *Cell*, 74(4):609–619, 1993. URL: https://www.sciencedirect.com/science/article/pii/009286749390509O, doi:10.1016/0092-8674(93)90509-O.

[95] T. Sato, M. Hanada, S. Bodrug, S. Irie, N. Iwama, L. H. Boise, C. B. Thompson, E. Golemis, L. Fong, and H. G. Wang. Interactions among members of the bcl-2 protein family analyzed with a yeast two-hybrid system. *Proceedings of the National Academy of Sciences of the United States of America*, 91(20):9238–9242, 1994. URL: https://www.pnas.org/doi/10.1073/pnas.91.20.9238, doi:10.1073/pnas.91.20.9238.

[96] T. W. Sedlak, Z. N. Oltvai, E. Yang, K. Wang, L. H. Boise, C. B. Thompson, and S. J. Korsmeyer. Multiple bcl-2 family members demonstrate selective dimerizations with bax. *Proceedings of the National Academy of Sciences of the United States of America*, 92(17):7834–7838, 1995. URL: https://www.pnas.org/doi/10.1073/pnas.92.17.7834, doi:10.1073/pnas.92.17.7834.

[97] Jonathan F. Lovell, Lieven P. Billen, Scott Bindner, Aisha Shamas-Din, Cecile Fradin, Brian Leber, and David W. Andrews. Membrane binding by tbid initiates an ordered series of events culminating in membrane permeabilization by bax. *Cell*, 135(6):1074–1084, 2008. URL: https://www.sciencedirect.com/science/article/pii/S0092867408014396, doi:10.1016/j.cell.2008.11.010.

[98] S. K. Chiou, L. Rao, and E. White. Bcl-2 blocks p53-dependent apoptosis. *Molecular and cellular biology*, 14(4):2556–2563, 1994. URL: https://journals.asm.org/doi/10.1128/mcb.14.4.2556-2563.1994, doi:10.1128/mcb.14.4.2556-2563.1994.

[99] A. Kelekar, B. S. Chang, J. E. Harlan, S. W. Fesik, and C. B. Thompson. *Molecular and cellular biology*, 17(12):7040–7046, 1997. URL: https://journals.asm.org/doi/10.1128/MCB.17.12.7040, doi:10.1128/MCB.17.12.7040.

[100] Feng-Ting Liu, Adrian C. Newland, and Li Jia. Bax conformational change is a crucial step for puma-mediated apoptosis in human leukemia. *Biochemical and Biophysical Research Communications*, 310(3):956–962, 2003. URL: https://www.sciencedirect.com/science/article/pii/S0006291X03018990, doi:10.1016/j.bbrc.2003.09.109.

[101] Tilman Oltersdorf, Steven W. Elmore, Alexander R. Shoemaker, Robert C. Armstrong, David J. Augeri, Barbara A. Belli, Milan Bruncko, Thomas L. Deckwerth, Jurgen Dinges, Philip J. Hajduk, Mary K. Joseph, Shinichi Kitada, Stanley J. Korsmeyer, Aaron R. Kunzer, Anthony Letai, Chi Li, Michael J. Mitten, David G. Nettesheim, ShiChung Ng, Paul M. Nimmer, Jacqueline M. O'Connor, Anatol Oleksijew, Andrew M. Petros, John C. Reed, Wang Shen, Stephen K. Tahir, Craig B. Thompson, Kevin J. Tomaselli, Baole Wang, Michael D. Wendt, Haichao Zhang, Stephen W. Fesik, and Saul H. Rosenberg. An inhibitor of bcl-2 family proteins induces regression of solid tumours. *Nature*, 435(7042):677–681, 2005. URL: https://www.nature.com/articles/nature03579, doi:10.1038/nature03579.

[102] Mark F. van Delft, Andrew H. Wei, Kylie D. Mason, Cassandra J. Vandenberg, Lin Chen, Peter E. Czabotar, Simon N. Willis, Clare L. Scott, Catherine L. Day, Suzanne Cory, Jerry M. Adams, Andrew W. Roberts, and David C. S. Huang. The bh3 mimetic abt-737 targets selective bcl-2 proteins and efficiently induces apoptosis via bak/bax if mcl-1 is neutralized. *Cancer Cell*, 10(5):389–399, 2006. URL: https://www.sciencedirect.com/science/article/pii/S1535610806002911, doi:10.1016/j.ccr.2006.08.027.

[103] M. P. Kline, S. V. Rajkumar, M. M. Timm, T. K. Kimlinger, J. L. Haug, J. A. Lust, P. R. Greipp, and S. Kumar. Abt-737, an inhibitor of bcl-2 family proteins, is a potent inducer of apoptosis in multiple myeloma cells. *Leukemia*, 21(7):1549–1560, 2007. URL: https://www.nature.com/articles/2404719, doi:10.1038/sj.leu.2404719.

[104] Katelyn L. O'Neill, Kai Huang, Jingjing Zhang, Yi Chen, and Xu Luo. Inactivation of prosurvival bcl-2 proteins activates bax/bak through the outer mitochondrial membrane. *Genes & Development*, 30(8):973–988, 2016. URL: http://genesdev.cshlp.org/content/30/8/973, doi:10.1101/gad.276725.115.

[105] S. N. Farrow, J. H. White, I. Martinou, T. Raven, K. T. Pun, C. J. Grinham, J. C. Martinou, and R. Brown. Cloning of a bcl-2 homologue by interaction with adenovirus e1b 19k. *Nature*, 374(6524):731–733, 1995. URL: https://www.nature.com/articles/374731a0, doi:10.1038/374731a0.

[106] T. Chittenden, E. A. Harrington, R. O'Connor, C. Flemington, R. J. Lutz, G. I. Evan, and B. C. Guild. Induction of apoptosis by the bcl-2 homologue bak. *Nature*, 374(6524):733–736, 1995. URL: https://www.nature.com/articles/374733a0, doi:10.1038/374733a0.

[107] M. C. Kiefer, M. J. Brauer, V. C. Powers, J. J. Wu, S. R. Umansky, L. D. Tomei, and P. J. Barr. Modulation of apoptosis by the widely distributed bcl-2 homologue bak. *Nature*, 374(6524):736–739, 1995. URL: https://www.nature.com/articles/374736a0, doi:10.1038/374736a0.

[108] Min-Sik Kim, Sneha M. Pinto, Derese Getnet, Raja Sekhar Nirujogi, Srikanth S. Manda, Raghothama Chaerkady, Anil K. Madugundu, Dhanashree S. Kelkar, Ruth Isserlin, Shobhit Jain, Joji K. Thomas, Babylakshmi Muthusamy, Pamela Leal-Rojas, Praveen Kumar, Nandini A. Sahasrabuddhe, Lavanya Balakrishnan, Jayshree Advani, Bijesh George, Santosh Renuse, Lakshmi Dhevi N. Selvan, Arun H. Patil, Vishalakshi Nanjappa, Aneesha Radhakrishnan, Samarjeet Prasad, Tejaswini Subbannayya, Rajesh Raju, Manish Kumar, Sreelakshmi K. Sreenivasamurthy, Arivusudar Marimuthu, Gajanan J. Sathe, Sandip Chavan, Keshava K. Datta, Yashwanth Subbannayya, Apeksha Sahu, Soujanya D. Yelamanchi, Savita Jayaram, Pavithra Rajagopalan, Jyoti Sharma, Krishna R. Murthy, Nazia Syed, Renu Goel, Aafaque A. Khan, Sartaj Ahmad, Gourav Dey, Keshav Mudgal, Aditi Chatterjee, Tai-Chung Huang, Jun Zhong, Xinyan Wu, Patrick G. Shaw, Donald Freed, Muhammad S. Zahari, Kanchan K. Mukherjee, Subramanian Shankar, Anita Mahadevan, Henry Lam, Christopher J. Mitchell, Susarla Krishna Shankar, Parthasarathy Satishchandra, John T. Schroeder, Ravi Sirdeshmukh, Anirban Maitra, Steven D. Leach, Charles G. Drake, Marc K. Halushka, T. S. Keshava Prasad, Ralph H. Hruban, Candace L. Kerr, Gary D. Bader, Christine A. Iacobuzio-Donahue, Harsha Gowda, and Akhilesh Pandey. A draft map of the human proteome. *Nature*, 509(7502):575–581, 2014. URL: https://www.nature.com/articles/nature13302, doi:10.1038/nature13302.

[109] Human proteome map, 30.11.2022. URL: http://www.humanproteomemap.org/protein.php?hpm_id=578.

[110] Human proteome map, 30.11.2022. URL: http://www.humanproteomemap.org/protein.php?hpm_id=581.

[111] Kristopher A. Sarosiek, Cameron Fraser, Nathiya Muthalagu, Patrick D. Bhola, Weiting Chang, Samuel K. McBrayer, Adam Cantlon, Sudeshna Fisch, Gail Golomb-Mello, Jeremy A. Ryan, Jing Deng, Brian Jian, Chris Corbett, Marti Goldenberg, Joseph R. Madsen, Ronglih Liao, Dominic Walsh, John Sedivy, Daniel J. Murphy, Daniel Ruben Carrasco, Shenandoah Robinson, Javid Moslehi, and Anthony Letai. Developmental regulation of mitochondrial apoptosis by c-myc governs age- and tissue-specific sensitivity to cancer therapeutics. *Cancer Cell*, 31(1):142–156, 2017. URL: https://www.sciencedirect.com/science/article/pii/S1535610816305542, doi:10.1016/j.ccell.2016.11.011.

[112] Tullia Lindsten, Andrea J. Ross, Ayala King, Wei-Xing Zong, Jeffrey C. Rathmell, Helena A. Shiels, Eugen Ulrich, Katrina G. Waymire, Patryce Mahar, Kenneth Frauwirth, Yifeng Chen, Michael Wei, Vicki M. Eng, David M. Adelman, M.Celeste Simon, Averil Ma, Jeffrey A. Golden, Gerard Evan, Stanley J. Korsmeyer, Grant R. MacGregor, and Craig B. Thompson. The combined functions of proapoptotic bcl-2 family members bak and bax are essential for normal development of multiple tissues. *Molecular Cell*, 6(6):1389–1399, 2000. URL: https://www.sciencedirect.com/science/article/pii/S1097276500001362, doi:10.1016/S1097-2765(00)00136-2.

[113] M. C. Wei, W. X. Zong, E. H. Cheng, T. Lindsten, V. Panoutsakopoulou, A. J. Ross, K. A. Roth, G. R. MacGregor, C. B. Thompson, and S. J. Korsmeyer. Proapoptotic bax and bak: a requisite gateway to mitochondrial dysfunction and death. *Science (New York, N.Y.)*, 292(5517):727–730, 2001. URL: https://www.science.org/doi/10.1126/science.1059108, doi:10.1126/science.1059108.

[114] W. X. Zong, T. Lindsten, A. J. Ross, G. R. MacGregor, and C. B. Thompson. Bh3-only proteins that bind pro-survival bcl-2 family members fail to induce apoptosis in the absence of bax and bak. *Genes & Development*, 15(12):1481–1486, 2001. URL: http://genesdev.cshlp.org/content/15/12/1481.long, doi:10.1101/gad.897601.

[115] Kurt Degenhardt, Ramya Sundararajan, Tullia Lindsten, Craig Thompson, and Eileen White. Bax and bak independently promote cytochrome c release from mitochondria. *The Journal of biological chemistry*, 277(16):14127–14134, 2002. URL: https://www.sciencedirect.com/science/article/pii/S0021925819610185, doi:10.1074/jbc.M109939200.

[116] C. Wang and R. J. Youle. Predominant requirement of bax for apoptosis in hct116 cells is determined by mcl-1's inhibitory effect on bak. *Oncogene*, 31(26):3177–3189, 2012. URL: https://www.nature.com/articles/onc2011497, doi:10.1038/onc.2011.497.

[117] Jules P.P. Meijerink, Ewald J.B.M. Mensink, Kun Wang, Thomas W. Sedlak, Annet W. Slöetjes, Theo de Witte, Gabriel Waksman, and Stanley J. Korsmeyer. Hematopoietic malignancies demonstrate loss-of-function mutations of-bax. *Blood*, 91(8):2991–2997, 1998. URL: https://ashpublications.org/blood/article/91/8/2991/107623/Hematopoietic-Malignancies-Demonstrate-Loss-of, doi:10.1182/blood.V91.8.2991.2991{\textunderscore}2991{\textunderscore}2997.

[118] Yanwei Luo, Xinye Wang, Heran Wang, Yang Xu, Qiuyuan Wen, Songqing Fan, Ran Zhao, Shihe Jiang, Jing Yang, Yukun Liu, Xiayu Li, Wei Xiong, Jian Ma, Shuping Peng, Zhaoyang Zeng, Xiaoling Li, Joshua B. Phillips, Guiyuan Li, Ming Tan, and Ming Zhou. High bak expression is associated with a favorable prognosis in breast cancer and sensitizes breast cancer cells to paclitaxel. *PLOS ONE*, 10(9):e0138955, 2015. URL: https://journals.plos.org/plosone/article?id=10.1371/journal.pone.0138955#pone-0138955-t001,, doi:10.1371/journal.pone.0138955.

[119] Konstantina Athanasopoulou, Panagiotis G. Adamopoulos, Glykeria N. Daneva, and Andreas Scorilas. Decoding the concealed transcriptional signature of the apoptosis-related bcl2 antagonist/killer 1 (bak1) gene in human malignancies. *Apoptosis*, 27(11-12):869–882, 2022. URL: https://link.springer.com/article/10.1007/s10495-022-01753-w#Sec17, doi:10.1007/s10495-022-01753-w.

[120] Douglas R. Green. The mitochondrial pathway of apoptosis part ii: The bcl-2 protein family. *Cold Spring Harbor perspectives in biology*, 14(6), 2022. URL: https://cshperspectives.cshlp.org/content/14/6/a041046.full, doi:10.1101/cshperspect.a041046.

[121] Motoshi Suzuki, Richard J. Youle, and Nico Tjandra. Structure of bax: Coregulation of dimer formation and intracellular localization. *Cell*, 103(4):645–654, 2000. URL: https://www.sciencedirect.com/science/article/pii/S0092867400001677, doi:10.1016/S0092-8674(00)00167-7.

[122] Tudor Moldoveanu, Qian Liu, Ante Tocilj, Mark Watson, Gordon Shore, and Kalle Gehring. The x-ray structure of a bak homodimer re-

veals an inhibitory zinc binding site. *Molecular Cell*, 24(5):677–688, 2006. URL: https://www.sciencedirect.com/science/article/pii/S1097276506007039, doi:10.1016/j.molcel.2006.10.014.

[123] Embl-ebi. Emboss needle < pairwise sequence alignment < embl-ebi, 19.04.2022. URL: https://www.ebi.ac.uk/Tools/psa/emboss_needle/.

[124] Fábio Madeira, Matt Pearce, Adrian R. N. Tivey, Prasad Basutkar, Joon Lee, Ossama Edbali, Nandana Madhusoodanan, Anton Kolesnikov, and Rodrigo Lopez. Search and sequence analysis tools services from embl-ebi in 2022. *Nucleic acids research*, 2022. URL: https://europepmc.org/article/MED/35412617, doi:10.1093/nar/gkac240.

[125] Frank Edlich, Soojay Banerjee, Motoshi Suzuki, Megan M. Cleland, Damien Arnoult, Chunxin Wang, Albert Neutzner, Nico Tjandra, and Richard J. Youle. Bcl-x(l) retrotranslocates bax from the mitochondria into the cytosol. *Cell*, 145(1):104–116, 2011. URL: https://www.sciencedirect.com/science/article/pii/S0092867411001863, doi:10.1016/j.cell.2011.02.034.

[126] Franziska Todt, Zeynep Cakir, Frank Reichenbach, Frederic Emschermann, Joachim Lauterwasser, Andrea Kaiser, Gabriel Ichim, Stephen W. G. Tait, Stephan Frank, Harald F. Langer, and Frank Edlich. Differential retrotranslocation of mitochondrial bax and bak. *The EMBO journal*, 34(1):67–80, 2015. URL: https://www.embopress.org/doi/full/10.15252/embj.201488806, doi:10.15252/embj.201488806.

[127] A. Nechushtan, C. L. Smith, I. Lamensdorf, S. H. Yoon, and R. J. Youle. Bax and bak coalesce into novel mitochondria-associated clusters during apoptosis. *The Journal of cell biology*, 153(6):1265–1276, 2001. URL: https://rupress.org/jcb/article/153/6/1265/47802/Bax-and-Bak-Coalesce-into-Novel-Mitochondria, doi:10.1083/jcb.153.6.1265.

[128] A. Gross, J. Jockel, M. C. Wei, and S. J. Korsmeyer. Enforced dimerization of bax results in its translocation, mitochondrial dysfunction and apoptosis. *The EMBO journal*, 17(14):3878–3885, 1998. URL: https://www.embopress.org/doi/full/10.1093/emboj/17.14.3878, doi:10.1093/emboj/17.14.3878.

[129] Peter E. Czabotar, Dana Westphal, Grant Dewson, Stephen Ma, Colin Hockings, W. Douglas Fairlie, Erinna F. Lee, Shenggen Yao, Adeline Y. Robin, Brian J. Smith, David C. S. Huang, Ruth M. Kluck, Jerry M. Adams, and Peter M. Colman. Bax crystal structures reveal how bh3 domains activate

bax and nucleate its oligomerization to induce apoptosis. *Cell*, 152(3):519–531, 2013. URL: https://www.sciencedirect.com/science/article/pii/S009286741201553X, doi:10.1016/j.cell.2012.12.031.

[130] Stephanie Bleicken, Gunnar Jeschke, Carolin Stegmueller, Raquel Salvador-Gallego, Ana J. García-Sáez, and Enrica Bordignon. Structural model of active bax at the membrane. *Molecular Cell*, 56(4):496–505, 2014. URL: https://www.sciencedirect.com/science/article/pii/S1097276514007795, doi:10.1016/j.molcel.2014.09.022.

[131] Grant Dewson, Tobias Kratina, Huiyan W. Sim, Hamsa Puthalakath, Jerry M. Adams, Peter M. Colman, and Ruth M. Kluck. To trigger apoptosis, bak exposes its bh3 domain and homodimerizes via bh3:groove interactions. *Molecular Cell*, 30(3):369–380, 2008. URL: https://www.sciencedirect.com/science/article/pii/S1097276508002657, doi:10.1016/j.molcel.2008.04.005.

[132] Tirtha Mandal, Seungjin Shin, Sreevidya Aluvila, Hui-Chen Chen, Carter Grieve, Jun-Yong Choe, Emily H. Cheng, Eric J. Hustedt, and Kyoung Joon Oh. Assembly of bak homodimers into higher order homooligomers in the mitochondrial apoptotic pore. *Scientific Reports*, 6(1):30763, 2016. URL: https://www.nature.com/articles/srep30763, doi:10.1038/srep30763.

[133] Richard W. Birkinshaw, Sweta Iyer, Daisy Lio, Cindy S. Luo, Jason M. Brouwer, Michelle S. Miller, Adeline Y. Robin, Rachel T. Uren, Grant Dewson, Ruth M. Kluck, Peter M. Colman, and Peter E. Czabotar. Structure of detergent-activated bak dimers derived from the inert monomer. *Molecular Cell*, 81(10):2123–2134.e5, 2021. URL: https://www.sciencedirect.com/science/article/pii/S1097276521001829, doi:10.1016/j.molcel.2021.03.014.

[134] G. Dewson, S. Ma, P. Frederick, C. Hockings, I. Tan, T. Kratina, and R. M. Kluck. Bax dimerizes via a symmetric bh3:groove interface during apoptosis. *Cell Death & Differentiation*, 19(4):661–670, 2012. URL: https://www.nature.com/articles/cdd2011138, doi:10.1038/cdd.2011.138.

[135] Rachel T. Uren, Martin O'hely, Sweta Iyer, Ray Bartolo, Melissa X. Shi, Jason M. Brouwer, Amber E. Alsop, Grant Dewson, and Ruth M. Kluck. Disordered clusters of bak dimers rupture mitochondria during apoptosis. *eLife Sciences Publications, Ltd*, 2017. URL: https://elifesciences.org/articles/19944.

[136] Jason M. Brouwer, Ping Lan, Angus D. Cowan, Jonathan P. Bernardini, Richard W. Birkinshaw, Mark F. van Delft, Brad E. Sleebs, Adeline Y. Robin, Ahmad Wardak, Iris K. Tan, Boris Reljic, Erinna F. Lee, W. Douglas Fairlie, Melissa J. Call, Brian J. Smith, Grant Dewson, Guillaume Lessene, Peter M. Colman, and Peter E. Czabotar. Conversion of bim-bh3 from activator to inhibitor of bak through structure-based design. *Molecular Cell*, 68(4):659–672.e9, 2017. URL: https://www.sciencedirect.com/science/article/pii/S1097276517308365, doi:10.1016/j.molcel.2017.11.001.

[137] Angus D. Cowan, Nicholas A. Smith, Jarrod J. Sandow, Eugene A. Kapp, Yepy H. Rustam, James M. Murphy, Jason M. Brouwer, Jonathan P. Bernardini, Michael J. Roy, Ahmad Z. Wardak, Iris K. Tan, Andrew I. Webb, Jacqueline M. Gulbis, Brian J. Smith, Gavin E. Reid, Grant Dewson, Peter M. Colman, and Peter E. Czabotar. Bak core dimers bind lipids and can be bridged by them. *Nature Structural & Molecular Biology*, 27(11):1024–1031, 2020. URL: https://www.nature.com/articles/s41594-020-0494-5, doi:10.1038/s41594-020-0494-5.

[138] S. Y. Hsu, A. Kaipia, E. McGee, M. Lomeli, and A. J. Hsueh. Bok is a pro-apoptotic bcl-2 protein with restricted expression in reproductive tissues and heterodimerizes with selective anti-apoptotic bcl-2 family members. *Proceedings of the National Academy of Sciences of the United States of America*, 94(23):12401–12406, 1997. URL: https://www.pnas.org/doi/full/10.1073/pnas.94.23.12401, doi:10.1073/pnas.94.23.12401.

[139] Raed Shalaby, Arzoo Diwan, Hector Flores-Romero, Vanessa Hertlein, and Ana J. Garcia-Saez. Visualization of bok pores independent of bax and bak reveals a similar mechanism with differing regulation. *Cell Death & Differentiation*, pages 1–11, 2022. URL: https://www.nature.com/articles/s41418-022-01078-w, doi:10.1038/s41418-022-01078-w.

[140] Fabien Llambi, Yue-Ming Wang, Bernadette Victor, Mao Yang, Desiree M. Schneider, Sébastien Gingras, Melissa J. Parsons, Janet H. Zheng, Scott A. Brown, Stéphane Pelletier, Tudor Moldoveanu, Taosheng Chen, and Douglas R. Green. Bok is a non-canonical bcl-2 family effector of apoptosis regulated by er-associated degradation. *Cell*, 165(2):421–433, 2016. URL: https://www.sciencedirect.com/science/article/pii/S0092867416301283, doi:10.1016/j.cell.2016.02.026.

[141] F. Ke, A. Voss, J. B. Kerr, L. A. O'Reilly, L. Tai, N. Echeverry, P. Bouillet, A. Strasser, and T. Kaufmann. Bcl-2 family member bok is widely expressed but its loss

has only minimal impact in mice. *Cell Death & Differentiation*, 19(6):915–925, 2012. URL: https://www.nature.com/articles/cdd2011210, doi:10.1038/cdd.2011.210.

[142] Francine F. S. Ke, Hannah K. Vanyai, Angus D. Cowan, Alex R. D. Delbridge, Lachlan Whitehead, Stephanie Grabow, Peter E. Czabotar, Anne K. Voss, and Andreas Strasser. Embryogenesis and adult life in the absence of intrinsic apoptosis effectors bax, bak, and bok. *Cell*, 173(5):1217–1230.e17, 2018. URL: https://www.sciencedirect.com/science/article/pii/S0092867418305671, doi:10.1016/j.cell.2018.04.036.

[143] R. M. Kluck, E. Bossy-Wetzel, D. R. Green, and D. D. Newmeyer. The release of cytochrome c from mitochondria: a primary site for bcl-2 regulation of apoptosis. *Science (New York, N.Y.)*, 275(5303):1132–1136, 1997. URL: https://www.science.org/doi/10.1126/science.275.5303.1132, doi:10.1126/science.275.5303.1132.

[144] J. C. Goldstein, N. J. Waterhouse, P. Juin, G. I. Evan, and D. R. Green. The coordinate release of cytochrome c during apoptosis is rapid, complete and kinetically invariant. *Nature Cell Biology*, 2(3):156–162, 2000. URL: https://www.nature.com/articles/ncb0300_156, doi:10.1038/35004029.

[145] S. S. Smaili, Y. T. Hsu, K. M. Sanders, J. T. Russell, and R. J. Youle. Bax translocation to mitochondria subsequent to a rapid loss of mitochondrial membrane potential. *Cell Death & Differentiation*, 8(9):909–920, 2001. URL: https://www.nature.com/articles/4400889, doi:10.1038/sj.cdd.4400889.

[146] Liying Zhou and Donald C. Chang. Dynamics and structure of the bax-bak complex responsible for releasing mitochondrial proteins during apoptosis. *Journal of cell science*, 121(Pt 13):2186–2196, 2008. URL: https://journals.biologists.com/jcs/article/121/13/2186/30224/Dynamics-and-structure-of-the-Bax-Bak-complex.

[147] Kresten Bertelsen, Jerzy Dorosz, Sara Krogh Hansen, Niels Chr Nielsen, and Thomas Vosegaard. Mechanisms of peptide-induced pore formation in lipid bilayers investigated by oriented 31p solid-state nmr spectroscopy. *PLOS ONE*, 7(10):e47745, 2012. URL: https://journals.plos.org/plosone/article?id=10.1371/journal.pone.0047745#pone.0047745-Wi1, doi:10.1371/journal.pone.0047745.

[148] Yamunadevi Subburaj, Katia Cosentino, Markus Axmann, Esteban Pedruezo-Villalmanzo, Eduard Hermann, Stephanie Bleicken, Joachim Spatz, and Ana J.

García-Sáez. Bax monomers form dimer units in the membrane that further self-assemble into multiple oligomeric species. *Nature Communications*, 6(1):8042, 2015. URL: https://www.nature.com/articles/ncomms9042, doi:10.1038/ncomms9042.

[149] Grant Dewson, Tobias Kratina, Peter Czabotar, Catherine L. Day, Jerry M. Adams, and Ruth M. Kluck. Bak activation for apoptosis involves oligomerization of dimers via their alpha6 helices. *Molecular Cell*, 36(4):696–703, 2009. URL: https://www.sciencedirect.com/science/article/pii/S1097276509008211, doi:10.1016/j.molcel.2009.11.008.

[150] Matthew G. Annis, Erinn L. Soucie, Paulina J. Dlugosz, Jorge A. Cruz-Aguado, Linda Z. Penn, Brian Leber, and David W. Andrews. Bax forms multispanning monomers that oligomerize to permeabilize membranes during apoptosis. *The EMBO journal*, 24(12):2096–2103, 2005. URL: https://www.embopress.org/doi/full/10.1038/sj.emboj.7600675, doi:10.1038/sj.emboj.7600675.

[151] Dana Westphal, Grant Dewson, Marie Menard, Paul Frederick, Sweta Iyer, Ray Bartolo, Leonie Gibson, Peter E. Czabotar, Brian J. Smith, Jerry M. Adams, and Ruth M. Kluck. Apoptotic pore formation is associated with in-plane insertion of bak or bax central helices into the mitochondrial outer membrane. *Proceedings of the National Academy of Sciences of the United States of America*, 111(39):E4076–85, 2014. URL: https://www.pnas.org/doi/10.1073/pnas.1415142111, doi:10.1073/pnas.1415142111.

[152] Hector Flores-Romero, Uris Ros, and Ana J. Garcia-Saez. Pore formation in regulated cell death. *The EMBO journal*, 39(23):e105753, 2020. URL: https://www.embopress.org/doi/full/10.15252/embj.2020105753, doi:10.15252/embj.2020105753.

[153] Fujiao Lv, Fei Qi, Zhi Zhang, Maorong Wen, Justin Kale, Alessandro Piai, Lingyu Du, Shuqing Wang, Liujuan Zhou, Yaqing Yang, Bin Wu, Zhijun Liu, Juan Del Rosario, Justin Pogmore, James J. Chou, David W. Andrews, Jialing Lin, and Bo OuYang. An amphipathic bax core dimer forms part of the apoptotic pore wall in the mitochondrial␣membrane. *The EMBO journal*, 40(14):e106438, 2021. URL: https://www.embopress.org/doi/full/10.15252/embj.2020106438.

[154] Adeline Y. Robin, Sweta Iyer, Richard W. Birkinshaw, Jarrod Sandow, Ahmad Wardak, Cindy S. Luo, Melissa Shi, Andrew I. Webb, Peter E.

Czabotar, Ruth M. Kluck, and Peter M. Colman. Ensemble properties of bax determine its function. *Structure*, 26(10):1346–1359.e5, 2018. URL: https://www.sciencedirect.com/science/article/pii/S0969212618302521, doi:10.1016/j.str.2018.07.006.

[155] Michael A. Dengler, Adeline Y. Robin, Leonie Gibson, Mark X. Li, Jarrod J. Sandow, Sweta Iyer, Andrew I. Webb, Dana Westphal, Grant Dewson, and Jerry M. Adams. Bax activation: Mutations near its proposed non-canonical bh3 binding site reveal allosteric changes controlling mitochondrial association. *Cell Reports*, 27(2):359–373.e6, 2019. URL: https://www.sciencedirect.com/science/article/pii/S2211124719303560, doi:10.1016/j.celrep.2019.03.040.

[156] Noah B. Bloch, Thomas E. Wales, Michelle S. Prew, Hannah R. Levy, John R. Engen, and Loren D. Walensky. The conformational stability of pro-apoptotic bax is dictated by discrete residues of the protein core. *Nature Communications*, 12(1):4932, 2021. URL: https://www.nature.com/articles/s41467-021-25200-7, doi:10.1038/s41467-021-25200-7.

[157] Jarrod J. Sandow, Iris Kl Tan, Alan S. Huang, Shashank Masaldan, Jonathan P. Bernardini, Ahmad Z. Wardak, Richard W. Birkinshaw, Robert L. Ninnis, Ziyan Liu, Destiny Dalseno, Daisy Lio, Giuseppi Infusini, Peter E. Czabotar, Andrew I. Webb, and Grant Dewson. Dynamic reconfiguration of pro-apoptotic bak on membranes. *The EMBO journal*, 40(20):e107237, 2021. URL: https://www.embopress.org/doi/full/10.15252/embj.2020107237, doi:10.15252/embj.2020107237.

[158] Laura E. Sperl, Florian Rührnößl, Anita Schiller, Martin Haslbeck, and Franz Hagn. High-resolution analysis of the conformational transition of pro-apoptotic bak at the lipid membrane. *The EMBO journal*, 40(20):e107159, 2021. URL: https://www.embopress.org/doi/full/10.15252/embj.2020107159, doi:10.15252/embj.2020107159.

[159] Geetika Singh, Cristina D. Guibao, Jayaraman Seetharaman, Anup Aggarwal, Christy R. Grace, Dan E. McNamara, Sivaraja Vaithiyalingam, M. Brett Waddell, and Tudor Moldoveanu. Structural basis of bak activation in mitochondrial apoptosis initiation. *Nature Communications*, 13(1):250, 2022. URL: https://www.nature.com/articles/s41467-021-27851-y, doi:10.1038/s41467-021-27851-y.

[160] Philipp Wolf, Axel Schoeniger, and Frank Edlich. Pro-apoptotic complexes of bax and bak on the outer mitochondrial membrane. *Biochimica et biophysica acta. Molecular cell research*, 1869(10):119317, 2022. URL: https://www.sciencedirect.com/science/article/pii/S0167488922001094, doi:10.1016/j.bbamcr.2022.119317.

[161] Justin P. Pogmore, David Uehling, and David W. Andrews. Pharmacological targeting of executioner proteins: Controlling life and death. *Journal of Medicinal Chemistry*, 64(9):5276–5290, 2021. URL: https://pubs.acs.org/doi/10.1021/acs.jmedchem.0c02200, doi:10.1021/acs.jmedchem.0c02200.

[162] Lena Große, Christian A. Wurm, Christian Brüser, Daniel Neumann, Daniel C. Jans, and Stefan Jakobs. Bax assembles into large ring-like structures remodeling the mitochondrial outer membrane in apoptosis. *The EMBO journal*, 35(4):402–413, 2016. URL: https://www.embopress.org/doi/full/10.15252/embj.201592789, doi:10.15252/embj.201592789.

[163] Raquel Salvador-Gallego, Markus Mund, Katia Cosentino, Jale Schneider, Joseph Unsay, Ulrich Schraermeyer, Johann Engelhardt, Jonas Ries, and Ana J. García-Sáez. Bax assembly into rings and arcs in apoptotic mitochondria is linked to membrane pores. *The EMBO journal*, 35(4):389–401, 2016. URL: https://www.embopress.org/doi/full/10.15252/embj.201593384, doi:10.15252/embj.201593384.

[164] Raquel Salvador Gallego. *Characterization of Bax and Drp1 during apoptosis with advanced microscopy techniques: Characterization of Bax and Drp1 during apoptosis with advanced microscopy techniques*. PhD thesis, Eberhard Karls Universität Tübingen. URL: https://ub01.uni-tuebingen.de/xmlui/handle/10900/72929.

[165] Laura A. Gillies, Han Du, Bjoern Peters, C. Michael Knudson, Donald D. Newmeyer, and Tomomi Kuwana. Visual and functional demonstration of growing bax-induced pores in mitochondrial outer membranes. *Molecular biology of the cell*, 26(2):339–349, 2015. URL: https://www.molbiolcell.org/doi/10.1091/mbc.E13-11-0638.

[166] Nicholas R. Ader, Patrick C. Hoffmann, Iva Ganeva, Alicia C. Borgeaud, Chunxin Wang, Richard J. Youle, and Wanda Kukulski. Molecular and topological reorganizations in mitochondrial architecture interplay during bax-mediated steps of apoptosis. *eLife*, 8, 2019. URL: https://elifesciences.org/articles/40712, doi:10.7554/eLife.40712.

[167] Katia Cosentino, Vanessa Hertlein, Andreas Jenner, Timo Dellmann, Milos Gojkovic, Aida Peña-Blanco, Shashank Dadsena, Noel Wajngarten, John S. H. Danial, Jervis Vermal Thevathasan, Markus Mund, Jonas Ries, and Ana J. Garcia-Saez. The interplay between bax and bak tunes apoptotic pore growth to control mitochondrial-dna-mediated inflammation. *Molecular Cell*, 82(5):933–949.e9, 2022. URL: https://www.sciencedirect.com/science/article/pii/S1097276522000089, doi:10.1016/j.molcel.2022.01.008.

[168] Shashank Dadsena, Louise E. King, and Ana J. García-Sáez. Apoptosis regulation at the mitochondria membrane level. *Biochimica et biophysica acta. Biomembranes*, 1863(12):183716, 2021. URL: https://www.sciencedirect.com/science/article/abs/pii/S0005273621001644, doi:10.1016/j.bbamem.2021.183716.

[169] Takahiro Yamazaki and Lorenzo Galluzzi. Bax and bak dynamics control mitochondrial dna release during apoptosis. *Cell Death & Differentiation*, 29(6):1296–1298, 2022. URL: https://www.nature.com/articles/s41418-022-00985-2, doi:10.1038/s41418-022-00985-2.

[170] David W. Andrews. The case for brakes: Why restrain the size of bax and bak pores in outer mitochondrial membranes? *Molecular Cell*, 82(5):882–883, 2022. URL: https://www.sciencedirect.com/science/article/pii/S1097276522001605, doi:10.1016/j.molcel.2022.02.022.

[171] R. Hooke. *Micrographia Or Some Physiological Descriptions of Minute Bodies Made by Magnifying Glasses with Observations and Inquiries Thereupon*. Martyn, 1665. URL: https://ttp.royalsociety.org//ttp/ttp.html?id=a9c4863d-db77-42d1-b294-fe66c85958b3&type=book.

[172] A. van Leeuwenhoek. Observations, communicated to the publisher by mr. antony van leewenhoeck, in a dutch letter of the 9th octob. 1676. here english'd: concerning little animals by him observed in rain-well-sea- and snow water; as also in water wherein pepper had lain infused. *Philosophical Transactions of the Royal Society of London*, 12(133):821–831, 1677. URL: https://royalsocietypublishing.org/doi/10.1098/rstl.1677.0003, doi:10.1098/rstl.1677.0003.

[173] M. Knoll and E. Ruska. Das elektronenmikroskop. *Zeitschrift für Physik*, 78(5-6):318–339, 1932. URL: https://link.springer.com/article/10.1007/BF01342199, doi:10.1007/BF01342199.

[174] O. SHIMOMURA, F. H. JOHNSON, and Y. SAIGA. Extraction, purification and properties of aequorin, a bioluminescent protein from the luminous hydromedusan, aequorea. *Journal of Cellular and Comparative Physiology*, 59(3):223–239, 1962. URL: https://onlinelibrary.wiley.com/doi/10.1002/jcp.1030590302, doi:10.1002/jcp.1030590302.

[175] M. Minsky. Memoir on inventing the confocal scanning microscope. *Scanning*, 10(4):128–138, 1988. URL: https://onlinelibrary.wiley.com/doi/abs/10.1002/sca.4950100403, doi:10.1002/sca.4950100403.

[176] Markus Sticker, Rebecca Elsässer, Markus Neumann, and Horst Wolff. How to get better fluorescence images with your widefield microscope: A methodology review. *Microscopy Today*, 28(6):36–43, 2020. doi:10.1017/S155192952000156X.

[177] Axiom Optics. Confocal microscopy, 07.02.2022. URL: https://www.axiomoptics.com/application/confocal-microscopy/.

[178] E. Abbe. Beiträge zur theorie des mikroskops und der mikroskopischen wahrnehmung. *Archiv für Mikroskopische Anatomie*, 9(1):413–468, 1873. URL: https://link.springer.com/article/10.1007/BF02956173, doi:10.1007/BF02956173.

[179] S. W. Hell and J. Wichmann. Breaking the diffraction resolution limit by stimulated emission: stimulated-emission-depletion fluorescence microscopy. *Optics letters*, 19(11):780–782, 1994. URL: https://opg.optica.org/ol/fulltext.cfm?uri=ol-19-11-780&id=12352, doi:10.1364/ol.19.000780.

[180] T. A. Klar, S. Jakobs, M. Dyba, A. Egner, and S. W. Hell. Fluorescence microscopy with diffraction resolution barrier broken by stimulated emission. *Proceedings of the National Academy of Sciences of the United States of America*, 97(15):8206–8210, 2000. URL: https://www.pnas.org/doi/10.1073/pnas.97.15.8206, doi:10.1073/pnas.97.15.8206.

[181] Francesca Bottanelli, Emil B. Kromann, Edward S. Allgeyer, Roman S. Erdmann, Stephanie Wood Baguley, George Sirinakis, Alanna Schepartz, David Baddeley, Derek K. Toomre, James E. Rothman, and Joerg Bewersdorf. Two-colour live-cell nanoscale imaging of intracellular targets. *Nature Communications*, 7(1):10778, 2016. URL: https://www.nature.com/articles/ncomms10778, doi:10.1038/ncomms10778.

[182] Eric Betzig, George H. Patterson, Rachid Sougrat, O. Wolf Lindwasser, Scott Olenych, Juan S. Bonifacino, Michael W. Davidson, Jennifer Lippincott-Schwartz, and Harald F. Hess. Imaging intracellular fluorescent proteins at nanometer resolution. *Science (New York, N.Y.)*, 313(5793):1642–1645, 2006. URL: https://www.science.org/doi/10.1126/science.1127344, doi:10.1126/science.1127344.

[183] Samuel T. Hess, Thanu P. K. Girirajan, and Michael D. Mason. Ultra-high resolution imaging by fluorescence photoactivation localization microscopy. *Biophysical journal*, 91(11):4258–4272, 2006. URL: https://www.sciencedirect.com/science/article/pii/S0006349506721403, doi:10.1529/biophysj.106.091116.

[184] Michael J. Rust, Mark Bates, and Xiaowei Zhuang. Sub-diffraction-limit imaging by stochastic optical reconstruction microscopy (storm). *Nature Methods*, 3(10):793–795, 2006. URL: https://www.nature.com/articles/nmeth929, doi:10.1038/nmeth929.

[185] Michael Hensel, Jürgen Klingauf, and Jacob Piehler. Imaging the invisible: resolving cellular microcompartments by superresolution microscopy techniques. *Biological Chemistry*, 394(9):1097–1113, 2013. URL: https://www.degruyter.com/document/doi/10.1515/hsz-2012-0324/html, doi:10.1515/hsz-2012-0324.

[186] Mark Bates, Jan Keller-Findeisen, Adrian Przybylski, Andreas Hüper, Till Stephan, Peter Ilgen, Angel R. Cereceda Delgado, Elisa D'Este, Alexander Egner, Stefan Jakobs, Steffen J. Sahl, and Stefan W. Hell. Optimal precision and accuracy in 4pi-storm using dynamic spline psf models. *Nature methods*, 19(5):603–612, 2022. URL: https://www.nature.com/articles/s41592-022-01465-8, doi:10.1038/s41592-022-01465-8.

[187] Francisco Balzarotti, Yvan Eilers, Klaus C. Gwosch, Arvid H. Gynnå, Volker Westphal, Fernando D. Stefani, Johan Elf, and Stefan W. Hell. Nanometer resolution imaging and tracking of fluorescent molecules with minimal photon fluxes. *Science (New York, N.Y.)*, 355(6325):606–612, 2017. URL: https://www.science.org/doi/10.1126/science.aak9913, doi:10.1126/science.aak9913.

[188] Klaus C. Gwosch, Jasmin K. Pape, Francisco Balzarotti, Philipp Hoess, Jan Ellenberg, Jonas Ries, and Stefan W. Hell. Minflux nanoscopy delivers 3d multicolor nanometer resolution in cells. *Nature methods*, 17(2):217–224, 2020. URL:

https://www.nature.com/articles/s41592-019-0688-0, doi:10.1038/s41592-019-0688-0.

[189] Lynn M. Ostersehlt, Daniel C. Jans, Anna Wittek, Jan Keller-Findeisen, Kaushik Inamdar, Steffen J. Sahl, Stefan W. Hell, and Stefan Jakobs. Dna-paint minflux nanoscopy. *Nature methods*, pages 1–4, 2022. URL: https://www.nature.com/articles/s41592-022-01577-1, doi:10.1038/s41592-022-01577-1.

[190] J. C. Goldstein, R. M. Kluck, and D. R. Green. A single cell analysis of apoptosis: Ordering the apoptotic phenotype. *Annals of the New York Academy of Sciences*, 926:132–141, 2000. URL: https://nyaspubs.onlinelibrary.wiley.com/doi/full/10.1111/j.1749-6632.2000.tb05607.x.

[191] R. J. Isfort, D. B. Cody, G. Lovell, and C. J. Doersen. Analysis of oncogenes, tumor suppressor genes, autocrine growth-factor production, and differentiation state of human osteosarcoma cell lines. *Molecular carcinogenesis*, 14(3):170–178, 1995. URL: https://onlinelibrary.wiley.com/doi/abs/10.1002/mc.2940140306, doi:10.1002/mc.2940140306.

[192] Katerina M. Niforou, Athanasios K. Anagnostopoulos, Konstantinos Vougas, Christos Kittas, Vassilis G. Gorgoulis, and George T. Tsangaris. The proteome profile of the human osteosarcoma u2os cell line. *Cancer genomics & proteomics*, 5(1):63–78, 2008. URL: https://cgp.iiarjournals.org/content/5/1/63.long.

[193] Y. Nemoto and P. de Camilli. Recruitment of an alternatively spliced form of synaptojanin 2 to mitochondria by the interaction with the pdz domain of a mitochondrial outer membrane protein. *The EMBO journal*, 18(11):2991–3006, 1999. URL: https://www.embopress.org/doi/full/10.1093/emboj/18.11.2991, doi:10.1093/emboj/18.11.2991.

[194] Antje Keppler, Susanne Gendreizig, Thomas Gronemeyer, Horst Pick, Horst Vogel, and Kai Johnsson. A general method for the covalent labeling of fusion proteins with small molecules in vivo. *Nature biotechnology*, 21(1):86–89, 2003. URL: https://www.nature.com/articles/nbt765, doi:10.1038/nbt765.

[195] Eirini P. Papapetrou and Axel Schambach. Gene insertion into genomic safe harbors for human gene therapy. *Molecular therapy : the journal of the American Society of Gene Therapy*, 24(4):678–684, 2016. URL: https://www.sciencedirect.com/science/article/pii/S1525001616309911, doi:10.1038/mt.2016.38.

[196] Kun Qian, Cindy Tzu-Ling Huang, Hong Chen, Lisle W. Blackbourn, Yuejun Chen, Jingyuan Cao, Lin Yao, Cornall Sauvey, Zhongwei Du, and Su-Chun Zhang. A simple and efficient system for regulating gene expression in human pluripotent stem cells and derivatives. *Stem cells (Dayton, Ohio)*, 32(5):1230–1238, 2014. URL: https://academic.oup.com/stmcls/article/32/5/1230/6444484, doi:10.1002/stem.1653.

[197] Gražvydas Lukinavičius, Keitaro Umezawa, Nicolas Olivier, Alf Honigmann, Guoying Yang, Tilman Plass, Veronika Mueller, Luc Reymond, Ivan R. Corrêa, Zhen-Ge Luo, Carsten Schultz, Edward A. Lemke, Paul Heppenstall, Christian Eggeling, Suliana Manley, and Kai Johnsson. A near-infrared fluorophore for live-cell super-resolution microscopy of cellular proteins. *Nature Chemistry*, 5(2):132–139, 2013. URL: https://www.nature.com/articles/nchem.1546, doi:10.1038/nchem.1546.

[198] Marahaini Musa. Cell proliferation study of human osteosarcoma cell line (u2os) using alamar blue assayand live cell imaging. *IOSR Journal of Dental and Medical Sciences*, 8(2):60–65, 2013. URL: http://www.iosrjournals.org/iosr-jdms/papers/Vol8-issue2/M0826065.pdf, doi:10.9790/0853-0826065.

[199] Georgyi V. Los, Lance P. Encell, Mark G. McDougall, Danette D. Hartzell, Natasha Karassina, Chad Zimprich, Monika G. Wood, Randy Learish, Rachel Friedman Ohana, Marjeta Urh, Dan Simpson, Jacqui Mendez, Kris Zimmerman, Paul Otto, Gediminas Vidugiris, Ji Zhu, Aldis Darzins, Dieter H. Klaubert, Robert F. Bulleit, and Keith V. Wood. Halotag: a novel protein labeling technology for cell imaging and protein analysis. *ACS chemical biology*, 3(6):373–382, 2008. URL: https://pubs.acs.org/doi/10.1021/cb800025k, doi:10.1021/cb800025k.

[200] Mariusz Karbowski, Yang-Ja Lee, Brigitte Gaume, Seon-Yong Jeong, Stephan Frank, Amotz Nechushtan, Ansgar Santel, Margaret Fuller, Carolyn L. Smith, and Richard J. Youle. Spatial and temporal association of bax with mitochondrial fission sites, drp1, and mfn2 during apoptosis. *The Journal of cell biology*, 159(6):931–938, 2002. URL: https://rupress.org/jcb/article/159/6/931/33282/Spatial-and-temporal-association-of-Bax-with, doi:10.1083/jcb.200209124.

[201] J. Xiang, D. T. Chao, and S. J. Korsmeyer. Bax-induced cell death may not require interleukin 1 beta-converting enzyme-like proteases. *Proceedings of the National Academy of Sciences of the United States of Amer-*

ica, 93(25):14559–14563, 1996. URL: https://www.pnas.org/doi/10.1073/pnas.93.25.14559, doi:10.1073/pnas.93.25.14559.

[202] J. G. Pastorino, S. T. Chen, M. Tafani, J. W. Snyder, and J. L. Farber. The overexpression of bax produces cell death upon induction of the mitochondrial permeability transition. *The Journal of biological chemistry*, 273(13):7770–7775, 1998. URL: https://www.sciencedirect.com/science/article/pii/S0021925818617594, doi:10.1074/jbc.273.13.7770.

[203] Grant Dewson. Interplay of bcl-2 proteins decides the life or death fate. *The Open Cell Signaling Journal*, 3:3–8, 2011. URL: https://benthamopen.com/FULLTEXT/TOCELLSJ-3-3, doi:10.2174/1876390101103010003.

[204] Nicholas M. George, Jacquelynn J. D. Evans, and Xu Luo. A three-helix homo-oligomerization domain containing bh3 and bh1 is responsible for the apoptotic activity of bax. *Genes & Development*, 21(15):1937–1948, 2007. URL: http://genesdev.cshlp.org/content/21/15/1937, doi:10.1101/gad.1553607.

[205] K. Wang, A. Gross, G. Waksman, and S. J. Korsmeyer. Mutagenesis of the bh3 domain of bax identifies residues critical for dimerization and killing. *Molecular and cellular biology*, 18(10):6083–6089, 1998. URL: https://journals.asm.org/doi/10.1128/MCB.18.10.6083, doi:10.1128/MCB.18.10.6083.

[206] Stephen W. G. Tait and Douglas R. Green. Mitochondria and cell death: outer membrane permeabilization and beyond. *Nature reviews. Molecular cell biology*, 11(9):621–632, 2010. URL: https://www.nature.com/articles/nrm2952, doi:10.1038/nrm2952.

[207] Luca Scorrano, Mona Ashiya, Karolyn Buttle, Solly Weiler, Scott A. Oakes, Carmen A. Mannella, and Stanley J. Korsmeyer. A distinct pathway remodels mitochondrial cristae and mobilizes cytochrome c during apoptosis. *Developmental Cell*, 2(1):55–67, 2002. URL: https://www.sciencedirect.com/science/article/pii/S1534580701001162, doi:10.1016/S1534-5807(01)00116-2.

[208] Martin Ott, John D. Robertson, Vladimir Gogvadze, Boris Zhivotovsky, and Sten Orrenius. Cytochrome c release from mitochondria proceeds by a two-step process. *Proceedings of the National Academy of Sciences of the United States of America*, 99(3):1259–1263, 2002. URL: https://www.pnas.org/doi/full/10.1073/pnas.241655498, doi:10.1073/pnas.241655498.

[209] Alam Nur-E-Kamal, Stephane R. Gross, Zui Pan, Zita Balklava, Jianjie Ma, and Leroy F. Liu. Nuclear translocation of cytochrome c during apoptosis. *The Journal of biological chemistry*, 279(24):24911–24914, 2004. URL: https://www.jbc.org/article/S0021-9258(20)66383-9/fulltext, doi:10.1074/jbc.C400051200.

[210] Luiz C. Godoy, Cristina Muñoz-Pinedo, Laura Castro, Simone Cardaci, Christopher M. Schonhoff, Michael King, Verónica Tórtora, Mónica Marín, Qian Miao, Jian Fei Jiang, Alexandr Kapralov, Ronald Jemmerson, Gary G. Silkstone, Jinal N. Patel, James E. Evans, Michael T. Wilson, Douglas R. Green, Valerian E. Kagan, Rafael Radi, and Joan B. Mannick. Disruption of the m80-fe ligation stimulates the translocation of cytochrome c to the cytoplasm and nucleus in nonapoptotic cells. *Proceedings of the National Academy of Sciences of the United States of America*, 106(8):2653–2658, 2009. URL: https://www.pnas.org/doi/10.1073/pnas.0809279106, doi:10.1073/pnas.0809279106.

[211] Johannes Schindelin, Ignacio Arganda-Carreras, Erwin Frise, Verena Kaynig, Mark Longair, Tobias Pietzsch, Stephan Preibisch, Curtis Rueden, Stephan Saalfeld, Benjamin Schmid, Jean-Yves Tinevez, Daniel James White, Volker Hartenstein, Kevin Eliceiri, Pavel Tomancak, and Albert Cardona. Fiji: an open-source platform for biological-image analysis. *Nature methods*, 9(7):676–682, 2012. URL: https://www.nature.com/articles/nmeth.2019, doi:10.1038/nmeth.2019.

[212] K. Pearson. Vii. mathematical contributions to the theory of evolution.—iii. regression, heredity, and panmixia. *Philosophical Transactions of the Royal Society of London. Series A, Containing Papers of a Mathematical or Physical Character*, 187:253–318, 1896. URL: https://royalsocietypublishing.org/doi/abs/10.1098/rsta.1896.0007, doi:10.1098/rsta.1896.0007.

[213] E. M. M. Manders, F. J. Verbeek, and J. A. Aten. Measurement of co-localization of objects in dual-colour confocal images. *Journal of Microscopy*, 169(3):375–382, 1993. URL: https://onlinelibrary.wiley.com/doi/abs/10.1111/j.1365-2818.1993.tb03313.x, doi:10.1111/j.1365-2818.1993.tb03313.x.

[214] Kenneth W. Dunn, Malgorzata M. Kamocka, and John H. McDonald. A practical guide to evaluating colocalization in biological microscopy. *American journal of physiology. Cell physiology*, 300(4):C723–42, 2011. URL: https://journals.physiology.org/doi/full/10.1152/ajpcell.00462.2010, doi:10.1152/ajpcell.00462.2010.

[215] Gene set - u2os, 25.08.2022. URL: https://maayanlab.cloud/Harmonizome/gene_set/U2OS/CCLE+Cell+Line+Gene+Expression+Profiles.

[216] Cell line u2os - compound sensitivity profile | cansar black, 25.08.2022. URL: https://cansarblack.icr.ac.uk/cell-line/U-2-OS/copy-number/chromosome/19.

[217] Beomjong Song, Soyeon Yang, Gue-Ho Hwang, Jihyeon Yu, and Sangsu Bae. Analysis of nhej-based dna repair after crispr-mediated dna cleavage. *International journal of molecular sciences*, 22(12), 2021. URL: https://www.mdpi.com/1422-0067/22/12/6397/htm.

[218] K. G. Wolter, Y. T. Hsu, C. L. Smith, A. Nechushtan, X. G. Xi, and R. J. Youle. Movement of bax from the cytosol to mitochondria during apoptosis. *The Journal of cell biology*, 139(5):1281–1292, 1997. URL: https://rupress.org/jcb/article/139/5/1281/819/Movement-of-Bax-from-the-Cytosol-to-Mitochondria, doi:10.1083/jcb.139.5.1281.

[219] Kristopher A. Sarosiek, Triona Ni Chonghaile, and Anthony Letai. Mitochondria: gatekeepers of response to chemotherapy. *Trends in Cell Biology*, 23(12):612–619, 2013. URL: https://www.sciencedirect.com/science/article/pii/S0962892413001360, doi:10.1016/j.tcb.2013.08.003.

[220] Louise E. King, Ricardo Rodriguez-Enriquez, Robert Pedley, Charlotte E. L. Mellor, Pengbo Wang, Egor Zindy, Michael R. H. White, Keith Brennan, and Andrew P. Gilmore. Apoptotic priming is defined by the dynamic exchange of bcl-2 proteins between mitochondria and cytosol. *Cell Death & Differentiation*, 29(11):2262–2274, 2022. URL: https://www.nature.com/articles/s41418-022-01013-z, doi:10.1038/s41418-022-01013-z.

[221] Tomomi Kuwana, Louise E. King, Katia Cosentino, Julian Suess, Ana J. Garcia-Saez, Andrew P. Gilmore, and Donald D. Newmeyer. Mitochondrial residence of the apoptosis inducer bax is more important than bax oligomerization in promoting membrane permeabilization. *Journal of Biological Chemistry*, 295(6):1623–1636, 2020. URL: https://www.jbc.org/article/S0021-9258(17)49861-9/fulltext, doi:10.1074/jbc.RA119.011635.

[222] Marie K. Schwinn, Leta S. Steffen, Kris Zimmerman, Keith V. Wood, and Thomas Machleidt. A simple and scalable strategy for analysis of endogenous protein dynamics. *Scientific Reports*, 10(1):8953, 2020. URL: https://www.nature.com/articles/s41598-020-65832-1, doi:10.1038/s41598-020-65832-1.

[223] Mazen W. Karaman, Sanna Herrgard, Daniel K. Treiber, Paul Gallant, Corey E. Atteridge, Brian T. Campbell, Katrina W. Chan, Pietro Ciceri, Mindy I. Davis, Philip T. Edeen, Raffaella Faraoni, Mark Floyd, Jeremy P. Hunt, Daniel J. Lockhart, Zdravko V. Milanov, Michael J. Morrison, Gabriel Pallares, Hitesh K. Patel, Stephanie Pritchard, Lisa M. Wodicka, and Patrick P. Zarrinkar. A quantitative analysis of kinase inhibitor selectivity. *Nature Biotechnology*, 26(1):127–132, 2008. URL: https://www.nature.com/articles/nbt1358, doi:10.1038/nbt1358.

[224] Thomas P. Hopp, Kathryn S. Prickett, Virginia L. Price, Randell T. Libby, Carl J. March, Douglas Pat Cerretti, David L. Urdal, and Paul J. Conlon. A short polypeptide marker sequence useful for recombinant protein identification and purification. *Bio/Technology*, 6(10):1204–1210, 1988. URL: https://www.nature.com/articles/nbt1088-1204, doi:10.1038/nbt1088-1204.

[225] Tiberiu S. Mihaila, Carina Bäte, Lynn M. Ostersehlt, Jasmin K. Pape, Jan Keller-Findeisen, Steffen J. Sahl, and Stefan W. Hell. Enhanced incorporation of subnanometer tags into cellular proteins for fluorescence nanoscopy via optimized genetic code expansion. *Proceedings of the National Academy of Sciences of the United States of America*, 119(29):e2201861119, 2022. URL: https://www.pnas.org/doi/abs/10.1073/pnas.2201861119, doi:10.1073/pnas.2201861119.

[226] H. Düssmann, M. Rehm, C. G. Concannon, S. Anguissola, M. Würstle, S. Kacmar, P. Völler, H. J. Huber, and J. H. M. Prehn. Single-cell quantification of bax activation and mathematical modelling suggest pore formation on minimal mitochondrial bax accumulation. *Cell Death & Differentiation*, 17(2):278–290, 2010. URL: https://www.nature.com/articles/cdd2009123, doi:10.1038/cdd.2009.123.

[227] S. Angermüller, G. Künstle, and G. Tiegs. Pre-apoptotic alterations in hepatocytes of tnfalpha-treated galactosamine-sensitized mice. *The journal of histochemistry and cytochemistry : official journal of the Histochemistry Society*, 46(10):1175–1183, 1998. URL: https://journals.sagepub.com/doi/10.1177/002215549804601009, doi:10.1177/002215549804601009.

[228] J. Kwong, H. L. Choi, Y. Huang, and F. L. Chan. Ultrastructural and biochemical observations on the early changes in apoptotic epithelial cells of the rat prostate induced by castration. *Cell and Tissue Research*, 298(1):123–136, 1999. URL: https://link.springer.com/article/10.1007/s004419900057, doi:10.1007/s004419900057.

[229] G. Feldmann, D. Haouzi, A. Moreau, A. M. Durand-Schneider, A. Bringuier, A. Berson, A. Mansouri, D. Fau, and D. Pessayre. Opening of the mitochondrial permeability transition pore causes matrix expansion and outer membrane rupture in fas-mediated hepatic apoptosis in mice. *Hepatology*, 31(3):674–683, 2000. URL: https://aasldpubs.onlinelibrary.wiley.com/doi/10.1002/hep.510310318, doi:10.1002/hep.510310318.

[230] M. Vogler, D. Dinsdale, X-M Sun, K. W. Young, M. Butterworth, P. Nicotera, M. J. S. Dyer, and G. M. Cohen. A novel paradigm for rapid abt-737-induced apoptosis involving outer mitochondrial membrane rupture in primary leukemia and lymphoma cells. *Cell Death & Differentiation*, 15(5):820–830, 2008. URL: https://www.nature.com/articles/cdd200825, doi:10.1038/cdd.2008.25.

[231] A. Sesso, J. E. Belizário, M. M. Marques, M. L. Higuchi, R. I. Schumacher, A. Colquhoun, E. Ito, and J. Kawakami. Mitochondrial swelling and incipient outer membrane rupture in preapoptotic and apoptotic cells. *The Anatomical Record: Advances in Integrative Anatomy and Evolutionary Biology*, 295(10):1647–1659, 2012. URL: https://anatomypubs.onlinelibrary.wiley.com/doi/10.1002/ar.22553, doi:10.1002/ar.22553.

[232] Ons M'Saad and Joerg Bewersdorf. Light microscopy of proteins in their ultrastructural context. *Nature Communications*, 11(1):3850, 2020. URL: https://www.nature.com/articles/s41467-020-17523-8, doi:10.1038/s41467-020-17523-8.

[233] Stuart Berg, Dominik Kutra, Thorben Kroeger, Christoph N. Straehle, Bernhard X. Kausler, Carsten Haubold, Martin Schiegg, Janez Ales, Thorsten Beier, Markus Rudy, Kemal Eren, Jaime I. Cervantes, Buote Xu, Fynn Beuttenmueller, Adrian Wolny, Chong Zhang, Ullrich Koethe, Fred A. Hamprecht, and Anna Kreshuk. ilastik: interactive machine learning for (bio)image analysis. *Nature methods*, 16(12):1226–1232, 2019. URL: https://www.nature.com/articles/s41592-019-0582-9, doi:10.1038/s41592-019-0582-9.

[234] John S. H. Danial and Ana J. Garcia-Saez. Quantitative analysis of super-resolved structures using asap. *Nature methods*, 16(8):711–714, 2019. URL: https://www.nature.com/articles/s41592-019-0472-1, doi:10.1038/s41592-019-0472-1.

[235] Zhi Zhang, Sabareesh Subramaniam, Justin Kale, Chenyi Liao, Bo Huang, Hetal Brahmbhatt, Samson G. F. Condon, Suzanne M. Lapolla, Franklin A.

Hays, Jingzhen Ding, Feng He, Xuejun C. Zhang, Jianing Li, Alessandro Senes, David W. Andrews, and Jialing Lin. Bh3-in-groove dimerization initiates and helix 9 dimerization expands bax pore assembly in membranes. *The EMBO journal*, 35(2):208–236, 2016. URL: https://www.embopress.org/doi/full/10.15252/embj.201591552, doi:10.15252/embj.201591552.

[236] Jason M. Brouwer, Dana Westphal, Grant Dewson, Adeline Y. Robin, Rachel T. Uren, Ray Bartolo, Geoff V. Thompson, Peter M. Colman, Ruth M. Kluck, and Peter E. Czabotar. Bak core and latch domains separate during activation, and freed core domains form symmetric homodimers. *Molecular Cell*, 55(6):938–946, 2014. URL: https://www.sciencedirect.com/science/article/pii/S1097276514006091, doi:10.1016/j.molcel.2014.07.016.

[237] Shenggen Yao, Dana Westphal, Jeffrey J. Babon, Geoff V. Thompson, Adeline Y. Robin, Jerry M. Adams, Peter M. Colman, and Peter E. Czabotar. Nmr studies of interactions between bax and bh3 domain-containing peptides in the absence and presence of chaps. *Archives of Biochemistry and Biophysics*, 545:33–43, 2014. URL: https://www.sciencedirect.com/science/article/pii/S000398611400006X, doi:10.1016/j.abb.2014.01.003.

[238] R. Sundararajan, A. Cuconati, D. Nelson, and E. White. Tumor necrosis factor-alpha induces bax-bak interaction and apoptosis, which is inhibited by adenovirus e1b 19k. *The Journal of biological chemistry*, 276(48):45120–45127, 2001. URL: https://www.jbc.org/article/S0021-9258(19)82720-5/fulltext, doi:10.1074/jbc.M106386200.

[239] Valery Mikhailov, Margarita Mikhailova, Kurt Degenhardt, Manjeri A. Venkatachalam, Eileen White, and Pothana Saikumar. Association of bax and bak homo-oligomers in mitochondria. bax requirement for bak reorganization and cytochrome c release. *The Journal of biological chemistry*, 278(7):5367–5376, 2003. URL: https://www.sciencedirect.com/science/article/pii/S0021925819328509, doi:10.1074/jbc.M203392200.

[240] Sweta Iyer, Rachel T. Uren, Michael A. Dengler, Melissa X. Shi, Etsuko Uno, Jerry M. Adams, Grant Dewson, and Ruth M. Kluck. Robust autoactivation for apoptosis by bak but not bax highlights bak as an important therapeutic target. *Cell Death & Disease*, 11(4):268, 2020. URL: https://www.nature.com/articles/s41419-020-2463-7, doi:10.1038/s41419-020-2463-7.

[241] Florian J. Bock, Egor Sedov, Elle Koren, Anna L. Koessinger, Catherine Cloix, Désirée Zerbst, Dimitris Athineos, Jayanthi Anand, Kirsteen J. Campbell, Karen

Blyth, Yaron Fuchs, and Stephen W. G. Tait. Apoptotic stress-induced fgf signalling promotes non-cell autonomous resistance to cell death. *Nature Communications*, 12(1):6572, 2021. URL: https://www.nature.com/articles/s41467-021-26613-0, doi:10.1038/s41467-021-26613-0.

[242] Paolo Armando Gagliardi, Maciej Dobrzyński, Marc-Antoine Jacques, Coralie Dessauges, Pascal Ender, Yannick Blum, Robert M. Hughes, Andrew R. Cohen, and Olivier Pertz. Collective erk/akt activity waves orchestrate epithelial homeostasis by driving apoptosis-induced survival. *Developmental Cell*, 56(12):1712–1726.e6, 2021. URL: https://www.sciencedirect.com/science/article/pii/S1534580721004366, doi:10.1016/j.devcel.2021.05.007.

[243] New England Biolabs. Nebuilder, 22.08.2022. URL: https://nebuilder.neb.com/#!/.

[244] Till Stephan, Christian Brüser, Markus Deckers, Anna M. Steyer, Francisco Balzarotti, Mariam Barbot, Tiana S. Behr, Gudrun Heim, Wolfgang Hübner, Peter Ilgen, Felix Lange, David Pacheu-Grau, Jasmin K. Pape, Stefan Stoldt, Thomas Huser, Stefan W. Hell, Wiebke Möbius, Peter Rehling, Dietmar Riedel, and Stefan Jakobs. Micos assembly controls mitochondrial inner membrane remodeling and crista junction redistribution to mediate cristae formation. *The EMBO journal*, 39(14):e104105, 2020. URL: https://www.embopress.org/doi/full/10.15252/embj.2019104105, doi:10.15252/embj.2019104105.

[245] Joerg Schnitzbauer, Maximilian T. Strauss, Thomas Schlichthaerle, Florian Schueder, and Ralf Jungmann. Super-resolution microscopy with dna-paint. *Nature Protocols*, 12(6):1198–1228, 2017. URL: https://www.nature.com/articles/nprot.2017.024, doi:10.1038/nprot.2017.024.